Oagile Jomo Kanyeto

# INVESTIGATION OF THE BEHAVIOUR OF LATERALLY LOADED THIN-JOINTED CONCRETE-BLOCK MASONRY PANELS

A thesis submitted for the degree of Doctor of Philosophy to

Kingston University London, Kingston Upon Thames

 November 2006

# ABSTRACT

This masonry research investigated the structural response of masonry wall panels when subjected to static lateral loads. The lateral load capacity and deformational characteristics of two full-scale wall panels, constructed with dense concrete blocks and laid in thin joint mortar of 3 mm thickness, have been studied experimentally and with numerical models. Linear elastic equations have been employed to predict the distribution of moments and failure load of the panels. The necessary material properties were determined from a series of small scale tests involving a total of 24 wallettes. The wallettes were built and tested in accordance with the British Standards recommendations as outlined in BS 5628: Part 1, and complied with the European code, EN 1996-1-1. The research found that, when subjected to lateral loads, concrete block masonry built using thin layer mortar behaves as a homogeneous elastic plate and fail in a brittle manner. Recommendations on the application of elastic theory concepts as the basis for development of material constitutive laws have been made based on the fact that linear elastic equations have been tested against experimental data and found to be valid.

# ACKNOWLEDGEMENTS

I wish to start by offering my sincere gratitude to Dr Anton Fried, who was my Director of Study for most part of my research project. His constant encouragement, inspiration and guidance throughout the entire duration of the research work made my studies very interesting and stress free. I also wish to thank Professors John Roberts and Eddie Bromhead for their important roles in the supervision of this research. Thanks are also offered to Professor Mukesh Limbachiya who willingly became my surrogate Director of Studies after the departure of Dr Fried. Professor Mukesh Limbachiya's support, guidance and advice towards the end of my study are highly appreciated.

Many thanks are offered to Colin Bradsell, Peter Wells, Ron Adey, John Ordish and Glyn Davies of Kingston University for their technical assistance. This research would not have been completed without their experience and full support.

Last but not least, I would like to thank my family, friends and colleagues for their continuous encouragement and believe in me.

This project was supported by Hanson Building Products, who supplied and built all the specimens and provided valuable guidance for which thanks are offered. In particular, the support of Paul Ragatski of Hanson Building Products is acknowledged.

The research project was entirely funded by the University of Botswana as part of its Staff Training and Development Programme. The University of Botswana also provided maintenance support throughout the duration of the research work. This sponsorship is highly appreciated.

# TABLE OF CONTENTS

## CHAPTER 3: EVALUATION OF ANALYTICAL METHODS



## CHAPTER 4: TESTING PROGRAMME

## CHAPTER 6: ANALYSIS AND DESIGN PROCEDURE



## CHAPTER 7: VALIDATION OF ELASTIC THEORY



## CHAPTER 8: CONCLUSIONS



## REFERENCES

## APPENDICES

# List of Figures

# List of Tables

# List of Symbols

$x$ , $y$ rectangular axes in the plane of a slab

$f_{tx}$ - the horizontal flexural strength

$f_{ty}$ - the vertical flexural strength

$f_{kx}$ – characteristic flexural tensile strength parallel to bed joints.

H - wall height

t - wall thickness

L - length of wall

$m_x$ bending moment per unit width in the $x$ direction

$m_y$ bending moment per unit width in the $y$ direction

$m_{xy}$ torsional moment per unit width

q uniformly distributed load per unit area of an element

$\sigma_b$ Bending Stress

$E$ modulus of elasticity,

$I = \frac{bt^3}{12}$ is the second moment of area of thickness $t$ and width $b$ ,

$u$ maximum lateral deflection, which occurs at the mid-span,

$P$ applied point load

$L$ support span,

$a$ distance between support and loading point

$v$ Poisson's ratio

$w$ uniformly distributed load per unit area of a wall panel

$m_{cx}$ moment capacity per unit length in the x-direction

$m_{cy}$ moment capacity per unit length in the x-direction

Z section modulus per unit width

D flexural rigidity

$w_x$ failure load with respect to the bed joints

$w_y$ failure load with respect to the perpend joints

$\alpha_x$ bending moment coefficient in the direction of the x-axis

$\alpha_y$ bending moment coefficient in the y-direction

$f_u$ mean modulus of rapture of the blocks (UMOR)

$f_b$ mean flexural tensile strength of the bed joints

$\beta_1$ , $\beta_2$ numerical coefficients given in Table A1.1, Appendix 1(a)

$D_x$ flexural rigidity with respect to the x-axis

$D_y$ flexural rigidity with respect to the y-axis

$E_x, E_y$ modulus of elasticity with respect to the x- and y-axes, respectively.

# CHAPTER 1: INTRODUCTION

## 1.1 MASONRY

Masonry is an age-old material that represents a permanence of feature [Cowan, 1977] which human beings find attractive. The material is relatively cheap and durable, can provide infinite flexibility in plan form and offer attractive external appearance. However, the design of masonry buildings in accordance with modern structural engineering principles is quite new. It was not until the middle of the twentieth century that sufficient information was available to permit the preparation of codes of practice [Hendry, 1981] containing essential data on masonry strength and reduction factors for slenderness and strength. For a considerable period of time prior to this masonry was eclipsed by steel and concrete as a structural material for large buildings. The application of structural engineering principles to the design of masonry elements since the 1950s has resulted in the re-adoption of this material for many applications. Since that period, the whole field of research in masonry construction has been developing remarkably, as reflected by the holding of regular conferences devoted to the subject since the late 1960s. Hence, a considerable literature exists on most problems encountered in masonry applications.

Masonry structures can last for millennia, but are also vulnerable to destruction, which can arise from many sources: the passing of time, carelessness in construction, acts of God [Nichols, 2000]. This current research seeks to understand the response of the material to some of these forces. When testing masonry to explore its properties, techniques to accelerate failure and weathering are adopted. Nevertheless, experimental work should be designed to mirror the real destructive forces that exist in nature and establish the design limits of masonry [Baker, 1912]. These include earthquakes, wind or waves. These environmental loads occur in a random pattern often striking without discernible reason.

The use of masonry as a structural material, particularly in applications requiring tensile strength such as in basement construction, and the incidents arising from improper use of masonry, continually require research to provide accurate and convenient design methods based on theoretical analysis and experimental results. Although research on masonry wall panels subjected to lateral loading is well documented, it has failed to provide reliable design and analysis techniques that can accurately predict experimental results. The current research aims to provide an answer to this design problem.

One of the significant outcomes of masonry research has been the development of new materials and construction practices, providing enhanced physical and mechanical properties. Nowadays, masonry components can be erected by gluing bricks or concrete blocks together. Owing to the homogeneous appearance of such masonry, architects are especially fond of this new technique [Martens, 2000]. It is the engineer's duty to explore the strength characteristics of this revolutionary product in order to provide robust structures.

The writings of Heyman (1998) explain how economic forces shape the use of primary construction materials. He perceives the fundamental principle of engineering as seeking to make use of any material to create structures that are sound and yet with no superfluous elements, save those deemed by the designer. The ease of execution of glued masonry should allow a significant reduction of construction time and volume of mortar, with favourable consequences on the total costs. Economic forces will define the scale of thin layer masonry use, but in the current research, no attempt has been made to quantify economic benefits, which have been reported by others [Valluzzi, 2002].

**1.2 DEFINITION OF THE PROBLEM**

Unreinforced masonry design in the UK is currently undertaken in accordance with BS5628: Part 1:1992, the code of practice for structural use of unreinforced masonry [BSI, 1992]. The design procedure is based on moment coefficients derived from Yield Line analysis and experimental results [Haseltine, 1977]. Although the typical crack patterns for walls appear similar to yield lines and several researchers have reported good agreement between predicted failure loads and test results, the pragmatic justification for using a theory based on ductile behaviour for a brittle material like masonry is difficult for many to accept [Middleton and Drysdale, 1995]. Until recently, the code only covered masonry structures built using conventional mortar, with no reference to using thin joint mortar.

A seminar of The British Masonry Society in year 2000 aimed at providing full discussion and recommendations for change of materials behaviour, strength and design methods, both old and new, for laterally loaded masonry walls [British

Masonry Society, Winter 2000]. A total of ten recommendations were made, three of which are re-stated below:

1. A number of forms of masonry construction should be added to BS5628 in relation to flexural strength including: thin layer mortar, lightweight mortar and lime mortars.
2. The current basis of designing the lateral loading of walls by the use of the yield line method is still felt to offer the best solution.
3. In the longer term it might prove possible to use finite element modelling to predict the lateral loading capacities of masonry walls, and include this in the codification process.

Based on the above commentary, the gathering of additional information to gain insight into the behaviour of laterally-loaded masonry wall panels is justified. Hence, a research programme has been undertaken at Kingston University to address these issues.

It is hoped that this research will be of service to structural engineers and researchers by enabling them to extend their knowledge of masonry behaviour, and that it will contribute towards development of a structural design theory for thin-jointed masonry wall panels subjected to lateral loading.

## 1.3 RESEARCH OBJECTIVES AND METHODOLOGY

The principal objectives of this research were to:

I. Examine the performance of a few selected analytical techniques in predicting the behaviour of laterally-loaded masonry walls, by comparing their predictions to experimental results.

II. Study the response of thin jointed unreinforced masonry wall panels subjected to laterally-applied uniformly distributed loading.

III. Investigate the potential of numerical finite element modelling in predicting the load capacities and behaviour of thin jointed masonry walls.

IV. Establish a relationship between the flexural tensile strength of masonry constituents when tested in a masonry-composite and when tested individually.

V. Derive analysis and design equations for thin layer masonry wall panels, to be used in the development of design codes.

The objectives of the research have been addressed though the following programme:

I. Review of literature
II. Physical testing of small- and large-scale wall panels, and masonry units.
III. Numerical finite element modelling of full-scale wall models.
IV. Application of linear elastic theory concepts to define material behaviour

**1.4 THESIS STRUCTURE**

The main areas of this thesis are presented through eight chapters. The first chapter is introductory by nature, describing the problem that the investigation aimed to address as well as presenting the methodology employed to achieve this objective.

Chapter 2 and 3 present a review of the available literature. In Chapter 2, historical developments of the use of masonry as an engineering material are reviewed, with emphasis on the aspects related to the out-of-plane behaviour of the material. The purpose of this review is to assess the existing knowledge of the structural engineering aspects of masonry construction, and to establish the framework for addressing the challenges of the current research and of the future of masonry research in general. Chapter 3 makes an assessment of the application of engineering concepts to laterally loaded un-reinforced masonry wall panels. The review covers research work that has formed the basis of some design codes, as well as other research work aimed at material characterization for numerical modelling purposes. Due to the limited availability of data on thin-jointed masonry, the review in these two chapters is predominantly on conventionally-constructed masonry walls.

Details of the experimental study are outlined in Chapter 4 and include the data acquisition procedure and results obtained from the tests. A number of photographs and diagrams of the testing equipment and specimens are provided to assist with the explanation of the research method. Interpretation of the observations is presented with the help of graphs, tables and sketches. Appendix 4 presents the complete set of experimental results including photographs of the tested panels.

A detailed analysis of the deformational characteristics of thin jointed masonry walls is presented in Chapter 5. Mathematical relationships and engineering properties of the material are derived from the experimental results. Appendix 1 presents the detailed derivations of the mathematical formulae quoted in Chapter 5. Details of a numerical finite element analysis programme are described in this chapter, and the results are presented. The chapter concludes by recommending a theoretical basis for the prediction of material behaviour.

A demonstration of the applicability of elastic theory for prediction of the behaviour of thin-jointed concrete-block masonry wall panels is presented in Chapter 6. In Chapter 7, linear elastic analysis equations are tested against experimental data recorded by other researchers, and relevant discussions are presented.

Concluding remarks and recommendations for further work are provided in Chapter 8. The chapter presents a summary of the advantages of thin-jointed concrete-block masonry as compared to the conventional system, and its current and potential future applications in the construction industry are briefly discussed. The final sections of the chapter then summarise the benefits of the results of the current investigation and provide recommendations for further work on thin jointed concrete block masonry structures.

# CHAPTER 2: A REVIEW OF LATERAL BEHAVIOUR OF UNREINFORCED MASONRY WALLS

## 2.1 INTRODUCTION

A review, oriented towards the development of analytical and numerical analysis procedures, of the out-of-plane behaviour of masonry walls is presented in this chapter. The study examines the historical developments of masonry analysis and design in the last five decades. It is recognized that accurate numerical and analytical models can only evolve if an adequate materials description is available. Hence, the review begins by considering the factors that influence strength properties of masonry walls when subjected to lateral loads that can be classified as static. Conclusions are then drawn from the reviewed works, which are followed by some recommendations for further research work.

Appropriate combination of material properties, as well as reasonable representation of failure modes and mechanisms, should lead to the development of an accurate method of prediction of the behaviour of masonry walls. According to Sinha (1994), a rational approach can evolve if the failure criterion and the material's behaviour in bi-axial bending are fully understood. Once a rational analytical technique is formulated, and the flexural properties used in it are compatible with actual flexural resistances, Fried (1989) contends that accurate predictions of wall capacity should then be possible. So far, comparisons between predicted and observed results have often failed to provide the necessary level of confidence in prediction models resulting in unacceptably high partial safety factors. The research work reported here was undertaken with the objective of contributing towards the formulation of rational techniques for prediction and design of masonry walls subjected to lateral loads and, in particular, to considering if these are appropriate for thin joint glued masonry.

The current degree of sophistication of numerical modelling of masonry is reaching a state comparable with that used in concrete and steel design. Also with numerical modelling having developed into a mature analytical field, interest is shifting towards development of reliable analytical expressions and procedures that are simple and cheap enough for use in any design office. At present this would suggest the use of spreadsheets for masonry design. Masonry dwellings from before the second world war were designed and constructed using a combination of common sense and 'rules of thumb' without resorting to major structural analysis and design. However, the construction of complex modern structures, which are required to save materials and be environmentally friendly, obviously necessitates formal structural analysis and design procedures. This has, in the past half century, led to the gathering of experimental data and the formulation of mathematical models, with the objective of providing a formal unified design approach for masonry structures. The outcome has been the development of modern design standards based on a mixture of empirical rules, extensive numerical and experimental research, and finite element based analysis. The UK code, BS 5628: Part 1 [BSI, 1992], for example, employs a method of design that is derived from the yield line theory for concrete slabs and adapted empirically to fit a wide range of wall types. And the design method in the previous version of the Australian code, AS 3700 [Standards Australia, 1988], is a modified strip method, and, therefore, utilizes the likely crack lines of the walls under question. Because of the different analytical basis, predicted wall capacities obtained using various codes vary widely. Later in this chapter, these issues are addressed by reviewing research work that has been instrumental in the development of some current code provisions.

## 2.2 FACTORS INFLUENCING LATERAL STRENGTH

### 2.2.1 Introduction

Masonry is a composite material consisting of units and mortar, each of which is a composite material on its own. The bonding of the units to the mortar and the factors influencing its strength are still little understood. The problem is compounded by variations of environmental conditions and workmanship.

In the last 30 years, numerous analytical techniques to predict the failure of masonry panels have been developed. However, considerable differences between the predictions by the analytical techniques still exist. It is apparent, from the available literature, that, these differences are a direct result of several influencing factors and the role that each factor is made to play in a particular analytical technique. Factors that have been employed in most analytical techniques include; material properties, boundary conditions, wall geometry, and the mode of failure of wall panels. In this chapter, the influences of these factors on the out-of-plane behaviour of masonry panels are reviewed. The section starts by examining several suggested failure criteria and a number of observed modes of failure.

### 2.2.2 Failure Criteria

The distribution of moments and the failure criterion of brickwork walls spanning in one direction have been studied by a number of workers [Baker, 1979; Christianen, 1995; Gazzola and Drysdale, 1986; Guggisberg and Thurlimann, 1990; Lourenco, 2000]. When walls span in the vertical direction, failure usually occurs when the tensile bond strength is exceeded at the interface between the units and the bed joints. Sinha's (1994) tests revealed that the moment-curvature relationship is linear until failure, at which point the load capacity immediately drops to nearly zero. For horizontally spanning panels, the overlapping bricks in alternate courses may force the units to fail in tension or horizontal joints to fail in combined torsional shear and tension. For this failure mode, Sinha found that the moment-curvature relationship is linear up to about 80% of the failure load and then becomes non-linear until failure occurs. Sinha's tests suggest that laterally loaded masonry walls in vertical bending behave in a brittle manner, while there is some degree of ductility in the case of horizontal bending. Some researchers [Brooks and Abu Baker, 1998; Christiansen, 1995; Bouzeghoub and Riddington, 1994; Hansen, 2001] have revealed that the flexural strength for failure perpendicular to the bed joints is 2.5 to 4 times larger than the strength for failure parallel to the bed joints.

As the preceding discussion indicates, the behaviour of masonry walls in one direction is relatively simple. The problem gets more complicated when masonry is subjected to bi-axial bending. Relatively little is known about the interaction relationships for biaxial flexural tension. A detailed experimental programme in biaxial bending was carried out by Baker (1979). He reported that, for the case where both moments produce tension on the same face of the specimen, an elliptical interaction exists between the horizontal flexural strength, $f_{ktx}$, and the vertical flexural strength, $f_{kty}$, as shown in Figure 2.1. A sketch of Baker's test set-up is also shown in Fig.2.1. According to Lourenco (2001), however, it is highly debatable that this test set-up will give the flexural strength failure envelope Baker suggests for masonry, and also, because masonry is anisotropic, the principal moments alone are not adequate to fully describe its out-of-plane behaviour. He contends that complete out-of-plane behaviour should include three moment components ($M_{xx}$, $M_{yy}$ and $M_{xy}$), or the principal moments and one angle, $\theta$, which measures the orientation of the principal axes with respect to the material axes. Baker's failure criterion was shown by Lawrence (1983) to under-estimate the failure strength of laterally loaded masonry panels. Several other researchers [Schubert 1994; van der Pluijm et al 1995] performed experiments to gain insight into the problem of bi-axial bending. In most tests, failure has been observed to occur, generally, as a combination of tension and shear in the mortar joints, except for a few cases where cracking through the units has also been observed.

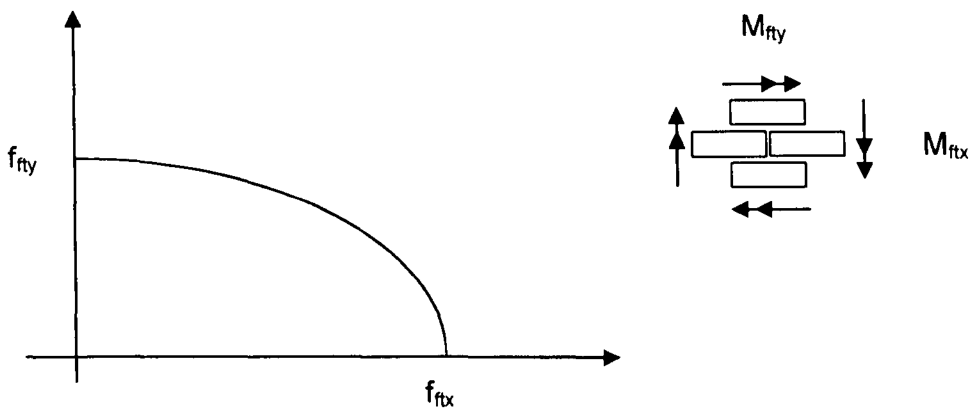


**Figure 2.1**: Failure criteria in biaxial bending according to Baker [Baker, 1979]

More recently, some experimental work into bi-axial bending has been reported by Duarte (2000), who arranged brickwork specimens in the shape of "combed cross-beams", as shown in Figure 2.2. Two types of specimens were built. In the first, all the joints were filled with 1:3 cement mortar, while in the second type only the central part was built in 1:3 mortar, the arms being made with epoxy resin in order to prevent premature failure in shear or bending. The load was manually applied by a hydraulic jack in small increments. Reactions were recorded at each of the four arms, and the lateral deflection near the centre of the cross was measured. Duarte concluded that the failure mode was a combination of shear and tension, and that after cracking there was no evidence of yielding of the material as the bending moments were not kept constant. He also noted that orthogonal material properties are important in predicting the lateral load behaviour of masonry walls by elastic analysis. Duarte observed some reserve of strength in horizontal bending after initial cracking as the load cells kept recording reactions until the failure load, but he associated it with membrane action.

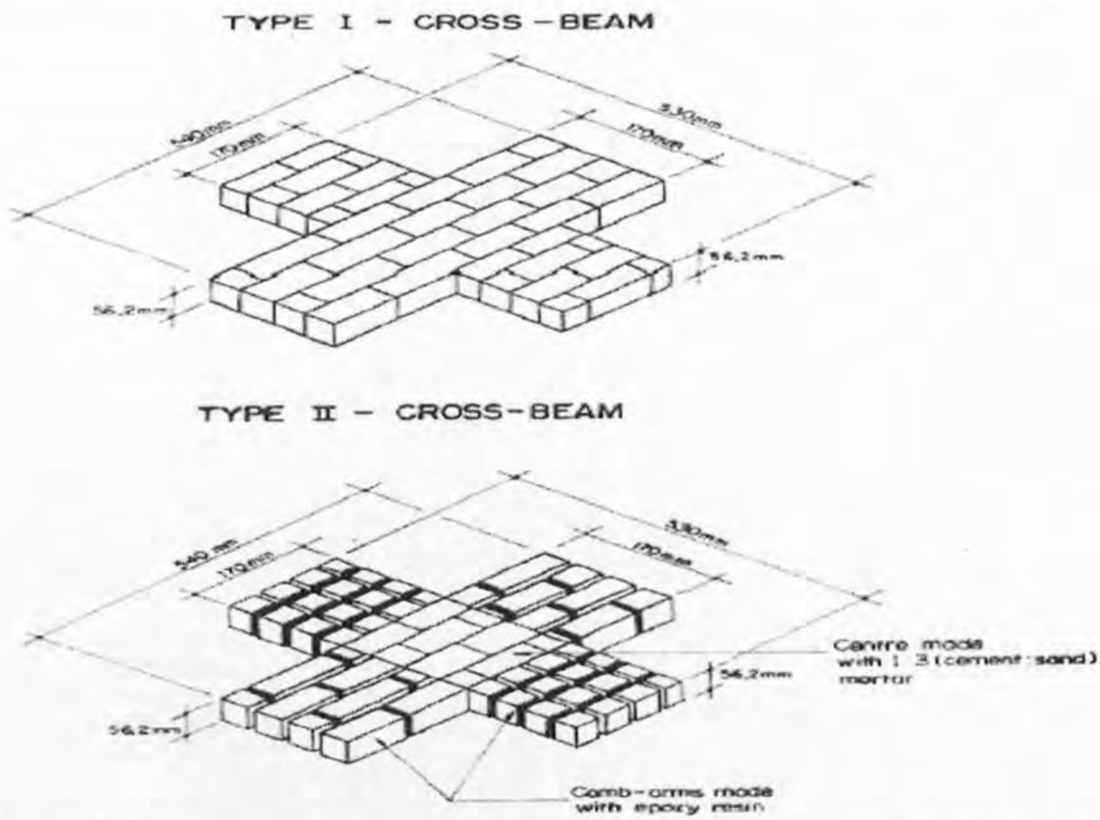


**Figure 2.2**: The "combed cross-beams" specimens used to test bi-axial bending by Duarte (2000).

The literature cited above has attempted to describe masonry failure mechanisms from the experimental viewpoint. Development of constitutive numerical models and then testing them against experimental results offers an alternative approach. Powerful constitutive models for numerical modelling of masonry structures have been developed by Lourenco (1998). Initially, he developed an anisotropic composite model for walls subjected to in-plane loading, which models masonry independently along the two orthogonal material axes, with different strengths and stress-strain diagrams. The model includes a Rankine-type failure criterion in tension and a Hill-type failure criterion in compression. As an extension to the in-plane model, Lourenco (2000) developed an out-of-plane model for masonry plates and shells. Without varying the in-plane response of the model, the modification enabled inclusion of all the six components of the stress and strain tensors. The abilities of both the in- and the out-of-plane models have been demonstrated by comparing their theoretical predictions with experimental results, which have been shown to yield good agreement.

### 2.2.3 Modes of Failure

When loaded to failure, laterally loaded un-reinforced masonry walls are characterised by the formation of fracture lines similar to the yield lines observed in reinforced concrete slabs. In some wall tests performed by Lawrence and Marshall (2000), the following observations regarding the patterns of the cracks have been reported. For panels supported on four sides, it was noted that the first crack was always along a bed joint at approximately the mid-height of the panel. Following the formation of this crack, the upper and lower halves of the panel behaved independently as panels with half the height of the original wall, each with supports on three sides and the top or (in the case of the top half) the bottom free. These observations were also noted by Cajdert and Losberg (1975), Lawrence (1983), Baker (1979), Anderson (1981) and Fried (1989), at various stages in the twenty years prior to Lawrence and Marshall's current test work. For walls with two adjacent sides supported, cracks were observed to develop and radiate approximately from the corner, generally following the mortar joints in a direction dictated by the proportions of the bricks. The diagonal cracks continued until they met a free edge, another crack, or the edge of an opening. When diagonal cracks radiating from the bottom corners intersected, a vertical crack was formed that ran to the top edge of the panel (if it was unsupported) or to the intersection of the opposite diagonal cracks (if the top edge was supported).

Hansen (2001) observed that although failure in the bed joints occurs in the interface between the brick and the mortar joint, it alternates between the brick below and the brick above the mortar. The two failure surfaces are joined by oblique cracks running through the mortar from one surface to another, as shown in Figure 2.3. According to Hansen, it is these oblique cracks which give the bond its strength. On the observed ductility, Hansen argues that it comes from the shear-torsion failure in the bed joints. This ductility vanishes when a very strong mortar is used, due to replacement of the shear-torsion failure by a bending failure in the bricks. He found that the post peak ductility is not dependent on brick and mortar type, but depends on whether or not the bed joints are involved in the failure.

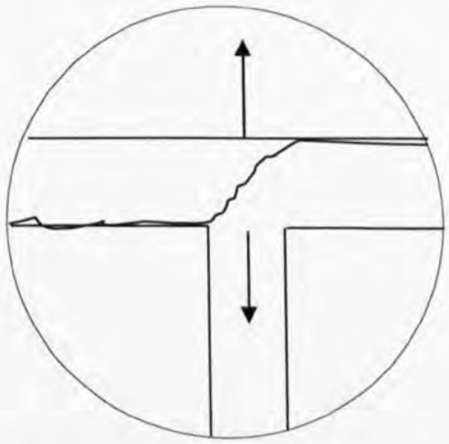

**Figure 2.3**: Alternating interface failure between the brick below and the brick above the mortar, according to Hansen (2001).

Fried (1989) noted that when B-wallettes failed, if the bond was very good, the bond generally occurred along the top of the joint even when perpends entered from above. However, when bond was weaker, the impact of perpends entering the bed joints became evident. Here, the perpend effectively strengthened the bed mortar at the intersection causing de-bonding to alternate between the upper and lower faces of the joint, depending on whether the perpend entered the bed joint from above or below, see Figure 2.4.

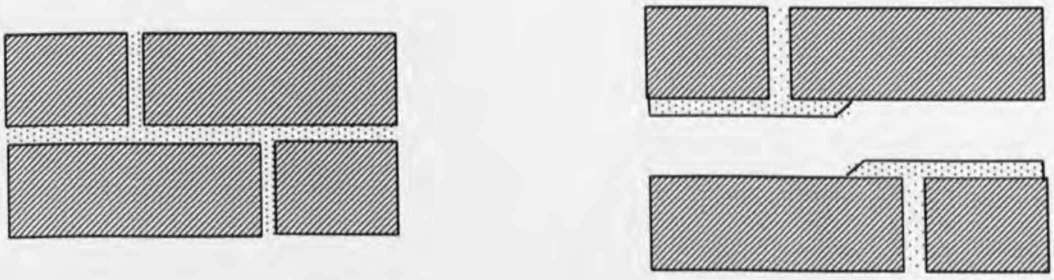

(a) joint before failure

(b) joint after failure

**Figure 2.4**: Alternate de-bonding between upper and lower faces of the joint, according to Fried (1989).

The purpose of analysing failure modes is to enable any relationships between these and the out-of-plane strength properties. It was the resemblance to yield lines in reinforced concrete slabs that prompted the use of yield line theory in masonry subjected to lateral loading in BS 5628: Part 1. The virtual work method applied by Lawrence and Marshall (2000) is also based on the panel failure modes. These points are further discussed in section 2.3.

### 2.2.4 Influence of Material Properties

#### 2.2.4.1 Effects of Material Properties on the Tensile Bond Strength

Tensile bond strength between masonry units and mortar is the most critical factor in determining resistance of non load-bearing masonry walls to lateral loads. Bond strength is influenced by material properties such as: surface texture, water absorption and moisture content of the units; composition, additives, sand grading, air content and water retention of the mortar; and some environmental factors such as dust on the units, temperature, humidity, workmanship and curing conditions. It is not always possible to consider each of these factors separately, hence the effects of all of these parameters on the bond strength are briefly discussed here.

An investigation of flexural bond strength by Lawrence and Page (1994) refers to earlier work by several researchers which showed that the bond is primarily mechanical, and that brick surface characteristics are important. The work describes the bond formation as being the mechanical interlocking of hydration products in the surface pores of the unit. Unit suction rate plays an important role in this bonding process, especially with clay bricks. According to Jung (1988), the suction rate is important in the first few minutes during the transfer of water from mortar to unit. Other workers [Fried and Li, 1994; Grandet, 1973], however, report that unit suction is also important throughout the period until setting of the cement gel is complete. In brick-masonry tests conducted by Christiansen (1995), it was observed that there is an optimum brick suction rate, at which the mortar and unit will form a bond with the highest possible flexural strength. Suction rates below and above the optimum rate result in lower bond strengths.

Cement content of the mortar is another factor that influences the strength of the bond. However, its influence is still not easily quantifiable. It has been reported [Lawrence and Page, 1994] that, while increasing cement content in the mortar increases the mortar cube strength, there is no proof of the same effect on the bond strength. On the other hand, Borchelt and Tann (1996) found that the higher the cement content, the higher the flexural strength of the masonry. It might be argued that this improved masonry flexural strength stems from improved bond strength, which suggests that bond formation, as being the mechanical interlocking of hydration products in the surface pores of the unit, may well be significant.

The water content of the mortar may be more critical than the content of cement. In tests conducted by the author, it was found that a variation of a few percent of the water content alters the flexural strength by a considerable amount. It has been found [Christiansen, 1995] that, for bricks with a high suction rate, slightly altering the water content of the mortar can alter the flexural strength by 200 – 300%. It is further noted that when the suction rate is moderate, the influence of the water content is less important.

The effects of other mortar constituents have also been reported. Results of some experiments [Lawrence and Page, 1994] have shown that the use of air entrainers can reduce strength while overdosing produces a marked reduction in strength. This trend was also corroborated by tests at the University of Newcastle, Australia, after the Newcastle earthquake in December 1989 [Page, 1992]. It has been observed that sands containing a high proportion of fine silica particles result in poor bond between the mortar and the units. According to Lawrence and Page, this is due to clogging of the surface pores of the brick by the fine inert silica particles, thus preventing the effective mechanical interlock to form a strong bond. A comparable argument was alluded to by Wakefield (1996) when he reported on his tests of the effects of mortar on masonry.

The effects of age and curing conditions on bond strength have been reported in the literature, but, as with other parameters, the results are not consistent. Some work [Jung, 1988] has reported a continued increase of strength with age, without, however, revealing the rate of increase of such strength. Anecdotal evidence suggests bond reduces considerably as masonry ages over 5 years.

The above discussion shows that, despite many investigations over recent decades, the present knowledge of the mechanism of bonding and the factors influencing bond strength in given circumstances, is still inadequate. Groot et al (1994) note that, because there are so many factors influencing bond strength, its investigation requires very careful experimental techniques and a broadly based approach.

#### 2.2.4.2 Effects of Material Properties on Masonry Flexural Strength

Laterally loaded masonry panels fail in different modes. Close investigations of the various failure modes reveal that lateral strength is not always governed by the bond failure. In cases where failure involves rupture of the units, the masonry flexural tensile strength will be partly related to some properties of the units. Some of the workers who have investigated these phenomena include Hansen (2001), Fried (1989), Guggisberg and Thurlimann (1990), and Hughes et al (2000).

Hansen (2001) investigated flexural tensile strength and ductility of masonry walls by means of deformation controlled tests. He used five different types of clay bricks and two different mortars. The weaker mortar was an 8:12:17 (cement: lime: sand by weight), with compressive strength of 3.8 N/mm$^2$ and tensile flexural strength of 1.51 N/mm$^2$. The stronger mix with a ratio of 65:35:650 (cement: lime: sand by weight), had a compressive strength of 11.5 N/mm$^2$ and flexural tensile strength of 3.65 N/mm$^2$. The bricks varied in suction rates from 2.0 to 3.2 kg/m$^2$/mm and compressive strengths varied from 26 to 66 N/mm$^2$. Hansen found that strong mortars did not generally produce higher flexural strengths than weak mortars, and in some cases, weak mortars produced higher tensile flexural strengths. Bricks with high suction rates gave the lowest flexural strengths, whether bending about the horizontal or the vertical axes. There was no apparent relationship between the flexural strength and the compressive strength of the brick.

Fried (1989) examined the effects of properties of the units on the flexural strength of brick masonry in the horizontal direction. He considered four different failure modes of wallettes in the horizontal direction. In the first mode, failure was completely through the units, which would occur if the unit modulus of rapture (UMOR) was less than the tensile bond strength between brick and mortar. In two modes, failure was through the perpend joints and straight through the middle of the brick. In these modes, part of the flexural strength would be obtained from the UMOR and part from flexural resistance in the perpend joints. In the fourth mode, failure followed the mortar joints, that is, down the perpend joint, along the bed joint, and then down the perpend joint. In this mode, the horizontal flexural strength was due to the flexural bond strength in the perpend joints and torsional shear strength in the bed joints. By examining these failure mechanisms closely, Fried concluded that the horizontal flexural strength of masonry is related to some combination of UMOR and tensile bond. However, contrary to Hansen's conclusion, no evidence of a universal relationship between horizontal flexural strength and the water absorption of clay bricks was found. It was also noted, however, that in cases where part of the flexural tensile strength is obtained by bond failure within the perpend joints, the strength may be related to the water absorption. Fried refers to other workers who have established a relationship between the water absorption of clay bricks and the tensile bond of masonry that is consistent with the recommendations of BS 5628: Part 1. Their work revealed that bricks with high water absorption rates produce bond of low flexural tensile strength, and visa-versa. Indeed, in yet another study carried out by Fried and Li (1994), this conclusion was substantiated.

### 2.2.5 Boundary Conditions

It is well documented that the nature of supports plays a vital role in the strength of civil engineering structures. Un-reinforced masonry wall panels are no exception. Tests carried out by Lourenco et al (1998) showed that the failure load of wall panels decreases once the number of fixed edges is reduced. However, they also observed that the ductility increases significantly with a reduction of the number of fixed supports.

Analysis undertaken by Schubert (1994) revealed that, in simply supported panels, strength is enhanced when the two vertical edges are changed from simple to fixed supports. He observed that as the aspect ratio decreases, the enhancement of panel strength increases due to the predominant strength being in the horizontal direction. For panels supported on three edges (with differing boundary conditions) but always free along the top edge, it is reported that the effect of a built-in base is greatest at low aspect ratios – defined as height/length. On the same token, the effect of built-in vertical edges is greatest at low aspect ratios when the horizontal direction contributes more to strength.

Much work in the literature [Sinha, 1978; Reeh, 1994; Sjostrand, 1994; Schultz 2000] reveals that boundary conditions of masonry walls subject to out-of-plane behaviour have significant influence on the strength characteristics. This is one area where some consistency of wall behaviour has been observed, the only shortcoming being the inability to quantify the degree of fixity of the edges. Recent work by Sui et al (2006) aims at developing a numerical technique which analyses and updates a panel's stiffness in the vicinity of the boundaries to minimise the error between experimental load capacities and theoretical predictions. Their work recognizes that numerical models often fail to accurately predict strength properties of masonry wall panels due to misrepresentation of the boundary conditions in the models. Thus, the proposed numerical model updates the stiffness of the elements of the panel close to the boundaries, effectively altering the degree of fixity of the panel edge to approach the real conditions. While this research is in the right direction, it fails to demonstrate how the modified stiffness can be applied to panels that have not been physically tested, or how the technique can be employed to predict the stiffness of a panel under design. Clearly, more work still remains to be done regarding the influence of boundary conditions in the theoretical predictions of the behaviour of laterally loaded masonry wall panels.

### 2.2.6 Geometric Properties

For wall panels with similar boundary conditions and built using the same masonry components, it has been observed [Lourenco, 2001] that the response of low aspect ratio panels is slightly less ductile than for panels of larger aspect ratios. Since aspect ratio in these experiments was defined as length/height, the observation about the ductility implies that, as horizontal bending becomes more dominant, masonry panels exhibit some ductility. It can be deduced that the ductility is a result of the torsional shear strength, of the bed joints. When the aspect ratio is defined as above, an enhancement of strength is observed as the aspect ratio increases due to the predominant strength being in the horizontal direction [Schubert, 1994]. Panels with aspect ratio close to one, that is, nearly-square panels, tend to be stronger than rectangular panels due to the effect of two-way internal force distribution being more prominent in square panels.

Failure modes are also influenced by the geometry of masonry panels. At low aspect ratios (when Aspect Ratio is defined as length/height) failure in masonry panels occurs at the mid-height of the panel next to one of the sides, the predominance of strength coming from the vertical direction. As the aspect ratio increases, the position suddenly moves to the centre point of the panel, when the horizontal strength contributes most to panel capacity. Failure occurs at the above mentioned positions when panels have symmetrical boundary conditions, that is, either simply supported all round, fully fixed all round, or opposite sides having similar supports.

In BS 5628: Part 1 (1992), wall thickness is a parameter which affects the flexural strength of concrete blockwork, but as bricks in the UK are all the same, thickness is not of influence in these units.

## 2.3 ANALYTICAL AND NUMERICAL MODELLING

Having taken into consideration all the factors influencing the lateral strength of walls, it would be advantageous if a reliable analytical expression could be developed. In recent decades, several analytical techniques to predict the behaviour of masonry panels have been postulated, and in 1989, Fried investigated the capability of some selected analytical techniques. He found that considerable differences between the predictions existed. Large variations in the predictions come as little surprise since the expressions have been derived using different basic assumptions and approaches, such as; material properties, modes of failure or assumed failure criteria.

Considering several different panels, Hagsten and Nielsen (2000), and Lourenco (2000) identified possible modes of failure for the derivation of the equations governing masonry behaviour. Hagsten and Nielsen's method was based on the masonry failure mechanism that assumed a modified Coulomb yield criterion for both the normal and shear stresses. The masonry was modelled as a rigid-perfectly plastic, three-phase composite, comprising bricks, mortar and the interface between the mortar and the bricks. They formulated an expression of internal energy dissipation in terms of the uni-axial tensile and compressive strengths, and the principal strain increments. Then an expression for the external work was formulated, which was the well known 'force multiplied by displacement'. When these expressions were equated, the solution gave the load-carrying capacity of the wall panel. Some comparisons of the calculated results from the model with test results were made, and good agreement between the two was found.

It is very important to note some adjustments that Hagsten and Nielsen made in formulating their model. Firstly, as mentioned above, the Coulomb friction hypothesis was modified so as to avoid over-estimating the tensile strength. Of more importance, however, were the modifications in the form of "effectiveness factors" that had to be introduced to account for the assumptions of rigid, perfectly plastic material modelling. The workers acknowledge that the assumptions of rigid, perfectly plastic behaviour in masonry are incorrect, and therefore, the effectiveness factors were necessary in their model. Although the factors are not reported in the work referred to, it is reported that they are dependent upon the masonry-unit properties and the type of mortar.

Lourenco (2000) proposed a yield criterion that combined the advantages of plasticity concepts with a representation of anisotropic material behaviour, incorporating different hardening/softening behaviour along each material axis. A curved shell element formulation was used, which makes two basic assumptions: zero shear stresses in the transverse direction and, plane surfaces before deformations remain plane after deformations. The adopted plane stress anisotropic yield criterion included a Hill type criterion for compression and a Rankine-type criterion for tension (the reader is referred to Lourenco (2000) for these formulations). The model was capable of producing different behaviours in the two orthogonal directions, a typical characteristic of masonry behaviour in flexure. The moment-curvature diagrams plotted by Lourenco show that the model performed very well when compared to test results.

Evidence of reasonable predictions using various analytical expressions does exist. However, the major problem is their lack of consistency for any type of wall panel. Fried (1989) carried out a detailed comparison of analytical techniques with regard to their ability to predict lateral behaviour of masonry walls. A total of seven different techniques were considered: three strip methods, a principal stress method, a method based on the elastic plate theory, a modified version of the principal stress method termed 'the normal moment method', and the yield line method, were investigated. The comparisons were in terms of predictions of cracking and ultimate loads of brickwork and blockwork masonry panels. Comparing the results with test values, it was found that some techniques gave reasonable predictions for the ultimate loads, while others gave good predictions for the cracking loads. It was also found that the ability of the techniques to predict the test results depended on the boundary conditions of the walls, as well as on the aspect ratio of the panels. Varying the material properties was also found to have some effect on the relative accuracy of the predictions by various techniques.

Analysis of the literature considered above confirms that derivation of a rational expression is not straight forward but, with good account of the influencing factors, solutions to this problem are possible. It is apparent that most of the influencing factors are known, but the extent of their influence is difficult to quantify. However, given the need for designers to be provided with guidelines for the design of masonry structures, codes of practice of several countries have adopted some of the procedures. The next section reviews some research work that has been instrumental in the development of the methods of design appearing in the British and Australian codes of practice.

## 2.4 DESIGN PROCEDURES

### 2.4.1 Introduction

In the preceding sections of this review, the factors influencing flexural behaviour of masonry walls were discussed. There are two important reasons why gaining an insight into this structural property is important. Firstly, the need to carry out structural analysis of masonry walls and ensure their adequacy to fulfil their intended purpose cannot be over-emphasised. Secondly, it is not enough for a structure to fulfil its intended function in terms of strength, but this has to be achieved economically. This is the purpose of structural design.

Prior to the 1970's limited research work had been carried out in the area of lateral behaviour of masonry, most of which focused on determining experimentally, properties such as the bond strength between the mortar and bricks, and masonry flexural strength, so enabling the orthogonal strength ratio between the major principal directions to be obtained. Very few attempts at predicting lateral load capacity, or formulating flexural design expressions for masonry panels, were made. Fried (1989) refers to The New Zealand Pottery and Ceramics Research Association as being one of the first to publish a design note concerned with lateral loading. In Britain, preliminary guidelines on lateral loading were presented in 1965, and in America the Structural Clay Products Institute produced a lateral design code for Structural Brickwork Masonry in 1969 [Gazzola et al, 1995]]. According to Lawrence and Page (1994), very little guidance on the design of laterally loaded panels was provided by the first Australian Brickwork Code, CA 47 – 1969.

### 2.4.2 BS 5628: Part 1

Research in Britain carried out in the early 1970's by Haseltine, West and Tutt (1977) resulted in a breakthrough in the development of a design method for laterally loaded masonry panels. Their work led directly to the method of design included in the British Code of Practice, BS 5628: Part 1, first published in 1978. Haseltine et al tested a large number of brickwork panels with different support conditions. Most of the walls tested were supported along three edges -- two vertical edges and the base. Based on their work, they published values of flexural strengths along the two major orthogonal directions. Several design theories, including elastic plate theory and yield line method, were examined for a limited range of variables such as aspect ratio, flexural strength, reciprocal of the square of wall length, etc. The result of the work was the proposal of a method of design based on the use of bending moment coefficients obtained from yield line theory. The moment coefficient values are only given for simply supported or continuous edges, with no values for partial restraint. The research work also gave recommendations for partial safety factors for materials and loads, varying according to the degree of construction and manufacturing control.

The application of the yield line theory in the design of brittle masonry panels did not go without criticism. Many researchers [Baker, 1979; Fried, 1989; Haseltine et al, 1978; Lawrence, 1995; Lourenco, 2001; Lovegrove, 1988; Sinha and Ng, 1994; Sinha, 1978] have argued against this and many have carried out tests to investigate the applicability of the method. Most of the work has concluded that the yield line method does produce reasonable results but, still without concrete theoretical basis or rationale as to why it works.

In 1994 Haseltine, de Verkey and Tutt (1994) analysed the results of 20 full-size masonry walls tested at the University of Plymouth and four others tested at British Ceramic Research Limited (BCRL). Their work used yield line theory to predict resistances of the tested walls using characteristic flexural strengths obtained from BS 5628: Part 1 and mean flexural strengths from the wallette results obtained in the test programme. The purpose of the work was to investigate how closely the yield line method of analysis predicted the ultimate resistances. Haseltine et al found that the use of BS 5628: Part 1 values of characteristic flexural strength produced resistances which compare badly with the test pressures. In all the cases that were compared, BS 5628 over-estimated the ultimate resistances of the walls. The resistances calculated using the experimental mean flexural strength values, on the other hand, compared well with the test results. The poor predictions produced by the BS 5628: Part 1 method were attributed to the fact that the characteristic strengths given in the Code were generally higher than the wallette strengths. However, the results were still found to be acceptable because they all fell above the minimum global factor of safety line. As a result, the researchers concluded that the use of the yield line approach for the design of laterally loaded wall panels was justified.

### 2.4.3 AS 3700

Of all the codes of practice in the world, perhaps the Australian code has undergone the most reviews and upgrading. The first ever masonry code, SAA Brickwork Code, CA 47-1969, was published in 1969 and based on British codes of the time [Lawrence and Page, 1994]. According to Lawrence and Page, an amendment concerning lateral load was issued in 1983, and in 1988 a revised Australian Masonry Code, AS 3700 [Standards Australia, 1988], was published. The 1988 code contained an empirical strip method of design for laterally loaded wall panels, where the ultimate load capacity of a wall was considered to be the sum of a vertically spanning strip and a horizontally spanning one. This code was revised ten years later and led to the publication of the 1998 version [Standards Australia, 1998].

The latest version of the Australian Code, AS 3700 (1998), utilizes a virtual work approach that was formulated by Lawrence and Marshall [Lawrence and Marshall, 2000]. The method was postulated from examination of wall cracking patterns and their behaviour, which makes it partly empirical and partly rational. It is now common knowledge that crack patterns in wall panels are influenced by boundary conditions. It is this knowledge of crack patterns that provided the basis upon which a failure mechanism was postulated. Design equations were developed by considering fully cracked panels and visualising a unit deflection of the panel and the resulting rotations along the crack lines. A classical virtual work equation was set-up by equating the incremental crack energy and the work done. The equation could then be solved for the load resisted by the cracked panel.

The major advantages of the method are reported to be its applicability to walls with any support configurations, and to walls with openings for windows and doors. It also deals with walls built using hollow or solid units, whether clay or concrete bricks, without any need for an empirical factor to allow for behavioural differences [Lawrence and Marshall, 2000]. The method has been tested against the published results of a large number of wall tests and is reported to have performed very well and, as a result, has been adapted into the revised Australian Masonry Structures Code, AS 3700 (1998).

## 2.5 SUMMARY

The literature study has reviewed the research activity involving masonry wall panels, particularly those subjected to out of plane loading, during the past five decades. The review commenced with a brief study of the influence of material properties on the strength and behaviour of masonry wall panels, and concluded with an assessment of mathematical concepts that form the basis of design and analysis procedures adopted by some design codes. It has clearly emerged from the review that tensile bond strength between masonry units and mortar is the most critical factor in determining resistance of non load-bearing masonry walls to lateral loads. This masonry property depends on the properties of the individual materials forming the masonry composite. The most important properties of the units include: surface texture, water absorption and moisture content, while for the mortar, the composition, additives, sand grading, air content and water retention are very influential. Some environmental factors such as dust on the units, temperature, humidity, workmanship and curing conditions also affect the strength of bonding in masonry structures. Despite the knowledge of the factors affecting the bond strength, the nature of bonding between the units and the mortar is still little understood. This makes it difficult to quantify the effects of the influencing factors.

The review has revealed that boundary conditions have significant influence on the strength characteristics of laterally loaded masonry walls. However, work is still needed to quantify the degree of fixity of the edges. More work is also needed to explain the nature of the failure patterns. Failure patterns resemble those of reinforced concrete slabs, and this phenomenon has not been adequately explained by the current theoretical knowledge.

Masonry has been used as an empirically designed material for many years. It is only in recent times that a proper formulation of the theory of masonry analysis has developed, leading to development of design codes. These codes now offer rational design rules developed from sound research but also using proven empirical rules. The early codes provided a basis for the design of compression members and were used to design many high-rise buildings from the late 1950s onwards. Guidelines on lateral loading were not included in codes until the 1970s. Masonry codes will continue to evolve as new ideas are tried and proven or discarded.

## 2.6 THIN JOINT MASONRY

### 2.6.1 New Technique

Labour costs are becoming increasingly high while experienced masons are increasingly scarce. As a result, it is expected that the introduction of automation and robotics will be the only way to produce high quality and low budget masonry. This idea has pushed the masonry industry to start up different research projects into alternative building methods for masonry structures. A revolutionary new concept was developed by Ankerplast and The Royal Association of Dutch Brick Manufacturers [Vekemans and Ruben, 2000], resulting from a continuous process of product development which started in 1989 [Martens, 2000]. The company developed the concept now known as thin layer mortar. The main objectives of the research were:

- to improve the labour conditions for the masons
- to develop a low budget building technique
- to enable new structural designs in veneer walls
- to create new architectural opportunities
- to guarantee high quality masonry

The following sections present an evaluation of the extent to which these objectives have been met.

### 2.6.2 Mechanical Properties and Quality Aspects

Using this new technique, high bond and flexural tensile strengths have been reported by several researchers. Valluzzi et al (2002) report compressive strengths up to 40% higher than conventional masonry. Results of tests performed at the laboratory of Ankerplast, at TNO-Bouw (NL), at the Technical University of Eindhoven (NL) and on various construction sites have been summarised by Vekemans and Ruben (2000) as follows:

Compressive strength – greater than 12.5 N/mm$^2$

Flexural bond strength – greater than 4.5 N/mm$^2$

Tensile bond strength – after 24 hrs – greater than 0.2 N/mm$^2$

– after 28 hrs – greater than 0.6 N/mm$^2$

These values provide some insight into the strength of thin layer mortar masonry.

Tests on thin-jointed Autoclaved Aerated Concrete (AAC) panels conducted by Ahmed (2005) at Kingston University laboratories showed a significant improvement of thermal and acoustic properties. The improvement of thermal performance is no surprise since in conventionally constructed AAC walls, most of the heat is lost through the mortar joints. Considering water penetration issues, Fudge (2000) contends that by varying the sequence of cavity-wall building when using thin layer mortar, the problem of trapped mortar on the cavity wall ties can be reduced. He maintains that this can in turn reduce the incidence of rain penetration through poorly constructed cavity walls. High water retentivity of thin layer mortar has been reported by Martens (2000), who contends that this diminishes the risk of efflorescence and growth of moss on the surface of the masonry.

The high durability of masonry is unquestionable. This is also valid for thin layer mortar masonry since the most vulnerable component, that is, the mortar, is thinner and has a higher quality than the traditional mortar. With regard to sustainable development, thin layer mortar masonry presents good prospects since it can be recycled as course aggregate for concrete, only possible because thin layer mortar masonry has a high and reliable compressive strength.

### 2.6.3 Labour Conditions

When thin layer mortar systems were applied in construction of brick facades, higher tensile bond strengths suggested new structural possibilities, not available with brick masonry using normal mortar. The high tensile strengths of this masonry enabled the prefabrication of veneer walls, which initiated an exploration of possible ways to create larger components. Vekemans and Ruben (2000) report on several initial projects that have been completed using prefabricated veneer walls of sizes reaching 7 metres in length, 2.65 metres high and only 100mm thick. These projects include a small electricity sub-station, which already existed and only needed a new façade, and two facades for a cable television building in Zoetermeer. It is reported that on completion the products did not look much different from a traditional brick façade. The biggest advantage is that these walls were constructed at floor level in a factory, which was very convenient for the bricklayers. Another significant improvement of the labour conditions for masons comes from the use of a mortar pump, which avoids repetitive action of taking up and laying down the bricks and the mortar.

### 2.6.4 Architectural Aspects

Because of the increased tensile and flexural bond strength that can be achieved in a thin layer mortar system, it is possible to achieve more radical structures, which are not possible using traditional construction methods. In addition, by utilising much thinner joints on both bed and header joints, it is possible to create a completely new appearance using bricks. Martens (2000), for example, suggests new masonry patterns being made by laying clay bricks with a frog on their side. Also, due to the high flexural strength of thin layer mortar masonry, it is possible to achieve thinner veneer walls, and large window openings can be spanned without steel or concrete lintels. The use of thin layer mortar masonry presents opportunities for new and exciting architectural designs.

### 2.6.5 Economy

Due to the fact that thin layer mortar masonry is a relatively new technique, interest so far has been focused on the set-up of proper systems for laying the thin joints and in the selection of the constituent materials in order to optimise the total performance of the masonry. As a result, costs are temporarily high. Once the systems are established, considerable savings in costs may be expected due to the following factors:

- increased speed of the build process
- reduction in the quantity of mortar
- reduction, or total elimination, of bed joint reinforcement
- increased scale of use

No evidence in the literature of a study focusing on the costs of thin layer masonry construction as compared to conventional masonry has been found. Since economic issues will always play a major role in construction, it is essential that such assessment be done. Nevertheless, it is evident [Ahmed, 2005; Fudge, 2000; Martens, 2000; Valluzzi et al, 2002; Vekemans and Ruben, 2000] that in the past few years, thin layer mortar masonry has become more widely used in several countries.

### 2.6.6 Design Aspects

The use of dense concrete blocks laid in thin joint mortar represents one of the most promising construction systems for load-bearing masonry walls, due to their enhanced mechanical properties. However, most research has so far focussed on exploiting these enhanced properties in the prefabrication of masonry units made with bricks and thin layer mortars [Adell, 2000; Vekemans and Ruben, 2000]. While some evidence exists [Valluzzi et al, 2002; Jabbar et al, 2006] of research carried out on thin jointed dense concrete-block masonry, this only deals with in-plane behaviour. The question of out-of plane behaviour was addressed by Adell (2000) when he tested a series of brick wall panels in four-point bending. Adell's work, however, did not deal with design issues, but only studied the crack patterns of the failed panels and recorded the failure loads and strains. Design issues are addressed by Martens (2000), who proposes a design procedure for brick masonry lintels based on elastic theory. He also demonstrates a practical design procedure for bed-joint reinforcement, which is necessary only as a safety means to guard against brittle failure. In fact, most of the studies conducted so far have found that thin jointed masonry behaves linearly and is highly brittle. Another significant finding has been the low scatter of experimental data as compared to conventional masonry. Consistency of test results is invaluable both in development of prediction models and in the setting of partial safety factors.

**2.6.7 Current Applications of Thin-Layer Concrete-Block Masonry**

Thin layer masonry has been in use for several years in different countries, particularly in Continental Europe [Martens, 2000], where masonry units of calcium silicate and autoclaved aerated concrete (AAC) are frequently used. In the UK, the market for thin layer masonry has been limited to Aircrete. The publication of a report from a Government Task Force [Department of the Environment, 1998], aimed at rethinking construction in the UK, helped to stimulate change in the industry [Fudge, 2000]. The motive behind 'rethinking construction' was the shortage of skilled labour for construction work, coupled with the growing need to improve the energy use in buildings. New methods of construction were investigated, including the types of solution that were being offered elsewhere. Prefabrication using thin-layer mortars, with as much off-site work as possible, offered a practical solution to the skills shortage of masons. For energy savings, thin layer mortar construction in combination with Aircrete blocks, which already accounted for some 70% of the inner leave of external cavity walling in the UK housing market [Fudge, 2000], provided the best possible solution. In the early stages of thin layer mortar construction, applications used materials that could be handled manually on site. Until very recently, thin layer mortar construction in the UK has been associated only with Aircrete blocks and very limited prefabrication using standard-size bricks.

Dense concrete blocks joined using thin layer mortar represents a promising construction system for load-bearing and non load-bearing masonry walls. Due to its advantages over conventional masonry, the system could be used for a wide range of applications in both domestic and commercial situations. The enhanced moisture and frost resistant properties of thin-jointed concrete blockwork make it ideal for the construction of the inner and outer leaves of external cavity walls. The combination of higher strength and reduced sound transmittance properties makes the masonry suitable for single leave internal partition walls as well as solid external walls. The ease of execution in comparison with the conventional system ensures that panels are constructed quickly and cost-effectively. All types of internal and external finishes can easily be applied.

### 2.6.8 Potential Future Uses for Thin-Layer Blockwork Masonry

Basement Construction

Basements offer high standards of thermal performance, hence addressing the key environmental need to reduce the consumption of non-reusable energy sources. An assessment of potential basement usage in the UK by Tovey (1999) perceives basements as an excellent way of increasing space of a house within the same plot, as well as providing financial efficiency in areas of high land costs. In 1999, Roberts et al (1999), after realising that a design document published by the British Cement Association in 1997 excluded unreinforced masonry walls [Fried et al, 2002], published design guidance on unreinforced masonry basements. Their guidance provides a detailed method of design for typical UK dwelling construction. The method is a refinement of analytical techniques that already existed before, but are not economical for use with plain masonry because they give unrealistically thick wall sections [Roberts et al, 2002]. It is contended [Fried, 2005] that by refining the underlying design assumptions which form the basis of EC6, a 20% improvement in the performance of unreinforced conventional masonry can be achieved. Further, it is stated that it is unlikely to gain any more design economy for plain masonry walls by further refinement of the design assumptions for the masonry. Thin jointed concrete-block masonry could, however, provide additional improvements. With flexural tensile strengths of up to three times that of conventional masonry, thinner wall sections for basements can be achieved.

Prefabrication

The enhanced tensile bond strength of thin joint masonry is a great advantage for prefabrication applications. House builders constructing repeats of dwellings will find prefabrication of block walls a cost effective option. It doesn't require extensive deployment of site labour and avoids the volume of loose materials required for traditional masonry construction and their inherent handling problems. Prefabrication can be quality controlled giving a high standard of workmanship in factory conditions. It reduces potential for accidents and addresses on-site skill shortage. Building using prefabricated masonry elements constructed with thin layer mortar and standard-size bricks occurs in Holland, Belgium and Germany – the potential market gain with solid dense concrete blocks is more promising.

Public Sector Buildings

Fair-faced blockwork constructed using thin joints can be used in corridors in schools, hospitals, prisons and similar buildings. The advantages of fair-faced dense concrete blockwork are that it can be coloured during manufacture and requires no decoration after construction. The robustness of dense concrete blockwork deters graffiti and vandalism, hence the finish would require little maintenance.

### 2.6.9 Summary

The review in Section 2.6 above gives an account of the general research work that has been carried out on thin joint mortar masonry to date. Three important points have been identified as being most relevant to the current study.

Firstly, thin layer masonry is currently widely used in industry in association with Aircrete blocks to improve walls' thermal resistance but the technology, particularly in the UK, is rarely associated with solid dense concrete blocks or brickwork.

Secondly, the nature of the mortar and constituents of the material forming the block significantly enhance bond strength to the point where, in many instances, it exceeds block unit modulus of rupture (UMOR). For that reason, wall panels formed using thin joint masonry have lateral capacities dependant on the UMOR, not the tensile bond strength of the joint. Consequently, load capacity of walls built using thin joint technology in conjunction with solid dense concrete blocks or bricks with high UMOR's will be considerably higher than if the walls had been built using conventional mortar.

Lastly, in addition to enhanced mechanical properties, thin joint mortar masonry can provide designers with an improved degree of confidence in their design as compared to conventional masonry. Physical tests on wall panels constructed using thin joint technology have produced results with less scatter than experimental data obtained from conventional masonry tests. The variability of strength properties between identical panels is not as large as in conventional masonry. Hence, it may be feasible to reduce partial safety factors for materials when using thin joint mortar.

## 2.7 CONCLUSIONS

It can be concluded, based on the works that have been reviewed here, that:

- Tensile bond strength between masonry units and the mortar is the most critical factor in the flexural strength of non load-bearing masonry walls. Bond strength is influenced by several factors, such as material properties, boundary conditions, geometric properties, environmental factors and workmanship. A method of design, therefore, has to involve each of these factors in one way or another. However, different methods of obtaining the material properties of masonry from country to country mean that the outcome from the prediction models will vary accordingly, and analytical techniques will require factors which account for these differences.

- The literature implies that laterally loaded masonry walls in vertical bending behave in a brittle manner, while there is some degree of ductility in the case of horizontal bending. Theoretical knowledge is not able to adequately explain this observed ductility.

- Most of the factors influencing the lateral behaviour of masonry walls are known, but quantifying their effects is still a major stumbling block.

- Several analytical models to predict the flexural strength of masonry walls exist, but there is still large variability in the predictions. These variations render the models unreliable, and hence, make it very difficult to extend the application of these models into new areas.

- Much work still remains to be done in the area of lateral behaviour of masonry panels, and because of the many variables involved, future investigations require very carefully planned experimental techniques, which should, if possible, include some form of standardisation.

- The thin-joint system has great potential to revolutionize the building process, resulting in massive cost savings. The inherent speed of build enables quicker construction times, excellent thermal efficiency, reduced wastage of blocks and mortar, and a potentially cleaner site.

## 2.8 RECOMMENDATIONS

For conventional masonry, it is recommended that the testing procedures be standardised to eliminate the variations of results obtained by different workers at different places. Standardisation could be achieved by specifying basic flexural tests to evaluate the flexural bond strength and other bending properties. Because of the large variability of conventional masonry, it is often necessary to conduct tests on a number of equivalent sets of specimens built using the same materials. It is, therefore, essential to give guidance on the number of tests required in order to draw meaningful comparisons between sets of results. As an alternative, the relationship between different test methods could be established.

Finally, because they give inconsistent results, the methods of design contained in current codes of practice should be used with great care until more rational and dependable techniques are found.

# CHAPTER 3: EVALUATION OF ANALYTICAL METHODS

## 3.1 INTRODUCTION

Traditional structural analysis that has evolved from the work of Hooke was based on analytical solutions using elastic analysis [Hill, 1949]. In the last century, this approach has been altered in several ways. Firstly, plastic analysis was developed and secondly, with the advent of modern computers, numerical methods have been applied, in particular finite element analysis. Plastic analysis allows for the fact that at high stresses most materials become plastic, and consequently no longer behave linearly. Since at these higher stresses the structure is not behaving elastically, an elastic method of analysis is no longer valid and is, therefore, not a true indication of the distribution of moments in the structure.

Analytical techniques have been applied to masonry structures comparatively recently and are based on methods developed for elastic-plastic homogeneous materials, which are mostly metals. The theories were subsequently extended to cover other materials that exhibit limited elastic-plastic behaviour, such as reinforced concrete and timber. For example, Strip (elastic approach) and Yield Line (plastic approach) methods have found much success in the analysis of reinforced concrete plate structures such as slabs.

Although the use of structural analysis concepts in masonry is still in its infancy, it benefits from well established theories that have been successfully applied to other materials for over a century. Further, in recent decades, masonry researchers have gathered much evidence to suggest that masonry possesses properties comparable to those of other engineering materials, and hence, it should be possible to predict its behaviour using existing analytical and numerical models. In this chapter, some of the well established analytical techniques including Linear Plate theory, Yield Line method, and Strip methods, are employed to analyse laterally loaded masonry wall panels. Also considered is the Fracture Line theory, as well as numerical analysis using Finite Elements. Results from tests performed by other researchers in the past, and results obtained by the author, are used to compare the ability of these theories to accurately predict experimental data.

### 3.2 THE NEED FOR DESIGN FORMULAE

Throughout much of the early half of the last century, structural masonry was not treated as an engineered material in the same sense as steel, concrete and timber were. Rule of thumb procedures were applied for masonry construction, which resulted in excessively thick walls with consequent cost penalties and wastage of space within buildings. Haseltine et al (1977) note that, with the massive walls, the ability to resist such small loads as wind was never in question. As walls became thinner, and lower strength materials such as aerated concrete blocks were introduced, the need to carry out structural calculations could no-longer be avoided. Furthermore, it has been observed [Haseltine et al, 1977] that the narrowing of walls and the introduction of lower strength materials were accompanied by an increase in the pressure used to represent the effect of wind in design, i.e. the loads increased as the walls became more slender.

A new design theory should not be considered simply because of its novelty value but because it can explain, on the basis of sound physical principles, many old and successful design rules which are of an empirical nature [Davies, 1988]. It should also provide guidance for the design of unusual and innovative structures for which not even empirical design rules are available. This will give a designer the confidence to introduce bold and innovative designs, and to utilize new high-performance masonry materials. Designers, however, have to work within the rules embodied in the various national and international Codes of practice for the design of masonry structures. The committees charged with the revision and improvement of Codes will only include new design theories developed for masonry structures in the revised codes if they make a genuine improvement to the design rules. This research aims to address this issue.

### 3.3 EXISTING THEORIES

There are a number of theories on which prediction of lateral loading capacities of masonry walls can be based, these include: (a) elastic plate methods, (b) yield line theory, (c) finite elements, (d) strip method, and (e) fracture line theory. Analyses using these methods give quite different results when compared with experimental data, thus prompting researchers to focus on finding new techniques, or a rationale for existing methods. While there is some indication that each of these theories does give reasonable results under certain conditions, the results appear random and dependant on the specific testing programme undertaken. That is to say, there is no consistent evidence, so far, linking theory with all types of masonry walls. Consistent results only occur over specific sectors of the subject.

In the following sub-sections of this chapter, a selected number of the methods of analysis that were used to predict test findings are described. The results are presented in tabular and graphical forms, which are followed by discussion of the differences and similarities of the methods.

### 3.3.1 Elastic Plate Theory

Elastic plate theory would appear to be the most promising analytical technique since, in most of the tests recorded in literature, the load-deformation relationship for laterally loaded panels in the working range is nearly linear, as represented by the line OA in Figure 3.1. Allowance for the orthotropic properties of brickwork can also be made without any difficulty.

The European code, [Eurocode 6, 1996], in its design procedure, allows designers to choose between using the moment coefficients derived by the yield-line method and others. The moment coefficients shown in Table A3.1 (Appendix 3) were calculated using plate-bending equations derived by Timoshenko (1959), and are used to predict the lateral load capacity of walls presented in Table 3.1.

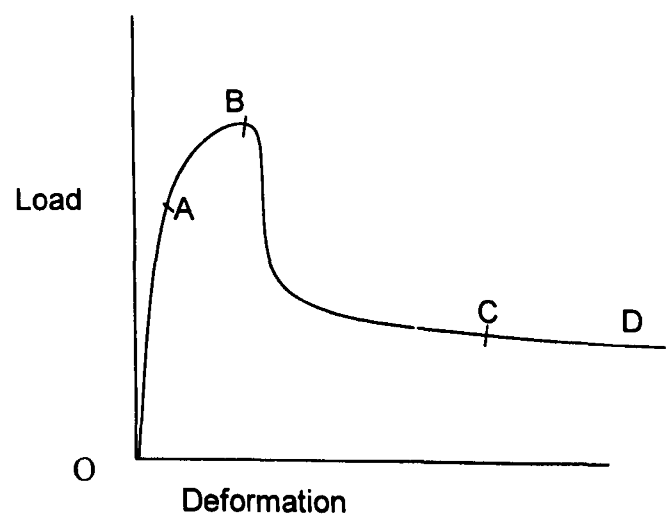


**Figure 3.1**: Typical Load-Deformation response of laterally loaded masonry panels for tension in the direction parallel to the bed joints.

### 3.3.2 Yield Line Theory

Yield line theory was developed for use with reinforced concrete, and assumes that the bending moment along a line or lines reaches a yield value, and stays constant until all parts of the line reach that yield value. Thus, a pattern of yield lines develops with constant moment along each line, when failure occurs. It has been argued by several researchers [Christiansen, 1995; Duarte, 1998; Fried, 1989; Lawrence, 1983; Lourenco, 2201; Sinha, 1977; Sinha, 1994] that, with masonry, this is theoretically unsound as it assumes the existence of plastic hinges which cannot exist in a brittle material. However, most Load-Deformation diagrams for laterally loaded masonry walls show a linear relationship at low values of applied stress, as shown in Figure 3.1 (region OA), and a moderate strain hardening behaviour prior to the attainment of the ultimate tensile capacity (region AB in Figure 3.1). Because of this shape of the Load-Deformation diagram, there is some justification in the application of an ultimate-load analysis concept for prediction of the tensile capacity.

The method of design of unreinforced masonry panels given in the British Code of practice, BS 5628: Part 1, is based on the yield line theory. In this chapter, yield line equations derived from energy principles considering panel mechanisms were used to calculate the failure loads. The yield line equations are presented in Appendix 1(b), and the failure loads determined by these equations are listed under the appropriate column of Table 3.1.

### 3.3.3 Finite Elements

Finite Element Analysis has been applied by many researchers [Page, 1978; Bouzeghoub and Reddington, 1994; Ghosh et al, 1994; Pande et al, 1994; Lourenco, 1997; Lange-Kornbak, 2000] to simulate the behaviour of masonry structures, and has often produced very good results when compared with experiments. The method is suitable for the prediction of failure loads, as well as stress distributions in the working stress range. Page (1978) used the method to investigate stress distributions in masonry walls and found that it was able to reproduce these with good accuracy. It was demonstrated, by Bouzeghoub and Reddington (1994), that there is no need to use 3-D finite elements since simpler 2-D elements are adequate to simulate the behaviour of masonry structures.

Although the finite element method is a good analysis tool, its biggest drawback is the effort and time it takes to idealise the structure, input the data and, interpret the results. As a result, the method is not suitable for design purposes. Designers need a simple analysis to make quick estimations of wall strength. Nevertheless, finite element analysis is invaluable in research applications.

In this research, a commercial finite element analysis package called ANSYS [ANSYS Inc., 2003] was used to predict the lateral load capacity of walls. A failure criterion was devised by the author, which utilises the properties of the walls obtained from tests. The predicted failure loads were determined from a combination of the actual properties obtained from tests and the results of a finite element stress analysis run, in which the wall model was loaded with a unit load. Each wall was modelled as a composite of two materials, that is, units and mortar, and discretized with eight-noded shell elements. Isotropic, linear elastic material properties were assigned to the elements, and these are summarised in Table 3.2. These values are approximately equal to the average values obtained from tests and recorded in [Lawrence, 1983]. A representation of the finite element mesh used in the analysis is shown in Figure 3.2. The predicted failure loads are listed in Table A3.2 (Appendix A3) and are also displayed in the appropriate column in Table 3.1.

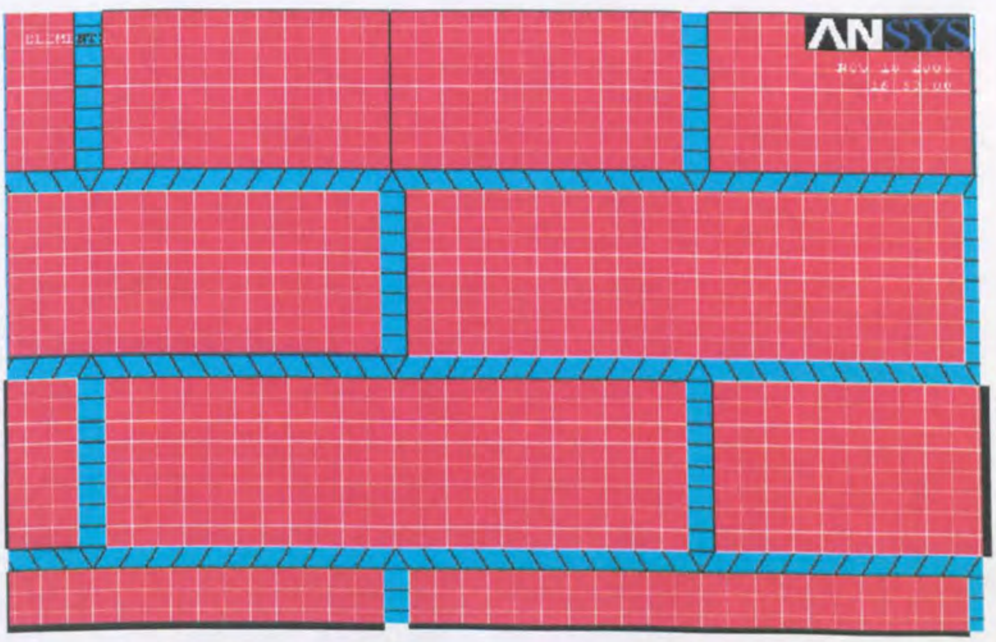


**Figure 3.2**: Finite Element mesh showing quadrilateral and triangular elements used to model the walls – courtesy of ANSYS Inc.

**Table 3.2**: Material properties for finite element modelling

| Masonry Constituent | Elastic modulus ($N/mm^2$) | Poisson's ratio |
|---|---|---|
| Block | $E_b$ = 22 000 | 0.15 |
| Mortar | $E_m$ = 6 000 | 0.125 |

**Table 3.1:** Theoretical and Experimental Failure Loads of Panels

| | | | Wall Dimensions | | | Predicted Failure Load, Wk (kPa) | | | | | Tests (Lawrence) (kPa) | | |
|---|---|---|---|---|---|---|---|---|---|---|---|---|---|
| Test no. | B.C. | fkx | H | t | L | YL | Elastic | Strip | Fract. Line | F.E. | Initial crack | Full crack | Ulti. Load |
| 8 | 1 | 1.96 | 3 | 0.11 | 6 | 4.57 | 2.37 | 4.07 | 2.79 | 2.30 | 1.6 | 3.0 | 3.2 |
| 12 | 1 | 1.93 | 2.5 | 0.112 | 2.5 | 10.58 | 13.48 | 7.33 | 8.05 | 6.96 | 7.6 | 8.6 | 8.6 |
| 18 | 1 | 2.06 | 2.5 | 0.109 | 3.75 | 6.75 | 5.82 | 6.13 | 4.33 | 3.63 | 2.9 | 4.9 | 4.9 |
| 22 | 1 | 1.98 | 2.5 | 0.111 | 5 | 5.61 | 3.51 | 5.84 | 3.62 | 2.54 | 3.1 | 4.7 | 4.7 |
| 27 | 1 | 1.93 | 2.5 | 0.109 | 6 | 5.90 | 2.47 | 5.61 | 3.73 | 3.92 | 1.9 | 3.1 | 3.1 |
| 32 | 1 | 2.33 | 3 | 0.109 | 6 | 5.88 | 2.76 | 4.88 | 3.95 | 3.26 | 1.7 | 3.5 | 3.5 |
| 6 | 2 | 1.93 | 3 | 0.11 | 6 | 10.81 | 6.84 | 6.24 | | 3.45 | 1.9 | 4.4 | 8.0 |
| 7 | 2 | 1.46 | 3 | 0.11 | 6 | 7.44 | 5.18 | 4.61 | | 3.02 | 2.3 | 4.4 | 8.1 |
| 13 | 2 | 2.08 | 2.5 | 0.112 | 2.5 | 23.19 | 30.12 | 11.80 | | 5.09 | 9.1 | 9.1 | 12.1 |
| 20 | 2 | 1.9 | 2.5 | 0.109 | 3.75 | 12.74 | 13.18 | 8.56 | | 3.05 | 3.6 | 5.2 | 11.6 |
| 23 | 2 | 2.22 | 2.5 | 0.111 | 5 | 12.16 | 11.54 | 9.95 | | 3.90 | 2.9 | 5.5 | 9.9 |
| 31 | 2 | 1.29 | 2.5 | 0.109 | 6 | 8.87 | 5.68 | 5.56 | | 5.38 | 1.8 | 4.2 | 6.9 |
| 33 | 2 | 1.87 | 3 | 0.109 | 6 | 10.83 | 6.51 | 6.12 | | 4.01 | 1.6 | 3.3 | 4.7 |
| 37 | 2 | 1.19 | 2.5 | 0.109 | 2.5 | 18.39 | 16.32 | 9.28 | | 6.23 | 9.0 | 10.7 | 24.0 |
| 9 | 3 | 2.32 | 3 | 0.112 | 6 | 6.12 | 9.49 | 5.05 | 8.17 | 1.24 | 1.6 | 2.5 | 5.5 |
| 14 | 3 | 2.06 | 2.5 | 0.112 | 2.5 | 19.41 | 28.24 | 9.81 | 19.08 | 8.33 | 11.3 | 11.3 | 20.0 |
| 19 | 3 | 1.76 | 2.5 | 0.109 | 3.75 | 8.85 | 13.85 | 5.75 | 9.94 | 4.57 | 4.3 | 4.8 | 6.7 |
| 24 | 3 | 2.56 | 2.5 | 0.111 | 5 | 10.01 | 14.81 | 8.02 | 12.94 | 4.14 | 2.9 | 5.0 | 6.4 |
| 30 | 3 | 1.35 | 2.5 | 0.109 | 6 | 4.95 | 5.94 | 4.05 | 6.49 | 2.94 | 2.3 | 4.7 | 4.7 |
| 34 | 3 | 1.77 | 3 | 0.109 | 6 | 6.95 | 6.86 | 4.28 | 7.92 | 2.75 | 2.2 | 3.0 | 3.9 |
| 38 | 3 | 1.37 | 2.5 | 0.109 | 2.5 | 14.18 | 17.79 | 7.81 | 17.99 | 5.54 | 9.0 | 9.0 | 18.8 |
| 16 | 4 | 2.17 | 2.5 | 0.109 | 2.5 | 13.95 | 7.07 | 4.15 | | 6.79 | 8.0 | 8.0 | 14.0 |
| 21 | 4 | 1.87 | 2.5 | 0.109 | 3.75 | 6.35 | 4.72 | 2.64 | | 2.63 | 3.6 | 3.9 | 4.0 |
| 25 | 4 | 2.09 | 2.5 | 0.111 | 5 | 4.90 | 5.86 | 2.51 | | 1.63 | 2.6 | 2.6 | 3.9 |
| 29 | 4 | 1.31 | 2.5 | 0.109 | 6 | 2.40 | 3.88 | 1.46 | | 0.74 | 2.4 | 2.4 | 3.5 |
| 35 | 4 | 1.79 | 3 | 0.109 | 6 | 3.14 | 3.36 | 1.69 | | 0.96 | 1.7 | 1.7 | 2.5 |
| 10 | 5 | 2.1 | 3 | 0.112 | 6 | 3.93 | 5.54 | 1.37 | | 1.72 | 1.7 | 1.7 | 1.7 |
| 15 | 5 | 2.09 | 2.5 | 0.112 | 2.5 | 8.42 | 17.93 | 4.15 | | 6.06 | 7.8 | 7.8 | 7.8 |
| 17 | 5 | 1.93 | 2.5 | 0.109 | 3.75 | 4.06 | 9.06 | 2.20 | | 3.74 | 3.4 | 3.4 | 3.4 |
| 26 | 5 | 1.99 | 2.5 | 0.111 | 5 | 2.92 | 7.43 | 1.96 | | 2.35 | 2.7 | 2.7 | 2.7 |
| 28 | 5 | 1.17 | 2.5 | 0.109 | 6 | 1.50 | 2.93 | 1.12 | | 1.25 | 2.3 | 2.3 | 2.3 |
| 36 | 5 | 1.36 | 3 | 0.109 | 6 | 1.59 | 3.40 | 1.14 | | 1.11 | 1.9 | 1.9 | 1.9 |

| Boundary categories (B.C.): | |
|---|---|
| 1 = all sides simply supported | H - Wall height |
| 2 = all sides built-in | t - wall thickness |
| 3 = simply supported top and bottom, built-in sides | L - length of wall |
| 4 = simply supported bottom, free top, built-in sides | |
| 5 = simply supported bottom and sides, free top | $f_{kx}$ – flexural tensile strength parallel to bed joints. |

### 3.3.4 Fracture Line Theory

The Fracture line method was proposed, and applied, by Sinha (1977) for the design of masonry wall panels resisting lateral loads [Hendry, 1981]. In this method, it is proposed that the variation of Young's modulus with direction should be taken into account, and that all deformations take place along the fracture lines only. Besides including stiffness orthotropy, the method does not differ much from yield line theory, since the resulting equilibrium equations are based on the cracked pattern of the wall, with assumed ultimate (constant) moments along the fracture lines. The assumed collapse mechanism is similar to that in the yield line theory but, since full plastic behaviour is not assumed, the failure regions are called fracture lines. As with the yield line method, it assumes that the individual parts of the failed panel rotate as rigid bodies, and the equations of equilibrium are derived from energy principles.

To the best of the author's knowledge, fracture line method is not incorporated in any code of practice, but it has been applied by several researchers, amongst them Sinha (1994) and Duarte (1998), for the prediction of failure pressures of panels with irregular shapes and panels with openings, with good agreement to test data. The coefficients in Table A3.1, which were later used to determine strengths of the walls in Table 3.1, were calculated from the equations in Appendix 1(c). The reader is referred to Sinha (1978) for the derivation and discussion of these formulae.

### 3.3.5 Strip Method

Consider the equation of equilibrium for a slab element, equation 3.1 below.

$$\frac{\partial^2 m_x}{\partial x^2} - \frac{2\partial^2 m_{xy}}{\partial x \partial y} + \frac{\partial^2 m_y}{\partial y^2} = -q \tag{3.1}$$

Where $x$ and $y$ are rectangular axes in the plane of the slab, $m_x$ and $m_y$ are the bending moments per unit width in the $x$- and $y$-directions, $m_{xy}$ is the torsional moment per unit width, and q the uniformly distributed load per unit area acting on the element. Equation (3.1) applies whether the slab is in the elastic or plastic range. The load $q$ on the right hand side can be arbitrarily apportioned between the terms on the left hand side. That is, the load can be carried by any combination of slab bending and/or twisting in the two directions. If the condition $m_{xy} = 0$ is chosen, the load will be carried entirely by the bending terms, that is, twist-free moment fields will result. This condition forms the basis of the strip method, thereby splitting the load into parts which are carried by an individual system of strips, designed as beams running in perpendicular directions.

Any combination of the moment fields, $m_x$ and $m_y$, that satisfies equation (3.1), the boundary conditions and the yield criterion, gives a valid lower bound solution. However, moments in proportions reasonably close to the distribution given by elastic theory are usually allocated. In cases where support conditions of the slab preserve the concept of strip method by providing twist-less strips, a good solution of the moment field within the slab will be obtained. However, in cases where the existence of twisting moments cannot be avoided, for example, panels supported on columns, a rather conservative solution can be expected.

The strip method was used by Lawrence (1983) to predict failure pressures for wall panels, and was found to give good agreement with experimental failure pressures. The method has also been incorporated [Lawrence and Page, 1994] into the 1988 version of the Australian code of practice, AS 3700 [Standards Australia, 1988].

The values in Table 3.1 were determined using Strip Method equations presented in Appendix 1(d). The equations were derived from equilibrium principles, in which the requirements of the Lower Bound Theorem were satisfied.

## 3.4 ANALYSIS OF RESULTS

The theories discussed above have been employed to predict the results of a series of wall panel tests that were carried out by Lawrence (1983). The panels used clay bricks laid in a 1:1:6 mortar (cement : lime : sand, by volume). Table 3.1 shows failure loads of the wall panels as predicted by the different theories, as well as the experimental results recorded during the testing programme. Three different failure stages were recorded during testing: the load at initial cracking; the load at the development of a full-crack pattern; and the ultimate failure load. The results are shown graphically in Figures 3.3 to 3.11.

### 3.4.1 General Performance of the Theoretical Techniques

In Figures 3.3(a) – (e), the failure loads of the panels as predicted using the theories above are compared to the experimental failure values. Figure 3.3(a) compares the results of the tests to the values predicted by elastic plate theory. It is apparent that elastic theory over-estimated the strengths of almost all of the walls that were tested. The values predicted by the theory exceeded the test values of every stage, that is, the cracking load, the full-crack load and the ultimate load. It can be concluded from this figure that, elastic theory is not a safe method to use for the prediction of flexural strength for these particular masonry walls.

Figure 3.3(b) compares the test values to the strengths predicted by the Strip method. Regarding the strengths of panels at the initial formation of cracks, the strip method over-estimated the failure loads of most panels. The full-crack loads were also generally over-estimated while the ultimate loads were under-estimated for most panels.

Figure 3.3(c) shows the comparison between test results and values predicted by the yield line method. It is observed that the yield line method over-estimated the load of initial crack formation for the majority of the panels. The load at full crack formation was predicted with better accuracy than the initial crack load. However, the prediction was still unsafe because most of the predicted values exceeded the test values. The yield line method performed relatively well for the prediction of the ultimate load, but again not for all panels. It was not a surprise that the yield line method predicted the ultimate load with more accuracy than it predicted the other load stages, because the method is based on the existence of a plastic mechanism.

Fracture line method predictions are compared with test values in Figure 3.3(d). It is apparent that the best predictions were for ultimate loads of the panels, and the worst were for initial crack load. This trend was expected since the method is based on formation of a plastic mechanism.

Figure 3.3(e) gives the results obtained by the Finite Element Analysis method. It is observed that the number of points close to the line of equality is greater in Figure 3.3(e) than in any other figure. In this graph, only the initial-crack load is shown. Clearly, more conservative predictions will occur for the full-crack and ultimate load test results.

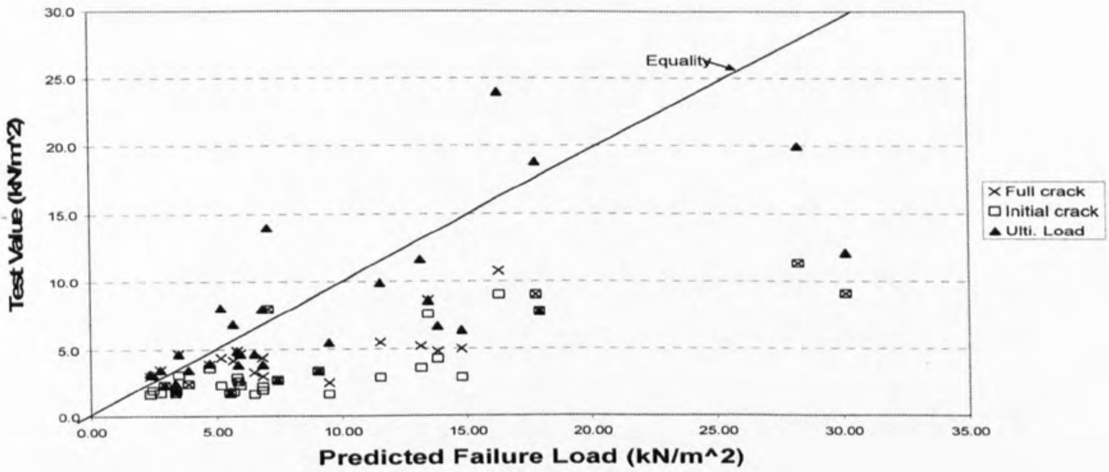


**Figure 3.3(a)**: Plate Theory versus Experiment

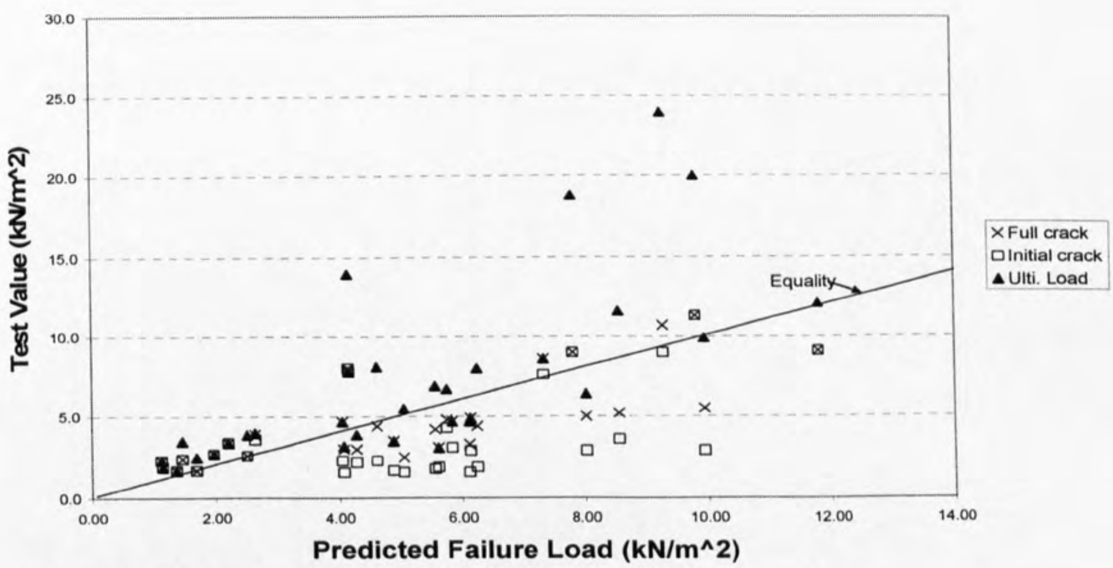


**Figure 3.3(b)**: Strip Method versus Experiment

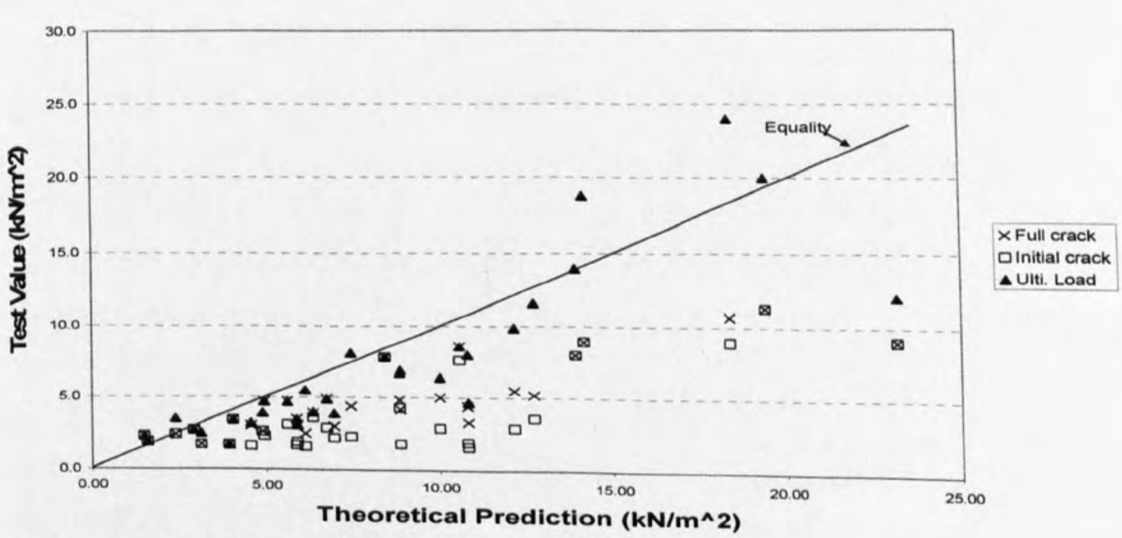


**Figure 3.3(c)**: Yield Line Method versus Experiment

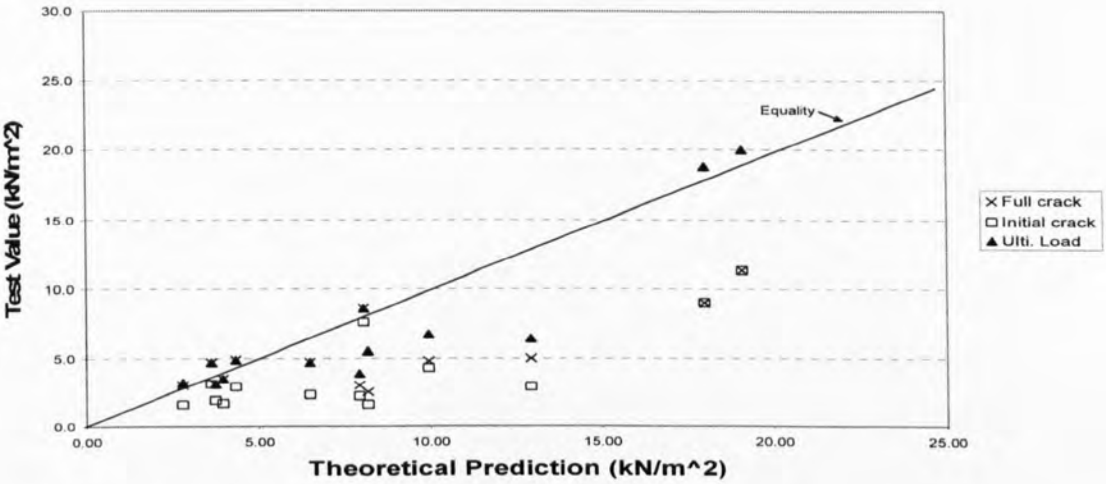


**Figure 3.3(d)**: Fracture Line Method versus Experiment

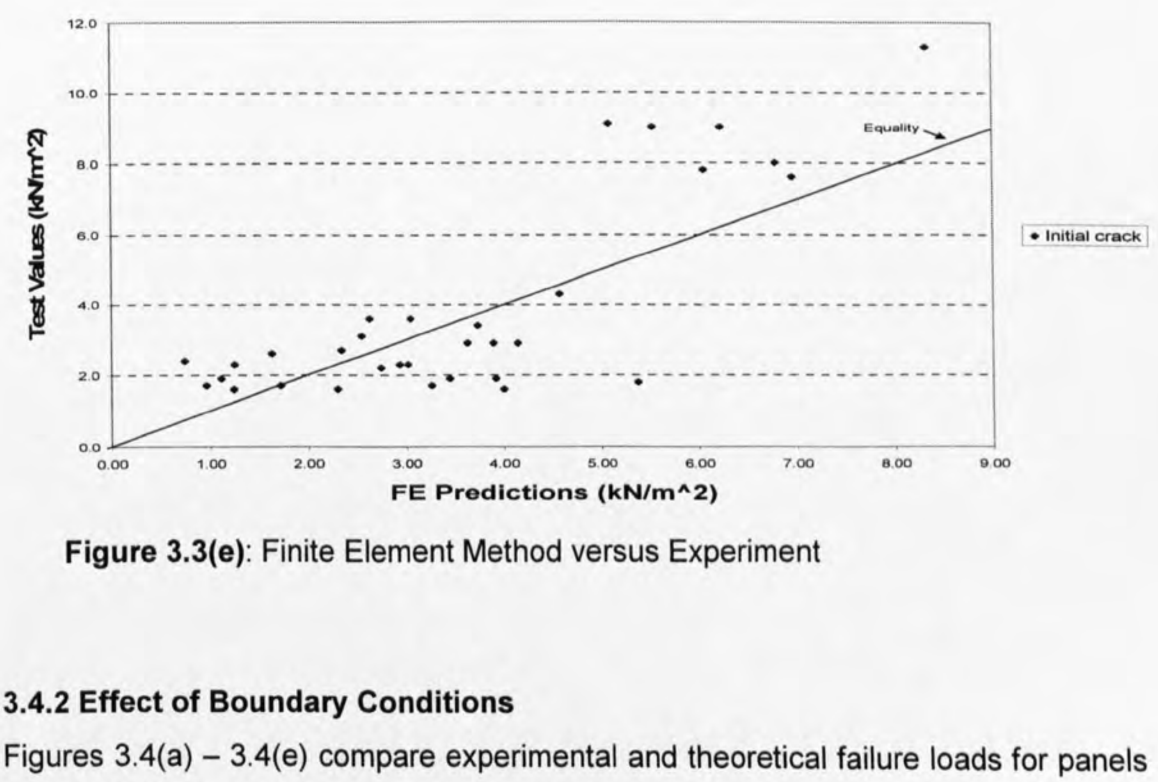


**Figure 3.3(e)**: Finite Element Method versus Experiment

### 3.4.2 Effect of Boundary Conditions

Figures 3.4(a) – 3.4(e) compare experimental and theoretical failure loads for panels of different boundary conditions. In Figure 3.4(a), predictions by elastic analysis for simply supported panels are compared to test values. The failure loads were over-estimated for all panels, but with the exception of two panels, the values fall within reasonable factor of safety margin (less than 1.5). For panels fully fixed on all edges (Figure 3.4(b)), elastic theory predicted values that are much higher than those obtained in the tests. The application of elastic theory assumes ideal boundary conditions. Since it is more difficult to obtain a fixed support than to obtain a simple support in laterally loaded wall tests, it can be argued that this difference is reflected by the results of these tests. For other support conditions, Figures 3.4(c) – 3.4(e), the margins of error were intermediate between those of simply supported and fully fixed panels.

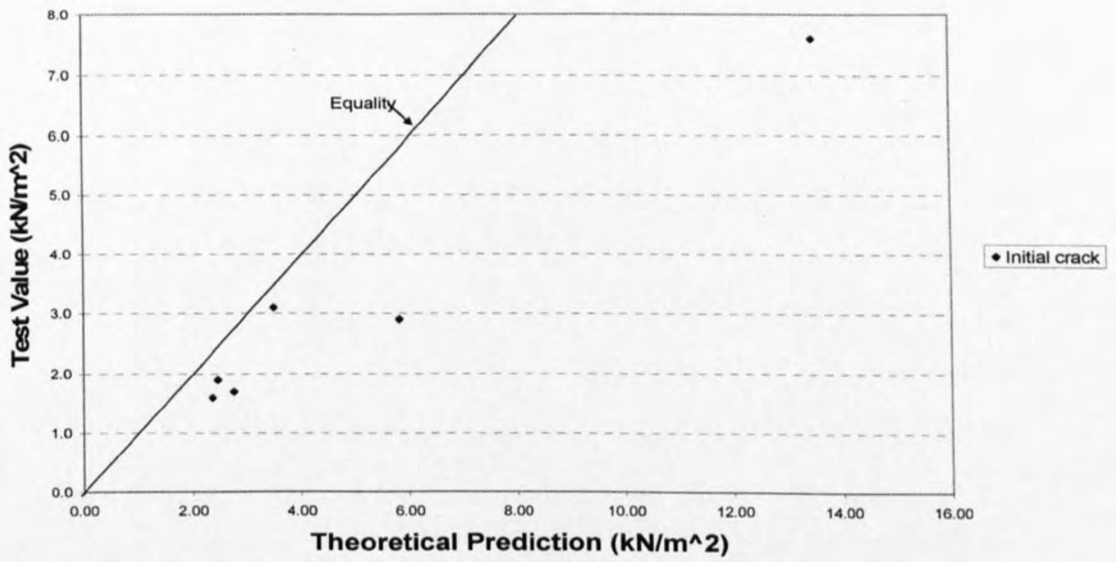


**Figure 3.4(a)**: Elastic Analysis versus Experiment – Simply Supported Panels

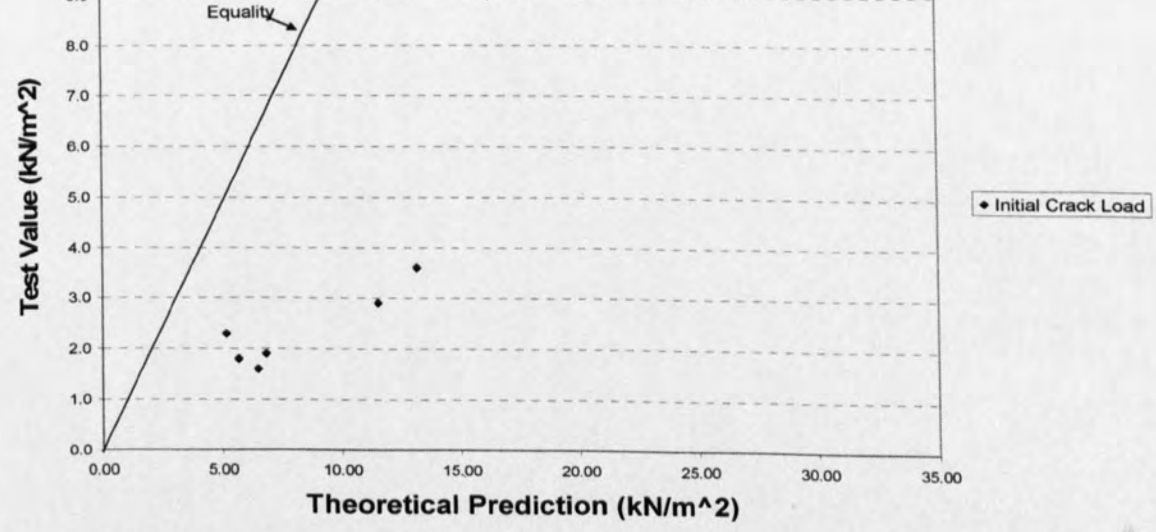


**Figure 3.4(b)**: Elastic Analysis versus Experiment – Fully Fixed Panels

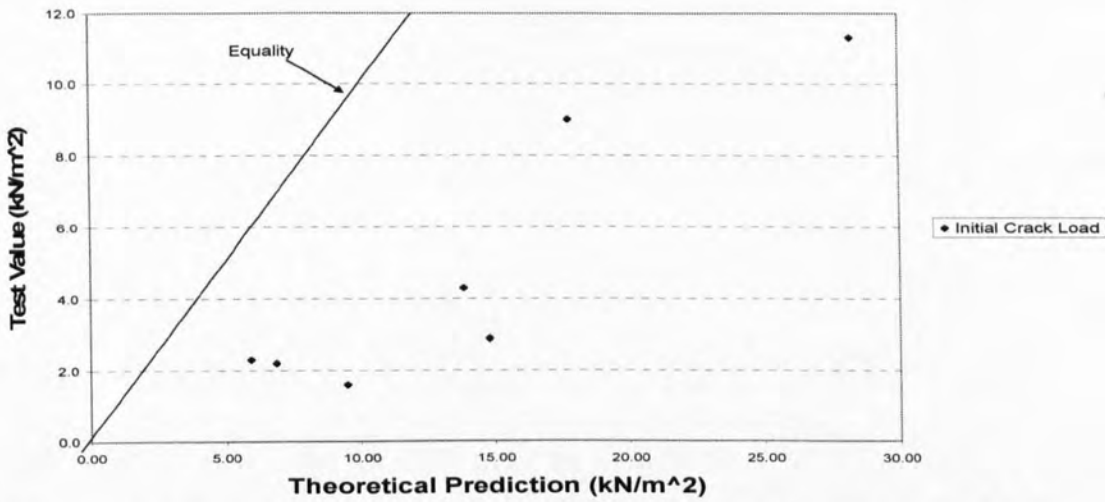


**Figure 3.4(c)**: Elastic Analysis versus Experiment – Simply Supported Top and Bottom, Built-in Sides.

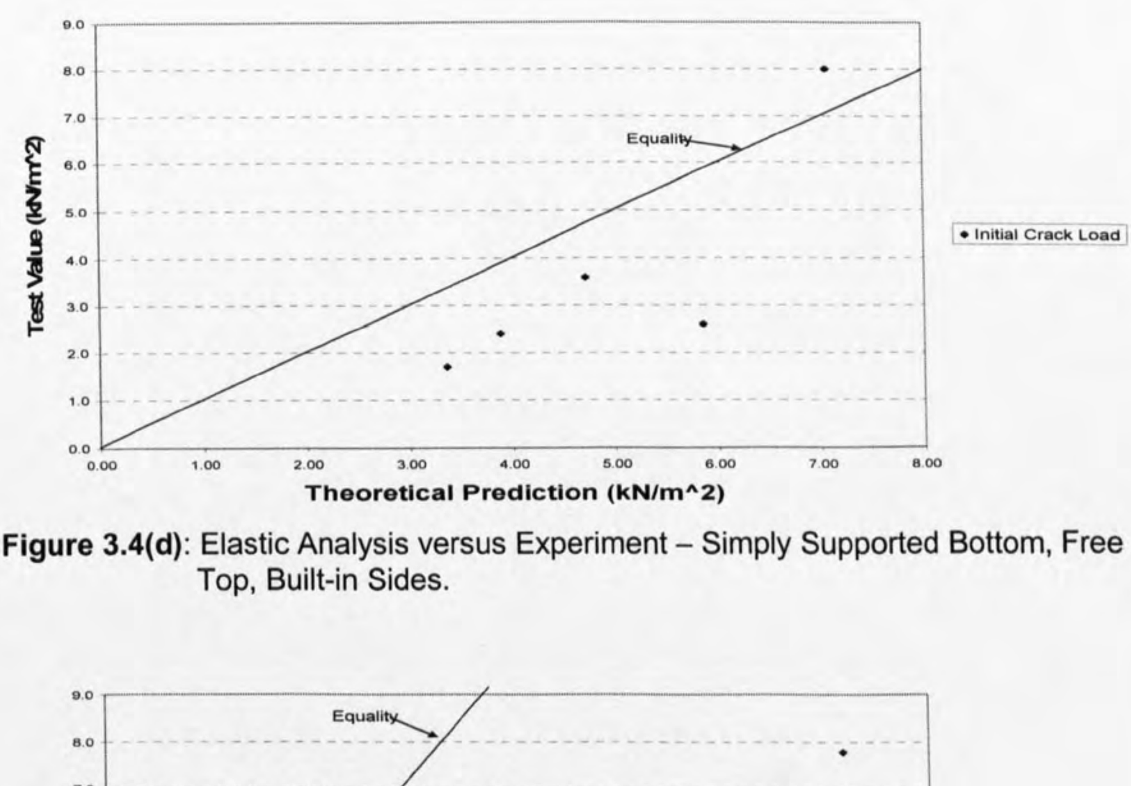


**Figure 3.4(d)**: Elastic Analysis versus Experiment – Simply Supported Bottom, Free Top, Built-in Sides.

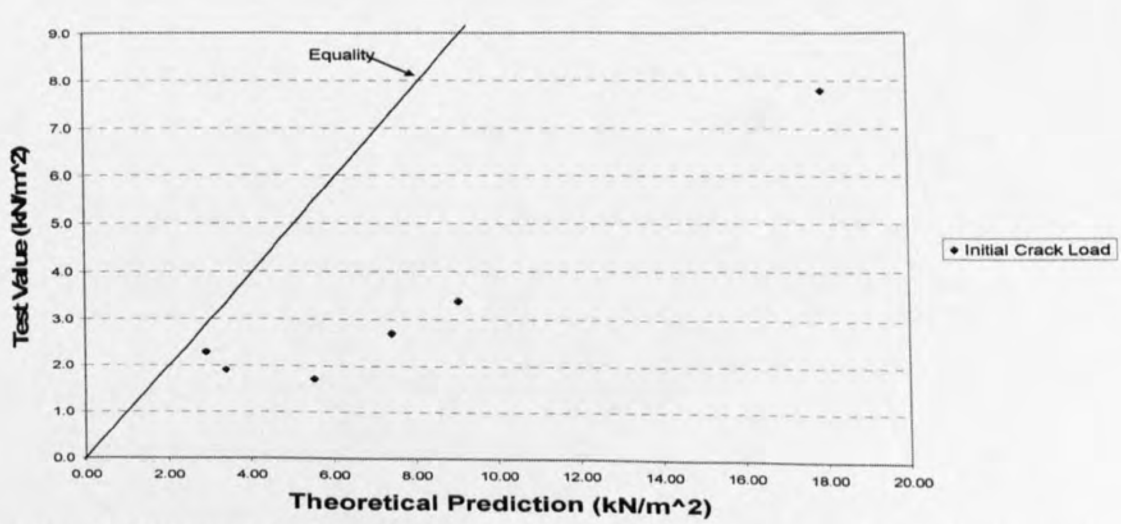


**Figure 3.4(e)**: Elastic Analysis versus Experiment – Simply Supported Bottom and Sides, Free Top.

The values predicted by the Strip method were compared to initial crack loads obtained in the tests, Figure 3.5(a) – 3.5(e). It can be seen from Figures 3.5(a) and 3.5(b) that the Strip method performed badly for both simply supported and fully fixed panels, but performed relatively well for the panels with mixed boundary conditions, Figures 3.5(c) – 3.5(e).

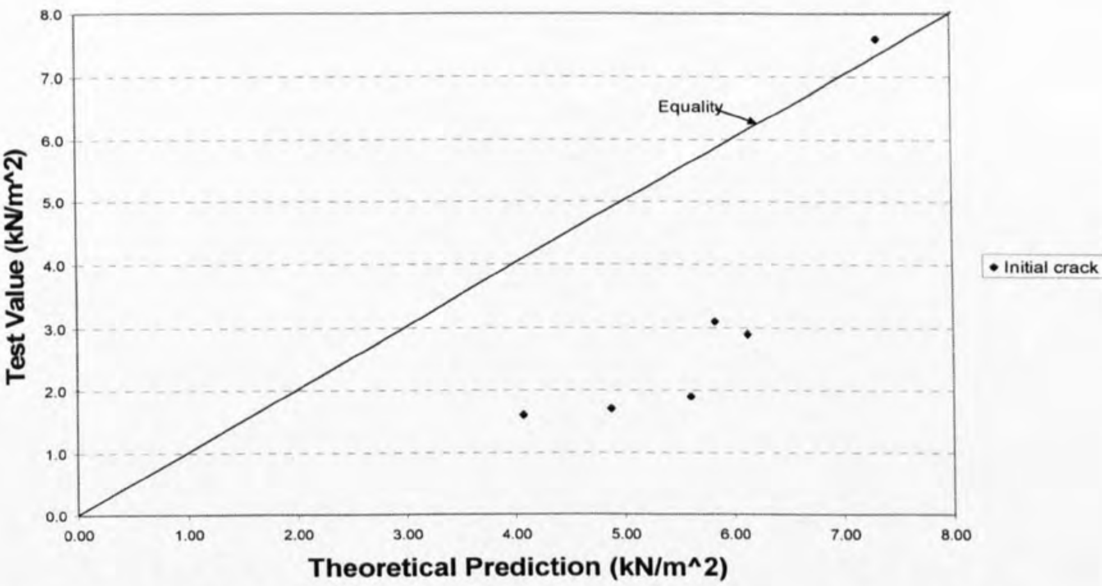


**Figure 3.5(a)**: Strip Method versus Experiment – Simply Supported Panels

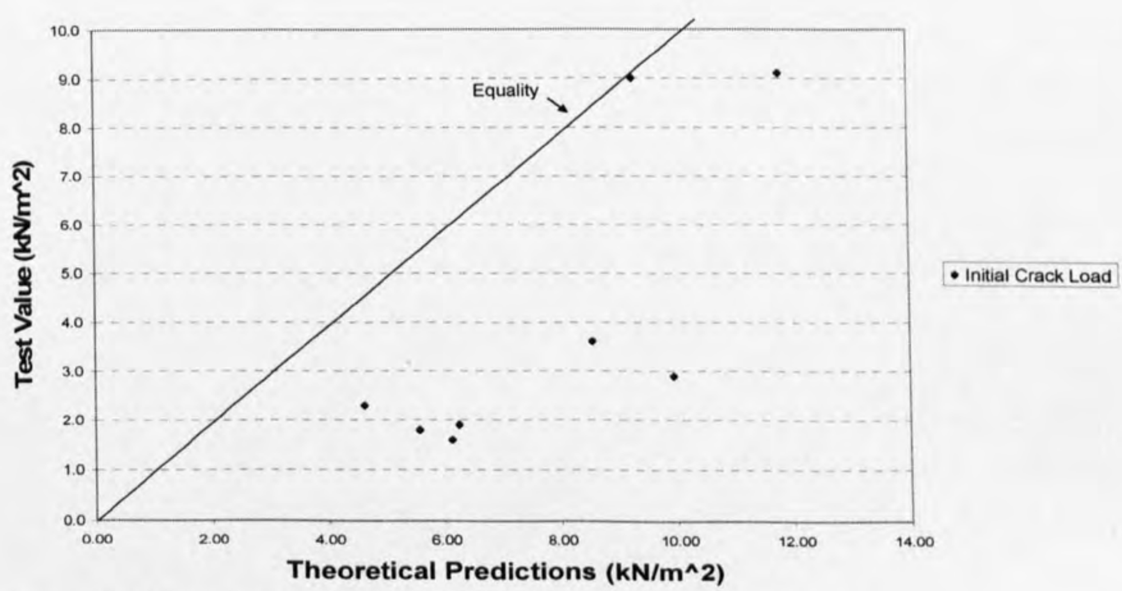


**Figure 3.5(b)**: Strip Method versus Experiment – All Edges Built-in

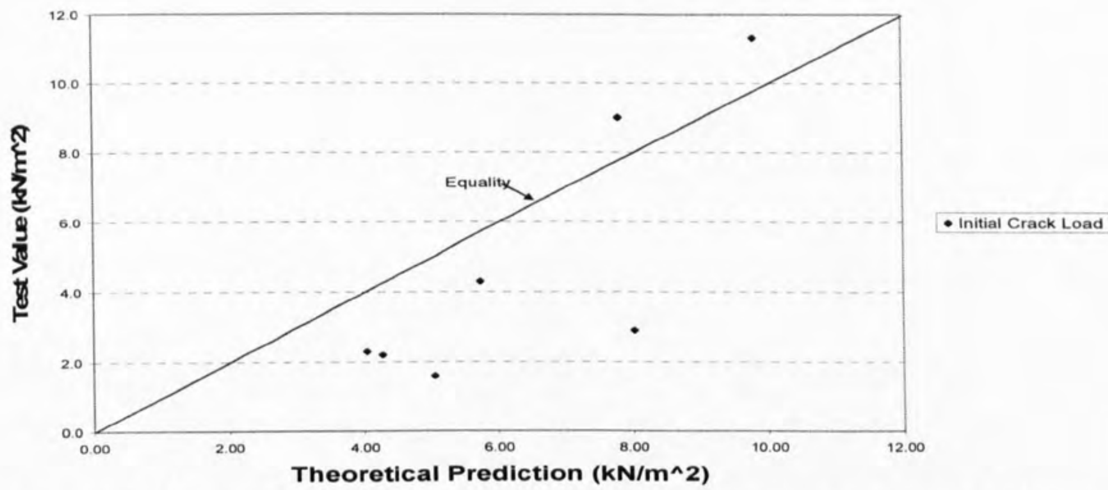


**Figure 3.5(c)**: Strip Method versus Experiment - Simply Supported Top and Bottom, Built-in Sides.

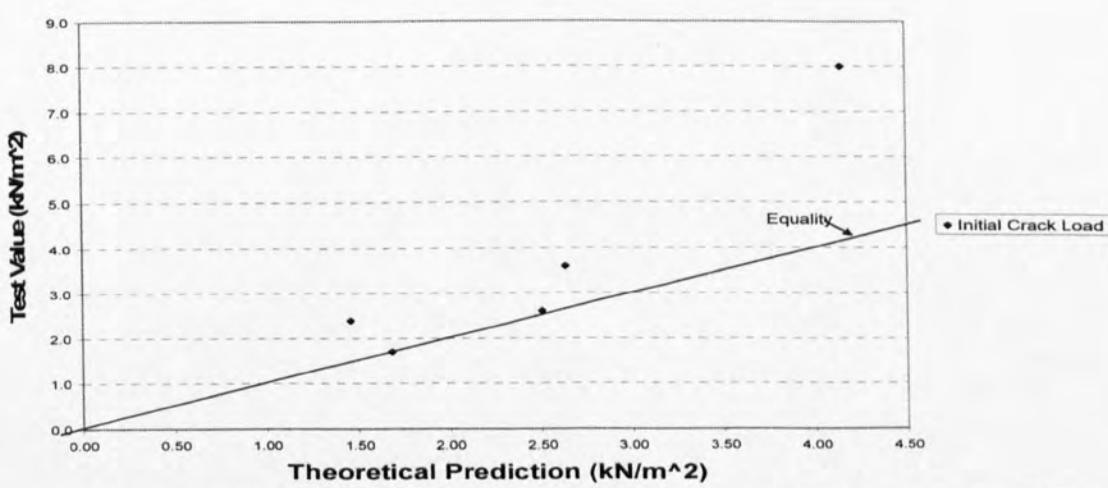


**Figure 3.5(d)**: Strip Method Experiment – Simply Supported Bottom, Free Top, Built-in Sides.

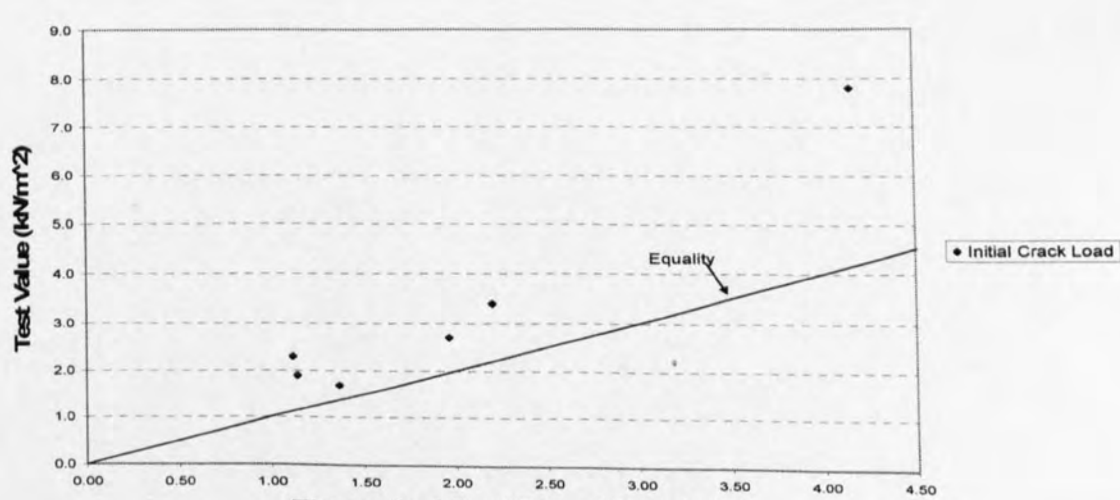


**Figure 3.5(e)**: Strip Method versus Experiment – Simply Supported Bottom and Sides, Free Top.

The influence of boundary conditions on the strengths predicted by the Yield Line method is demonstrated in Figures 3.6(a) to 3.6(e). In Figure 3.6(a) theoretical predictions for panels with simple supports are compared to test results. It is clear that Yield Line method over-estimated the ultimate strength of the simply supported wall panels considered in this study. For panels with all edges fixed, the method predicted the ultimate load relatively well, see Figure 3.6(b). These results demonstrate that some ductile response can be expected from panels with built-in edges, while it is not the case for simply supported panels. For panels with other support conditions, the Yield Line method continued to over-estimate the ultimate load of some wall panels, in a few cases by a factor larger than 2. The most worrying aspect, however, is the inconsistency of the predictions, that is, over-estimation of the failure load in some cases and under-estimation in other cases.

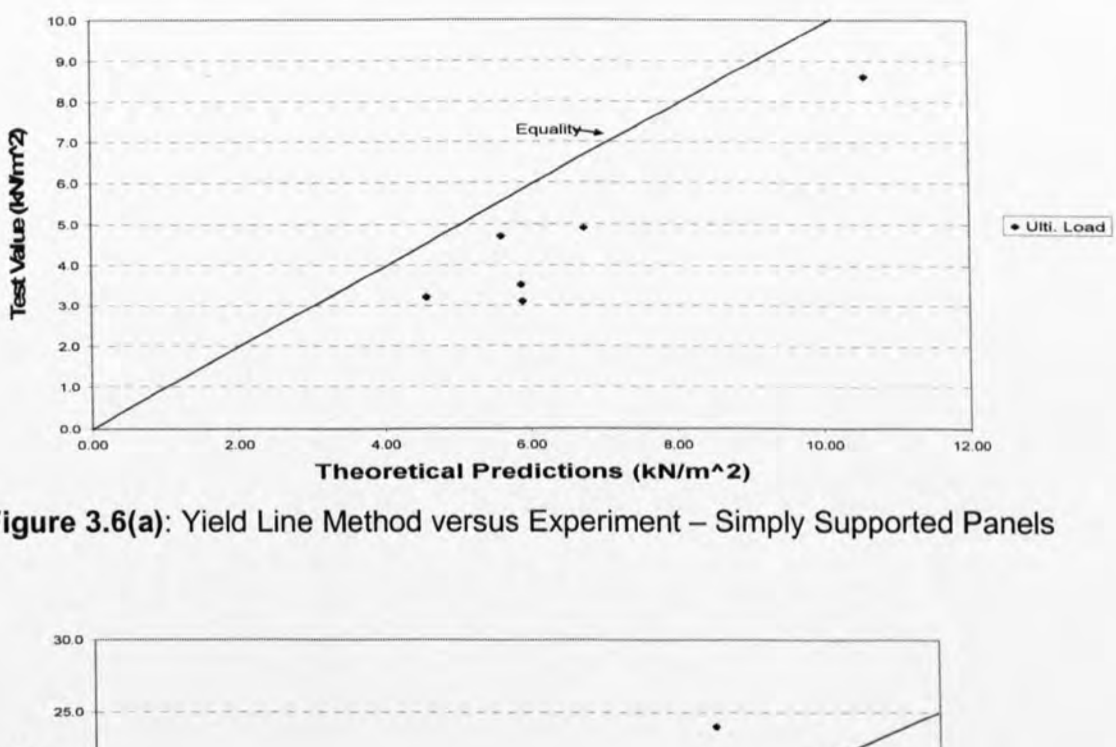


**Figure 3.6(a)**: Yield Line Method versus Experiment – Simply Supported Panels

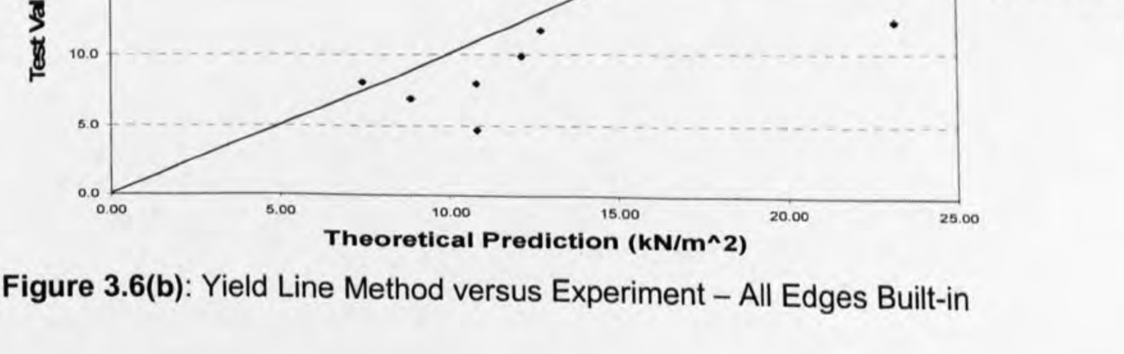


**Figure 3.6(b)**: Yield Line Method versus Experiment – All Edges Built-in

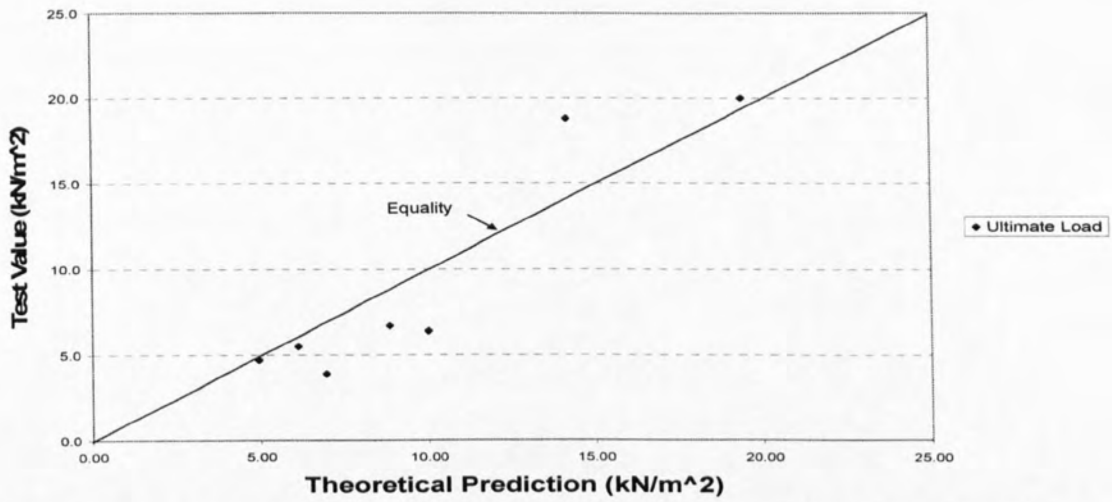


**Figure 3.6(c)**: Yield Line Method versus Experiment - Simply Supported Top and Bottom, Built-in Sides.

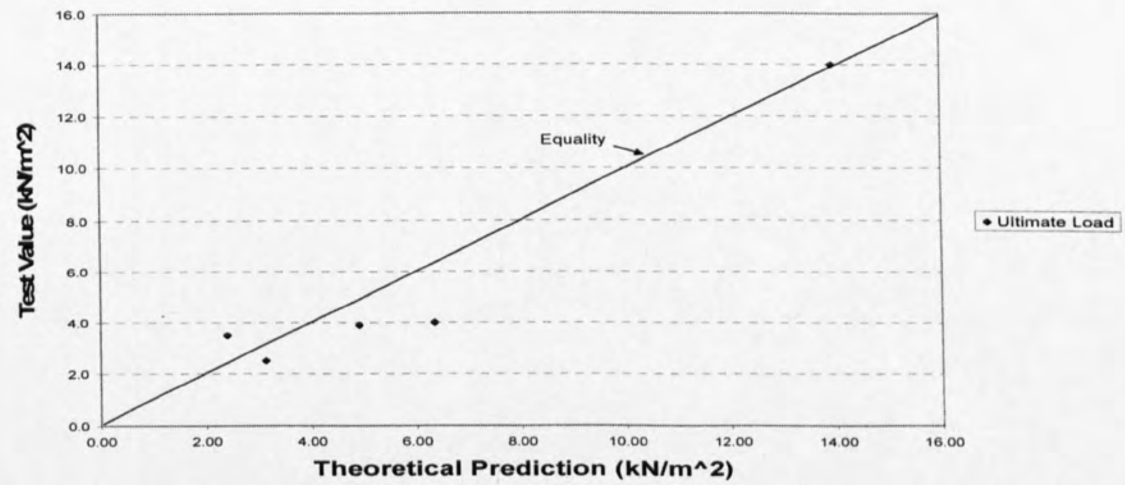


**Figure 3.6(d)**: Yield Line Method Experiment – Simply Supported Bottom, Free Top, Built-in Sides.

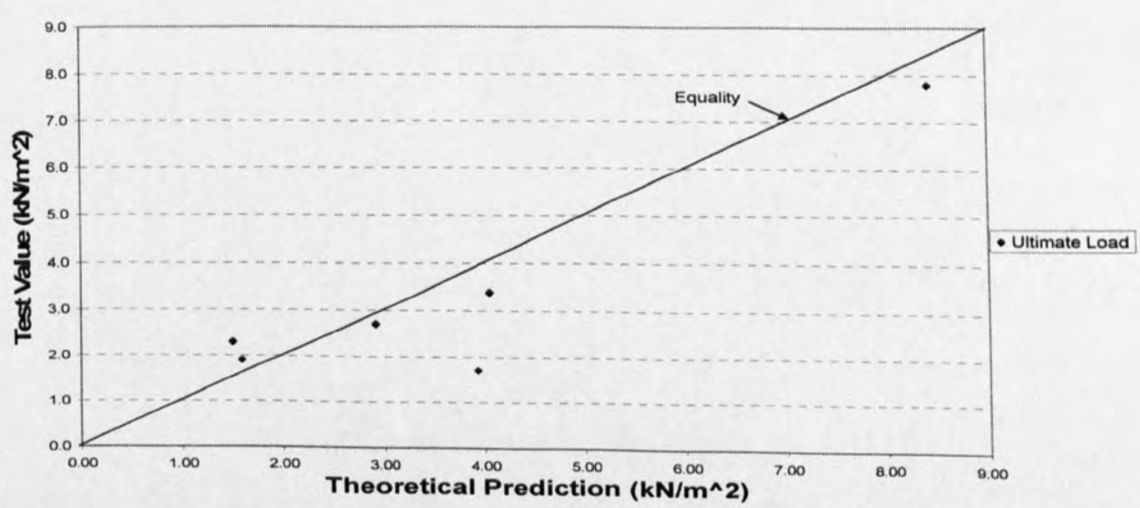


**Figure 3.6(e)**: Yield Line Method versus Experiment – Simply Supported Bottom and Sides, Free Top.

Fracture line method performed very well for simply supported panels, as can be seen from Figure 3.7(a). For panels with simple supports at top and bottom and fixed vertical edges, the Fracture Line method over-estimated the ultimate failure load for most wall panels, see Figure 3.7(b). However, a relatively low factor of safety value, say 1.5, would render these predictions acceptable, with the exception of only one panel.

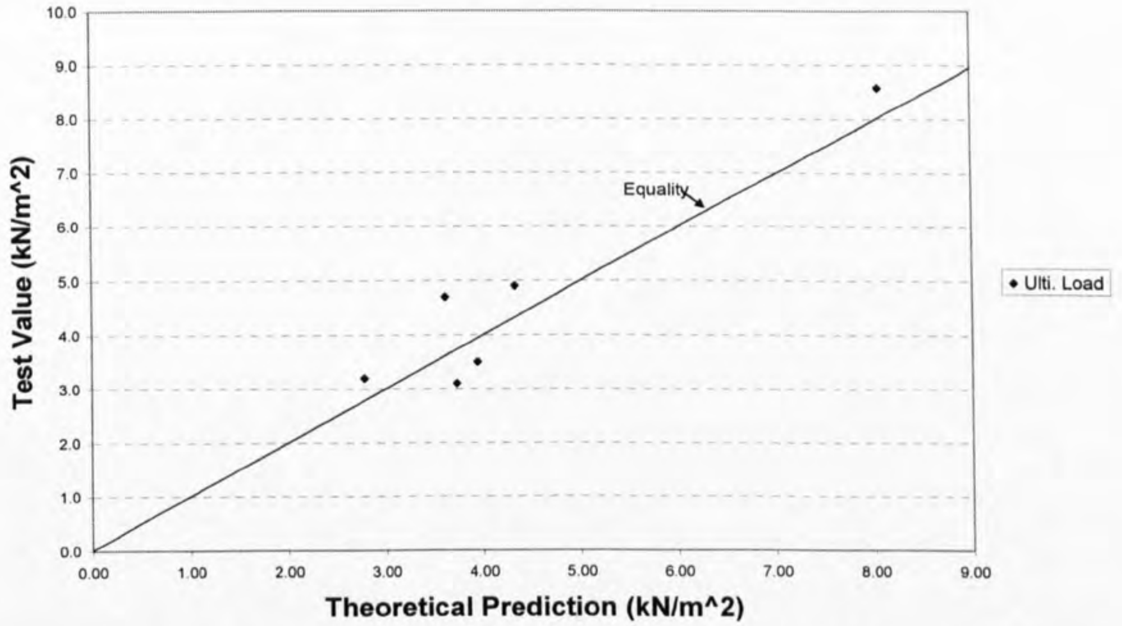


**Figure 3.7(a)**: Fracture Line Method versus Experiment – Simply Supported Panels

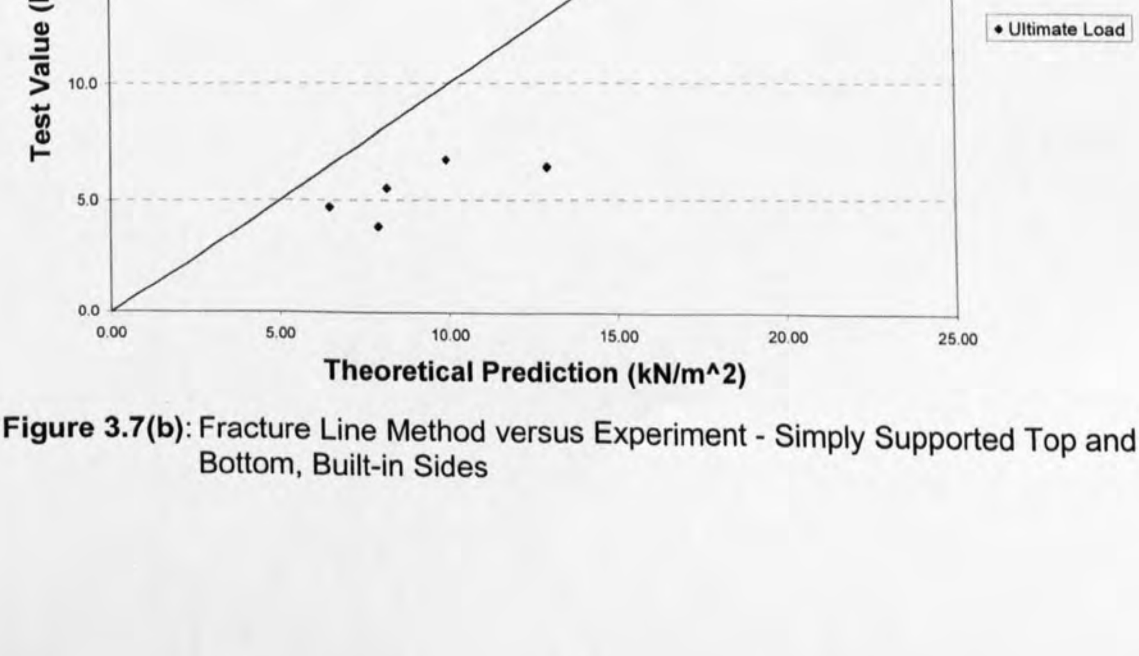


**Figure 3.7(b)**: Fracture Line Method versus Experiment - Simply Supported Top and Bottom, Built-in Sides

Finite Element Analysis results are displayed in Figure 3.3 (e), and in Figures 3.8(a) – (e). Examination of Figure 3.3(e) reveals that finite elements invariably under-estimated the strength of high-strength wall panels, while for the low-strength panels the predictions were not so consistent. It is also observed from Figures 3.1(a) – (e) that predictions by finite element method are closer to test results than predictions by all other theories. Figure 3.8(a) shows that the finite element method was able to yield good approximations of failure loads for most simply supported wall panels, but without consistency. The worst predictions by the finite element method were for panels with built-in supports, shown in Figure 3.8(b). For other support conditions the approximations were fairly good for low-strength panels, that is, panels of strength less than 5 kN/m$^2$.

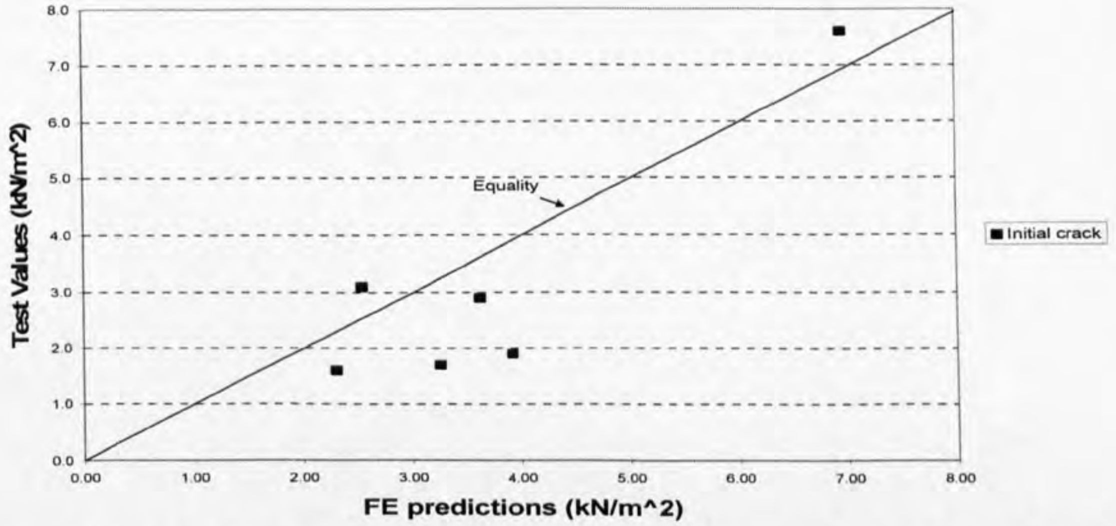


**Figure 3.8(a)**: Finite Element Method versus Experiment – Simply Supported Panels

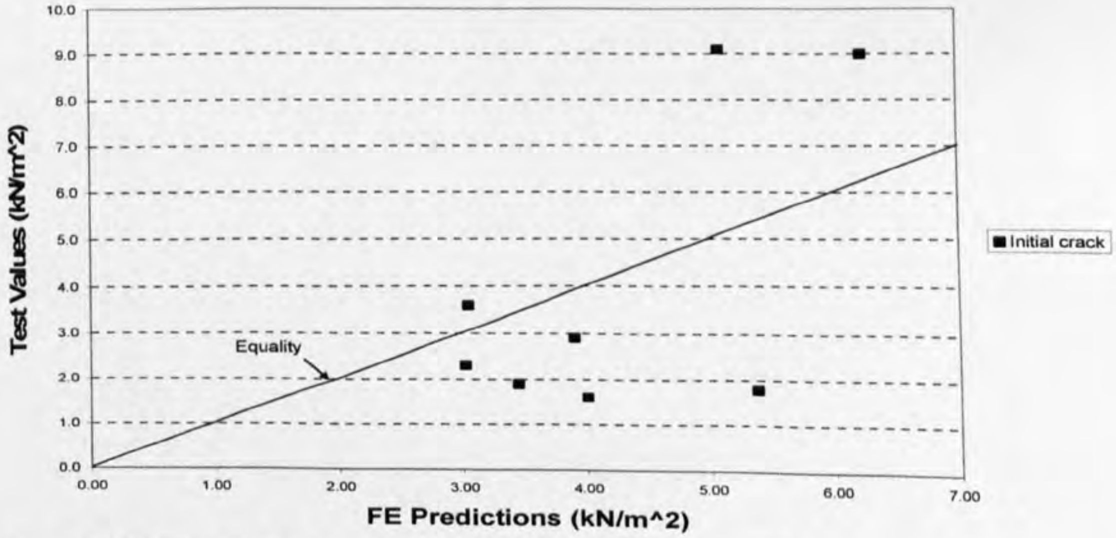


**Figure 3.8(b)**: Finite Element Method versus Experiment – All Edges Built-in

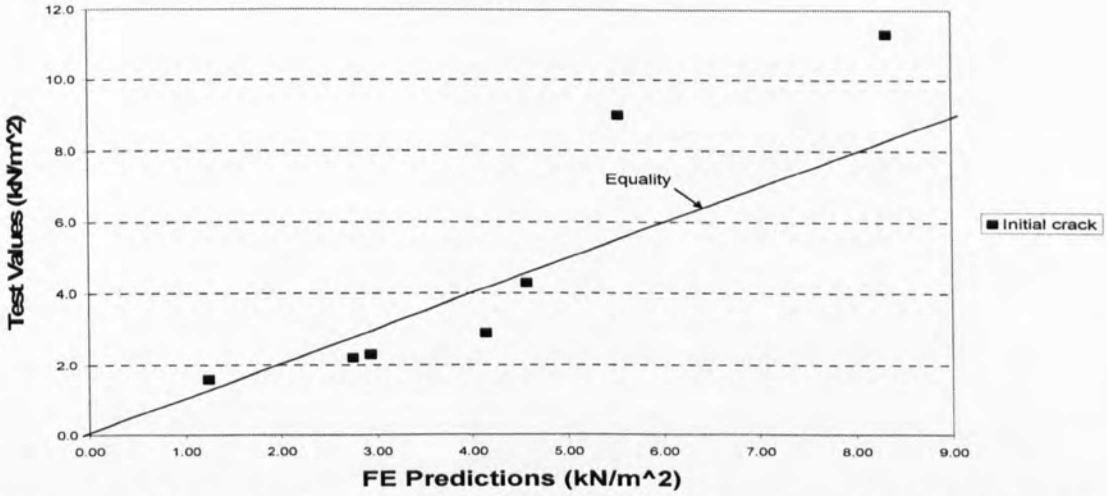


**Figure 3.8(c)**: Finite Element Method versus Experiment - Simply Supported Top and Bottom, Built-in Sides

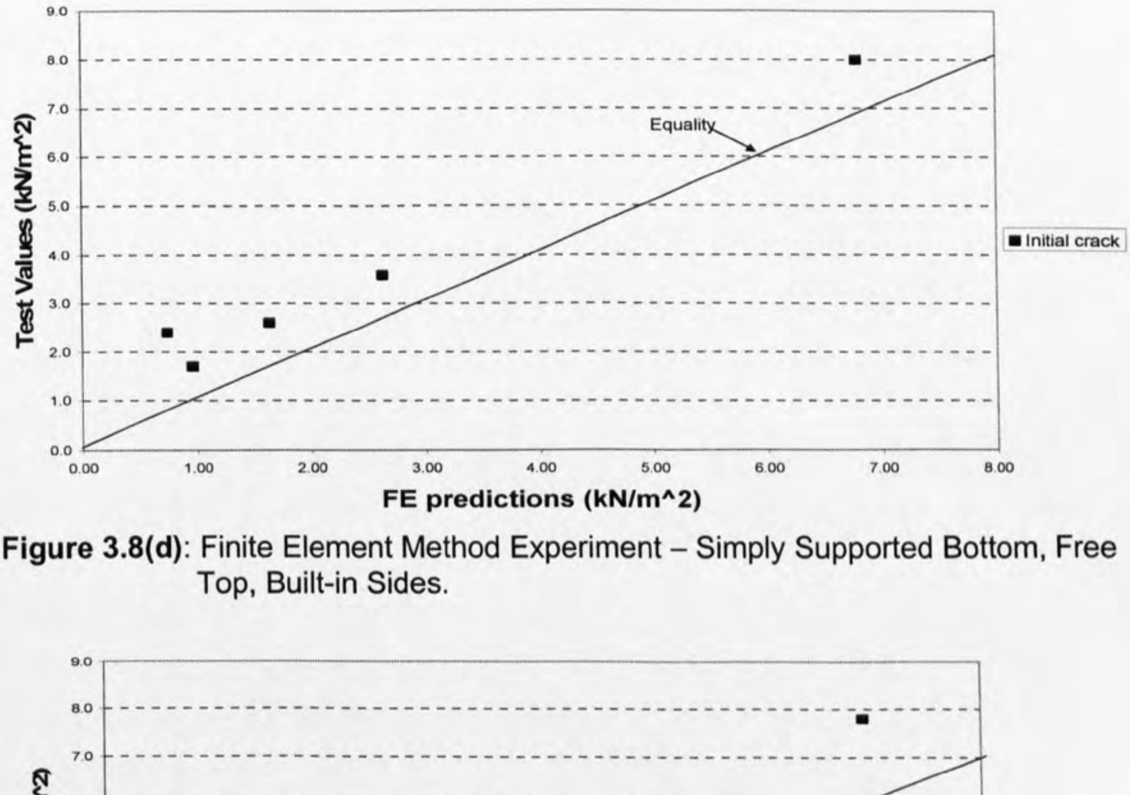


**Figure 3.8(d)**: Finite Element Method Experiment – Simply Supported Bottom, Free Top, Built-in Sides.

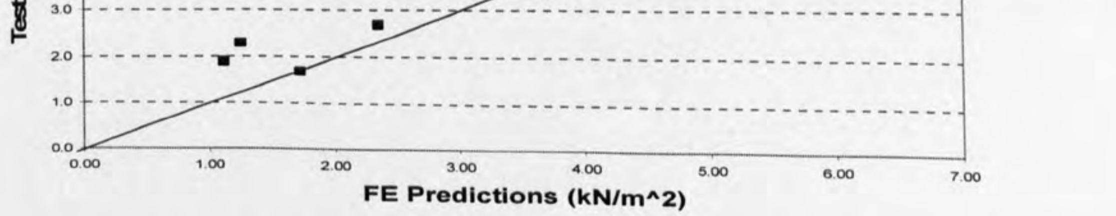


**Figure 3.8(e)**: Finite Element Method versus Experiment – Simply Supported Bottom and Sides, Free Top.

In general, all of the methods of analysis reviewed here reveal a high level of inconsistency and variability. An important observation from the Figures is that the results for simply supported panels are less scattered than those for panels with any other support conditions. This indicates that all theoretical methods reviewed here predicted the failure loads for simply supported panels with better accuracy than for panels with other support conditions. The methods also gave better approximations for panels with mixed boundary conditions as compared to panels with all built-in supports. It is observed that as the number of built-in edges increases, the theoretical predictions drift further from the test results. This trend can be associated with the values of the moment coefficients as they are derived on the assumption of full continuity at the built-in edges, but if the assumed built-in edge is not capable of full moment resistance, the assigned coefficient becomes faulty. With simple supports or free edges, the coefficients are more accurate. This confirms the significance boundary conditions have on the strength of masonry panels, with accurate predictions occurring when the boundary conditions assumed in the analysis nearly match the real conditions of the test panels.

A close observation of the test values in Table 3.1 reveals that the failure loads, that is, initial crack load, full crack and ultimate load, for panels with Boundary Condition 5 (free top and simply supported elsewhere) are identical. This implies that these panels did not carry additional load after initial formation of a crack. This shows that panels supported this way behave in a brittle manner as opposed to panels with other support conditions. Some researchers [Duarte, 2000; Guggisberg and Thurlimann, 1990] have observed that masonry panels become more brittle as the boundary conditions change from fully fixed to simple supports. This observation was also corroborated here. Panels with fully-fixed edges continued to support additional load after their full-crack pattern had developed, while the simply supported panels could not carry any additional load after the formation of full-crack patterns, see Table 3.1. Panels with fixed vertical edges and simple supports top and bottom (boundary condition 3, Table 3.1) were able to support additional load after the formation of a full-crack pattern, but to a lesser extent than panels with all edges fixed.

### 3.4.3 Effect of Aspect Ratio

In Figures 3.9(a) – 3.9(d), panels are categorised by their aspect ratio, and results from elastic theory are compared to test values. The aspect ratios for the tested panels ranged from 0.417 to 1, Figures 3.9(a) to 3.9(d), respectively. It is apparent from the figures that elastic theory gave inconclusive results with regards to the influence of aspect ratio on the panel strength.

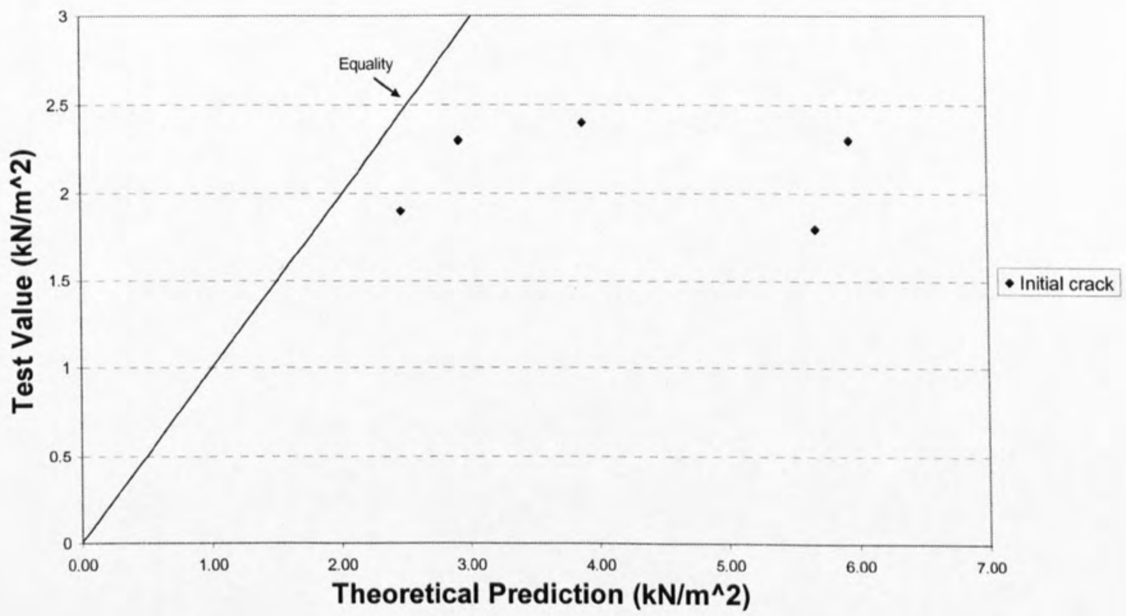


**Figure 3.9(a)**: Elastic Plate Theory versus Experiment – Aspect Ratio = 0.417

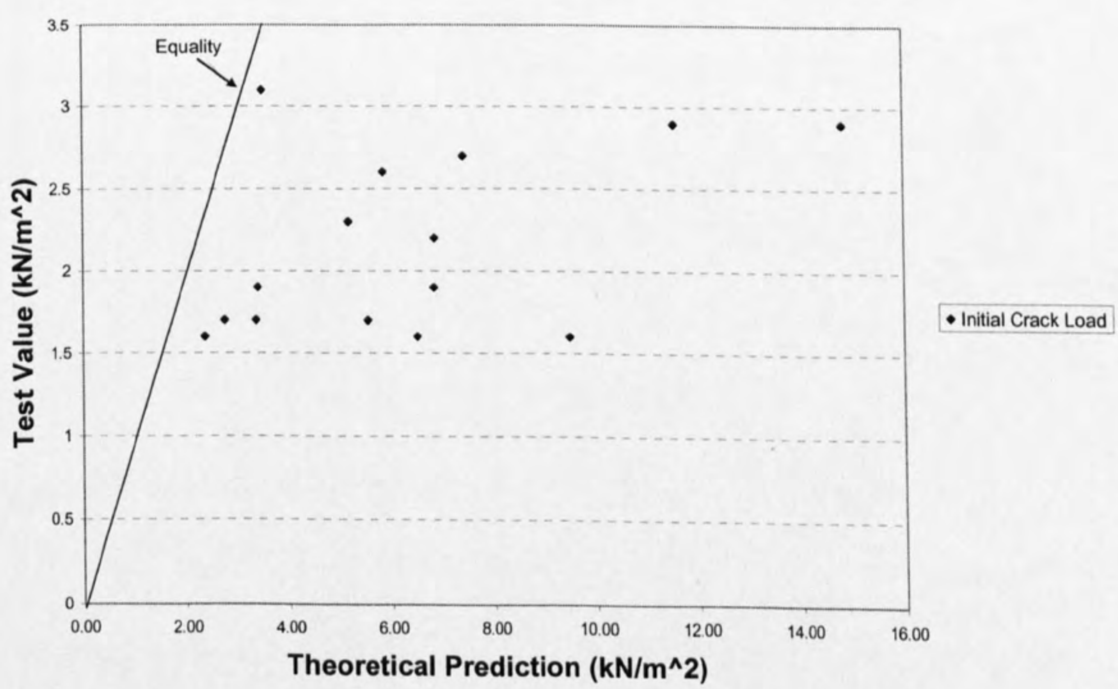


**Figure 3.9(b)**: Elastic Plate Theory versus Experiment – Aspect Ratio = 0.5

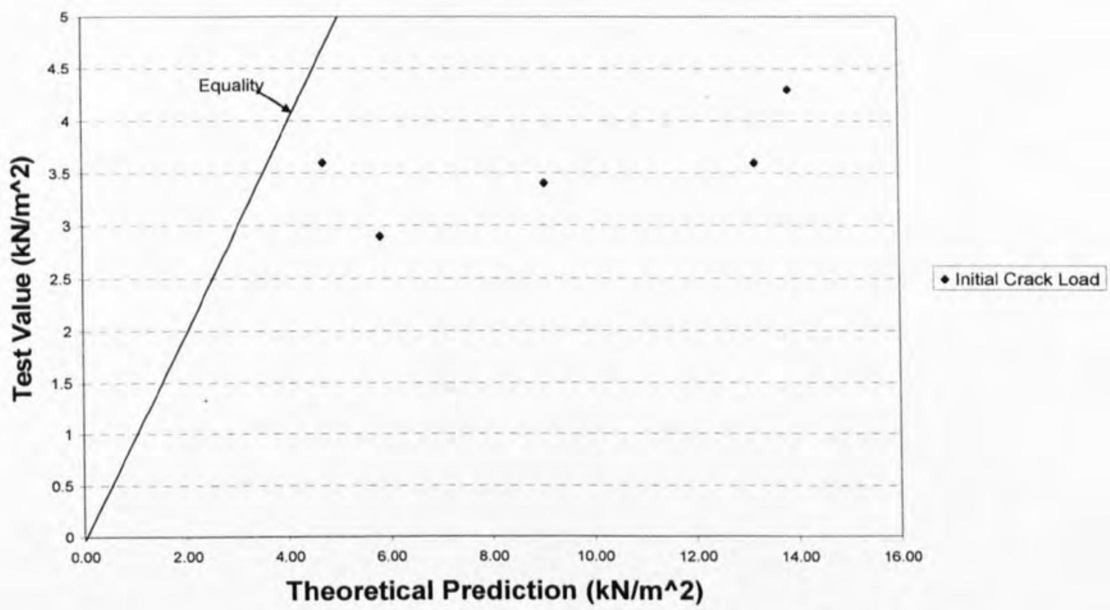


**Figure 3.9(c)**: Elastic Plate Theory versus Experiment – Aspect Ratio = 0.667

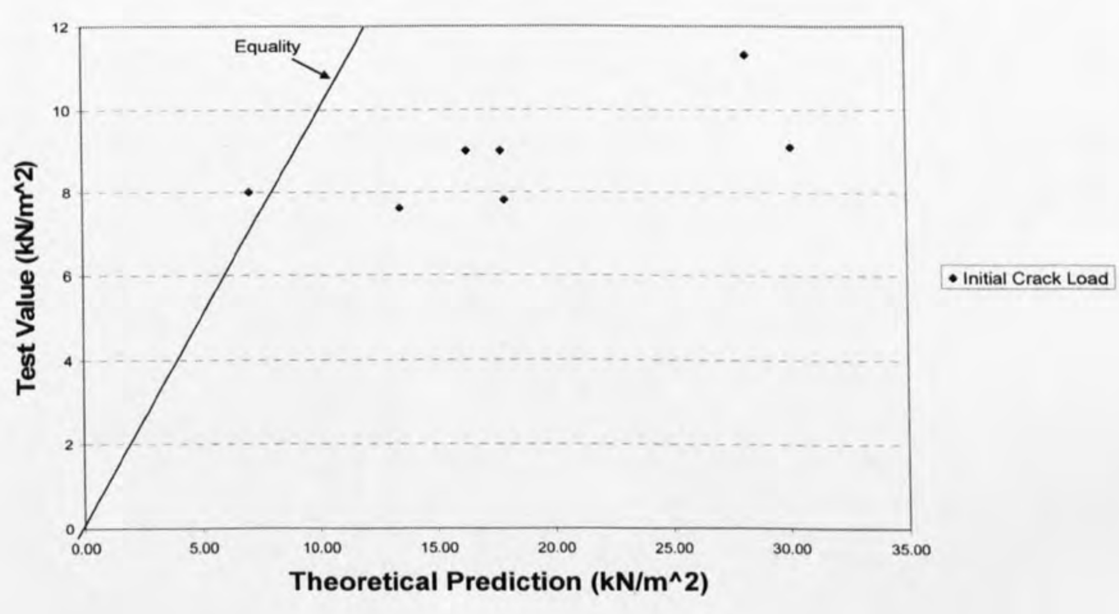


**Figure 3.9(d)**: Elastic Plate Theory versus Experiment – Aspect Ratio = 1

In Figures 3.10(a) to 3.10(d), the same is repeated for the yield line method. With this method, poor results were obtained for panels with aspect ratio of 0.5, while panels of other aspect ratios gave relatively good results. The effect of aspect ratio on the predictions by strip method was considered in Figures 3.11(a) to 3.11(d). Generally, this method gave the best results for all rectangular panels when compared to results by other methods. Predictions for square panels, however, were not as good.

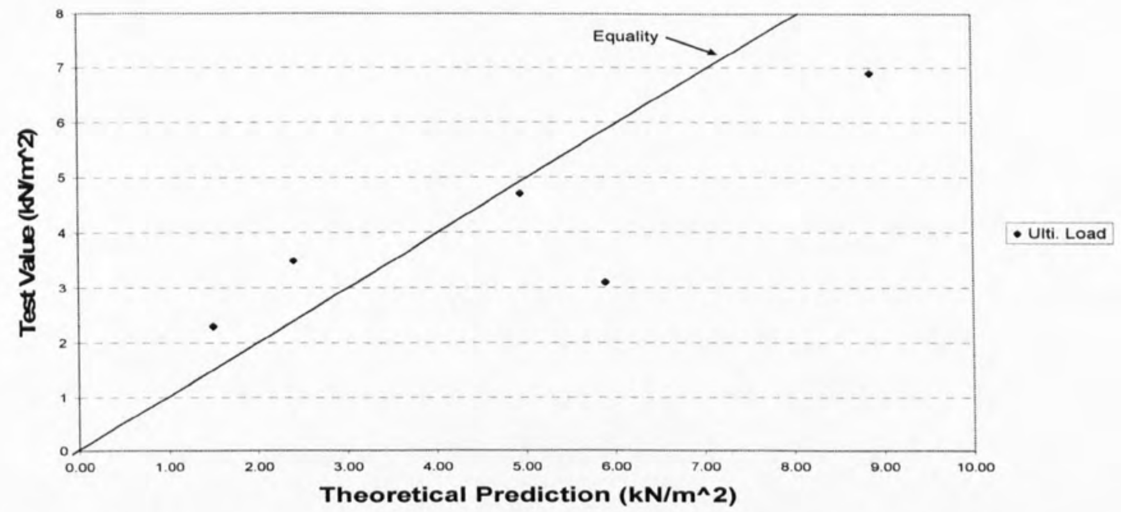


**Figure 3.10(a)**: Yield Line Method versus Experiment – Aspect Ratio = 0.417

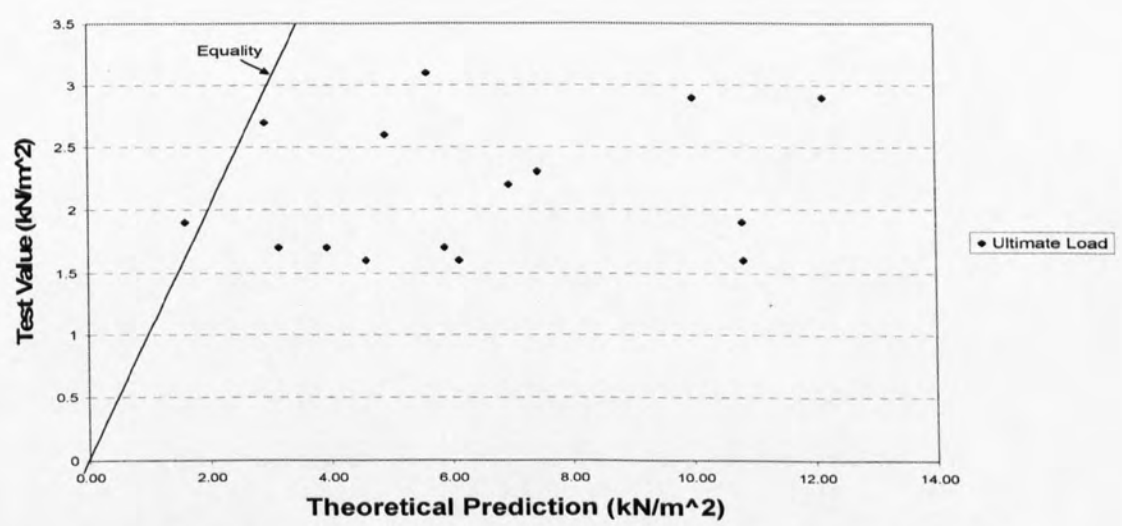


**Figure 3.10(b)**: Yield Line Method versus Experiment – Aspect Ratio = 0.5

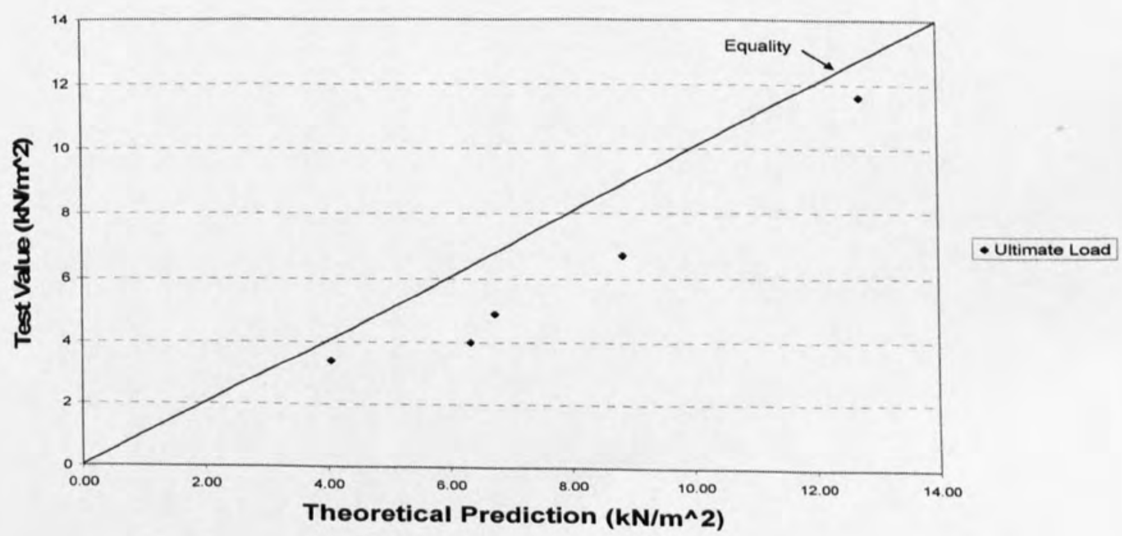


**Figure 3.10(c)**: Yield Line Method versus Experiment – Aspect Ratio = 0.667

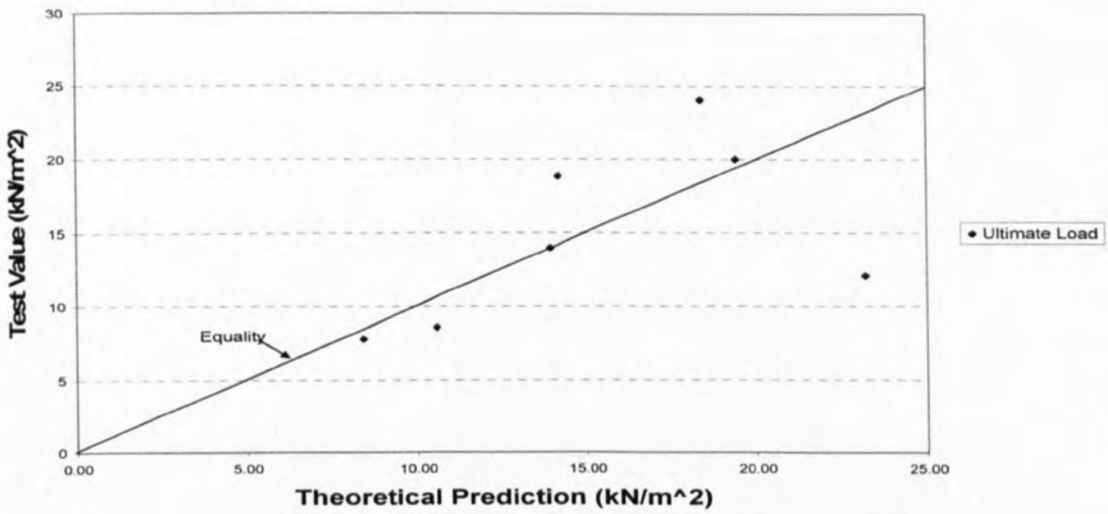


**Figure 3.10(d)**: Yield Line Method versus Experiment – Aspect Ratio = 1

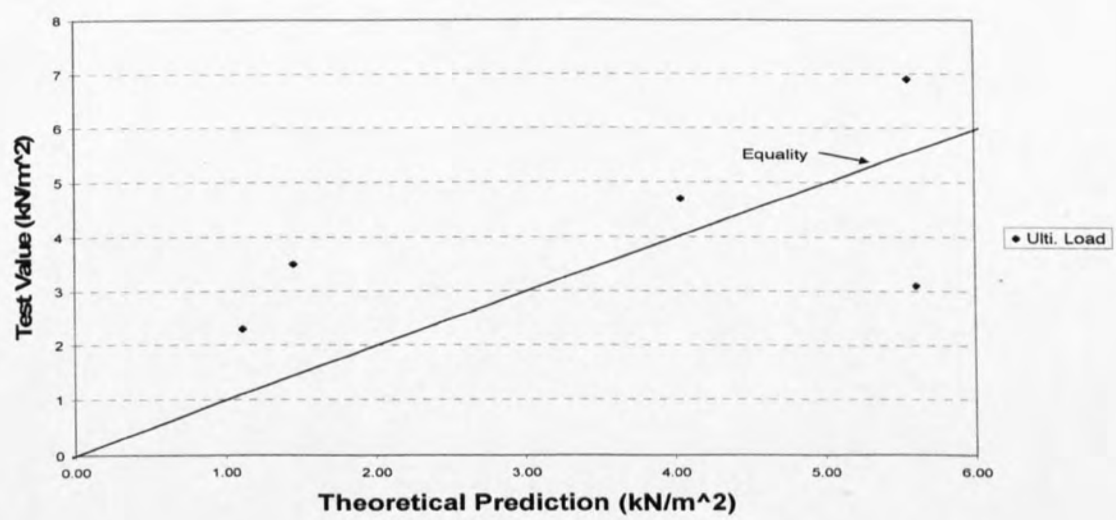


**Figure 3.11(a)**: Strip Method versus Experiment – Aspect Ratio = 0.417

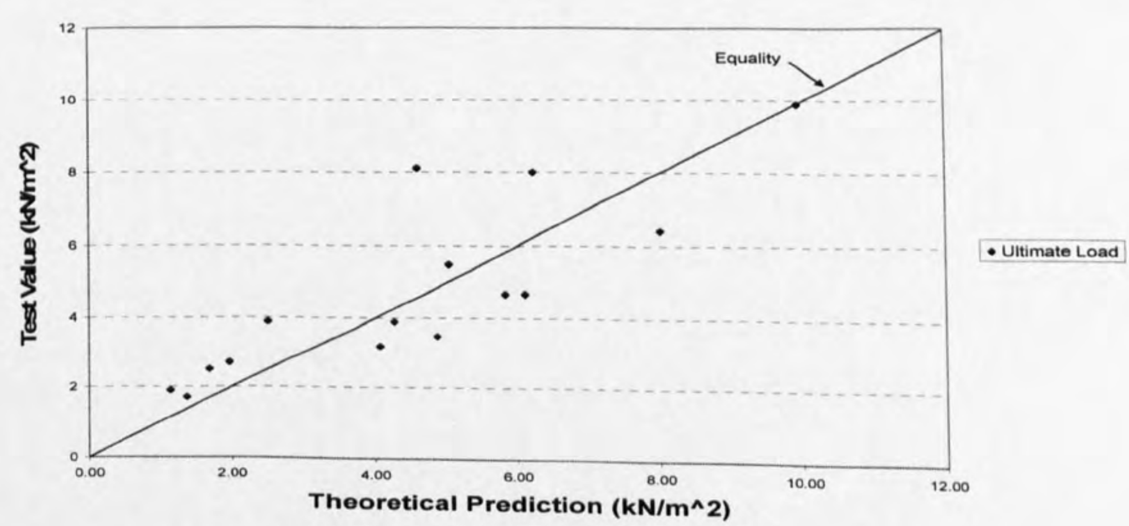


**Figure 3.11(b)**: Strip Method versus Experiment – Aspect Ratio = 0.5

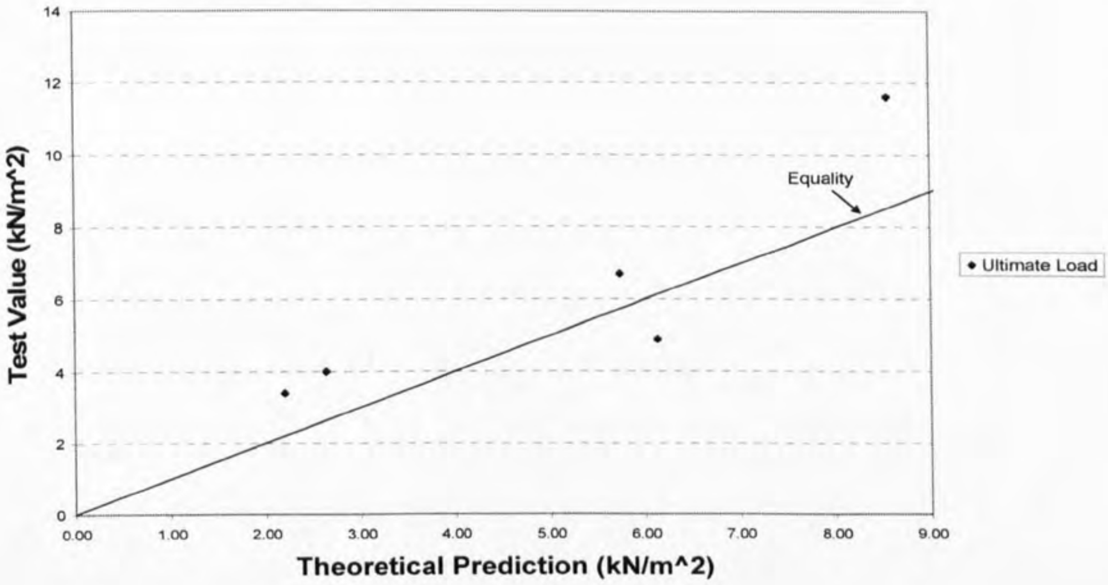


**Figure 3.11(c)**: Strip Method versus Experiment – Aspect Ratio = 0.667

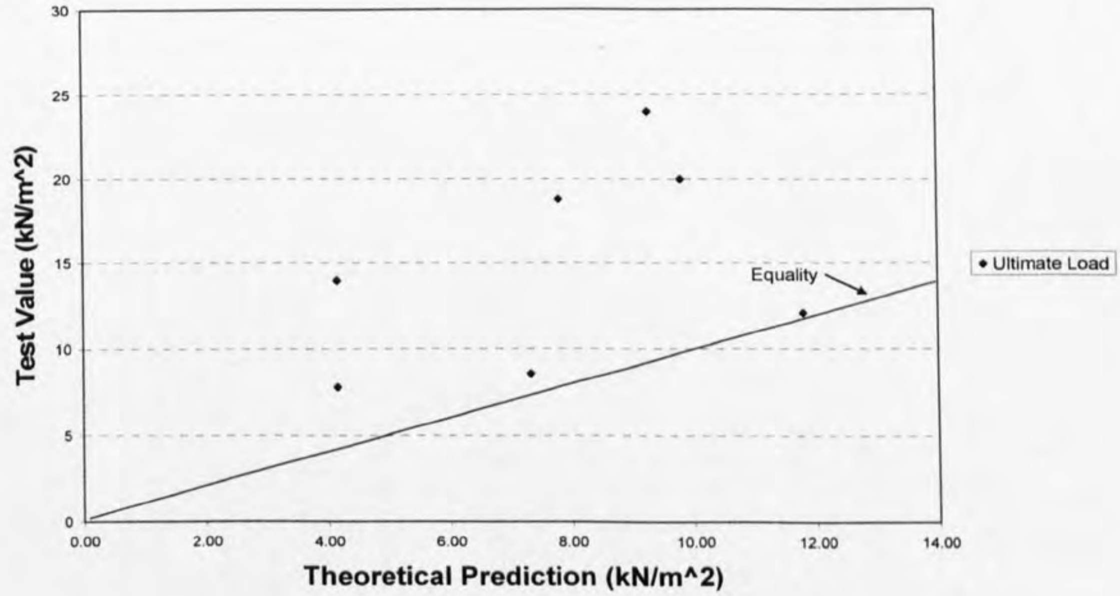


**Figure 3.11(d)**: Strip Method versus Experiment – Aspect Ratio = 1

### 3.5 COMPARISON BETWEEN THEORIES

It is very important to note here that the major task of this review was to compare the ability of the different theories to match the test results, as opposed to determining the load-carrying capacity of panels with different boundary conditions and aspect ratios. In Table 3.3 the ratios of predicted values to the test results are displayed. These ratios are then plotted in Figure 3.12. It is clear from the figure that, besides finite element analysis, the Strip method gives the best results for the walls tested as its values are closest to unity. It is also apparent from the figure that, in general, the elastic theory method over-estimated the load carrying capacity of these walls more than any other method. The yield line method gave the best results for panels with built-in edges. While all techniques (except Yield Line method) seemed to work relatively well in the case of simply supported panels, it was not easy to find a relationship between the test results and the predicted strength values since there was over-estimation in some cases and under-estimation in other cases. In that respect, all theoretical techniques performed not so well, as expected.

**Table 3.3: Ratio of Predicted Failure Load to Experimental Value**

| Test no. | Ratio of theory to tests (full crack pattern) | | | | Ratio of theory to tests (initial crack load) | | | | Ratio of theory to tests (ultimate load) | | | |
|---|---|---|---|---|---|---|---|---|---|---|---|---|
| | YL | Elastic | Strip | Fracture | YL | Elastic | Strip | Fracture | YL | Elastic | Strip | Fracture |
| 6 | 1.90 | 0.80 | 1.81 | | 3.10 | 1.30 | 2.95 | | 1.90 | 0.80 | 1.81 | |
| 7 | 0.65 | 1.27 | 0.49 | | 0.65 | 1.27 | 0.49 | | 0.65 | 1.27 | 0.49 | |
| 8 | 1.00 | 1.62 | 0.61 | 0.00 | 1.00 | 1.62 | 0.61 | 0.00 | 0.69 | 1.11 | 0.42 | 0.00 |
| 9 | 1.05 | 1.26 | 0.86 | 1.38 | 2.15 | 2.58 | 1.76 | 2.82 | 1.05 | 1.26 | 0.86 | 1.38 |
| 10 | 2.11 | 1.35 | 1.32 | | 4.93 | 3.15 | 3.09 | | 1.29 | 0.82 | 0.81 | |
| 12 | 2.46 | 1.56 | 1.42 | 0.00 | 5.69 | 3.60 | 3.28 | 0.00 | 1.35 | 0.86 | 0.78 | 0.00 |
| 13 | 1.69 | 1.18 | 1.05 | | 3.23 | 2.25 | 2.01 | | 0.92 | 0.64 | 0.57 | |
| 14 | 1.52 | 0.79 | 1.36 | 0.93 | 2.86 | 1.48 | 2.55 | 1.74 | 1.43 | 0.74 | 1.27 | 0.87 |
| 15 | 2.45 | 3.80 | 2.02 | | 3.83 | 5.93 | 3.16 | | 1.11 | 1.73 | 0.92 | |
| 16 | 2.31 | 3.26 | 0.80 | | 2.31 | 3.26 | 0.80 | | 2.31 | 3.26 | 0.80 | |
| 17 | 1.19 | 0.75 | 1.24 | | 1.81 | 1.13 | 1.88 | | 1.19 | 0.75 | 1.24 | |
| 18 | 2.21 | 2.10 | 1.81 | 0.00 | 4.19 | 3.98 | 3.43 | 0.00 | 1.23 | 1.17 | 1.00 | 0.00 |
| 19 | 2.00 | 2.96 | 1.60 | 2.59 | 3.45 | 5.11 | 2.77 | 4.46 | 1.56 | 2.31 | 1.25 | 2.02 |
| 20 | 1.89 | 2.25 | 0.96 | | 1.89 | 2.25 | 0.96 | | 1.26 | 1.50 | 0.64 | |
| 21 | 1.08 | 2.75 | 0.73 | | 1.08 | 2.75 | 0.73 | | 1.08 | 2.75 | 0.73 | |
| 22 | 1.68 | 0.79 | 1.39 | 1.13 | 3.46 | 1.62 | 2.87 | 2.32 | 1.68 | 0.79 | 1.39 | 1.13 |
| 23 | 3.28 | 1.97 | 1.85 | | 6.77 | 4.07 | 3.82 | | 2.30 | 1.39 | 1.30 | |
| 24 | 2.32 | 2.29 | 1.43 | 2.64 | 3.16 | 3.12 | 1.94 | 3.60 | 1.78 | 1.76 | 1.10 | 2.03 |
| 25 | 1.84 | 1.98 | 0.99 | | 1.84 | 1.98 | 0.99 | | 1.25 | 1.34 | 0.67 | |
| 26 | 0.84 | 1.79 | 0.60 | | 0.84 | 1.79 | 0.60 | | 0.84 | 1.79 | 0.60 | |
| 27 | 1.19 | 2.66 | 0.65 | 0.00 | 1.19 | 2.66 | 0.65 | 0.00 | 1.19 | 2.66 | 0.65 | 0.00 |
| 28 | 1.38 | 1.19 | 1.25 | | 2.33 | 2.01 | 2.12 | | 1.38 | 1.19 | 1.25 | |
| 29 | 1.84 | 2.88 | 1.20 | | 2.06 | 3.22 | 1.34 | | 1.32 | 2.07 | 0.86 | |
| 30 | 2.45 | 2.53 | 1.65 | 0.00 | 3.54 | 3.66 | 2.38 | 0.00 | 1.10 | 1.14 | 0.74 | 0.00 |
| 31 | 1.63 | 1.21 | 0.68 | | 1.76 | 1.31 | 0.73 | | 1.59 | 1.18 | 0.66 | |
| 32 | 1.23 | 1.57 | 0.85 | 0.94 | 1.39 | 1.77 | 0.96 | 1.06 | 1.23 | 1.57 | 0.85 | 0.94 |
| 33 | 2.55 | 3.31 | 1.30 | | 2.55 | 3.31 | 1.30 | | 1.92 | 2.49 | 0.98 | |
| 34 | 1.72 | 2.50 | 0.87 | 1.69 | 1.72 | 2.50 | 0.87 | 1.69 | 0.97 | 1.41 | 0.49 | 0.95 |
| 35 | 1.08 | 2.30 | 0.53 | | 1.08 | 2.30 | 0.53 | | 1.08 | 2.30 | 0.53 | |
| 36 | 1.74 | 0.88 | 0.52 | | 1.74 | 0.88 | 0.52 | | 1.00 | 0.51 | 0.30 | |
| 37 | 1.72 | 1.53 | 0.87 | | 2.04 | 1.81 | 1.03 | | 0.77 | 0.68 | 0.39 | |
| 38 | 1.58 | 1.98 | 0.87 | 2.00 | 1.58 | 1.98 | 0.87 | 2.00 | 0.75 | 0.95 | 0.42 | 0.96 |

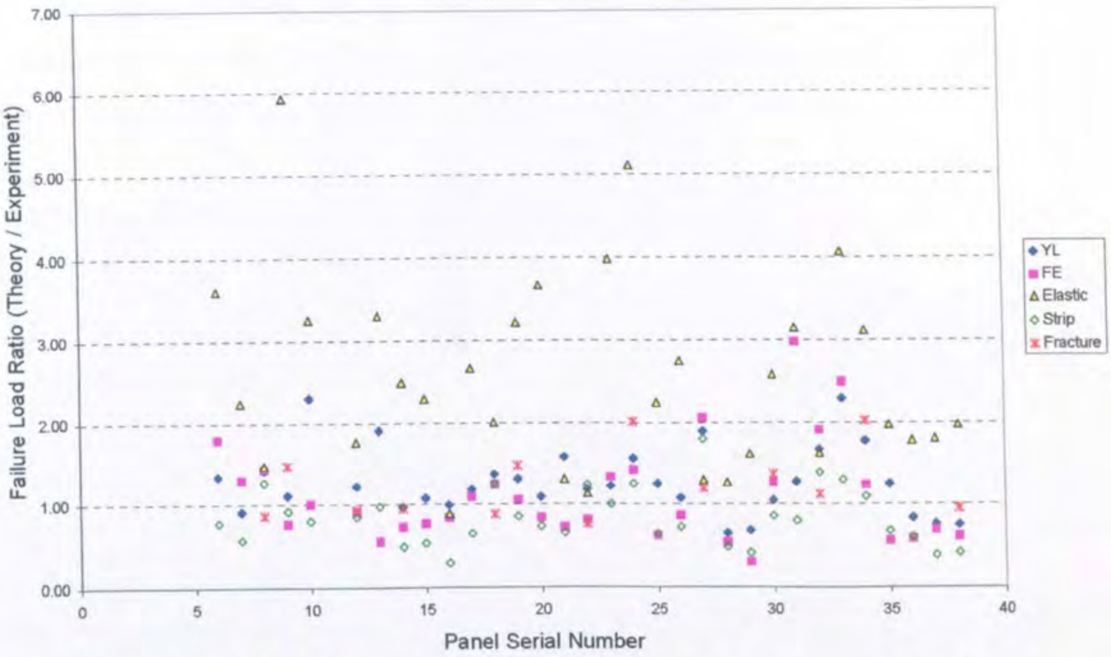


**Figure 3.12**: Ratios of Predicted Failure Strengths to Experimental Values

It could be accurately stated that the theoretical techniques performed differently for different types of panels. Yield Line method's predictions of ultimate failure loads for simply supported panels were very poor, while the method performed very well for other support conditions. The Fracture Line method attempts to improve the Yield Line method by taking material orthotropy into consideration. However, considering the results obtained by the two methods in this study, there was no apparent improvement in the predictions. The slight improvement noticed in the case of simply-supported panels is not enough to justify the extra tediousness of the resulting equations. Finite element analysis gave slightly better results than all other techniques reviewed in this study, with the exception of panels with built-in edges. However, as with other techniques, the predictions by Finite Element Analysis were inconsistent in the sense that some failure loads were over-estimated while others were under-estimated, and some by a factor larger than 2. Considering the amount of time spent on finite element modelling of the wall panels, the slight improvements are not justified unless in special cases where local strength values may be required, for example, when one is investigating a collapse. Elastic analysis performed very badly for all panels except for those simply supported on all edges. It is concluded that this method is not suitable for the analysis of clay-brick masonry wall panels built with conventional mortars. Strip method seemed to work relatively well for prediction of ultimate loads, though it also gave inconsistent results. Because of the simplicity of the Strip method, using it in the analysis of laterally loaded masonry panels would be relatively more efficient than using yield line or finite element methods.

The foregoing discussion clearly demonstrates the impossibility of drawing conclusions from the predictions of the existing theories, and illustrates the need to generate more test data and develop better prediction models.

### 3.6 CONCLUSIONS AND RECOMMENDATIONS

The following are the conclusions drawn from this review:

1. The methods used to predict lateral strength of wall panels are not consistent, and are unsafe in most cases. The predictions are sometimes random and cannot be easily correlated to test results.
2. Boundary conditions play a major role in the strength of masonry walls, and, results of theoretical methods can be greatly improved if a good representation of the boundary conditions can be made.
3. Different methods yield good approximations for different types of panels. The Strip method yields better results for rectangular panels as opposed to square panels, while Yield Line method gives better results for square panels than for rectangular panels. In general, the Yield Line method gives good predictions of ultimate load capacity of laterally loaded masonry panels.
4. There is not enough evidence to suggest that the use of more complex and tedious analysis techniques (such as Fracture Line method instead of Yield Line) improves predictions. Simple methods, such as Strip method, give reasonably good results, and with more efficiency.
5. A technique needs to be developed which enables the boundary conditions to be modified to reflect more truly actual rather than theoretical boundary conditions in walls.

It is recommended that:

1. More test data be generated, paying particular attention to boundary conditions.
2. Design of laterally-loaded masonry walls on the basis of the Yield line method be sustained (with great care) since all other currently known methods do not provide better solutions.
3. The possibility of applying more than one of the above-reviewed methods to derive a method of design be investigated.
4. The possibility of combining two or more of the above-reviewed methods with empirical methods be investigated.

# CHAPTER 4: TESTING PROGRAMME

## 4.1 INTRODUCTION

Codes of Practice for structural steelwork, concrete and timber, all include testing as an acceptable method of design, where calculations are not practicable or appropriate [Edwards, 1988], as does the code for masonry. Testing offers the opportunity to check the adequacy of existing structures, to base new structures on prototypes, and to improve analytical designs by incorporating real information on components into the calculations. The behaviour of the structure under test can be physically monitored and studied from the initial application of loads to collapse. Full-scale testing is, however, a luxury beyond the capacity of most structural practitioners in that it is clearly not possible to build a prototype bridge, dam, building, etc, and then test it to destruction in all situations. A more practical approach is, rather, to use a model of the full-size structure to determine the local stresses or loads so as to highlight vulnerable zones, and then to use full scale components to examine these critical areas. Such a philosophy was employed in this research by testing both wallettes and full-scale wall panels.

The prime motivation behind conducting experiments on models of structures is to minimise the costs; reductions coming from simpler loading equipment, reduced testing time and, ease of preparation and disposal of specimens after testing. In such experiments, it is essential to use standard models that have been proven to yield results representative of those of full-scale components, or models that can simulate as many scaleable non-dimensional parameters as possible. In the case of laterally loaded masonry walls, the British code BS5628: Part 1 [British Standards Institute, 1992] suggests standardised sizes of wallettes to be tested, as shown in Figure 4.1 and Figure 4.2. It recommends that in uni-axial flexure tests, the wallettes should be loaded with two line loads (four-point loading), oriented in such a way that the load is not applied directly over the mortar joints that are parallel to the load bearings. The four-point loading subjects the central portion of the panel to constant bending moment and zero shear force. Some researchers, amongst them Lawrence (1995) and Anderson (1982), have recommended that a horizontal orientation is more efficient if a state of pure bending is desired, especially for tensile loading perpendicular to the bed joints (vertical bending). However, since walls in real buildings have a vertical orientation, the vertical orientation approximates the real conditions in a better way, and has been adopted in the UK and Europe. This arrangement also allows forces and displacements to be measured with ease and accuracy, and deformations and crack propagations to be easily observed.

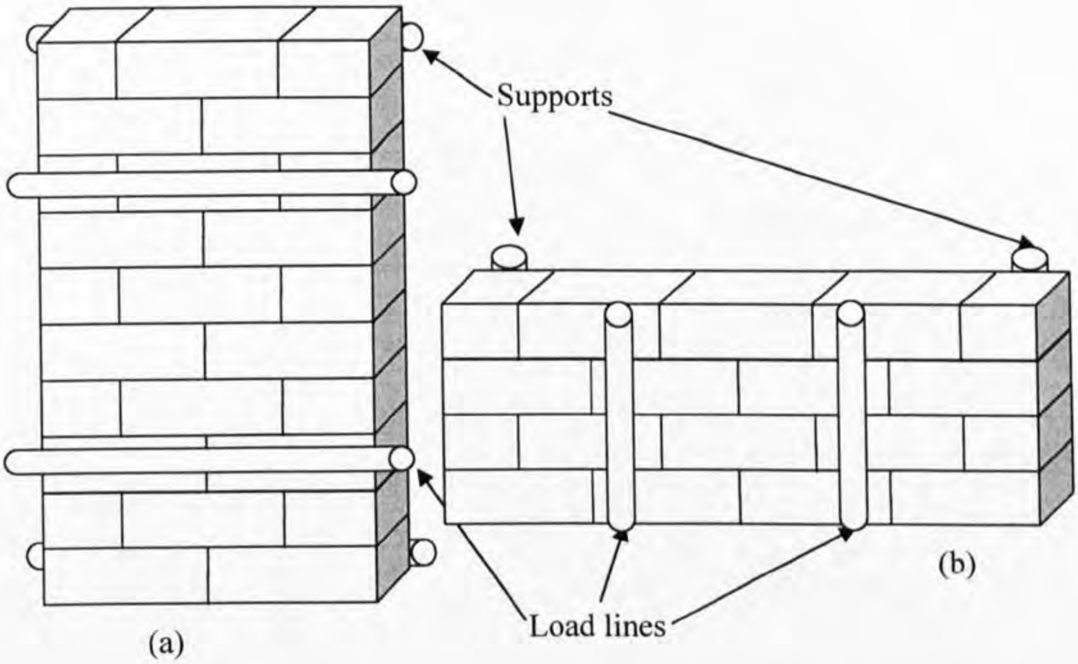


**Figure 4.1**: Brick wallettes for – (a) vertical bending test and, (b) horizontal bending test.

For tensile loading parallel to bed joints (horizontal bending), the load bearers are located as near as practicable midway between the nearest perpend joints, see Figures 4.1(b) and 4.2(b). The central region of the wallette is again subjected to constant bending moment and zero shear force. Unlike in the vertical bending tests, the upright orientation of the wallette in horizontal bending has less influence on the bending stresses, as the in-plane stress resulting from the effect of the self-weight is in a direction perpendicular to the bending stress being studied.

### 4.2.0 THE TESTS

Laboratory testing included 24 wallette specimens and two walls constructed using solid concrete blocks built using thin joint mortar. All blocks were 440mm long x 100mm wide x 215mm deep. Half of the specimens (one wall and twelve wallettes) were constructed using a "grey" block of strength 20N/mm$^2$ and density 1700kg/m$^3$ whilst the remainder were built using a "yellow" block of strength 14N/mm$^2$ and density 1400kg/m$^3$. Walls measured 2.65 x 1.75m and the wallettes were either 1.5 units long x 5 units high (665 x 1095mm) when tested about an axis parallel to the bed joints or 2.5 units long x 4 units high (1100 x 875mm high) when tested about an axis perpendicular to the bed joints (Figures 4.2(a) and (b)). Specimens were all built by an experienced mason at a brick/block producer in the Midlands in order to assess the potential of the process for prefabrication demonstrated by then transporting the specimens by lorry to Kingston University in SW London. The specimens were stored in the laboratory prior to testing.

In addition ten beams, constructed of the same grey blocks as above, were tested to determine the unit modulus of rupture (UMOR) of the blocks. A control test was also performed in order to determine the effects of the wallette test rig. All specimens and test procedures are described further in sections 4.2.1 – 4.2.4.

### 4.2.1 Wallette Testing

The sizes of the wallettes, as well as the testing procedure, complied with the recommendations of the British Standards Institution as outlined in BS 5628: Part 1, Appendix A.3, and conformed to BS EN 1052:2 [British Standards Institute, 1999].

In addition to the standard flexural test arrangement, deflection data was also obtained. Linear Variable Differential Transformers (LVDT's) were located at three points on each wallette, one near the mid-span and one near each support, see Figure 4.2. Magnetic bases attached the LVDT's to unloaded elements of the test rig. Loading was applied at a slow and repeatable rate using an hydraulic jack until failure of the specimen. With each test, the panel was initially loaded to 1 kN and left for 60 seconds before additional loading was applied. Displacement data was continuously gathered by data logger but only corroborated to load values at intervals of 0.5 kN. Curvatures of the wallettes were evaluated by subtracting the average displacement recorded by the LVDT's near the supports from the mid-span displacement. This information was used to determine other properties such as the flexural rigidity and the modulus of elasticity at different stress levels.

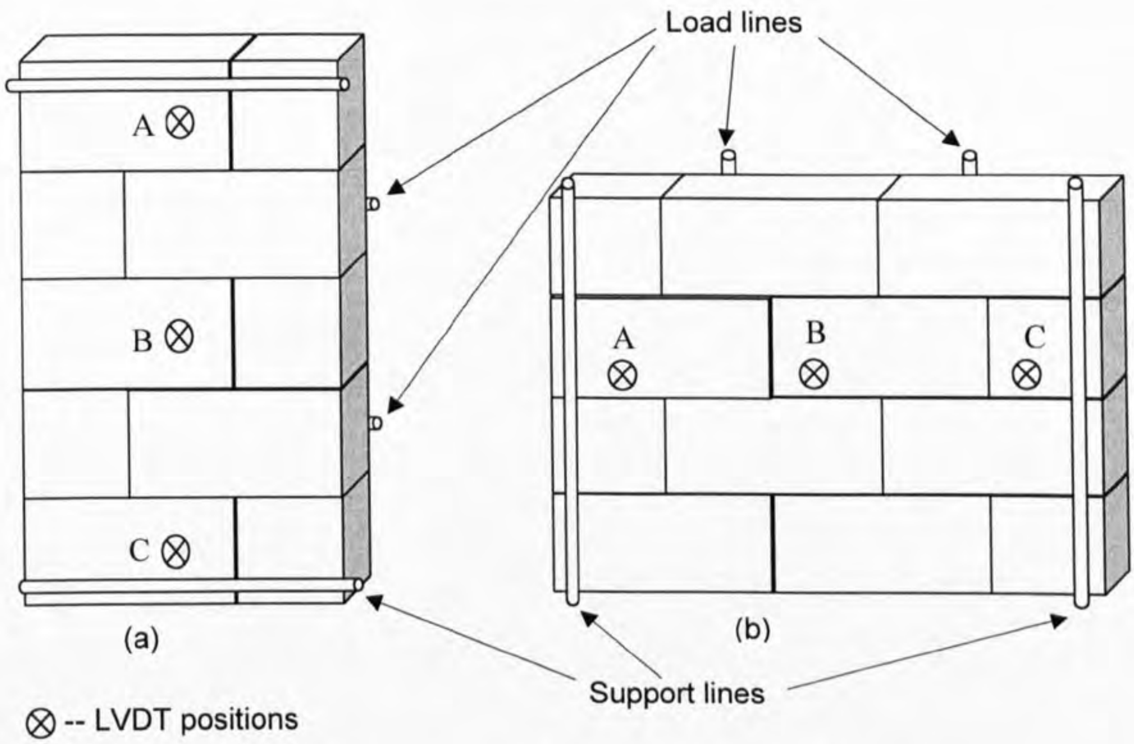


**Figure 4.2**: Block wallettes showing positions of LVDT's; (a) for vertical bending test, (b) for horizontal bending test

#### 4.2.2 Wall Testing

Figure 4.3 and section AA indicate a schematic view and section of the wall testing rig, with a wall in place. The all round simple support for the wall was provided using rubber hose attached to the bearing face of the test frame along all edges. The base of the wall was supported on a metal bearer designed to enable the wall to move laterally without restraint. Loading to the wall was uniformly distributed and provided by an air bag of similar area to the wall. Pressure was supplied by a pump and a data logger enabled the deformations of the front of the wall to be continuously monitored. One quarter of the wall was instrumented with LVDT's, their locations being shown in Figures 4.4 and 4.5. By assuming the walls behaved symmetrically, it was possible to determine the curvature along rows $R_1 - R_4$ or down columns $C_1 - C_5$ and, as with the wallettes, to use this information to determine the flexural rigidity and modulus of the material.

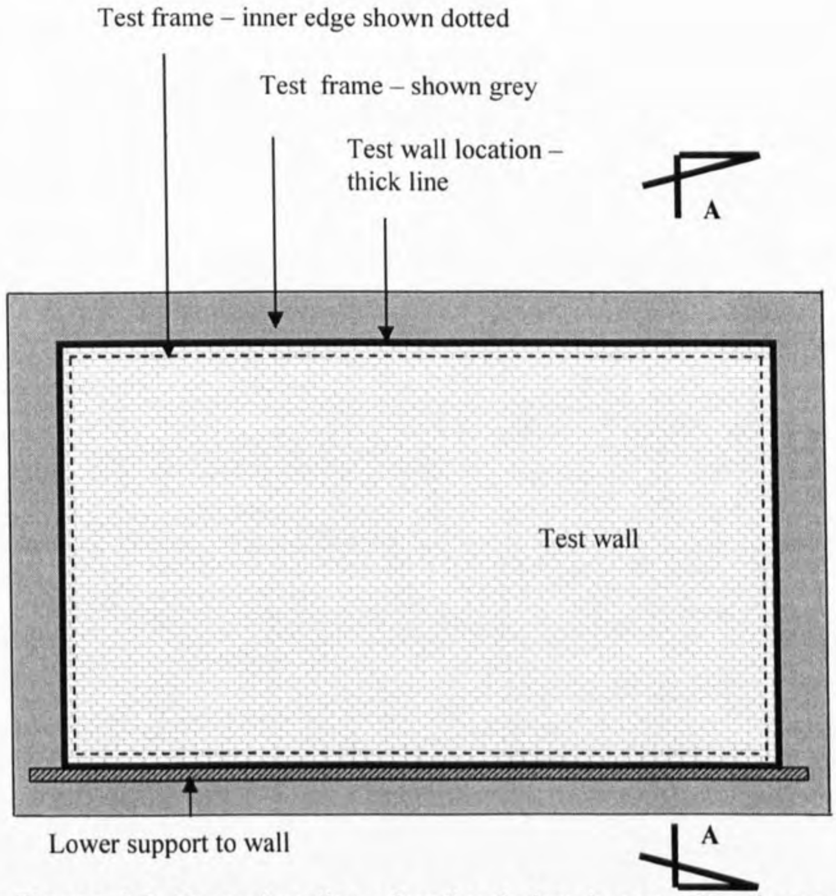


**Figure 4.3**: Rear elevation of wall not showing reaction frame

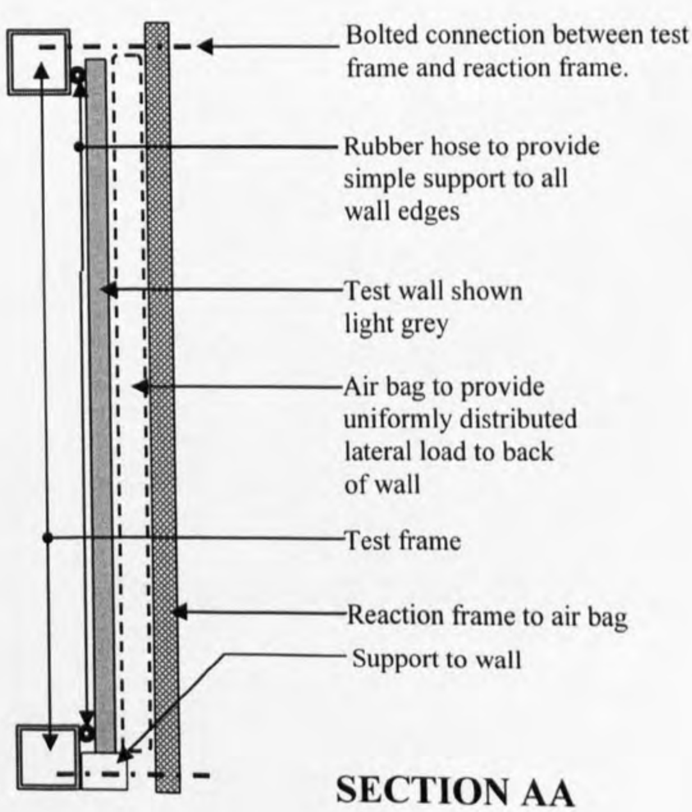

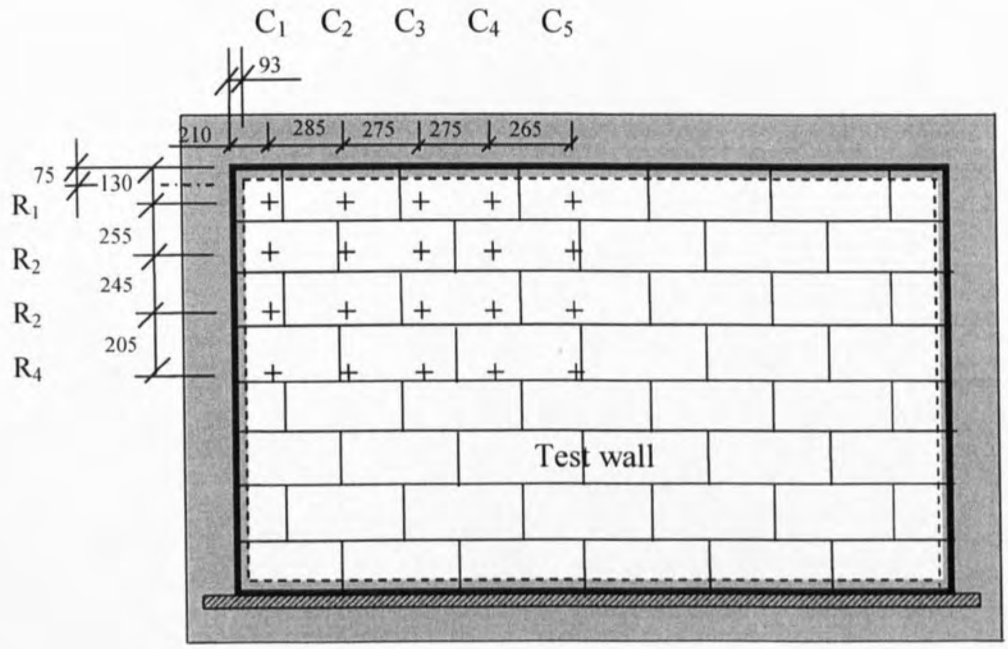


**Figure 4.4**: Location of LVDT's – Grey Wall

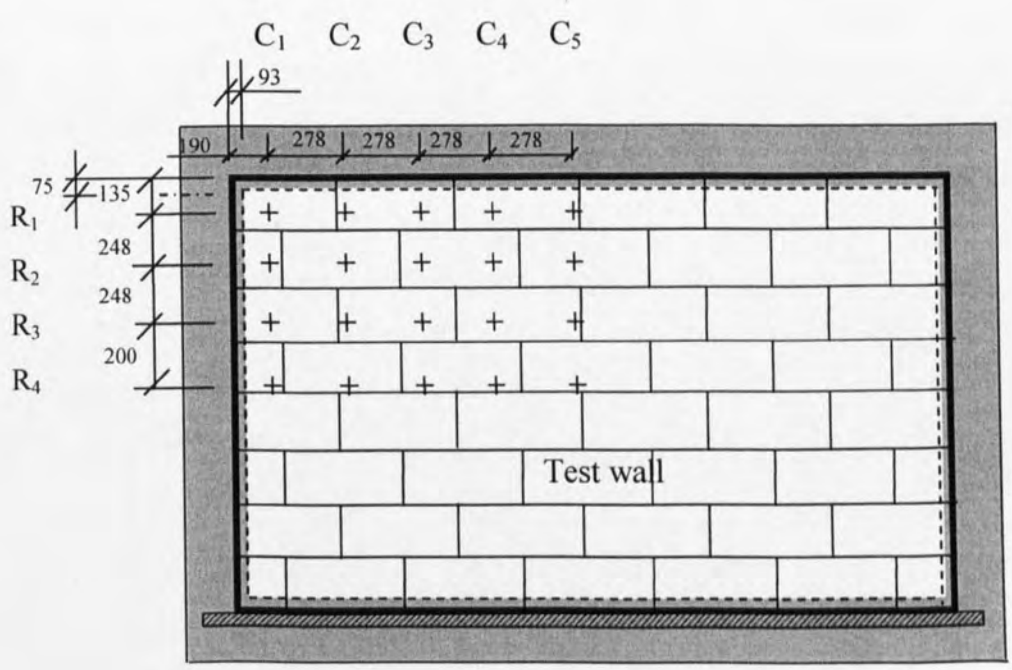


**Figure 4.5**: Location of LVDT's - Yellow Wall

### 4.2.3 Beam Testing

Following the wallette and wall tests, it was deemed relevant to determine the unit modulus of rupture (UMOR) of the blocks. Two types of beams were constructed using strong and quick-setting glue. In the Type-1 beam, blocks were attached end to end up their perpend faces, as shown in Figure 4.6(i). The beam was three blocks long, and a total of five beams were made. This beam enabled the horizontal UMOR of the material to be found. Type-2 beams were constructed by assembling the blocks as a stack bonded beam by gluing the bed joints together as shown in Figure 4.6(ii). Again, five of these beams were constructed. This second type of beam enabled the material UMOR to be determined in the vertical direction.

Testing of the beams was carried out as shown in Figure 4.7. The two ends were supported on smooth steel bearings and a central point load was applied using an hydraulic jack, attached to a data logger used to monitor the rate of load application and for recording the failure load. The load was gradually applied until failure of the beam occurred.

Beams similar to those described above and shown in Figure 4.6 (i) and (ii), were then constructed using thin-joint mortar in place of the super glue. The aim here was twofold: firstly to determine the UMOR of the blocks and secondly to determine whether the thin joint mortar utilised was stronger than the UMOR, which would imply the masonry behaves as a plate not conventional masonry, which de-bonds. The results of these tests are reported under section 4.3.

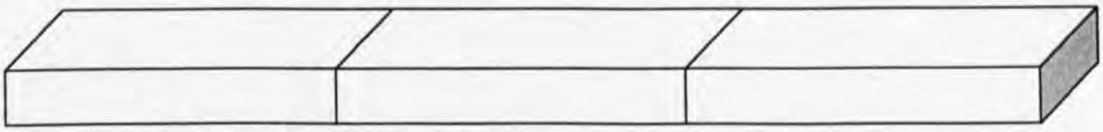

(i) Type-1 beam

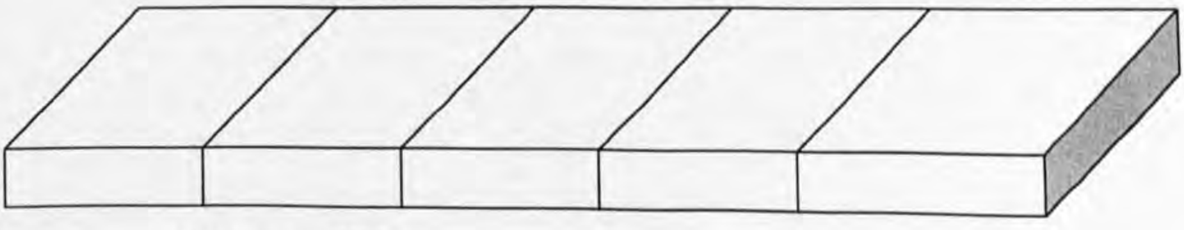

(ii) Type-2 beam

**Figure 4.6**: Block beams for determination of UMOR

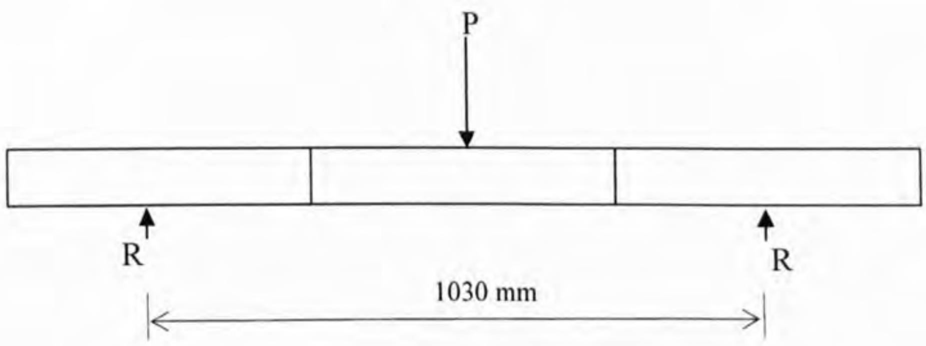


**Figure 4.7**: Beam test arrangement, Type-1 beam.

#### 4.2.4 Rig Calibration

In order to evaluate the effects of the test-rig used for wallette testing, a dummy test was carried out. The dummy test involved a rigid steel member of length 1.2 metres, with a square hollow cross-section of dimensions 200 mm by 200 mm by 10 mm thickness. The steel member was placed in the rig in a similar way to the wallettes, see Figure 4.8. Linear Variable Differential Transducers (LVDT's) were positioned at three different points on the steel member, as shown in Figure 4.9, then attached to the ground in order to measure the movement of the steel member relative to the ground. Due to the rigidity of the steel member, its displacements relative to the ground will be equal to those of the support members of the rig. Testing procedure similar to that of the wallettes was followed from this stage onwards. Two tests were performed, with the steel member placed in a horizontal position and then in a vertical position, as shown if Figures 4.8 and 4.9.

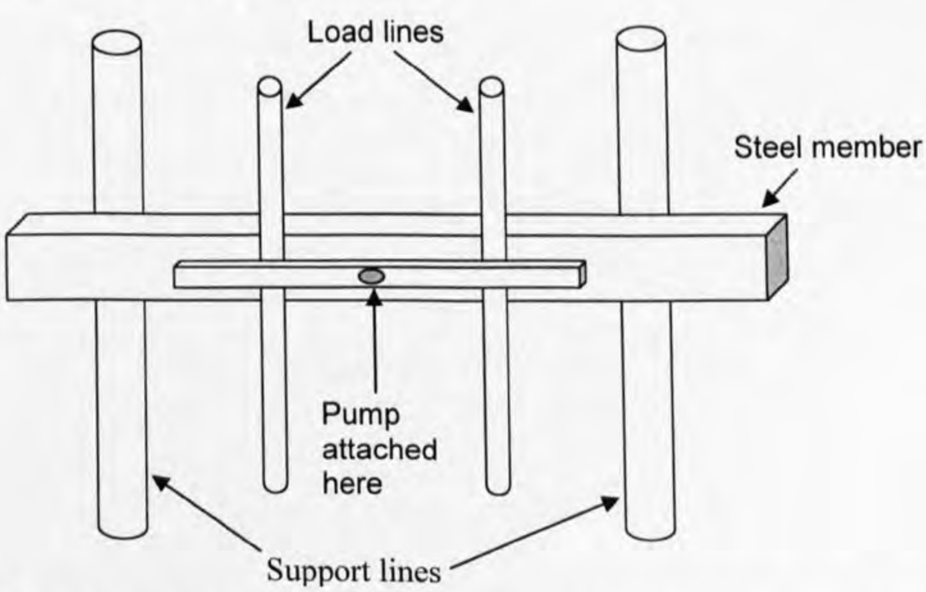


**Figure 4.8**: Rear view of the test rig with the rigid steel member placed in the horizontal position

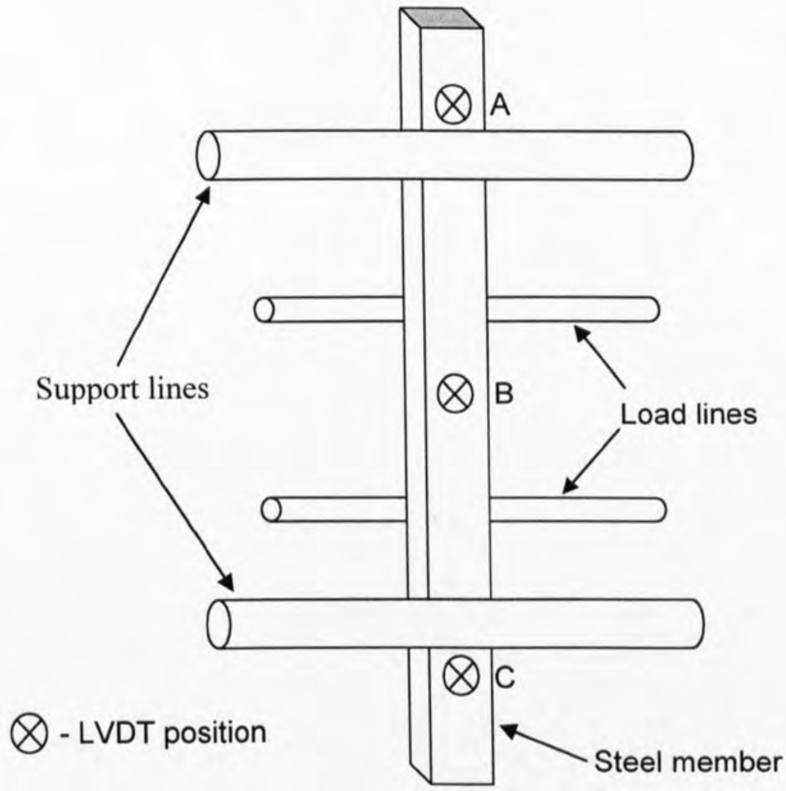


**Figure 4.9**: Front view of the test rig with the rigid steel member placed in the vertical position. Also notice the positions of the LVDT's.

## 4.3 TEST RESULTS

### 4.3.1 Grey Wallettes

B - Wallettes

The test results are summarised in Table 4.1, which presents failure loads, failure stresses and the positions of failure planes. Pictures of failed grey wallettes are displayed in Appendix 4(c), Slide 1 - 6. As can be seen from Table 4.1 and Slides 1 - 6, the failure planes in all of the wallettes ran through the blocks, and always within the region of constant maximum moment. In B-wallette number 4 (Table 4.1), the failure plane ran very close to the bed mortar joint, but close observation revealed that it still went through the units, as can be seen from Slide 4 in Appendix 4(c).

**Table 4.1**: Summary of B-wallette test results for grey unit types.

| Specimen reference number – Grey units | Load at failure (kN) | Stress at failure (N/mm$^2$) | Failure position |
|---|---|---|---|
| **B-wallette No. 1** | **9.5** | **1.03** | 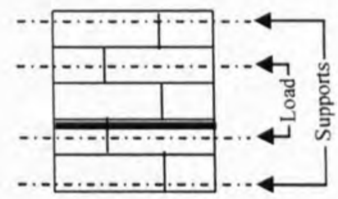 |
| **B-wallette No. 2** | **13.44** | **1.43** |  |
| **B-wallette No. 3** | **11.95** | **1.27** |  |
| **B-wallette No. 4** | **13.13** | **1.41** | 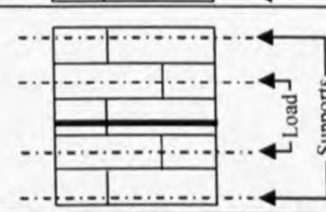 |
| **B-wallette No. 5** | **12.00** | **1.29** | 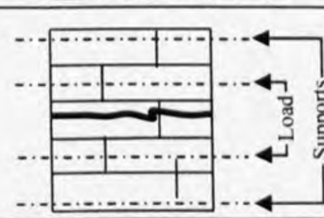 |
| **B-wallette No. 6** | **13.03** | **1.42** | 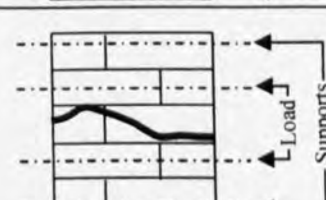 |
| **Averages** | **12.18** | **1.31** | |
| **Characteristic strength** | | **0.87** | |
| **Standard deviation** | | **0.15** | |

Load vs. displacement relationships for the grey wallettes tested in vertical bending are shown in Figure 4.10. It is observed that all of the graphs are nearly linear from the initial application of the load up to about one third (33%) of the ultimate load. For the range between one third and two thirds of the ultimate load, the graphs have an upward concave curvature. In the final third of the load range, the graphs again become almost linear, with steeper slopes. When the failure strength was reached, the wallettes failed instantaneously with an immediate and complete loss of strength.

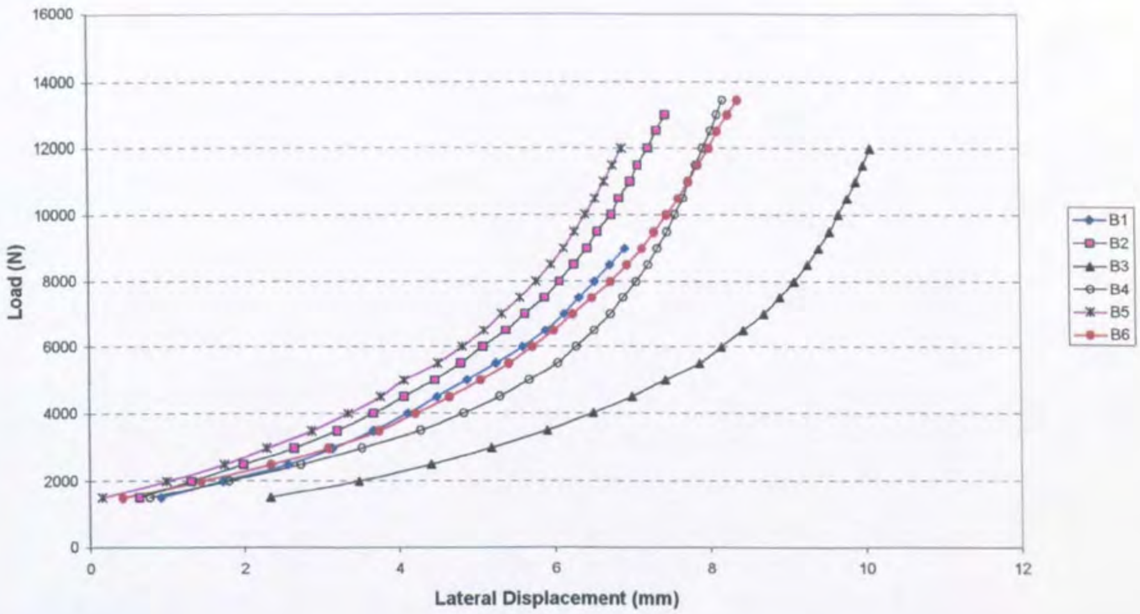


**Figure 4.10**: Load versus Displacement relationships for Grey wallettes tested in vertical bending.

P-Wallettes

The test results, together with the positions of failure planes, are summarised in Table 4.2. Pictures of the failed wallettes can be seen in Appendix 4(c), Slide 7 – 12. With the exception of P-wallette number 3 (Table 4.2), the failure planes in all wallettes ran vertically through the blocks in alternate courses, and very close to the block/mortar interface representing the perpend joints between the cracked blocks. For all wallettes, the failure plane was in the region of maximum and constant moment, that is, between the load lines. Wallette number 3 failed at a very low load, with the failure plane running diagonally through the second and third courses, as can be seen from Table 4.2. It was likely that material defects existed in the wallette before testing. For this reason, calculations of average strength and standard deviation were made both including and excluding the test value of this wallette, as noted under Table 4.2.

**Table 4.2**: Summary of P-wallette test results for grey unit types.

| Specimen reference number – Grey units | Load at failure (kN) | Stress at failure ($N/mm^2$) | Failure position |
|---|---|---|---|
| **P-wallette No. 1** | **15.06** | **1.47** | 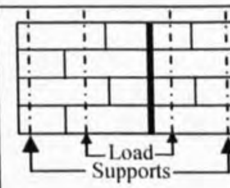 |
| **P-wallette No. 2** | **18.8** | **1.83** | 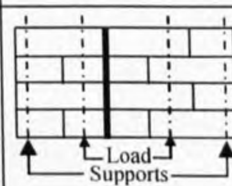 |
| **P-wallette No. 3** | **2.61** | **0.25** | 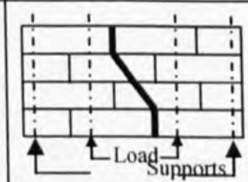 |
| **P-wallette No. 4** | **19.55** | **1.90** | 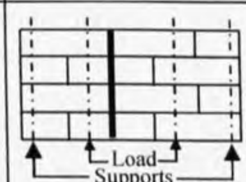 |
| **P-wallette No. 5** | **18.1** | **1.76** | 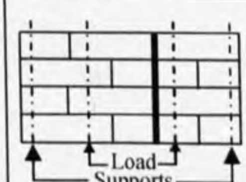 |
| **P-wallette No. 6 This wallette was not failed but the test discontinued for safety reasons** | **20.00** | **1.95** | 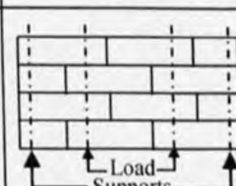 |
| **Averages** | **15.69 (18.30)** | **1.53 (1.78)** | |
| **Characteristic strength** | | **1.02 (1.19)** | |
| **Standard deviation** | | **0.65 (0.19)** | |

**Bracketed results exclude wallette No. 3.**

Observation of the failure planes revealed that even when the perpend joints were not fully filled, failure was never completely by de-bonding, as revealed by Slides 7 – 12 in Appendix 4(c). Rather, block material was always seen on either side of the failure plane.

Load vs. deformation relationships for the grey wallettes tested in horizontal bending are shown in Figure 4.11. All graphs, with the exception of P3, reveal an almost linear relationship from the application of load up to about one third (33%) of the failure load. Above this load, the graphs become non-linear until the failure strength is reached. However, the curvature maximises within the middle third of the graphs, while the top third is almost linear. Upon reaching the ultimate load, all wallettes failed instantaneously with an immediate and complete loss of strength.

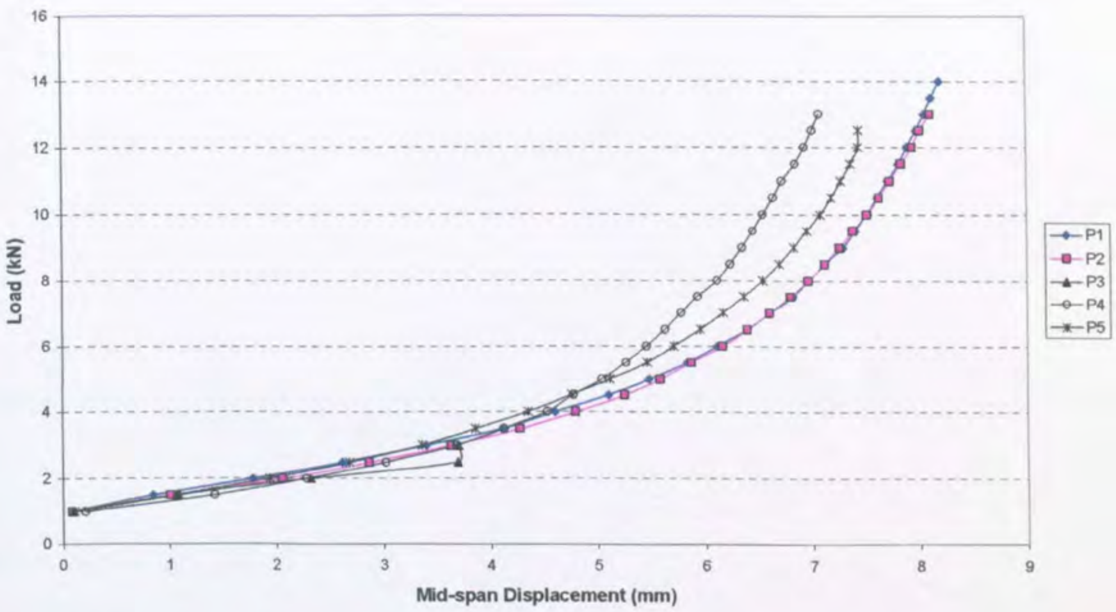


**Figure 4.11**: Load versus Displacement relationships for Grey P-wallettes (horizontal bending).

Figure 4.12 shows 'load versus displacement' relationship for P-wallette number 6 (Table 4.2). For this wallette, load was applied in three cycles: from 0 to 6 kN and then unloaded to 1 kN; then re-loaded up to 6 kN and unloaded again to 1 kN; and finally reloaded to failure. The graph shows that for the first cycle, the load-displacement relationship is almost linear up to 4 kN, thereafter becoming non-linear. For the second cycle, the graph is almost linear only up to 3.0 kN, and becomes non-linear for the rest of the loading history. There are, however, two linear sections for the final loading cycle; 0 – 2.5 kN, and 8 – 11.5 kN. Between 2 and 8 kN the graph shows an upward concave curvature. For safety reasons, testing of this wallette was terminated at 20 kN, that is, before failure was reached. Instrumentation was removed when a load of 12 kN was reached.

Discussions on the implications of the shapes of the graphs of Figure 4.8 - 4.12 are given under section 4.4.

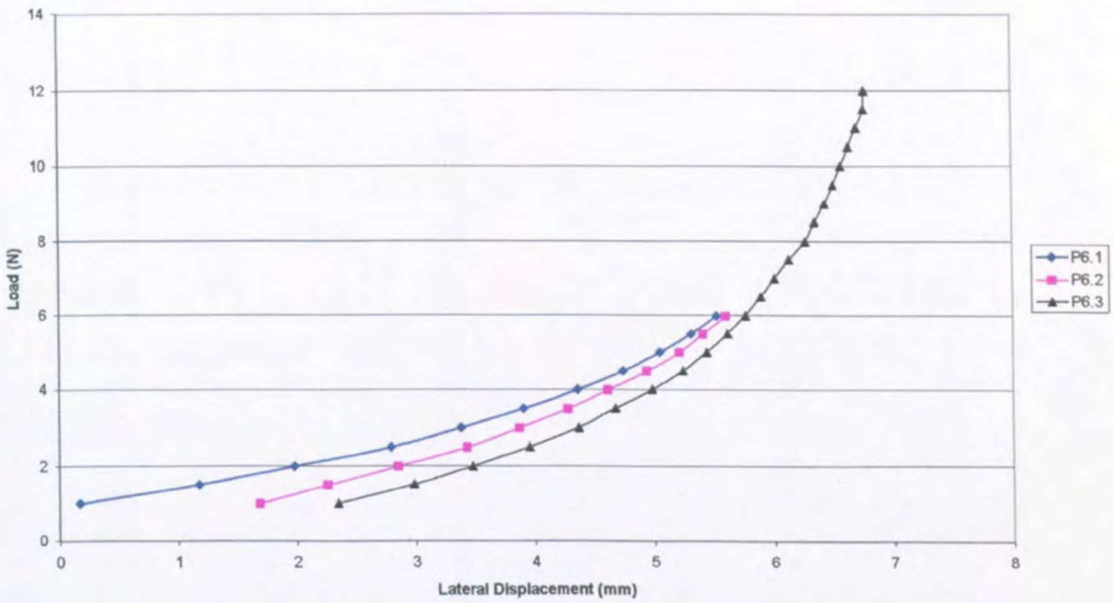


**Figure 4.12**: Load versus Displacement relationship for Grey wallette no.6 (tested in horizontal bending).

### 4.3.2 Yellow Wallettes

B-Wallettes

Table 4.3 summarises the test results, together with the positions of failure planes. Pictures of failed yellow wallettes are displayed in Appendix 4(c), Slide 13 - 18. Unlike with the grey blocks, the failure planes in the yellow wallettes ran very close to the mortar/block interface. With the exception of B-wallette No.1, all failure planes were within the region of constant maximum moment, that is, between the load lines. No Load-Deflection results were recorded for the yellow B-wallettes.

**Table 4.3**: Summary of B-wallette test results for yellow unit types.

| Specimen reference number – Yellow units | Load at failure (kN) | Stress at failure (N/mm$^2$) | Failure position |
|---|---|---|---|
| **B-wallette No. 1** | **7.18** | **0.78** | 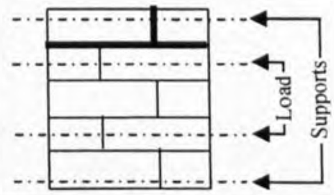  |
| **B-wallette No. 2** | **6.8** | **0.74** | 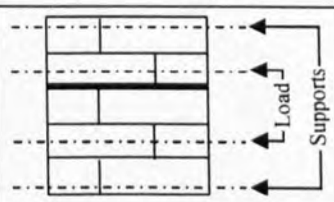  |
| **B-wallette No. 3** | **6.89** | **0.75** | 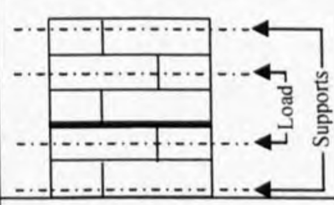  |
| **B-wallette No. 4** | **5.82** | **0.63** | 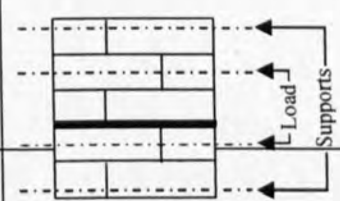  |
| **B-wallette No. 5** | **7.02** | **0.76** | 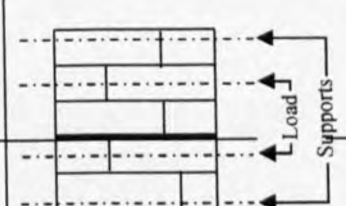  |
| **B-wallette No. 6** | **8.03** | **0.87** | 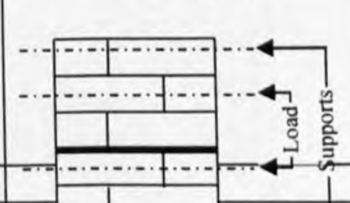  |
| **Averages** | **6.96** | **0.76** | |
| **Characteristic strength** | | **0.5** | |
| **Standard deviation** | | **0.08** | |

P-Wallettes

The test results, together with the positions of failure planes, are summarised in Table 4.4. All failure planes ran vertically through alternate block courses, and very close to the block/mortar interface for the intermediate courses. For all wallettes, the failure plane was in the region of maximum and constant moment, that is, between the load lines.

**Table 4.4**: Summary of P-wallette test results for yellow unit types.

| **Specimen reference number – Yellow units** | **Load at failure (kN)** | **Stress at failure ($N/mm^2$)** | **Failure position** |
|---|---|---|---|
| **P-wallette No. 1** | **12.5** | **1.22** | 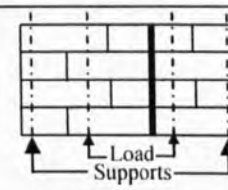  |
| **P-wallette No. 2** | **13.75** | **1.34** | 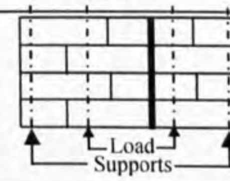  |
| **P-wallette No. 3** | **12.25** | **1.19** | 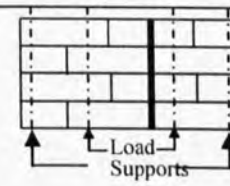  |
| **P-wallette No. 4** | **10.68** | **1.04** | 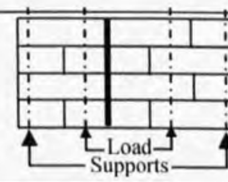  |
| **P-wallette No. 5** | **12.52** | **1.22** | 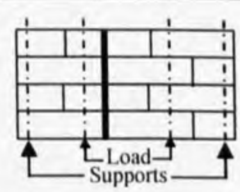  |
| **P-wallette No. 6** | **11.5** | **1.12** | 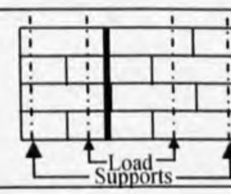  |
| **Averages** | **12.2** | **1.19** | |
| **Characteristic strength** | | **0.79** | |
| **Standard deviation** | | **0.1** | |

Pictures of failed wallettes are displayed in Appendix 4(c), Slide 19 - 24. Observation of the failure planes revealed that there was interface de-bonding between units and mortar in alternate courses, but not completely as some block material was always seen on either side of the failure plane.

Load vs. deformation relationships for the yellow wallettes tested in horizontal bending are shown in Figure 4.13. All graphs reveal an almost linear relationship from the application of load up to about one third (33 %) of the failure load. With the exception of P4 graph, the graphs are non-linear for the middle third of the loading history. In the final third of the load range the graphs become linear again until failure is reached. Failure of the wallettes was brittle and instantaneous, resulting in complete loss of strength.

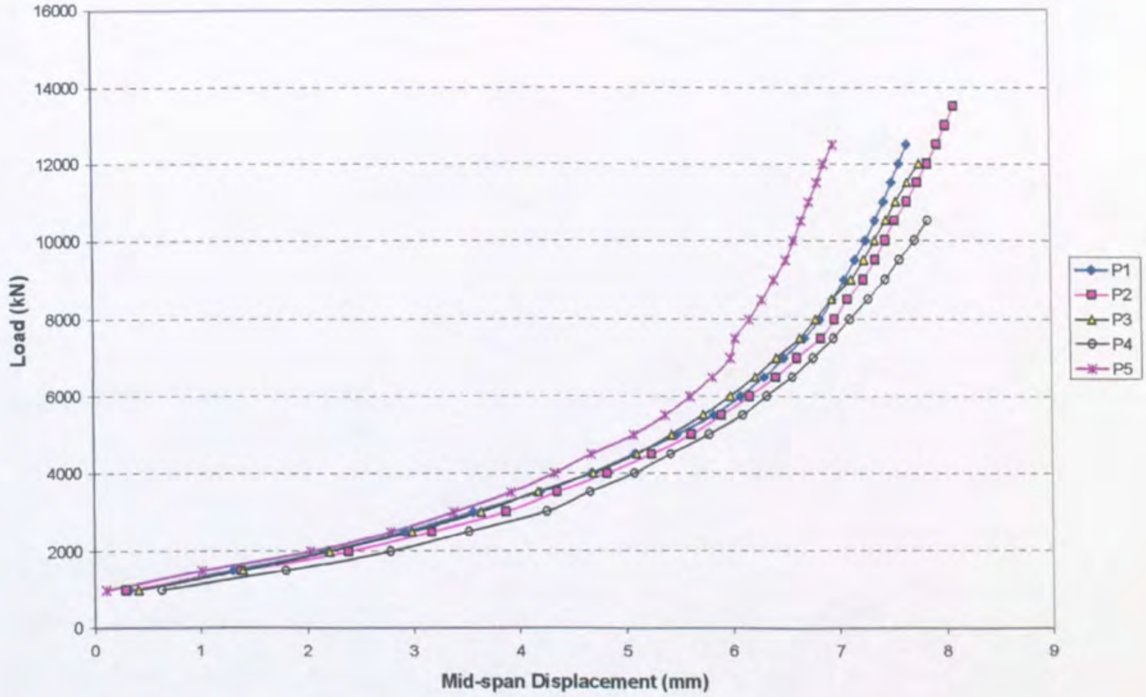


**Figure 4.13**: Load – Displacement relationships for yellow P-wallettes

Figure 4.14 shows the load vs. displacement relationship for P-wallette number 6 (Table 4.4). For this wallette, load was applied in three cycles: from 0 to 6 kN and then unloaded to 1 kN; then re-loaded up to 6 kN and unloaded again to 1 kN; and finally reloaded to failure. The graph shows that for the first cycle, the load-deformation relationship is almost linear up to 3.5 kN and then becomes non-linear. For the second cycle, the graph is almost linear only up to 2.5 kN, and becomes non-linear for the rest of the loading history. For the final cycle, there is a linear portion at the start, 0 – 2.5 kN, and at the end, of the graph, 8 – 11.5 kN. In between these regions, the graph is non-linear. Failure occurred by brittle and instantaneous mode at a load of 11.5 kN, resulting in complete loss of strength.

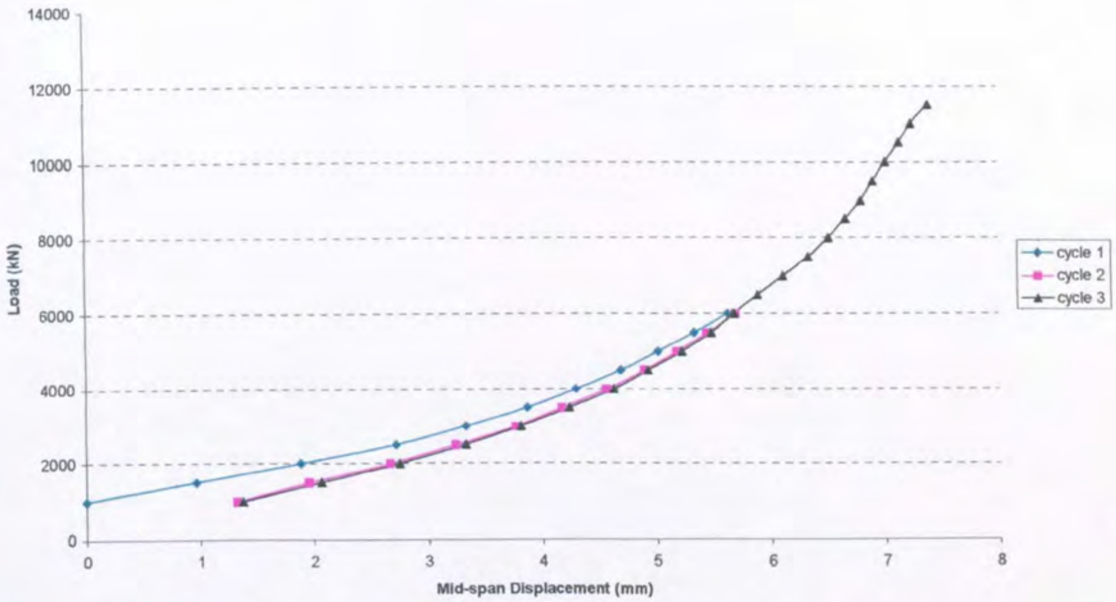


**Figure 4.14**: Load vs. Displacement graphs for yellow wallette no.6 (tested in horizontal bending)

### 4.3.3 Grey Wall

Load vs. deformation results at the centre of the wall are shown in Figure 4.15, and the wall crack pattern is shown in Figure 4.16. The initial crack in the grey wall occurred at a uniformly distributed load of 7.2kN/m$^2$ and a central displacement of 9.93 mm, and affected the left half of the wall. The crack occurred instantaneously and immediately the central displacement increased to 11.5 mm resulting in a pressure drop of 3kN/m$^2$. The pressure was then increased and a second crack occurred at the same load of 7.2kN/m$^2$ and a displacement of 14.36 mm. This crack affected the right hand side of the panel, was again instantaneous and resulted in the displacement increasing to 15.41 mm with a corresponding pressure loss of 1.7kN/m$^2$. At this point the LVDT's were removed and central deflection was estimated from this point forward. A third and fourth crack occurred at loads of 6.9 and 7.9 kN/m$^2$ respectively, the location of the cracks being as indicated in Figure 4.16 and the pattern as shown in Slide 29 of Appendix 4(c). With both cracks, the wall shifted outwards and there was a pressure loss to 4.2kN/m$^2$. Thereafter, increasing displacements occurred under a reasonably constant pressure of 4.2kN/m$^2$.

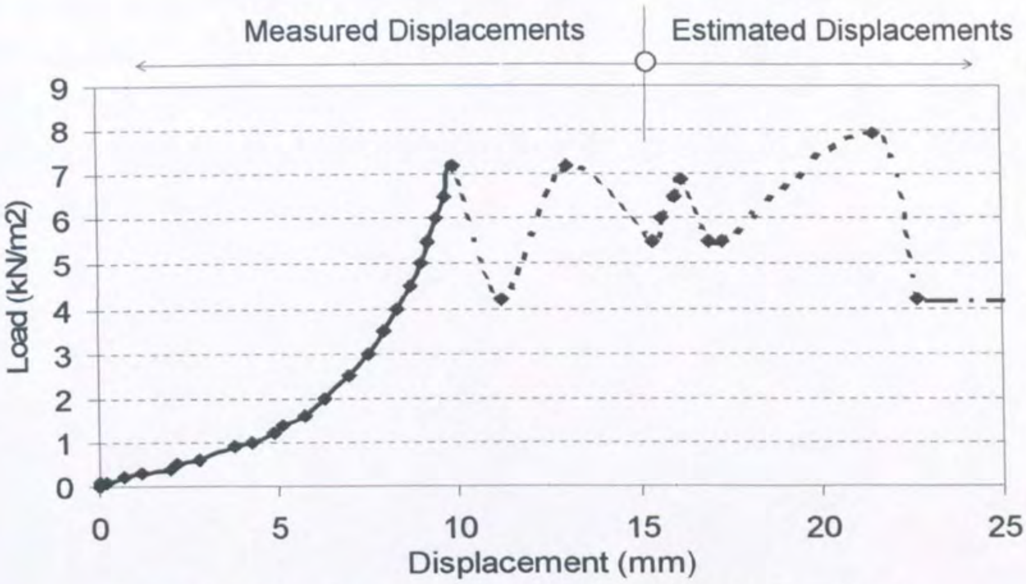


**Figure 4.15**: Load versus Central Displacement – Grey Wall

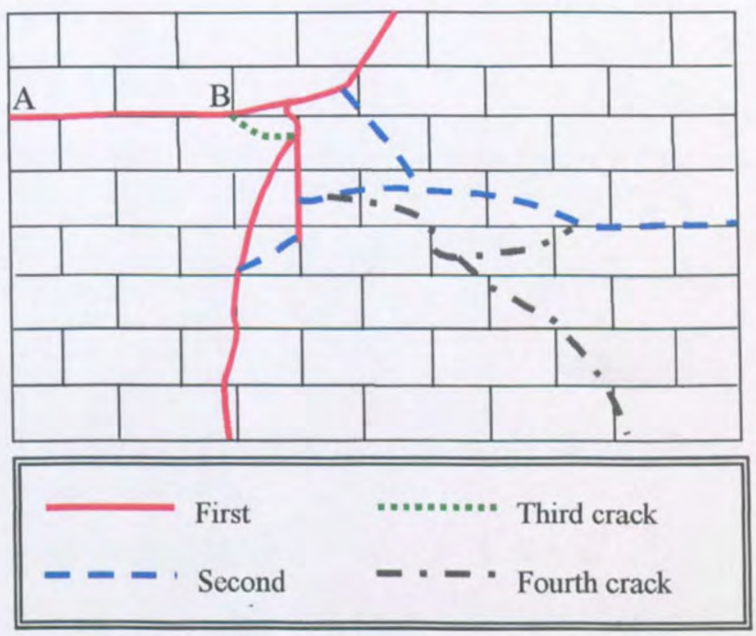


**Figure 4.16**: Crack pattern – Grey Wall

### 4.3.4 Yellow Wall

Load vs. deformation results at the centre of the wall are shown in Figure 4.17, and the wall crack pattern is shown in Figure 4.18. Slide 31 in Appendix 4(c) shows a picture of the wall with the cracks highlighted with a red marker. The first crack appeared instantaneously in the wall at a load of 6.0 kN/m$^2$, and a central displacement of 7.74 mm as shown in Figure 4.17. This crack pattern consisted of a horizontal crack at mid-height, running across the entire span, and two vertical cracks that initiated from the horizontal crack and terminated at the top and bottom edges of the panel, see Figure 4.18. The wall continued moving outwards to a new displacement of 15.82 mm. At this point the cracks had widened and the pressure dropped to 2.9kN/m$^2$, but was subsequently increased to 4.0kN/m$^2$. The test was terminated with a central displacement of 21.05 mm and wider cracks, without any other crack pattern having formed.

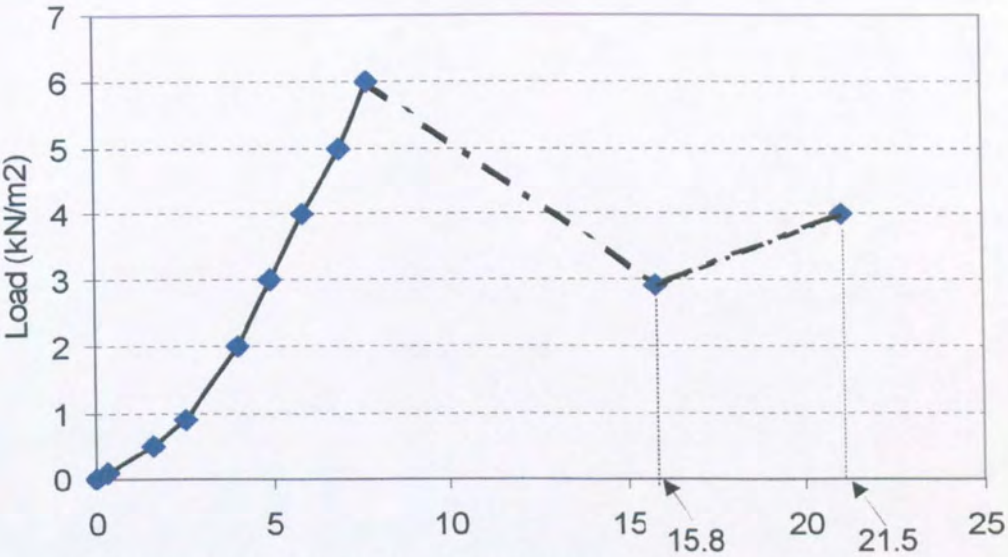


**Figure 4.17**: Load versus Central Displacement – Yellow Wall

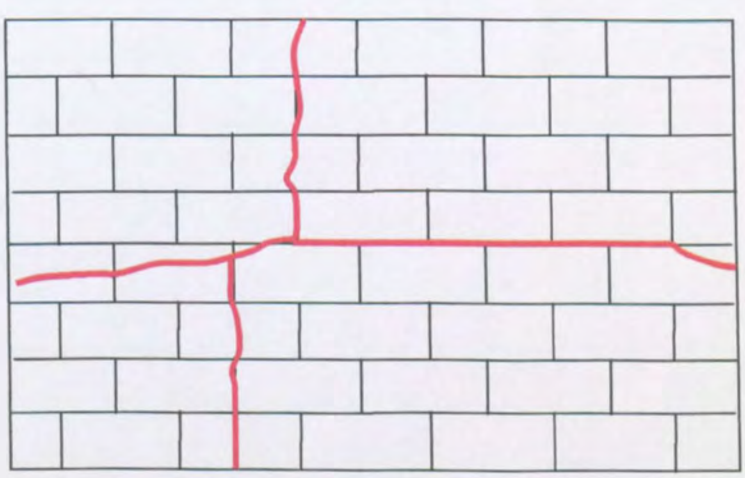

**Figure 4.18**: Crack pattern – yellow wall

### 4.3.5 Unit Modulus of Rupture Tests

#### 4.3.5.1 Single-Block Tests

Results of flexural tests performed on single grey blocks are presented in Table 4.5. The test set-up is shown in Figure 4.19.

**Table 4.5**: Failure stresses for single Grey blocks

| Block No. | Failure Load, P (kN) | Bending Moment, M (kNm) | Bending Stress, $\sigma_b$ (N/mm^2) |
|---|---|---|---|
| 1 | 8.440 | 822.900 | 2.244 |
| 2 | 8.340 | 813.150 | 2.218 |
| 3 | 8.040 | 783.900 | 2.138 |
| 4 | 9.040 | 881.400 | 2.404 |
| 5 | 8.540 | 832.650 | 2.271 |
| | | Mean Stress | 2.255 |
| | | Std Deviation | 0.10 |

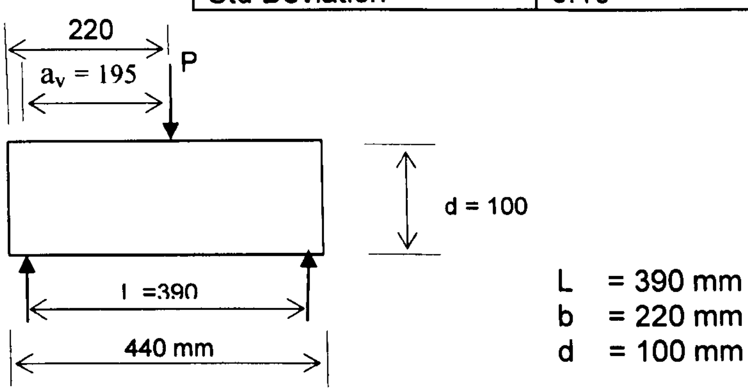


**Figure 4.19**: Flexural Test Set-up for single blocks

#### 4.3.5.2 Type-1 Beams

Type-1 beams, built using grey blocks, were three blocks long, attached end to end up their perpend faces, as shown in Figure 4.6(i), and tested as described in section 4.2.3. Table 4.6 presents the results for Type-1 beams made using super glue, and those for beams built with thin joint mortar are presented in Table 4.7.

**Table 4.6**: Failure stresses for glued Grey blocks

| Beam No. | Failure Load (kN) | Bending Moment (kNm) | Bending Stress (N/mm^2) | Comments |
|---|---|---|---|---|
| 1 | 3.074 | 0.792 | 2.159 | Middle block ruptured |
| 2 | 3.104 | 0.799 | 2.180 | middle block ruptured |
| 3 | 3.110 | 0.801 | 2.184 | middle block ruptured |
| 4 | 2.984 | 0.768 | 2.096 | middle block ruptured |
| 5 | 3.214 | 0.828 | 2.257 | middle block ruptured |
| | | Mean Stress | 2.175 | |
| | | Std. Deviation | 0.058 | |

**Table 4.7**: Failure stresses for Type-1 beams made using thin joint mortar – grey units

| Beam No. | Failure Load (kN) | Bending Moment (kNm) | Bending Stress (N/mm^2) | Comments |
|---|---|---|---|---|
| 1* | 0.994 | 0.256 | 0.698 | debonded at 1 joint |
| 2* | 1.244 | 0.320 | 0.874 | debonded at 1 joint |
| 3* | 1.534 | 0.395 | 1.077 | debonded |
| 4** | 1.444 | 0.372 | 1.014 | debonded |
| 5** | 1.394 | 0.359 | 0.979 | debonded |
| | | Mean Stress | 0.928 | |
| | | Std. Deviation | 0.148 | |

* Tested after 5 days
** Tested after 7 days

### 4.3.6 Type-2 Beams

Type-2 beams were described in section 4.2.3, and their configuration shown in Figure 4.6(ii). Table 4.9 summarises the test results for Type-2 beams constructed using thin joint mortar with grey units.

**Table 4.8**: Failure stresses for Type-2 beams made using thin joint mortar – grey units

| Beam No. | Failure Load (kN) | Bending Moment (kNm) | Bending Stress (N/mm^2) | Comments |
|---|---|---|---|---|
| 1* | 3.294 | 0.692 | 0.943 | de-bonded |
| 2* | 3.004 | 0.631 | 0.860 | de-bonded |
| 3** | 1.194 | 0.251 | 0.342 | de-bonded |
| 4** | 2.454 | 0.515 | 0.703 | de-bonded |
| 5** | 1.994 | 0.419 | 0.571 | de-bonded |
| | | Mean Stress | 0.684 | |
| | | Std. Deviation | 0.239 | |

* Tested after 5 days
** Tested after 7 days

### 4.3.7 Rig Calibration

The results of the dummy test are presented in Table 4.9 and Table 4.10.

**Table 4.9**: Movement of the test rig relative to the ground – horizontal position

| Load (kN) | Dial Gauge Readings (mm) A | B | C | Displacement (mm) A | B | C |
|---|---|---|---|---|---|---|
| 1 | 11.200 | 5.270 | 10.390 | 0.000 | 0.000 | 0.000 |
| 3 | 11.203 | 5.271 | 10.391 | 0.003 | 0.001 | 0.001 |
| 5 | 11.208 | 5.272 | 10.391 | 0.008 | 0.002 | 0.001 |
| 7 | 11.212 | 5.275 | 10.392 | 0.012 | 0.005 | 0.002 |
| 9 | 11.214 | 5.272 | 10.410 | 0.014 | 0.002 | 0.020 |
| 11 | 11.217 | 5.275 | 10.415 | 0.017 | 0.005 | 0.025 |
| 13 | 11.218 | 5.281 | 10.416 | 0.018 | 0.011 | 0.026 |
| 15 | 11.220 | 5.281 | 10.416 | 0.020 | 0.011 | 0.026 |

**Table 4.10**: Movement of the test rig relative to the ground – vertical position

| Load | Dial Gauge Readings (mm) | | | Displacement (mm) | | |
|---|---|---|---|---|---|---|
| (kN) | A | B | C | A | B | C |
| 1 | 11.240 | 5.290 | 10.380 | 0.000 | 0.000 | 0.000 |
| 3 | 11.242 | 5.280 | 10.380 | 0.002 | -0.010 | 0.000 |
| 5 | 11.243 | 5.290 | 10.381 | 0.003 | 0.000 | 0.001 |
| 7 | 11.243 | 5.292 | 10.382 | 0.003 | 0.002 | 0.002 |
| 9 | 11.242 | 5.292 | 10.382 | 0.002 | 0.002 | 0.002 |
| 11 | 11.243 | 5.294 | 10.381 | 0.003 | 0.004 | 0.001 |
| 13 | 11.243 | 5.294 | 10.382 | 0.003 | 0.004 | 0.002 |
| 15 | 11.244 | 5.295 | 10.384 | 0.004 | 0.005 | 0.004 |

## 4.4 ANALYSIS OF RESULTS

### 4.4.1 Wallettes

The LVDT's in the Rig Calibration tests recorded values of displacements in the order of one thousandth of a millimetre, see Table 4.9 and Table 4.10. These results confirm that the assumption of rigid supports of the rig is reasonably accurate. Thus, the LVDT readings recorded from the wallette tests are treated as absolute values, without any normalization being applied.

Data collected from wallette tests was used to plot the load-deflection graphs presented in Figures 4.10 to 4.14. Some points of interest about the graphs are noted. The shapes of the Load – Displacement graphs for both the grey and yellow-block wallettes are similar. All graphs show a near linear relationship between load and deflection for values of load below 33% of the ultimate. Above this load, the graphs display a non-linear relationship between the load and deflection until about 67% of the failure load is reached. In the final third of the loading history the graphs become almost linear again. Figure 4.20 shows a typical graph of one of the wallettes (Grey P-wallette No.2), highlighting the three regions described here. At failure, the load immediately dropped to zero showing that there was no reserve of strength after cracking, and that classic brittle failure had resulted.

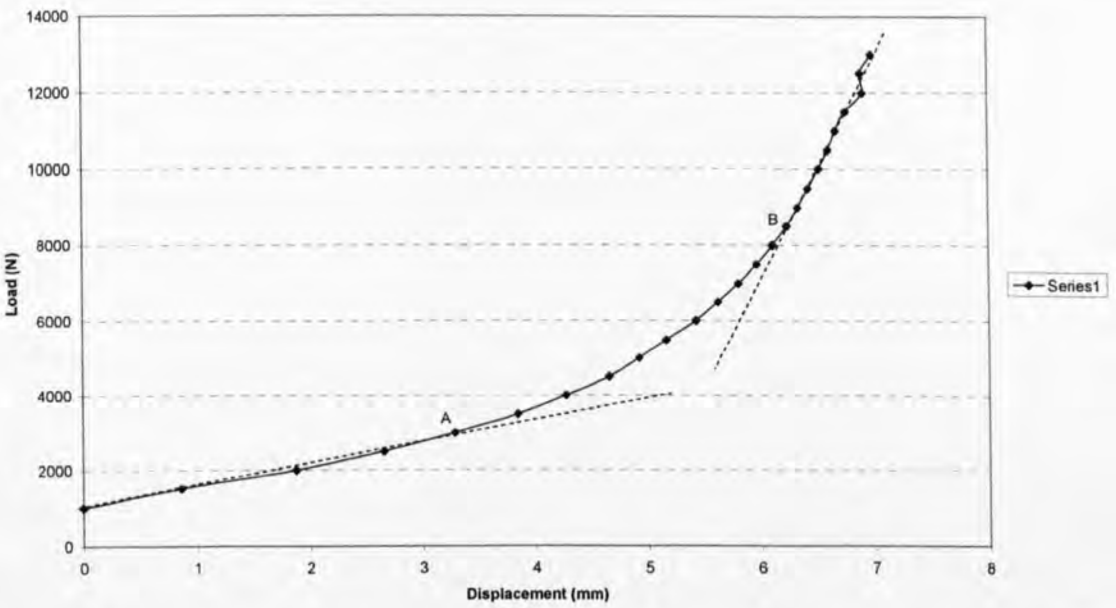


**Figure 4.20**: Typical Load – Deformation relationship for Thin-jointed Block wallettes tested at Kingston University.

The Load/Deformation graphs for the block wallettes tested in this project differ from typical graphs obtained for wallettes built from conventional mortars. Typical load-deformation response of conventionally constructed block wallettes was shown in Figure 3.1. In such wallettes, the initial linear elastic relationship is due to the fact that under low tensile stresses, cracks have not yet formed in the material, or if they have formed, their influence on the mechanical response of the material is not noticeable [Karihaloo, 1995]. With an increase in applied tensile stress, micro-cracks form at the mortar/block interface leading to non-linearity and stiffness reduction in region AB in Figure 3.1. For the thin-jointed block wallettes tested in this work, very different behaviour is observed. The Load - Displacement curve is initially near linear, then there is a non-linear part to the curve where stiffness increases, and finally another linear part until failure is reached, see Figure 4.20. Of paramount importance is the stiffness gain in the non-linear region. The stiffness gradually increases until it reaches a certain value (point B in Figure 4.20), and maintains this value until the failure stress is reached. It may be argued, therefore, that during initial stages of application of the load (region OA) there is very little micro-cracking, if any, in the material. It is postulated that the non-linear region of the graph (region AB) is a result of some weaker parts of the bond progressively failing, while the stronger parts are just beginning to get involved in the response of the joint, hence the observed stiffness enhancement. It appears, therefore, that when forming mortar joints using thin joint technology, the strength of bonding over the face varies. With load, the weaker areas fail but, overall, the remaining bond is stronger and stiffer than the failed parts, resulting in the unusual behaviour. With the grey units, the remaining stronger areas of bond are even stronger than the units, resulting in the units rupturing before de-bonding can take place. For the yellow units, the bond strength appears to be less than the Unit Modulus of Rupture (UMOR) of the units since de-bonding is visibly evident. With both units the weaker parts of the joint do not contribute significantly to its strength.

In Figures 4.21 and 4.22, deflections of the wallette-centre relative to two points close to the supports (points A and C, Figure 4.2) are displayed for P-wallettes. It can be clearly seen from these figures that the material reveals strong characteristics of linear behaviour from initial loading to collapse. Figure 4.23 displays the 'Load versus Relative Displacement' relationships for Grey B-wallettes. With the exception of wallette number 6, all other wallettes consistently show an increase of relative displacement with load increment. Linear characteristics are not revealed by the graphs of Figure 4.23, with the exception of graph B1, that is, for B-wallette number 1. It is noted again that no load/Displacement data was recorded for Yellow B-wallettes.

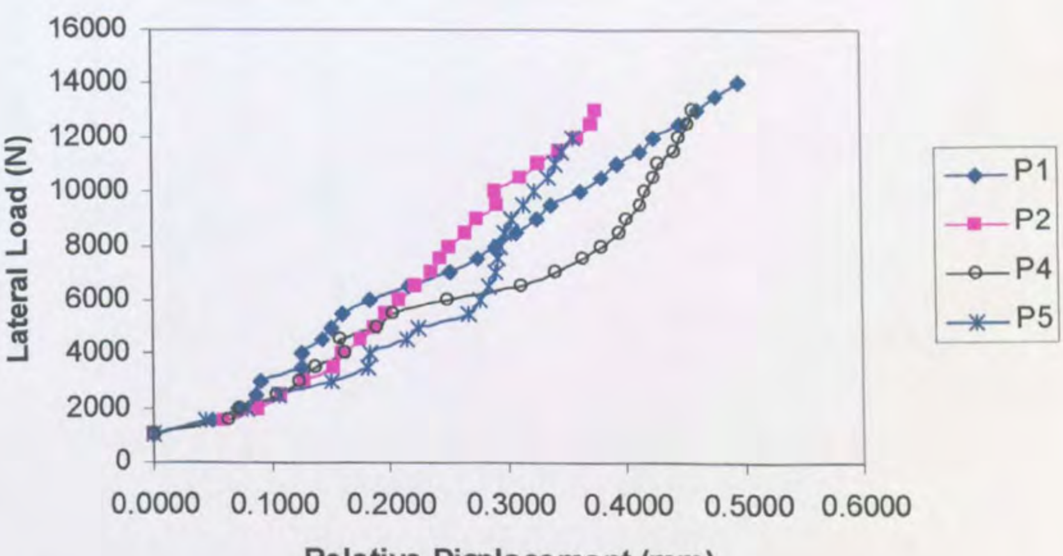


**Figure 4.21**: Displacement of Wallette Centre relative to outer points – Grey P-wallettes

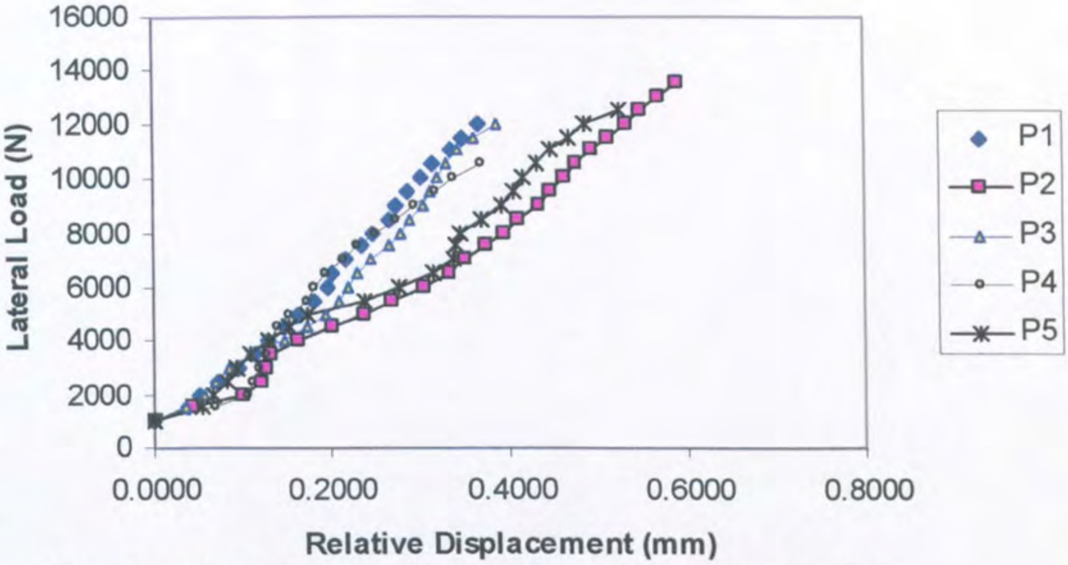


**Figure 4.22**: Displacement of Wallette Centre relative to outer points – Yellow P-wallettes

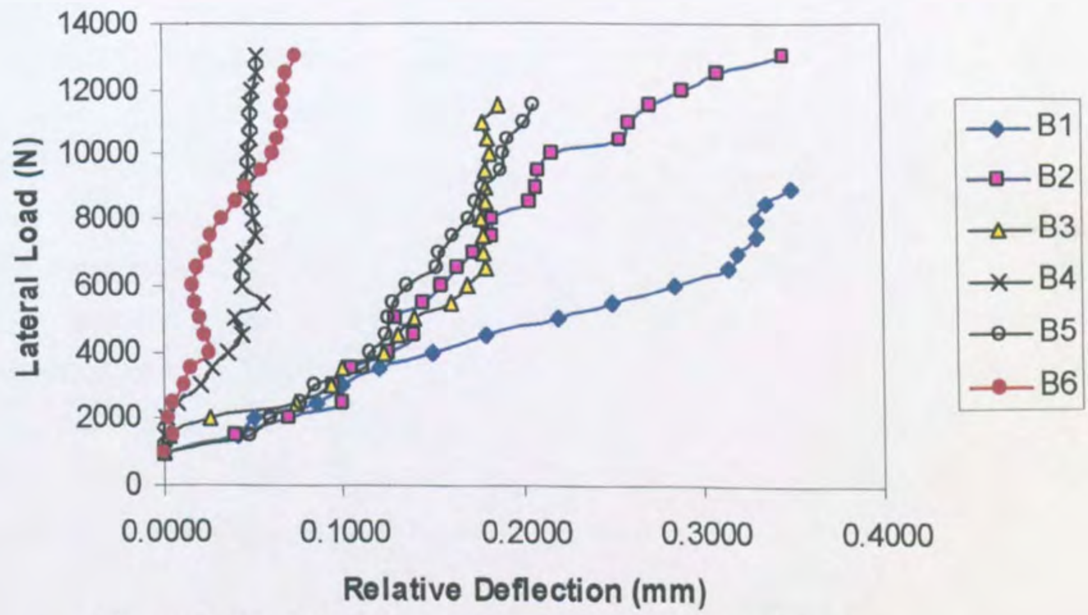


**Figure 4.23**: Displacement of Wallette-Centre relative to outer points – Yellow B-wallettes

Table 4.11 lists the mean failure loads, failure stresses and standard deviations, of the wallettes, both in vertical and horizontal bending. It is evident that the wallettes made from grey blocks were stronger than those made using yellow blocks. The mean failure stresses were 1.78 and 1.19 N/mm$^2$ for the grey and yellow blocks respectively in horizontal bending. In vertical bending, the corresponding values were 1.31 and 0.76 N/mm$^2$. The strengths of the yellow wallettes varied less than those of the grey wallettes, as indicated by the standard deviation values. For horizontal bending, the standard deviation for the yellow wallettes was 0.1 N/mm$^2$, compared to 0.19 N/mm$^2$ for the grey wallettes, whilst in vertical bending the corresponding values were 0.08 and 0.15 N/mm$^2$.

**Table 4.11**: Mean values of failure load, failure stress and standard deviation (on stresses) for Wallettes

| **Block Type** | **Bending direction** | **Mean Failure Load (kN)** | **Mean Strength (N/mm$^2$)** | **Standard Deviation** |
|---|---|---|---|---|
| Grey | Vertical (B) | 12.18 | 1.31 | 0.15 |
| | Horizontal (P) | 18.30 | 1.78 | 0.19 |
| Yellow | Vertical (B) | 6.96 | 0.76 | 0.08 |
| | Horizontal (P) | 12.2 | 1.19 | 0.10 |

### 4.4.2 Grey Blocks

B-wallettes

For bending leading to failure in a plane parallel to the bed joints (vertical bending), the failure plane generally ran through the units. In a few cases, however, failure initiated in the interface between the unit and the mortar, but progressed through the units, as can be seen from Slide 1 - 6 in Appendix 4(c). It is thought that failure may have initiated in the joint probably at locations without full mortar coverage but soon moved into the block adjacent to the joints as the joint strength increased. The description given in Section 4.4.1 may also help to explain this. Weaker bond areas within the joint may have initially failed by de-bonding, but adjacent stronger areas of bond resulted in failure moving the unit material. This explains why the mortar appeared to pluck parts of the unit away but close to the joint.

While conventional masonry in vertical bending generally fails by de-bonding between the units and the mortar, the interface in the grey wallettes proved to be stronger than the units, even when the joints were not completely filled with mortar.

P-wallettes

For bending leading to failure in a plane perpendicular to the bed joints (horizontal bending), all wallettes failed by developing cracks that ran almost vertically through a combination of units and head joints. Close observation revealed that although the failure plane ran very close to the perpend joints, there was actually very little de-bonding between the units and the mortar, see Slide 7 – 12, Appendix 4(c). As in vertical bending, failure was almost entirely through the units, indicating that the modulus of rupture of the units is less than the tensile flexural bond strength between the units and the mortar. Due to high flexural bond strength, no zig-zag failure (common in conventional masonry) occurred, that is, the bed joints did not experience any failure, which only would have occurred if the modulus of rupture of the units was greater than the tensile flexural bond strength in horizontal bending. For this form of failure to occur about an axis perpendicular to the bed joints indicates exceptionally good bond.

The tensile flexural strengths about the vertical and horizontal axes did not vary as much as has been observed in conventional masonry, see values in table 4.11. The orthogonal strength ratio was calculated from the mean values as 1.31/1.78, that is, 0.74. Comparative value for a designation (iii) mortar with these units from Table 3 of BS 5628: Part 1 is 1/2.4, that is, 0.42.

Figure 4.24 is a repeat of Figure 4.12, with dotted red lines added to highlight the linear sections of the graphs, and solid black lines highlighting unloading paths. The wallette was loaded and unloaded twice, and eventually loaded to failure. The graph suggests a degree of elastic behaviour for the material, since on removal of the load there is some strain recovery. However, not all of the strain is recovered, which also suggests some plastic strains. It could be that cracks start developing in the material at low stress values, but failure is initiated only when a certain crack width is reached. Therefore, the increase of non-linear behaviour in cycles 2 and 3 could be due to the material degrading, probably due to the formation of micro-cracks in the blocks and at the block/mortar interface, which can not be seen by a naked eye. Assuming that initially there are no micro cracks but, with the addition of lateral pressure, they start forming, and with subsequent unloading the cracks do not fully close and therefore the strain cannot be fully recovered. Then during the second load cycle, it would take less energy to deflect the wall equivalent distances as cracks exist from load cycle 1 and more cracks start forming at lower loads and hence there is a shorter linear section to the graph. In the final cycle, the cracks from load cycles 1 and 2 are sufficient to ensure there is an even shorter linear portion at the start of cycle 3. The graph then becomes non-linear, but becomes linear again at higher stresses until failure occurs. This behaviour was also discussed under section 4.4.1.

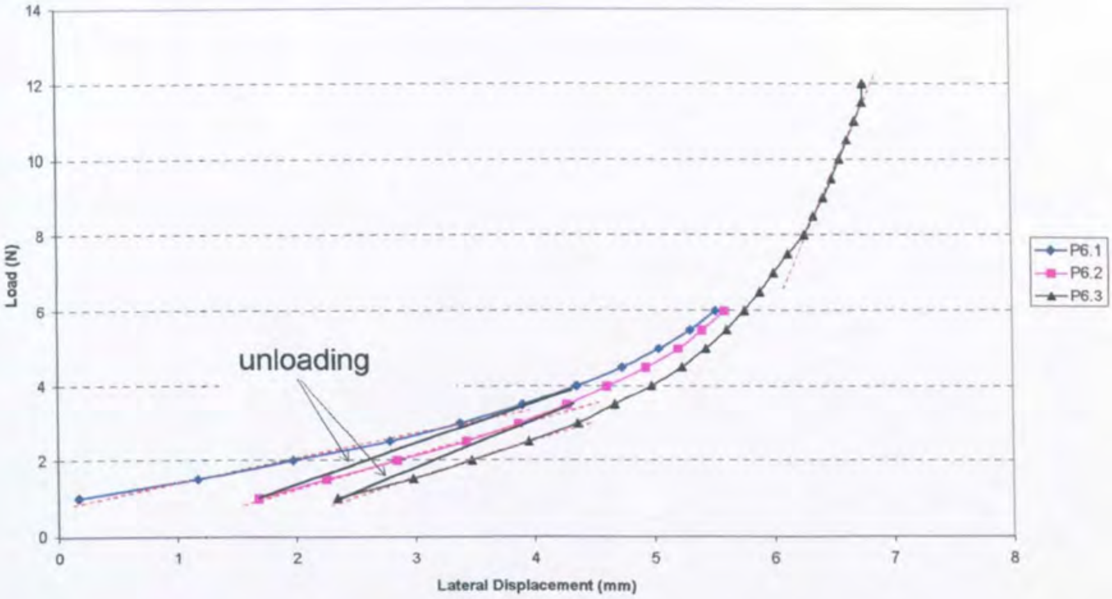


**Figure 4.24**: Load versus Displacement relationship for Grey wallette no.6, highlighting linear sections

The load-deformation behaviour plotted in Figure 4.24 reveals strange characteristics of the loading-unloading-reloading process. As described above, during the first stage of loading, the initial portion of the plot is linear becoming non-linear as the load increases. When the load is removed, the unloading path retraces the non-linear portion for a while, and then becomes linear but fails to return to the original point. The second unloading path is characterized by similar behaviour. The strangest characteristic of the graphs in Figure 4.24 is that the second and third loading paths have steeper slopes than the first. It was postulated earlier that the non-linear portion of the graphs might be as a result of the formation of micro-cracks. However, the slopes of the graphs suggest a stiffness gain in subsequent reloading. The most likely explanation for this behaviour is that cracking only eliminates local poorly bonded areas, leaving only the stiffer zones active.

### 4.4.3 Yellow Blocks

B-wallettes

Yellow-block wallettes in vertical bending failed by a combination of de-bonding and unit failure, as can be seen from Slide 13 - 18. Failure initiated in the interface between the unit and the mortar, but progressed partially through the units. The strength of these wallettes, therefore, is likely to depend on the properties of both the units and the bond between units and mortar.

P-wallettes

As with the grey wallettes in horizontal bending, all wallettes failed by developing cracks that ran vertically through units and head joints, as can be seen in Slides 19 - 24. Close observation, however, revealed that, unlike with the grey blocks, there was interface de-bonding between units and mortar in alternate courses, indicating that the bond in the yellow blocks is not as strong as that in the grey units, and less than the modulus of rupture of the units,. It appears that the wallette initially behaves as a plate, but de-bonding up the perpends at relatively low loads results in all the load being carried by the flexural capacity of the units bridging the perpend joints. Clearly, some load is also carried by the torsional resistance of the bed joints even though none of the bed joints failed when wallettes were tested in the horizontal bending position.

Figure 4.14 is a plot of deflection when loading and unloading wallette number 6 three times, eventually loading it to failure. Again, elastic material behaviour is suggested by the strain recovery revealed by the graph. However, as not all of the strain is recovered after the first loading cycle, it is likely plastic strains are occurring. The second and third cycles are broadly similar, suggesting that all the weaker parts have been eliminated during the first loading cycle. As with the grey wallette, steeper slopes at higher loads suggest some stiffness gain during the second and third loading cycles, when compared to the slope of lower loads.

### 4.4.4 Grey Wall

Observation of the cracking patterns suggests that a yield-line type of failure did not occur, at any of the peak loads or at ultimate load. Failure of the Grey Wall occurred in no less than four stages. After initial cracking, which revealed no particular pattern, there was an immediate pressure drop. Then there was some moment redistribution as the wall continued to take increased load until another pattern of cracks was formed, followed by a sudden pressure drop. With the application of more load, a third set of cracks developed, again, without any regular pattern. After these cracks, the load again fell, but on subsequent re-loading, a fourth crack resulted, after which the wall finally failed. At each of the stages described above, cracks generally ran through the blocks and across the mortar joints, see Slide 30 in Appendix 4(c). As in the case of the wallettes, the interfaces between the units and the mortar proved not to be regions of weakness. It is postulated the strength of this wall panel will depend more on the properties of the blocks than on the interface between the mortar and the units. Some of the continued stiffness in the wall after cracking can be associated with frictional shear strength in the cracked zones due to the self weight of the wall panel. With additional applied in-plane compressive stresses or gravity loads, residual shear and torsional strength can be expected.

The final crack pattern, with cracks coloured differently to indicate those that developed at different stages of the testing program, is shown in Figure 4.16 and pictured in Slide 29, Appendix 4(c). Looking at the crack stages again shows that every set of cracks divided the wall into smaller panels with different support conditions, and each of these sub-panels failed like a plate. The first set of cracks divided the wall into three sub-panels, as shown by the sketch in Figure 4.25(a). Figure 4.25(b) shows the typical crack patterns observed in similar panels of conventional masonry. Each of Sub-panels 1 and 2 (Figure 4.25) is supported along two edges and is relatively small compared to sub-panel 3. Therefore, the capacity of each of these sub-panels is likely to be higher than that of sub-panel 3. Sub-panel 3, on the other hand, is supported along 3 edges and free along the fourth (with only frictional shear stresses occurring along the crack line). Due to the differences of stiffness of the sub-panels, when further load was applied to the wall after the formation of the first crack, only sub-panel 3 failed, resulting in the formation of crack pattern 2 described in Figure 4.16.

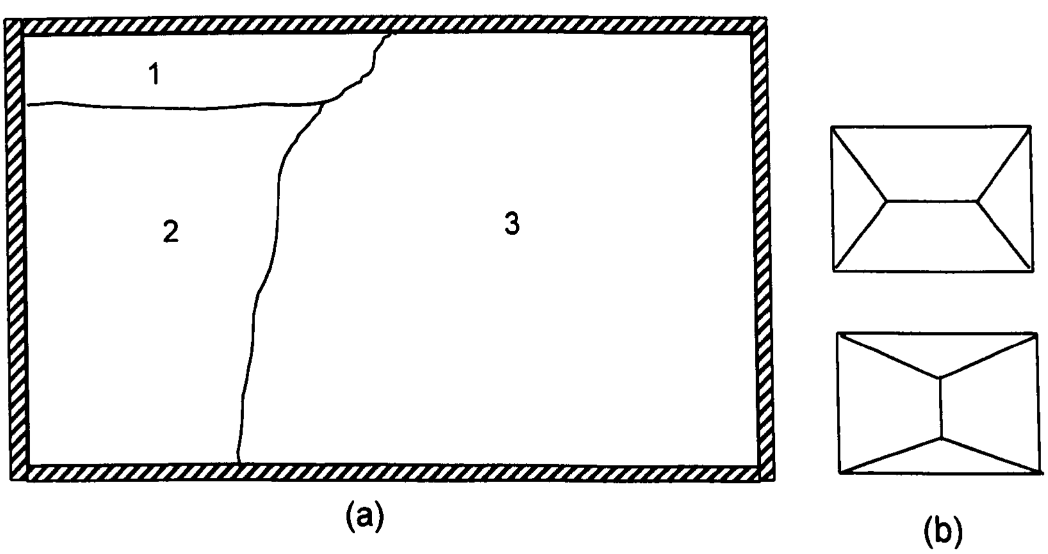


**Figure 4.25**: **(a)** Sketch showing three sub-panels of the grey wall after the first crack pattern occurred. **(b)** Typical crack patterns in similar panels built from conventional masonry.

Crack pattern 2 also divided sub-panel 3 into smaller sub-panels, 3a and 3b in Figure 4.26, each of which is supported along two adjacent edges. Sub-panel 3b, being the larger and therefore less stiff of the two, then failed by developing a crack that emanated very close to the intersection of the supported edges. This crack, which was referred to as crack pattern 3 in Figure 4.16, is shown in the sketch of sub-panel 3b in Figure 4.27. As mentioned above, the wall panel behaved like a plate at every stage of cracking. The capacities of each of the sub-panels were calculated using elastic analysis, and are presented in Chapter 7.

Very interestingly, the vast majority of cracks were through units. Nowhere is there the typical stepped-type of cracking that is observed in masonry walls built using conventional mortars.

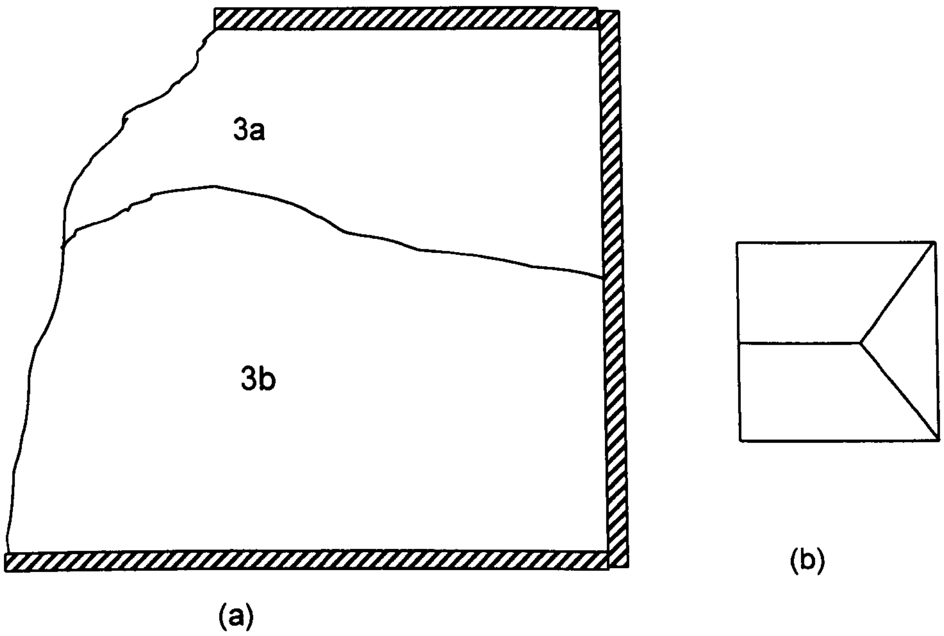


**Figure 4.26**: **(a)** A sketch of subsequent crack pattern of sub-panel 3 from Figure 4.25. **(b)** Typical crack pattern in similar panels built from conventional masonry.

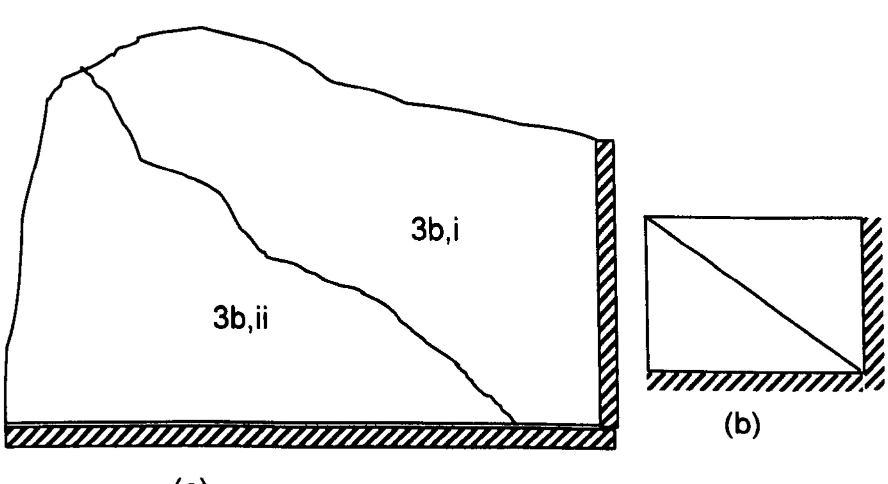


**Figure 4.27**: **(a)** Sub-division of sub-panel 3b into sub-panels 3b,i and 3b,ii. **(b)** Typical crack pattern in similar panels built from conventional masonry.

The load-deflection relations for the wall are plotted in Figure 4.28 and Figure 4.29. It is observed from the figures that some reserve of strength is present after initial cracking. This is a result of the frictional shear strength in the cracked zones. Figure 4.28 shows the load-deformation relationships across the mid-height of the grey panel, and Figure 4.29 shows the relationships down the mid-span of the panel. In both cases, it is observed that all curves are almost bi-linear, with the initial straight portion starting from zero stress to a value between 15% and 20% of the ultimate strength. From this value, the slopes of the graphs change sharply, culminating in the second linear portion. Through the test, wall stiffness unusually increases and as with wallettes, it is postulated that the strength of bonding over each face of the block varies, generally being weaker on the edges, but becoming stronger towards the centre of the face. This trend is substantiated by the observed failure planes, see Slide 34 in Appendix 4(c). With load application, the weaker areas fail but, overall, the remaining bond is stronger and stiffer than the failed parts, resulting in the unusual behaviour. It is believed that the sudden change of slope of the Load/Deflection graphs occurs when the weaker part of the bond has failed, and the bending strength begins to depend on the stronger part. After the sudden change of slope, the graphs indicate that the masonry stiffens under increasing stress, since the slopes of the graphs increase. However, the largest change of stiffness occurs during the formation of cracks as load is being redistributed. Unlike in the case of wallettes, the strength is not completely lost after initial cracking. Instead, the load drops to a lower value (from 7.2 to 3.1 N/mm$^2$, in this case) and was briefly held constant with increasing strain before it was increased again.

All graphs in Figure 4.28 (and those in Figure 4.29) are similar, but with varying magnitudes of displacements at different points on the wall, for a given load.

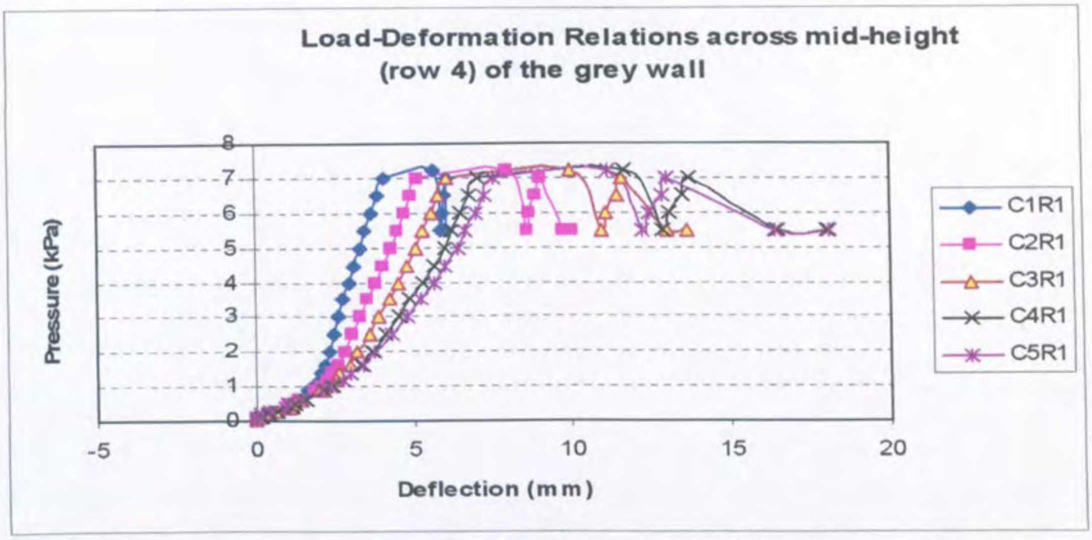


**Figure 4.28**: Load-Deformation Relations across mid-height (row 4) of the Grey Wall

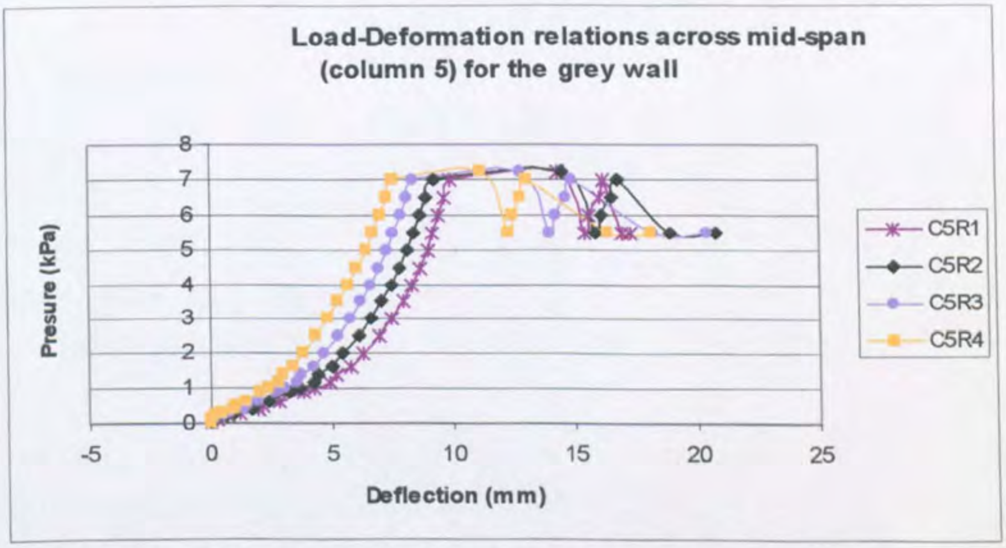


**Figure 4.29**: Load-Deformation Relations down mid-span (column 5) of the Grey Wall

### 4.4.5 Yellow Wall

Failure of the Yellow wall occurred in two stages. Initially, a crack pattern occurred instantaneously when a pressure of 6.0 kN/m$^2$ was reached, see Figure 4.18. Unlike with the Grey wall, the cracks in the Yellow wall initiated in the mortar joints, see Slide 32 in Appendix 4(c). The horizontal crack, which divided the wall into two equal sub-panels, ran along the bed joints along almost the entire span, only spreading into the units near the supports. The vertical crack probably initiated where the horizontal crack intersected perpend joints, in areas of high bending stresses, and ran vertically through alternate block courses and through the block/mortar interface for the intermediate courses. Although the horizontal and vertical cracks seemed to appear at the same time, it is believed that the horizontal crack formed first and the vertical one almost immediately afterwards. Immediately after cracking the pressure dropped to 2.9 kN/m$^2$ and displacement rose from 7.7 to 15.8 mm.

Further loading did not produce any new cracks, but only widened the existing ones. It was accompanied by a pressure increase from 2.9 to 4.0 kN/m$^2$ and a corresponding increase in deflection from 15.8 to 21.5 mm (see Figure 4.18). Initiating in the block/mortar interface and subsequently spreading into the units, the failure of the Yellow wall resembled that of the Yellow wallettes. Observations indicate, therefore, that the tensile strength of the joint when yellow blocks are used is slightly lower than the UMOR of the blocks. Regardless of the slightly lower tensile strength of the joint, the crack pattern suggests that the panel still behaved like a brittle plate. The cracks initiated in regions of maximum bending moment and ran in straight lines through the units and mortar joints, see Slide 31 in Appendix 4(c).

## 4.5 DISCUSSIONS

Figure 3.1 is very different from Figures 4.10 – 4.14, different analysis and design philosophies to apply. A design procedure based on the ultimate-load concept can be justified for a material that generates a Load-Deformation graph similar to Figure 3.1. On the other hand, the graphs of Figure 4.10 – 4.14 are predominately linear and do not reveal softening behaviour after attainment of the maximum load.

The variability of tensile flexural strengths determined from single-block tests, as well as those determined from stack-bonded beams, is small, see Tables 4.5 to 4.8. The number of samples in each test is relatively small, and such scatter may not be unexpected. However, the amount of testing was deemed adequate for a material characterisation that was part of a broader study, and for a material that had already shown low variability from wallette tests. It is noted also that variations are higher in beams constructed with the thin-joint mortar (Table 4.7 and 4.8) than in beams built with super glue (Table 4.6) or single blocks (Table 4.5). All beams constructed with super glue failed by rupturing of the middle block while those built with thin-layer mortar failed by de-bonding. This implies that the variation of the concrete in the block is lower than the variation in the bond strength.

The flexural tensile strength of the single-block beams differed slightly from that of the stack-bonded beams, see Table 4.12. This shows that for this masonry type, material properties of isolated geometries may not be very different from the properties of those same materials when in situ in the masonry composite. A contrary conclusion can be drawn with regards to conventional masonry, as eloquently expressed by Hughes et al (2000) when they remarked that the observed elasticity and Poisson's ratio of prismatic specimens of mortar will never be the same as those measured in the constrained bi-axial environment of a masonry bed joint. In the case of specimens tested in this work, slight differences can be associated with the influence of shear stresses, which will be expected to have more effect on the flexural tensile capacity in the single-block tests than in the stack-bonded beam tests. Shear stress becomes significant in flexural members as the shear-span/depth ratio ($a_v/d$ in Figure 4.19) decreases to values below 6. When single blocks were tested in flexure the shear-span/depth ratio was equal to 1.95 (see Figure 4.19), and therefore, their behaviour would approach that of deep beams. This resulted in a slightly larger value of the flexural tensile strength for the case of single-block tests. Similarly, the behaviour of wallettes tested under four-point loading may not exactly match that of full-scale wall panels in service, but only slight differences can be expected. During the process of developing an analytical model, values of parameters need to be chosen, and it is sensible and economical to use small-scale models to generate such parameters. The slight variations between the results obtained from different environments for this type of masonry will provide confidence when small-scale model results are applied to real situations. This aspect will be instrumental when values of safety factor for the material are chosen.

**Table 4.12**: Average flexural strengths of different specimens made from grey blocks

| Type of specimen | single block | stack beam |
|---|---|---|
| strength (N/mm$^2$) | 2.255 | 2.175 |

## 4.6 SUMMARY

This chapter has presented the experimental procedures undertaken to study the behaviour of thin jointed concrete block masonry walls. The results of the work are in terms of failure pattern, Load/Deformation graphs, failure loads and maximum deflections. A preliminary analysis of the experimental results was also given.

The results show that concrete blockwork masonry constructed with thin layer mortar has flexural strength values up to 3 times higher than conventional masonry, and that, depending on the units used, the unit/mortar interface is sometimes stronger than the units. This observation led to the conclusion that the flexural strength of such walls may depend on the Unit Modulus of Rupture of the blocks. Where the unit/mortar interface is weaker than the units, then the strength of the walls will depend on the properties of the units and the characteristics of the unit/mortar bond. When compared to conventional masonry, the variability of test data for this type of masonry was found to be very low, indicating that analytical models will be relatively less complicated to derive.

The results show a linear relationship between the flexural load and the lateral displacement both at low and at high stresses, and non-linear behaviour in-between these regions where stiffness increases. Crack patterns suggest homogeneous-plate behaviour and brittle failure.

### 4.7 CONCLUSIONS

The following conclusions are drawn from the experimental work presented in this chapter:

- The Load-Deformation graphs of the thin jointed concrete-block masonry tested in this research are Linear – Non Linear – Linear.

- The failure mode of the masonry is brittle. Failure is generally by a combination of de-bonding at mortar/unit interface and fracturing through the units.

- The flexural strength of the masonry built with grey blocks was greater than the strength of the yellow-block masonry. The average strengths of the grey-block masonry wallettes were 1.31 N/mm$^2$ and 1.78 N/mm$^2$, perpendicular and parallel to the bed joints, respectively. The average strengths of the yellow-block wallettes were 0.76 and 1.19 N/mm$^2$ in the vertical and horizontal directions, respectively.

- The variability of the flexural tensile strength values of the masonry wallettes tested in this research is low. The standard deviations were calculated as 0.15 and 0.19 N/mm$^2$ for grey-block wallettes in vertical and horizontal bending, respectively. The corresponding values for the yellow-block wallettes were 0.08 and 0.1 N/mm$^2$.

- The average unit modulus of rupture (UMOR) of the grey blocks was found to vary between 2.175 and 2.255 N/mm$^2$, depending on the geometry of the flexural test employed.

- When cyclic loading was applied to the thin jointed concrete-block wallettes in this research, the masonry indicated a degree of elastic behaviour by showing some stress-recovery. Plastic strains also resulted.

- Large-scale wall panels indicated load re-distribution after every cracking stage. Each of the resulting sub-panels failed like an elastic plate.

## 4.8 RECOMMENDATIONS FOR FURTHER WORK

The experimental work presented in this chapter has highlighted some important aspects which the current masonry research was not able to cover. Thus, the following are recommended for consideration in further investigations.

1. The high consistency and accuracy of the results obtained in this research will need to be challenged through more tests, involving varying types of support conditions and aspect ratios.

2. Because of their high flexural strengths and brittleness, failure of masonry wall panels built with concrete blocks and thin layer mortars is sudden. It is, therefore, recommended that further investigations should include panels with bed joint reinforcement. Bed joint reinforcement would not be expected to increase the flexural strength, but it would add ductility to the response of the masonry.

3. The modulus of elasticity was calculated by applying the beam-bending differential equation. It would be advantageous if flexural strains could be recorded during the testing programme so that this material property can also be evaluated from empirical stress/strain relationship.

4. Testing of wallette- and wall- specimens in this study was performed within 28 days of specimens being built. During this period, strength of the bond was assumed to have reached its maximum value. Future tests should include the effect of time on strength to verify this. Moreover, the strength characteristics for this material in the long term (beyond five years, say) still remain to be investigated.

# CHAPTER 5: PREDICTING MASONRY DEFORMATION CHARACTERISTICS AND FAILURE LOADS

## 5.1 INTRODUCTION

The experimental study presented in Chapter 4 investigated the deformational characteristics and strength of thin jointed concrete-block masonry walls subject to lateral loading. Preliminary analysis of the experimental data was made in the same chapter, Section 4.4, where it was discovered that this type of masonry exhibits some degree of linear homogeneous-plate behaviour. In this chapter, further analysis of the experimental results is presented, with the aim of verifying the linear plate-bending behaviour revealed by the experimental results of Chapter 4. In Section 5.2, the Load/Deformation graphs plotted from results of the wallette testing programme are examined further to verify correlation between test results, and also to assess the extent of linear behaviour of the material. This is followed in Sections 5.3 – 5.6 by analysis of the deformation characteristics of the wall panels. In Section 5.3, elastic modulus of the material is calculated using beam bending theory, in Section 5.4, analysis of the deflection data obtained from tests is presented, in Section 5.5, elastic plate theory equations are derived and employed to predict the critical deflection values of the walls, and in the final section, deformational characteristics of the walls are studied using the finite element method. The finite element model utilizes the concept of homogenization in order to check experimental observations against analysis.

## 5.2 LOAD/DEFORMATION RELATIONSHIPS OF THE WALLETTES

The 'Load versus Displacement' graphs of Figure 4.9 included experimental data from 1 kN to failure, so were extrapolated backwards to include behaviour of the wallettes between zero and 1 kN loading. This was achieved by first finding an approximate polynomial that fitted each graph, and then using the equation of the polynomial to plot the points between 0 and 1 kN. See Appendix 5(a) for the $4^{th}$ order polynomials that were used to approximate the equations of the graphs. The degree of correlation ($R^2$) between the original graph and the polynomial is also given under each figure, Figure A5.2 (i) – (iv), Appendix 5(a). It is noted that the $R^2$ values for all graphs are very close to unity, which indicates a very good correlation between the original graph and the approximate polynomial. The resulting graphs are presented in Figure 5.1, in dimensionless form. Also shown in Figure 5.1 (insert) is the dimensionless graph plotted from the average values of Graphs P1, P2, P4 and P5.

The graph was plotted using the data in Table A5.1, Appendix 5(a). The graphs of the yellow wallettes, Figure 4.11, were also extrapolated and normalized in the same manner, and these are shown in Figure 5.2. Source data for these wallettes is displayed in Appendix 5(a), in a similar manner to the grey wallettes data.

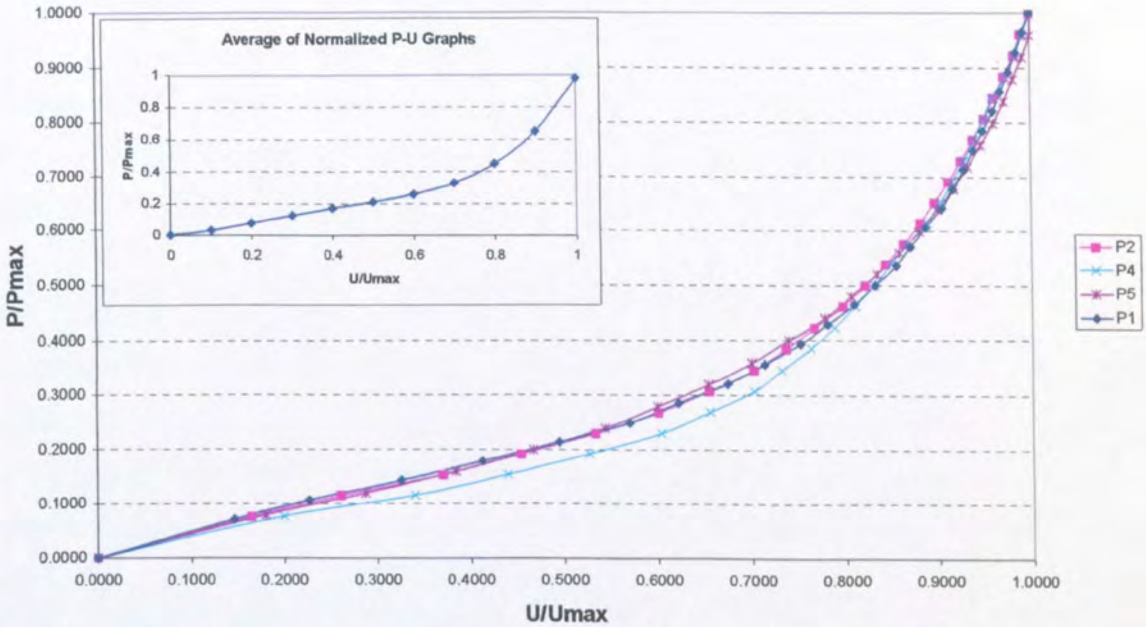


**Figure 5.1**: Normalized Load/Displacement Graphs of Grey P-Wallettes

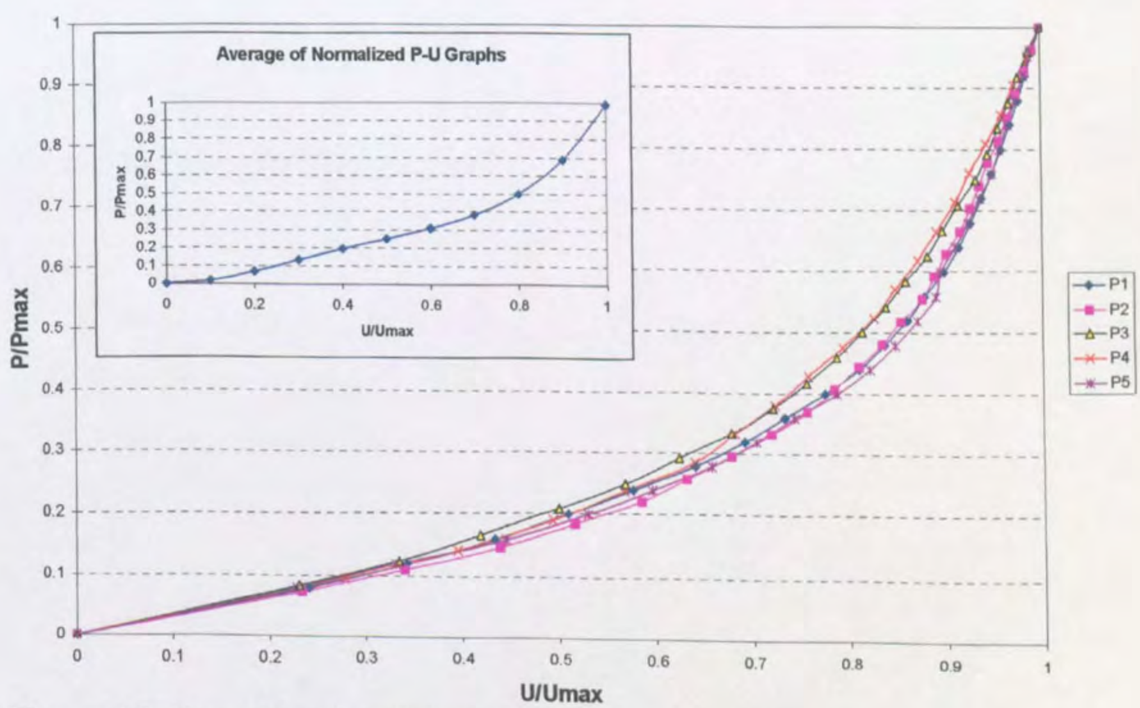


**Figure 5.2**: Normalized Load/Displacement Graphs of Yellow P-Wallettes

Normalized graphs are important for studying the general relationship between any two variables, in this case Load and Displacement, without consideration of their magnitudes. The dimensionless relationships shown in Figures 5.1 and 5.2 confirm the observation that was made in Section 4.3, that the Load/Deformation relationship is almost linear for the first one third of the ultimate load, non-linear in the middle third, and almost linear again in the last third of the loading history. This is particularly evident when the averages of the graphs are considered. Also to be noted is the remarkable similarity between the graphs, implying low variability between tests. Hence, a large number of specimens is not necessary to obtain a reasonably good estimate of the load/displacement relationship for this material.

## 5.3 ELASTIC MODULUS OF THE MASONRY

In order to determine the modulus of elasticity of the material the Load – Deflection data from the P-wallette tests were used. The variations of elastic modulus with applied bending stress for the grey-block and yellow-block wallettes are shown in Figure 5.4 and 5.5, respectively. These graphs were plotted using the data of Table A5.3 and A5.4, Appendix 5(a), respectively. The data in these tables was calculated using the deflection equation, Equation (5.1), the terms of which are defined in Figure 5.3. The equation was derived from simple beam-bending theory, the derivation being presented in Appendix 5(b).

$$EIu = \frac{1}{8}PaL^2 - \frac{1}{6}Pa^3 \qquad (5.1)$$

Where: $E$ is the modulus of elasticity,

$I = \frac{bt^3}{12}$ is the second moment of area of thickness $t$ and width $b$,

$u$ is the maximum lateral deflection, which occurs at the mid-span,

$P$ is the applied point load,

$L$ is the support span,

$a$ is the distance between support and loading point.

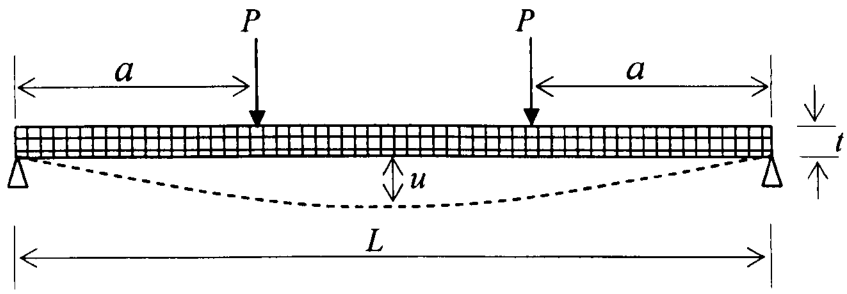


**Figure 5.3**: Definition of terms used in the beam-bending equation

The value of the deflection, $u$ in equation (5.1), was determined from the LVDT readings measured at three different points – one near the centre, and one near each support of the P-wallettes. It is apparent from Figures 5.4 and 5.5 that the modulus of elasticity varies slightly with bending stress. The modulus of elasticity for most grey wallettes moderately increases as the stress increases, particularly when the stress increases beyond 0.65 N/mm$^2$ (Figure 5.4). For wallette P1, however, the elastic modulus on average decreases until it reaches an almost constant value when the bending stress reaches 0.65 N/mm$^2$. Beyond this stress, the elastic modulus remains almost constant at a value of about 11000 N/mm$^2$. The load-deformation graphs of Figures 4.8 - 4.12 show that these wallettes gain stiffness as more loading is applied to them. This conclusion is generally substantiated by Figure 5.4. See Section 5.8 for further discussions of the implications of the Modulus versus Stress graphs.

The average value of the modulus of elasticity was calculated as 10890 N/mm$^2$ for grey wallettes, and this value is marked by a broken red line in Figure 5.4 (av. E = 10890 N/mm$^2$). The standard deviation was found to be 890 N/mm$^2$, which is about 8% of the mean value (Coefficient of Variation). This is another indicator of the consistency of results when thin layer concrete-block masonry walls are tested in flexure. For yellow wallettes the mean value was calculated as 10800 N/mm$^2$ with a standard deviation of 1425 N/mm$^2$, that, is 15% of the mean (Coeff. Of Var. = 15%). It is observed that, relative to the grey wallettes, the increase of stiffness for the yellow wallettes as the stress increases is insignificant.

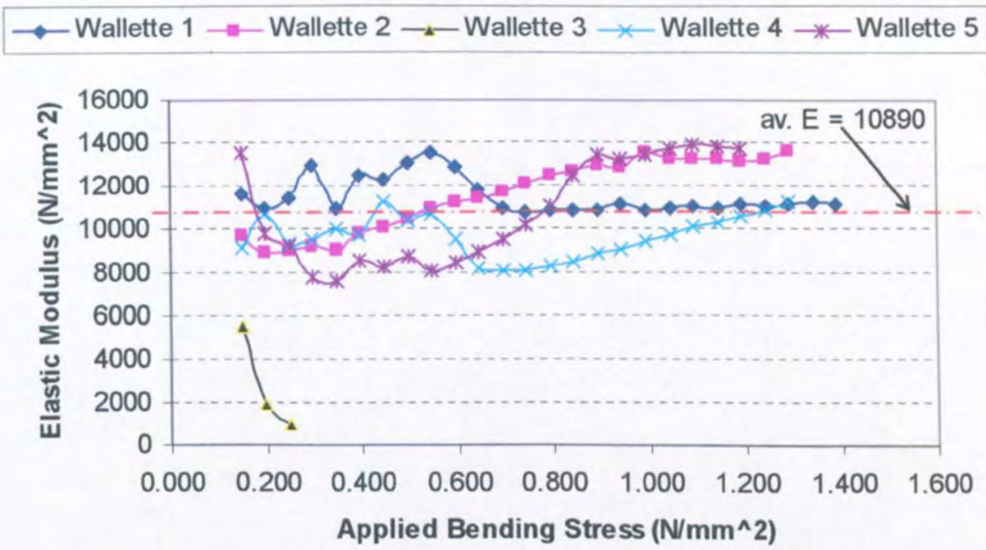


**Figure 5.4**: Variation of Elastic Modulus with tensile flexural stress for Grey wallettes tested in horizontal bending (Grey P-wallettes).

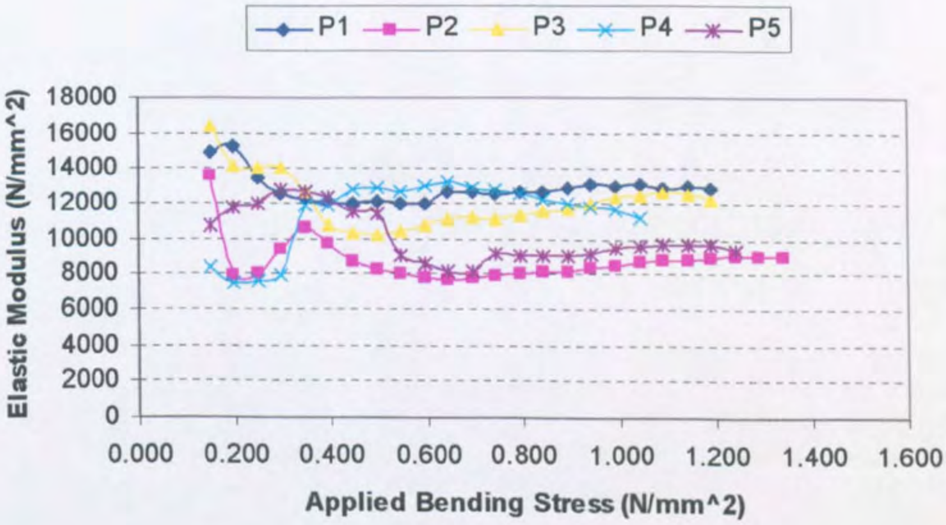


**Figure 5.5**: Variation of Elastic Modulus with tensile flexural stress for Yellow wallettes tested in horizontal bending (Yellow P-wallettes).

## 5.4 LOAD / DEFORMATION RELATIONSHIP OF WALLS - EXPERIMENT

Initially, displacements are examined using only the 20 data points available on the wall. Further analysis follows, which 'normalizes' the data effectively estimating zero deflection at the supports. Figures 4.4 and 4.5 show positions of the 20 LVDT's on the surface of each wall. The values of displacements along column 5, that is, down the mid-span, of the walls, and the values across row 4 (across mid-height) of the walls, are presented in Table 5.1 – Table 5.4. These values were used to plot the graphs of Displacement versus Position-on-the-wall, which are shown in Figures 5.6 – 5.9. The full Load versus Displacement data is given in Appendix 4(b).

**Table 5.1:** Displacement across mid-height — Grey Wall (Load = 7.2 kN/m$^2$)

| LVDT location (Fig. 4.4) | Distance from left edge (cm) | Displacement (mm) |
|---|---|---|
| support (no LVDT) | 0 | -- |
| C1R4 | 21 | 7.8693 |
| C2R4 | 49.5 | 8.2648 |
| C3R4 | 77 | 8.7461 |
| C4R4 | 104.5 | 9.2878 |
| C5R4 | 131 | 9.9271 |

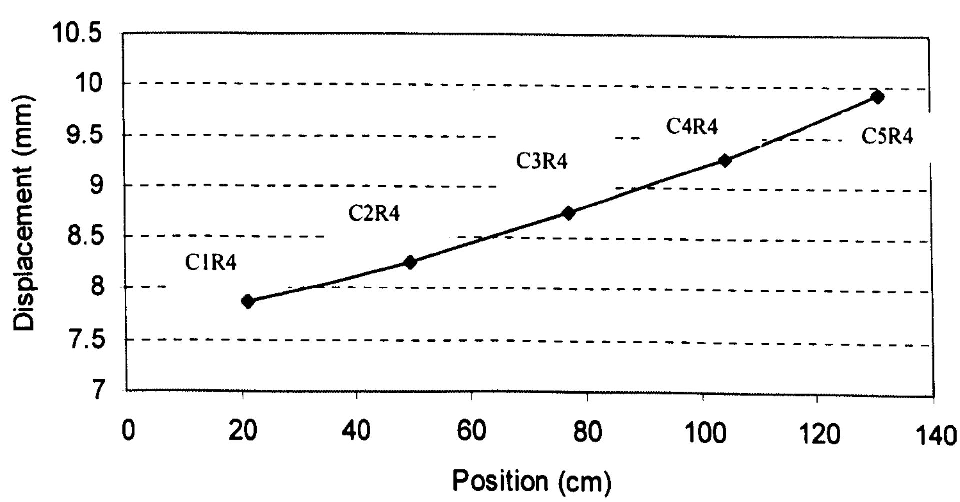


**Figure 5.6**: Displacement along Row 4 (mid-height)

**Table 5.2**: Displacement down mid-span — Grey Wall (Load = 7.2 kN/m²)

| LVDT location (Fig. 4.4) | Distance from top edge (cm) | Displacement (mm) |
|---|---|---|
| support (no LVDT) | 0 | -- |
| C5R1 | 13 | 7.8615 |
| C5R2 | 38.5 | 8.6185 |
| C5R3 | 63 | 9.3488 |
| C5R4 | 83.5 | 9.9271 |

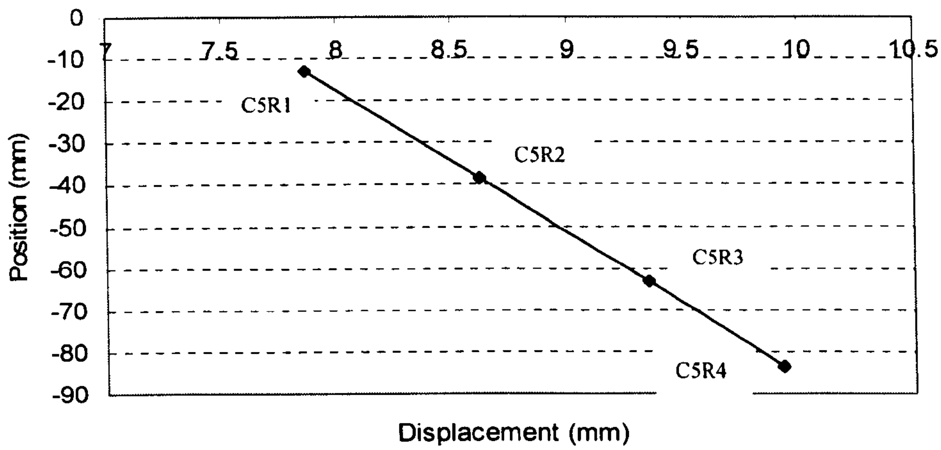


**Figure 5.7**: Displacement down Column 5 (mid-span)

**Table 5.3**: Displacement across mid-height — Yellow Wall (Load = 6 kN/m²)

| LVDT location (Fig. 4.5) | Distance from left edge (cm) | Displacement (mm) |
|---|---|---|
| support (no LVDT) | 0 | -- |
| C1R4 | 18 | 7.8121 |
| C2R4 | 45.8 | 8.3864 |
| C3R4 | 73.6 | 8.9145 |
| C4R4 | 101.4 | 9.1494 |
| C5R4 | 129.2 | 9.2226 |

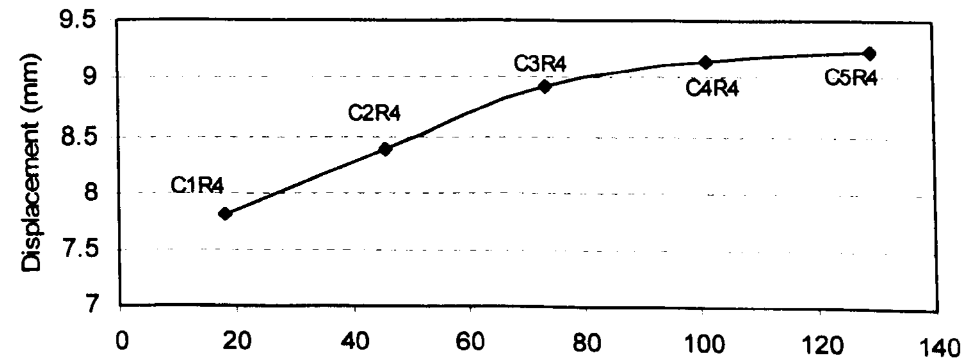


**Figure 5.8**: Displacement along Row 4 (mid-height)

**Table 5.4**: Displacement down mid-span — Yellow Wall (Load = 6 kN/m$^2$)

| LVDT location (Fig. 4.5) | Distance from top edge (cm) | Displacement (mm) |
|---|---|---|
| support (no LVDT) | 0 | - |
| C1R4 | 14.0 | 7.7357 |
| C2R4 | 63.6 | 8.1794 |
| C3R4 | 84.4 | 8.7162 |
| C4R4 | 38.8 | 9.2226 |

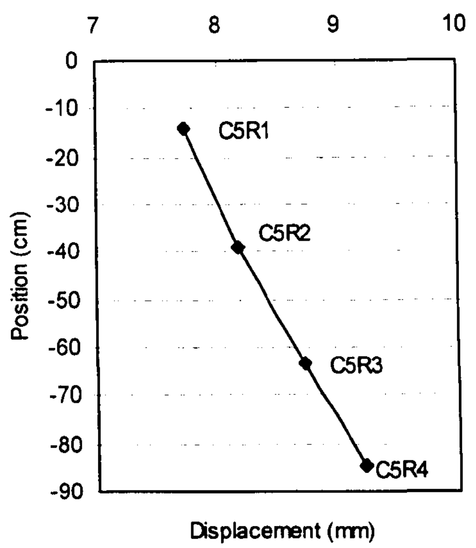


**Figure 5.9**: Displacement down Column 5 (mid-span)

It is clear from Figures 5.6 – 5.9 that a finite value of displacement at the supports has to be assigned. That is to say, assuming that the supports did not displace during the test would lead to a deflected shape with a kink at both the C1 and R1 positions on the walls. Clearly, this kind of shape cannot occur unless the wall has failed and formed a mechanism. It follows, therefore, that some displacement did take place at the supports, these being as a result of the compression of the rubber hoses. The magnitudes of these displacements were determined from extrapolation of the recorded values at the 20 instrumented points. Calculations of these values are in Appendix 5(c). Finally, assuming symmetry of the wall geometry about both the vertical and the horizontal axes, the deflected shapes of the entire walls were plotted, Figures 5.10 – 5.13. Figure 5.10 shows the deflected shape of the Grey wall as viewed from the top, while Figure 5.11 shows the deflected shape of the Grey wall as viewed from the side. The shape of the graph in Figure 5.10 suggests that failure occurred along a vertical crack, about 140 cm from the left. There still seems to be some curvature in Figure 5.11, which might suggest that failure may not have occurred yet. Hence, the figures suggest that failure may have occurred in the horizontal direction.

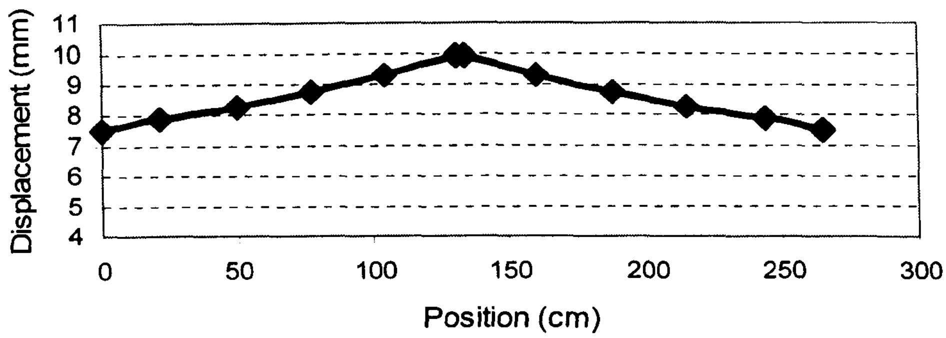


**Figure 5.10**: Plan view of deflected Grey Wall, Load = 7.2 kN/m$^2$.

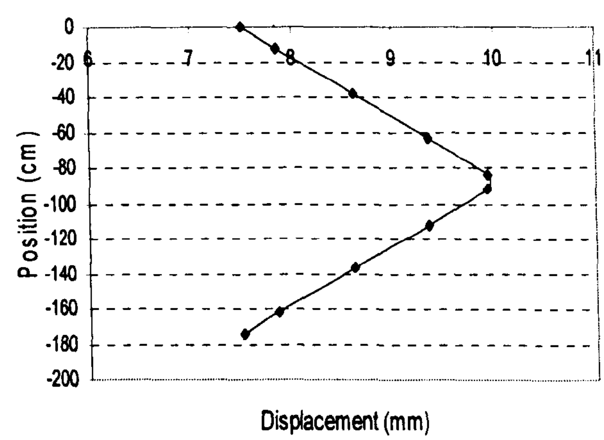


**Figure 5.11**: Side view of deflected Grey Wall, Load = 7.2 kN/m$^2$.

Figure 5.12 shows the deflected shape of the Yellow wall as viewed from the top, while Figure 5.13 shows the deflected shape of the Yellow wall as viewed from the side. Figure 5.12 suggests that no failure has taken place, as curvature is clearly present. Failure of the panel seems to have occurred along a horizontal crack, as suggested by the shape of Figure 5.13.

Detailed results of deflections at other points on the walls during the entire testing process are presented in Appendix 4(b).

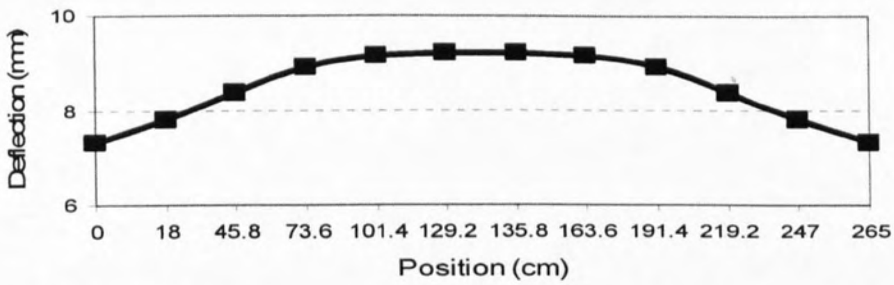


**Figure 5.12**: Plan view of deflected Yellow Wall, Load = 6 kN/m$^2$.

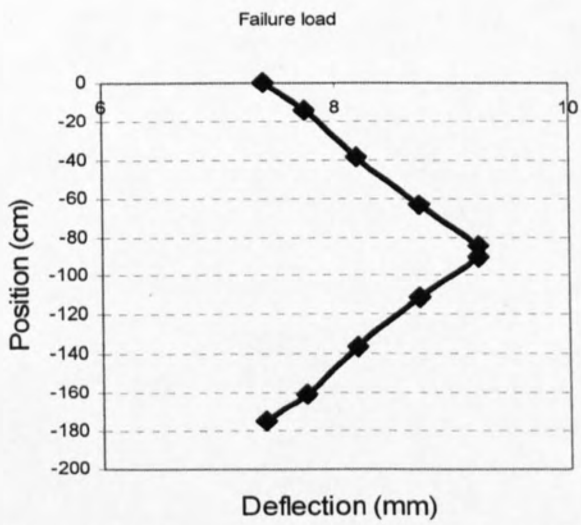


**Figure 5.13**: Side view of deflected Yellow Wall, Load = 6 kN/m$^2$.

## 5.5 LOAD / DEFORMATION RELATIONSHIPS - PREDICTIONS BY ELASTIC ANALYSIS

In this section, maximum values of deflection and failure loads of the wall panels are calculated using elastic theory equations. Derivations of the equations are presented in Appendix 1(a). Taking only the first term of the Series (A1.8) and (A1.9), the respective bending moments in the two directions can be approximated by using the following equations:

$$m_{x\max} = \frac{16w}{\pi^4} \frac{(1/L^2 + v/H^2)}{(1/L^2 + 1/H^2)^2} \tag{5.2}$$

$$m_{y\max} = \frac{16w}{\pi^4} \frac{(v/L^2 + 1/H^2)}{(1/L^2 + 1/H^2)^2} \tag{5.3}$$

Where $L$ and $H$ are, respectively, the length and height of the wall panel, $v$ is the Poisson's ratio of the material and $w$ is the uniformly distributed load per unit area of the wall panel.

The moment capacities per unit length in the two directions are given by:

$$m_{cx} = f_{tx}Z \tag{5.4}$$

$$m_{cy} = f_{ty}Z \tag{5.5}$$

where $f_{tx}$ is the flexural tensile strength of the masonry in horizontal bending, and $f_{ty}$ is the strength in the vertical direction. Z is the section modulus per unit width, and is given by

$$Z = \frac{t^2}{6}, \tag{5.6}$$

where $t$ is the wall thickness.

Equating equations (5.2) and (5.4) enables the critical value of load that would cause failure in the x-direction to be determined. Likewise, equations (5.3) and (5.5) yield the critical failure load in the y-direction. The lesser of these loads is assumed to be the failure load of the panel.

The maximum deflection at the centre of the wall is obtained from equation (5.7) (see Appendix 1(a) for the derivation of this equation)

$$U_{max} = \frac{16w}{\pi^6 D(\frac{1}{L^2} + \frac{1}{H^2})^2}, \quad (5.7)$$

where D is the flexural rigidity of the material, and is given by

$$D = \frac{Et^3}{12(1-\nu^2)}, \quad (5.8)$$

where E is the modulus of elasticity of the material, $t$ is the thickness of the panel and $\nu$ is Poisson's ratio.

The values of $f_{tx}$, $f_{ty}$ and E used in this section were obtained from wallette tests (Chapter 4), and are summarised in Table 5.5. A value of 0.15 for Poisson's ratio was used.

**Table 5.5**: Material properties of the masonry wall panels (mean values from wallette tests, see Table 4.1 – 4.4 and Figure 5.4 – 5.5)

| **Wall Panel** | **$f_{tx}$ (N/mm$^2$)** | **$f_{ty}$ (N/mm$^2$)** | **E (N/mm$^2$)** | $\nu$ |
|---|---|---|---|---|
| Grey Wall | 1.78 | 1.31 | 10900 | 0.15 |
| Yellow Wall | 1.19 | 0.76 | 10800 | 0.15 |

Using the values given in Table 5.5, the critical loads that would cause failure in the two directions, and the corresponding maximum deflections, were predicted and are presented in Table 5.6. Table 5.6 also presents the failure loads obtained by experiment.

**Table 5.6:** Elastic Theory predictions of Failure Load and Maximum Deflections

| **Wall Panel** | **$W_x$ (N/mm$^2$)** | **$W_y$ (N/mm$^2$)** | **Failure Load (kN/m$^2$)** | **Max. deflection (mm)** | **Failure Load (Experiment)** |
|---|---|---|---|---|---|
| Grey Wall | 14.6 | 7.8 | 7.8 | 0.631 | 7.2 kN/m$^2$ |
| Yellow Wall | 21.8 | 5.2 | 5.2 | 0.531 | 6.0 kN/m$^2$ |

## 5.6 LOAD / DEFORMATION RELATIONSHIPS – PREDICTIONS BY FINITE ELEMENT ANALYSIS

### 5.6.1 Introduction

The biggest challenge of numerical modelling in the field of masonry is to find the most suitable model to predict the behaviour of the material with reasonable accuracy. Recent research work has focused on the development of appropriate representation techniques for the desired analysis. Some of the techniques employed include: modelling masonry as a homogeneous material with smeared properties; modelling masonry as a composite of two materials, incorporating linear isotropic material properties along principal directions; representing masonry as a composite of two materials, incorporating linear orthotropic properties along the principal axes; representing masonry as a composite material with different non-linear material behaviours along each principal direction, as in the case of Tzamtzis and Asteris's (2002) and Lourenco's (2000) models. Masonry has also been modelled as a three phase composite, comprising of units, mortar and the interface, as in the case of Hagsten and Nielsen's (2000) models. In three-phase representations, contact elements have often been employed to model the interface. Each representation has its own merits and demerits, and a choice of one depends mainly on the objectives of the analysis and the accuracy desired. In this section, numerical models that were employed to augment the study are described, and their results are presented.

### 5.6.2 The Models

The two wall panels were modelled in a finite element analysis program, incorporating some important information obtained from the experimental tests on wallettes and block beams. It was ascertained from the wallette tests that the interface between the mortar and grey units was slightly stronger than the blocks, while for the yellow-block wallettes the bond strength was found to be slightly lower than the flexural tensile strength of the blocks. Furthermore, physical tests have shown that the elastic modulus of the blocks [Jabbar et al, 2006] and of the mortar [Valluzzi et al, 2002] are of the same order of magnitude, between 8850 N/mm$^2$ and 11000 N/mm$^2$. This information helped to simplify the numerical modelling process significantly, and led to the homogenisation technique being employed.

Homogenisation technique is a process that assumes a homogeneous distribution of stresses and strains across a medium. Other researchers that have used this technique include Lourenco and Rots (1997), and Lee et al (1994). Lee et al computed equivalent material properties of masonry employing a two-stage homogenisation of brick and mortar joints, and used the resulting stresses to compute properties in the constituent materials. They found that these macro stresses were in good agreement with those evaluated from 3-dimensional finite element analysis utilising a 20-noded solid element for each constituent material.

Lourenco and Rots (1997) demonstrated that homogenisation can be used for the calculation of linear characteristics of masonry where the macroscopic stresses induced by the structural loads vary slowly within the structure or where the characteristics of the basic cell (a periodic pattern associated with some frame of reference) change slowly within the structure. However, in the presence of non-linear behaviour, they state that the technique is likely to yield large errors. In this research, the numerical models were employed to study the masonry behaviour from initial application of the load until initial failure of the panel. During this loading history, the physical models revealed that there was no localised cracking or slipping at the interface, phenomena that are most responsible for the inelastic response of masonry.

The main advantage of using homogenisation techniques (in the case of linear analysis) is that, once the properties of the constituent materials are fully known, the composite behaviour of the material can be predicted without costly and necessarily large tests. In this study, the stresses developed in a masonry panel subject to a uniform lateral pressure were computed, and these were related to the flexural tensile strength of the blocks and mortar joints obtained from physical tests. The wall panels were discretized with quadratic, eight-nodded, thin shell elements, called 'Elastic 8Node 93' in ANSYS. These elements have six degrees of freedom at each node – three translations along the major axes, and three rotational degrees about the major axes. However, due to the model constraints, only three degrees are active, that is, the lateral translational degree and two rotational degrees about the x- and y-axes. As is required by thin shell theory, transverse shearing effects are excluded. Simple support conditions were assigned to describe the boundaries for all four edges of the wall panels.

Two different models for each wall were analysed. In Model 1, a constant value equivalent to the average modulus of elasticity of the wallettes was assigned to the material, see Table 5.7 for a summary of the material and geometric properties that were assigned to Model 1. In Model 2, the elastic modulus of masonry was defined using the stress/strain diagram plotted from the results of the wallette tests. Figure 5.14 shows the multi-linear graph that was used as the input data for the Grey wall. A typical finite element mesh of the walls is shown in Figure 5.15.

**Table 5.7**: Material Properties for Model1 used in FE modelling

| Panel | Size (L x h x t), m | E (N/mm$^2$) | Poisson's ratio |
|---|---|---|---|
| Grey Wall | 2.65 x 1.75 x 0.1 | 10900 | 0.15 |
| Yellow Wall | 2.65 x 1.75 x 0.1 | 10800 | 0.15 |

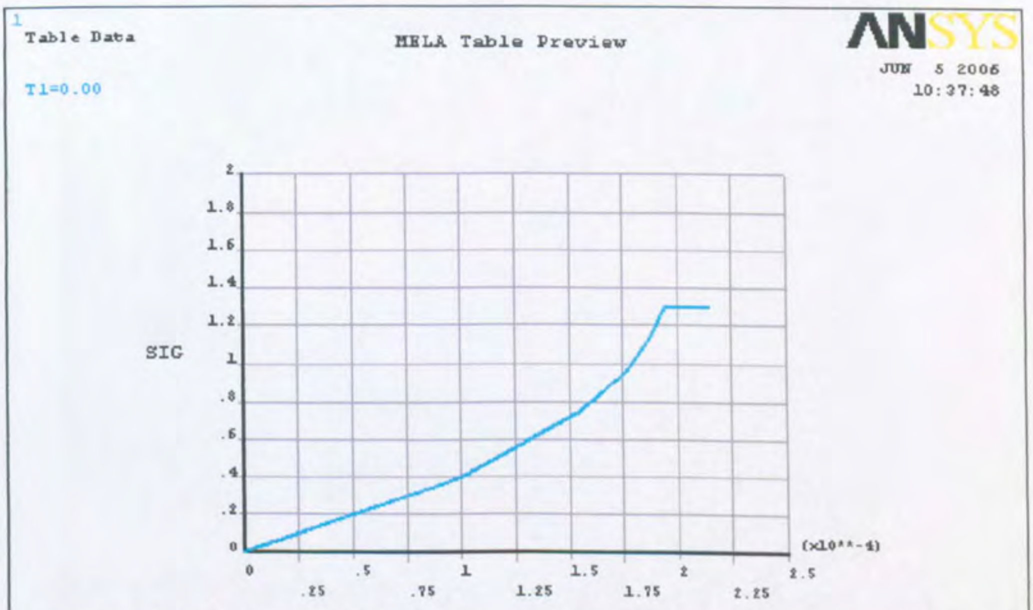


**Figure 5.14**: Stress-Strain relationship for determination of modulus of elasticity, used as input data for FEA model2

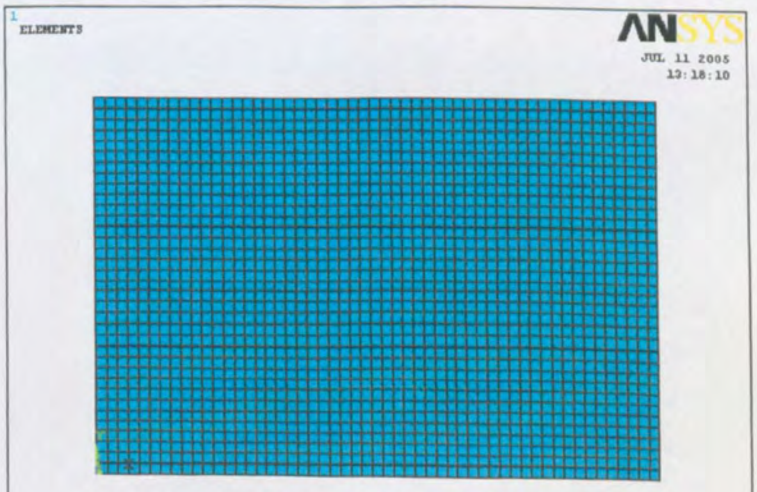


**Figure 5.15**: Typical finite element mesh

### 5.6.3 Results of Finite Element Analysis

**5.6.3.1 Model 1** (Constant E)

Figure 5.16 shows the deflection field of the Grey wall panel obtained using the ANSYS [ANSYS Inc, 2003] finite element program. The maximum deflection, which occurred at the centre of the panel, was found to be 0.602 mm. Figure 5.17 is the deflection plot of the Yellow panel, where the maximum value is displayed as 0.501 mm.

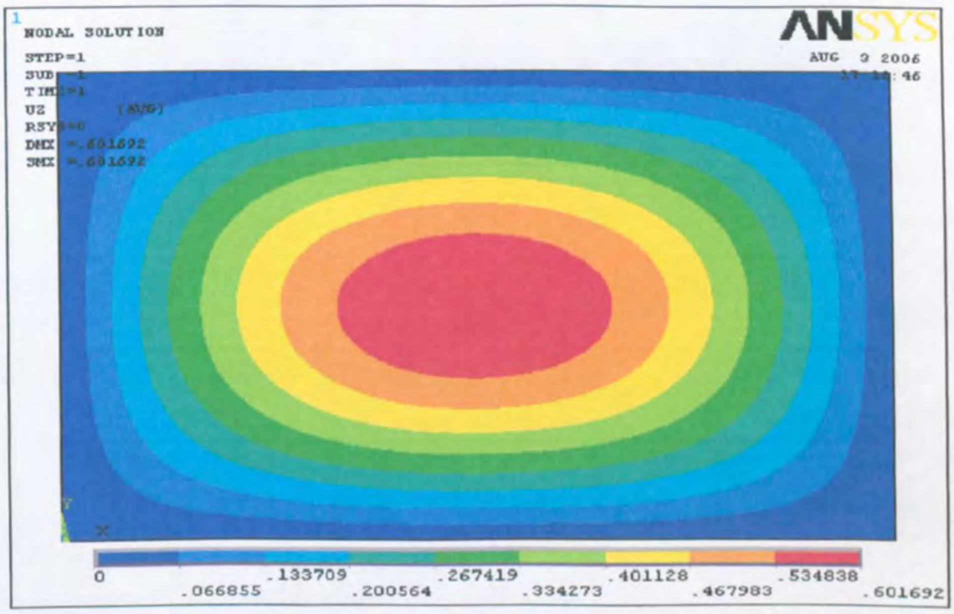


**Figure 5.16**: Deflection plot of Grey Wall, E = 10900 N/mm$^2$

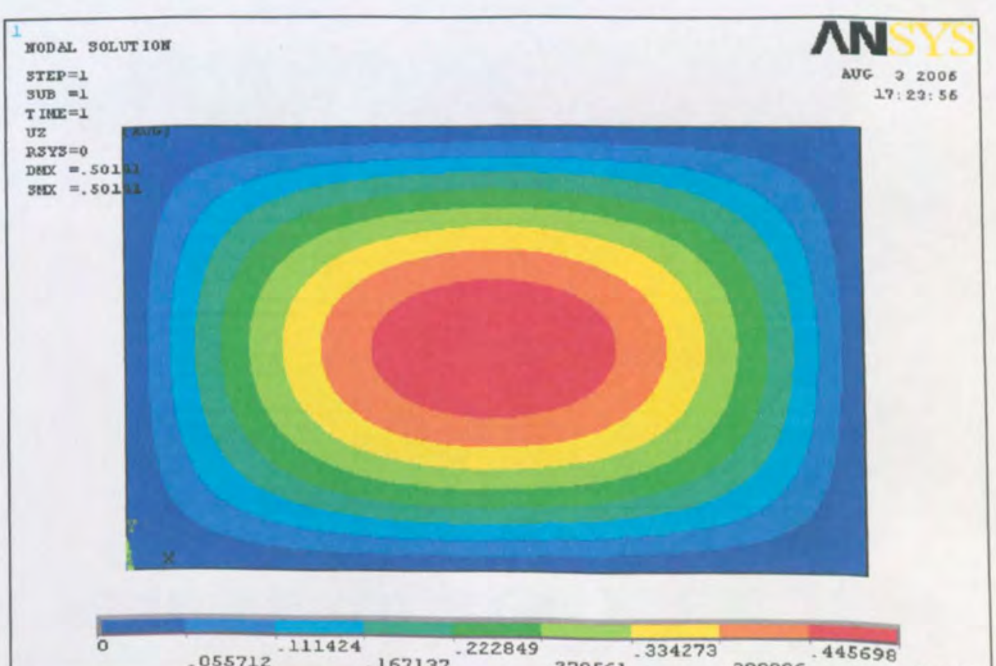


**Figure 5.17**: Deflection plot of Yellow Wall, E = 10800 N/mm$^2$

**5.6.3.2 Model 2** (Variable E)

Deflection plots for Model 2 are displayed in Figure 5.18 and 5.19, for the Grey and Yellow panels, respectively. The maximum values are 1.98 mm and 1.74 mm, respectively.

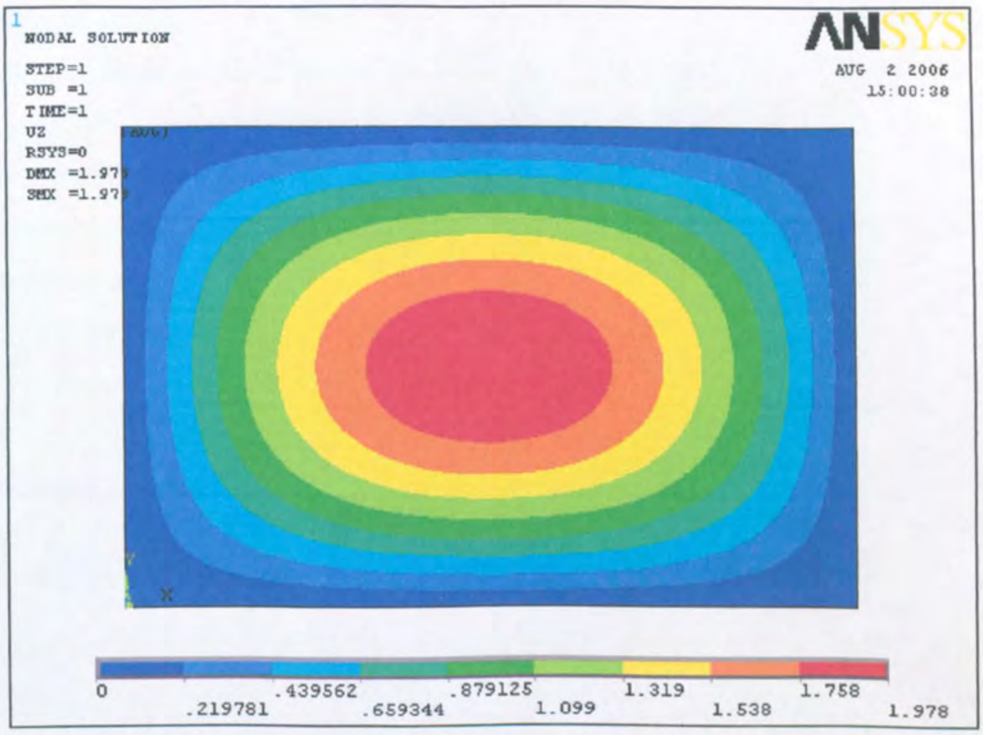


**Figure 5.18**: Deflection plot of Grey Wall when multi-linear stress/strain material behaviour is specified as input data for FEA

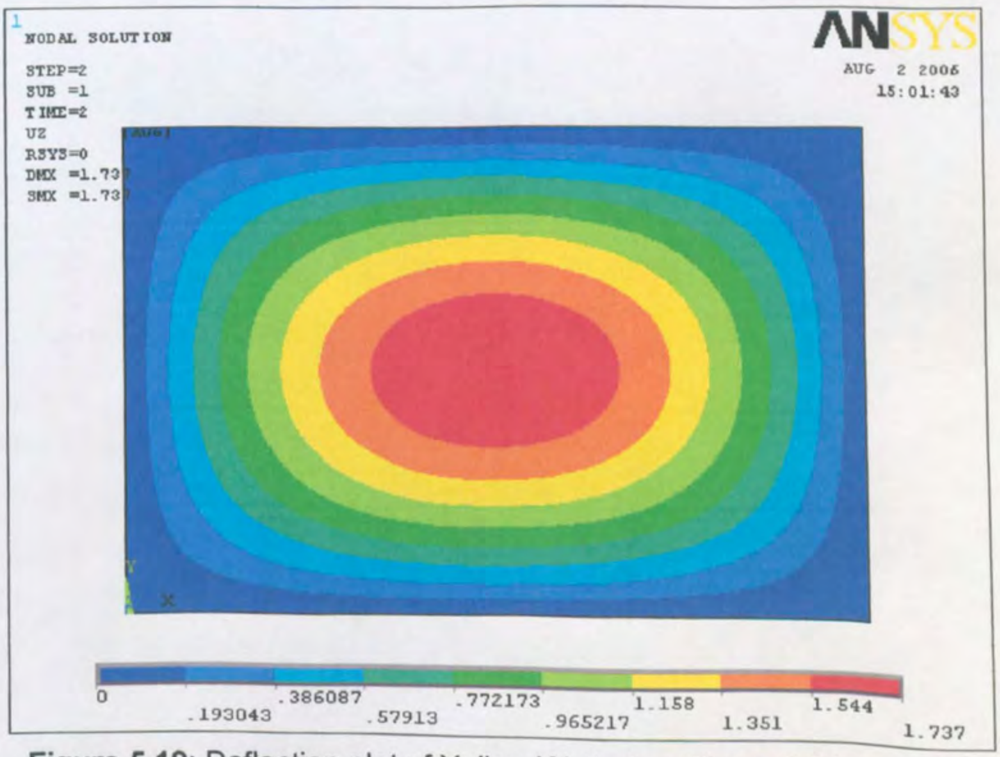


**Figure 5.19**: Deflection plot of Yellow Wall when Figure 5.6 is used as FEA input data

## 5.7 FAILURE LOADS OF WALLS - BS 5628 METHOD OF PREDICTION

The method of design for laterally loaded wall panels employed in BS 5628, the British code of practice for unreinforced masonry, utilises bending moment coefficients, α, derived using the Yield Line theory. The bending moment coefficients depend on the orthogonal ratio, μ, and the aspect ratio, H/L of the wall panel. The method also uses characteristic flexural tensile strengths. These were obtained using Appendix A.3.3 in BS 5628,. Table 5.8 summarises the factors used for the two walls in this study. The bending moment coefficients, α, were determined by interpolation between appropriate values given in Table 9 of BS 5628: Part 1. Results from this analysis are used to compare with the test and other analytical results to give an understanding of the reliability of code predictions. The comparisons are presented and discussed in Section 5.8.

**Table 5.8:** Values of orthogonal ratio μ, aspect ratio H/L, moment coefficient, α, and characteristic flexural tensile strengths, $f_{kx}$ and $f_{ky}$.

| Wall Panel | μ | H/L | α | $f_{kx}$ | $f_{ky}$ |
|---|---|---|---|---|---|
| Grey Wall | 0.73 | 0.66 | 0.031 | 1.19 | 0.87 |
| Yellow Wall | 0.63 | 0.66 | 0.034 | 0.79 | 0.5 |

Using the values given in Table 5.8, the failure load, $w$, for each wall panel was computed by application of equations (5.9). The results are presented in Table 5.9.

$$w_x = \frac{f_{kx} Z}{\alpha L^2}, \text{ in horizontal bending.} \tag{5.9a}$$

$$w_y = \frac{f_{ky} Z}{\mu \alpha L^2}, \text{ in vertical bending.} \tag{5.9b}$$

Where $f_{kx}$ and $f_{ky}$ are the characteristic flexural tensile strengths of the wallettes obtained in the tests of the current study (Table 4.1 - 4.4).

**Table 5.9**: Failure loads of the wall panels predicted using method of BS 5628

| Wall Panel | $w_x$ (kN/m²) | $w_y$ (kN/m²) | $w$ (kN/m²) |
|---|---|---|---|
| Grey Wall | 8.75 | 8.75 | 8.75 |
| Yellow Wall | 5.29 | 5.29 | 5.29 |

## 5.8 DISCUSSIONS

The Load versus Deformation relationships of wallettes plotted in Chapter 4, as well as the normalized graphs of Section 5.2, revealed a non-linear region sandwiched between two linear sections. In conventional masonry and reinforced concrete, the non-linear section follows a linear section and is a result of material degradation due to the formation of micro-cracks. For the concrete blockwork masonry constructed using thin layer mortar tested at Kingston University, the concave shape of the non-linear region implies stiffness gain. The calculated modulus of elasticity, particularly at stress levels over 0.4 N/mm$^2$ in Figure 5.4 and over 0.6 N/mm$^2$ in Figure 5.5, seem to substantiate this argument. However, the stiffness gain observed from Figures 5.4 and 5.5 is not as considerable as would be expected when one examines the Load/Deformation graphs (Figure 4.8 - 4.11). The contention that stiffness gain is due to weaker parts of the bond failing and leaving only stronger parts is still maintained, but it is evident that a significant part of the observed response may be as a result of the influence of the testing equipment. It was explained in Section 5.3 that compression of the rubber hoses attached along the load and support lines amplified the magnitudes of the measured displacements. At low stress levels, a significant part of the recorded displacements comprised of the compression of the rubber hoses. Hence, the Load/Deformation graphs may be influenced by the stiffness of the hoses and, consequently, may not be reliable at all loads.

It is noted further that, for all wallettes, the elastic modulus is unstable at low bending stresses, becoming more stable as the stress increases (see Figure 5.4 and 5.5). The stiffness calculations using the wallettes, however, should eliminate the effects of the support conditions by considering relative displacements of three different points on the wallette. Hence, the elastic modulus values are considered more reliable than the Load/Displacement graphs even at low stress levels. It would have been an added advantage if strain gages had been attached to the surfaces of the wallettes in order to give another perspective to the behaviour of the material.

In the walls, in order to eliminate the effects of the supports, relative deflections were examined in detail up the centre of the wall and across the mid-height of the panel. Central deflection across the panel, at location C5R4, was determined relative to the deflection at C1R4. In a similar manner, up the panel, deflection at C5R4 was found relative to C5R1. The measured deflections of the grey wall-centre were examined at 25%, 50% and 75% of the failure load, and just before failure, as shown in Table 5.10. The pressure corresponding to initial cracking (failure load) of the grey wall was

7.2 kN/m$^2$. Note that the deflections up the centre of the wall correspond to vertical bending, and those across the mid-height of the panel correspond to horizontal bending (Table 5.10). Assuming that the wall is linear elastic, the deflections should be linear and in accordance to elastic theory. The deflection at C5R4 at 50% of the failure load should be double the deflection at the same point when 25% of the failure load is applied. This is not revealed by the values of Table 5.10. Assuming elastic behaviour for the material, the results of Table 5.10, therefore, indicate an increasing stiffness as further loading is applied. This is consistent with the conclusion that was drawn before, namely that, the thin jointed blockwork tested in this study gains stiffness as lateral loading is increased.

**Table 5.10**: Relative deflections of grey wall-centre at different loading stages

| Mode of Bending | Deflection (mm) of the wall centre at: | | | |
|---|---|---|---|---|
| | **25% load** | **50% load** | **75% load** | **failure load** |
| Horizontal | 1.03 | 1.45 | 2.00 | 2.06 mm |
| Vertical | 1.03 | 1.62 | 2.05 | 2.07 mm |

Table 5.11 presents the deflections of the yellow wall-centre as measured relative to the deflections at C1R4 (horizontal bending) and C5R1 (vertical bending), at different stages of loading. The deflections of the yellow wall were examined at 33%, 50% and 83% of the failure load, and just before cracking. The failure load of the yellow wall was 6 kN/m$^2$. The discussion points raised above concerning the grey wall also apply here.

**Table 5.11**: Relative deflections of yellow wall-centre at different loading stages

| Mode of Bending | Deflection (mm) of the wall centre at: | | | |
|---|---|---|---|---|
| | **33% load** | **50% load** | **83% load** | **failure load** |
| Horizontal | 0.85 | 1.17 | 1.37 | 1.41 |
| Vertical | 0.91 | 1.23 | 1.47 | 1.49 |

Consider also the deformed shape of the walls at different stages of the loading process. Figure 5.20 is the deformed shape of the grey wall as viewed from the top (horizontal bending). Figure 5.21 is the same wall viewed from the side (vertical bending). Both Figure 5.20 and 5.21 show a 'dishing' effect of the deflected shape at low loads, particularly at 25% of the failure load. At 50% of the failure load, the 'dishing' effect is visible in Figure 5.20, and not so clear in Figure 5.21. The 'dishing' effect at low loads is an indication of rotation at a number of sections across the span or up the height of the panel. It is likely that these rotations take place at the mortar joints as the outer, weaker parts of the joints progressively fail. After the outer parts have failed, the remaining parts of the joints are stronger and the panel becomes stiffer, resulting in the deformed shape observed at higher loads. Hence, the shape of the deflected wall at loads above 50% of the failure load is due to the high stiffness of the mortar joints in this form of masonry construction. The high stiffness of the joints leads to the panel behaving as a plate.

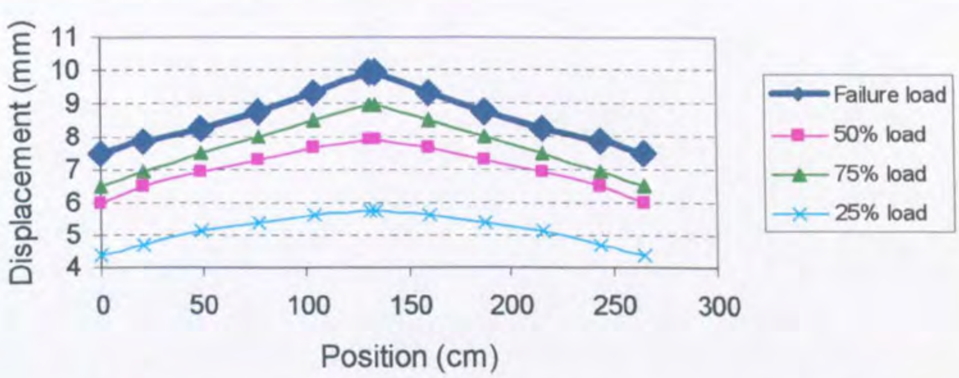


**Figure 5.20**: Plan view of deformed shape of the Grey Wall at different stages of loading

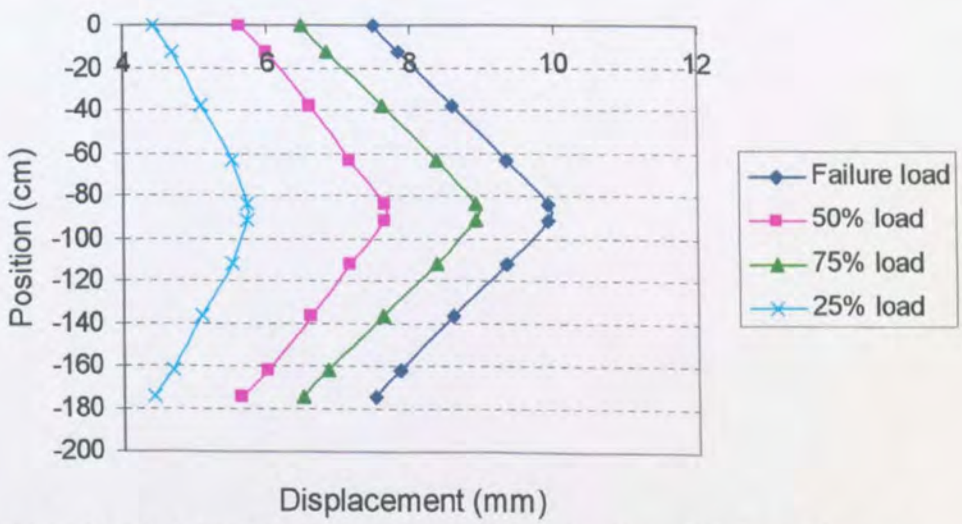


**Figure 5.21**: Side view of deformed shape of the Grey Wall at different stages of loading

Figure 5.22 and 5.23 show the deformed shapes of the yellow wall at different stages of loading. Again, the wall is viewed from both the top (Figure 5.22) and the side (Figure 5.23). Unlike in the case of the grey wall, the deformed shapes of the grey wall do not show a 'dishing' effect at low loads, neither are the shapes smooth at loads not exceeding 50% of the failure load. This may be as a result of uneven support conditions. Consider the supports along the edges of the panel when load is applied. Assuming the wall is linear elastic, if the panel is evenly supported along the edges, deflections will tend to be linear and in accordance with elastic theory. However, if some parts of the panel edges are not resting on the supports, the load will tend to be more concentrated around the supported strips of the panel, resulting if higher deflections in these vicinities. The deflected shapes of the yellow wall become smoother as loads increase beyond 50% (Figure 5.22 and 5.23). It can be deduced from this observation that the support along the edges of the panel evens out as the load increases, resulting in more uniform distribution of the load.

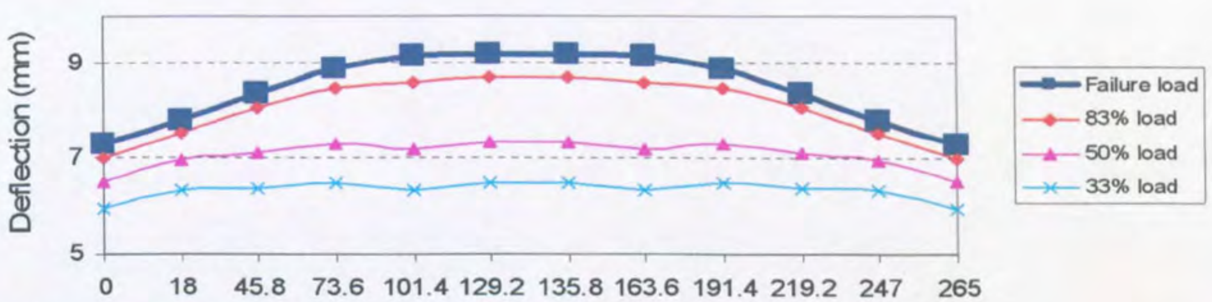


**Figure 5.22**: Plan view of deformed shape of the Yellow Wall at different stages of loading

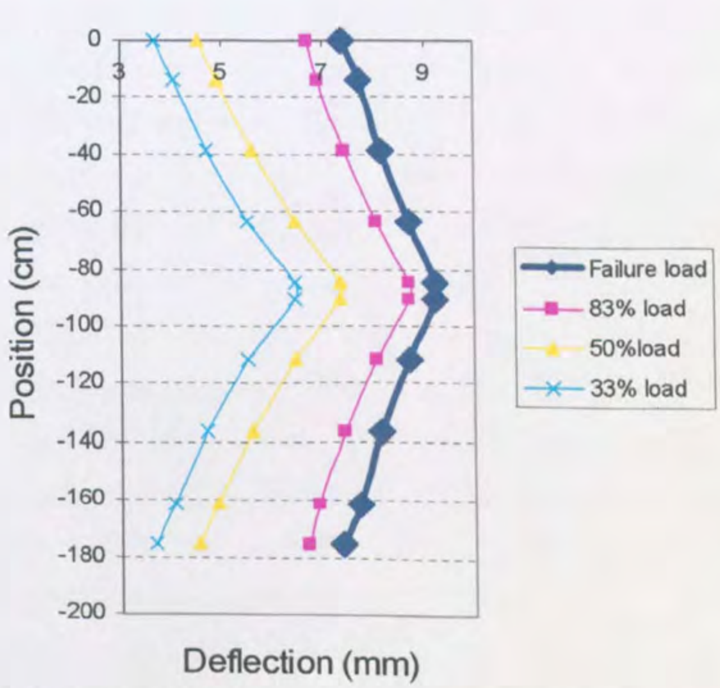


**Figure 5.23**: Side view of deformed shape of the Yellow Wall at different stages of loading

Finally, the critical deflections and failure loads as determined by; experiment, finite element analysis, the elastic plate theory, and the BS 5628 Part 1 method, are compared in Table 5.12 and Table 5.13, for both the Grey and Yellow walls.

**Table 5.12**: Comparison of Results for Grey Wall

| **Grey Wall** | Experiment | Elastic Analysis | BS 5628 | Finite Elements | |
|---|---|---|---|---|---|
| | | | | Model 1 | Model 2 |
| Failure Load ($kN/m^2$) | 7.2 | 7.8 | 8.8 | -- | -- |
| Max. Deflection (mm) | 2.44 | 0.631 | -- | 0.602 | 1.98 |
| | | | | | |

**Table 5.13**: Comparison of Results for Yellow Wall

| **Yellow Wall** | Experiment | Elastic Analysis | BS 5628 | Finite Elements | |
|---|---|---|---|---|---|
| | | | | Model 1 | Model 2 |
| Failure Load ($kN/m^2$) | 6.0 | 5.2 | 5.3 | -- | -- |
| Max. Deflection (mm) | 1.89 | 0.531 | -- | 0.501 | 1.74 |
| | | | | | |

Investigation of the above tables clearly shows that elastic theory yields better prediction of failure loads than the method of BS 5628. There is, however, a large discrepancy between the measured deflections and deflections predicted by elastic theory using a constant value of the elastic modulus (Model 1 results). The deflections predicted from the non-linear finite element analysis, whereby a multi-linear stress/strain behaviour was defined for the material (Model 2), are found to be much closer to the measured values. It is the contention of the author that the non-linear behaviour observed from the load/deflection graphs is partly a result of the effects of the experimental set-up and, therefore, may not be a true indication of the material behaviour. However, the results of Model 2 confirm that elastic theory is capable of reproducing reasonably good results if the numerical model incorporates the real conditions as much as practically possible. Moreover, the critical stresses on the walls just before failure (determined by finite element analysis, see Figure A2.1 – A2.2 in Appendix 2(b)) are found to almost match the average uni-axial failure strengths of the wallettes (see Table 4.1 – 4.4). Critical flexural tensile stress in the vertical direction on the Grey Wall just before cracking was calculated by linear elastic finite element analysis as 1.383 $N/mm^2$. For the Yellow Wall the corresponding critical flexural tensile stress was found to be 0.89 $N/mm^2$. When B-wallettes (vertical bending) were physically tested, the average flexural tensile strengths were 1.31 and 0.76 N/mm$^2$ for the grey and yellow wallettes, respectively.

## 5.9 CONCLUSIONS

The following conclusions are drawn from the analysis presented in this chapter:

- The normalized Load-Deformation graphs for any similar set of wallettes tested in this research programme are almost identical to each other. This implies low variability between tests. Hence, a large number of specimens is not necessary to obtain a reasonably good estimate of the load/displacement relationship for this material.

- The modulus of elasticity plotted against applied stress indicates that the recorded data is unstable at low stress levels, and becomes stable at high stress levels. Moreover, it was observed that the modulus of elasticity for the masonry increases slightly with increasing applied stress, which is a phenomenon that has never been observed in conventional masonry.

- The average value of the modulus of elasticity was found as 10890 N/mm$^2$ for grey-block wallettes, with a standard deviation of 890 N/mm$^2$, or 8% of the mean value. For yellow-block wallettes, the mean value was found as 10800 N/mm$^2$ with a standard deviation of 1425 N/mm$^2$, that is, 15% of the mean value.

- For the thin jointed concrete-block masonry wall panels tested here, Elastic theory yields better prediction of failure loads than the method of BS 5628.

- The great importance of an accurate modelling of the boundary conditions in finite element analysis has been demonstrated. When the experimental non-linear Load-Deformation graph (which may be a result of the boundary conditions) was used as input data for the finite element analysis programme, the deflections of the thin jointed masonry wall panels were predicted with a higher level of accuracy.

- Comparison between failure strength values of wallettes (uni-axial tests) and wall panels (biaxial tests) shows that failure of the masonry is initiated when the uni-axial tensile strength is reached in any one direction. When the uni-axial strength is reached, a crack develops normal to the direction of the critical stress, and the masonry fails in a brittle mode.

## 5.10 RECOMMENDATIONS FOR FUTURE WORK

In addition to plotting Load/Deformation graphs, Stress/Strain relationships plotted directly from the wallette tests should be considered. This would give another perspective of the response of the material against lateral loads.

Another important aspect to be considered is that of damage mechanics. Damage is seen as a decrease in elastic properties as a consequence of the decrease of the area that transmits internal forces, through the appearance and subsequent propagation of micro-cracks [Maugin, 1992]. Since in thin layer masonry panels tested in the current study, the modulus of elasticity appears to increase as micro-cracks are formed, a phenomenon opposite to damage appears to be observed. A detailed chemical and electron microscopic analysis could be undertaken to ascertain how the bond between glue mortar and concrete blocks is achieved. A preliminary optical microscopic study undertaken at Kingston University [Fried et al, 2005] has already indicated that the parent material of the block influences the thickness and nature of the bond zone.

# CHAPTER 6: ANALYSIS AND DESIGN PROCEDURE

## 6.1 INTRODUCTION

In conventional masonry, research activities aimed at developing design and analysis procedures for wall panels subjected to out-of-plane loading has resulted in widely varying techniques, due partly to the variability of mechanical properties of the material. The behaviour of laterally loaded masonry walls does not only depend on the characteristics of the constituent materials, but also on the environmental conditions and construction practices. Consequently, existing masonry design codes differ substantially in their treatment of this subject. The British Code [British Standards Institute, 1992] uses a design procedure based on moment coefficients derived from yield-line analysis and verified using experimental results [Sinha, 1978]. The Australian Code [Standards Australia, 1998] applies virtual work principles to predict the wall resistance, based on the tensile bond strength of the material, while in North America the design is governed by allowable tension stresses [The American Concrete Institute, 1992] and strengths [Canadian Standards Association, 1995] with the designer being responsible for performing an appropriate analysis. Due to the variety of conditions and building practices which exist across the European Union, the European Code [Eurocode 6, 1996] only gives general design procedures for laterally loaded panels, and recommends two approximate techniques – one utilizing moment coefficients determined from an appropriate theory, and the second approach based on the arching action of a wall between supports. These differences are due mainly to the unpredictability of conventional masonry as an engineering material.

Masonry wall-construction using thin layer mortar is a relatively new practice, but rapidly growing, particularly in Europe, mainly due to its enhanced performance [Building Research Establishment, 2006] when compared to conventional masonry. In addition to enhanced properties, experimental results also reveal a remarkable level of consistency between similar samples, see Chapter 4. From the engineering point of view, this is a crucial factor that will ensure simplicity in the process of development of prediction models, as well as ensuring uniform margins of safety in design. Despite its rapidly growing application, design codes do not yet offer any advice on how to size and design thin-jointed masonry. The work reported in this chapter should serve as a foundation for the development of constitutive models and design criteria for thin-jointed masonry wall panels, for eventual inclusion in design codes. It must be noted, however, that the current research is not so much a matter of re-inventing the wheel, but more a matter of identifying and ascertaining the appropriate theory for handling masonry structures made from concrete blocks and thin mortar joints.

The experimental results of Chapter 4, and the deformational analysis of Chapter 5, indicate that the behaviour of thin-jointed concrete-block masonry walls is elastic-brittle, hence, analytical techniques based on elastic theory are likely to provide rational design philosophy. Moreover, it was postulated in Chapter 5 that the material behaviour may be expressed in terms of block properties and the basic bond strength of the masonry. By using this approach, the need to test masonry beams or wallettes in flexure in order to predict the strength of walls is prevented, and the design requires fewer parameters.

## 6.2 ASSUMPTIONS FOR THE PROPOSED METHOD

As a starting point for the development of a design procedure for the panels of the current work, the following assumptions have been made.

- The distribution of bending moments on the surface of the panels is in accordance with elastic theory, and the stress-strain relationship is linear-elastic.

- Progressive cracking of the masonry, if any, in the working stress range does not cause any significant changes to the section under bending. Thus, the moment of area of the cross-section under consideration remains constant during loading until the ultimate load is reached, at which stage the stiffness is completely lost through brittle failure.

- In line with small deformation theory, plane sections before bending remain plane after deformations.

- Failure is initiated when the uni-axial strength is reached in any one direction, that is, when either the flexural tensile bond strength or the modulus of rupture of the units is attained.

## 6.3 MATHEMATICAL MODEL

### 6.3.1 Design Moments

The basis for the determination of design bending moments is the linear elastic characteristics exhibited by the material under lateral loads. The load-deformation relation is linear, and the lateral deflections of the wall can be determined by elastic plate theory. Because of the relatively high value of orthogonal ratio (0.65 for yellow blocks and 0.75 for grey blocks), it can be shown (Chapter 7) that assuming isotropy when calculating the moments does not lead to significant discrepancy in the predicted load capacities. However, orthotropic properties may be considered if desired by the analyst. The designer may choose to derive the elastic plate equations from first principles or to use moment coefficients that are widely available in literature. Timoshenko (1959) presents moment coefficients for both isotropic (Tables 29 - 47) and orthotropic (Table 80) elastic plates, for various orthogonal ratios and support conditions. In this section, the Navier solution [Timoshenko and Woinowsky-Krieger, 1959] is applied to derive bending moment coefficients for simply supported panels subjected to uniformly distributed load.

The expressions for the distribution of elastic bending moments on isotropic panels are derived in Appendix 1(a). The series (A1.8) of Appendix 1(a) can be written as:

$$m_x = \frac{16 q_0 L^2}{\pi^4}\left(1 + \frac{L^2 v}{H^2}\right) \sum_{m=1,3,...}^{\infty} \sum_{n=1,3,..}^{\infty} \frac{\sin\frac{m\pi x}{L} \sin\frac{n\pi y}{H}}{mn\left(m^2 + \frac{L^2 n^2}{H^2}\right)^2} \tag{6.1}$$

See Appendix 1(a) for the definition of terms in Equation (6.1). For a given material, that is $v =$ constant, the bending moment $m_x$ will depend on the length of the panel, $L$, and the aspect ratio, $\frac{L}{H}$. Hence, Equation (6.1) can be written as

$$m_x = \alpha_x q_0 L^2 \tag{6.2}$$

Where $$\alpha_x = \frac{16}{\pi^4}\left(1 + \frac{L^2 v}{H^2}\right) \sum_{m=1,3,...}^{\infty} \sum_{n=1,3,...}^{\infty} \frac{\sin\frac{m\pi x}{L} \sin\frac{n\pi y}{H}}{mn\left(m^2 + \frac{L^2 n^2}{H^2}\right)^2}, \tag{6.3}$$

is the bending moment coefficient in the direction of the x-axis. Similarly, the bending moment in the y-direction can be expressed as

$$m_y = \alpha_y q_0 L^2 \tag{6.4}$$

The bending moment coefficients $\alpha$ can be easily tabulated. Table 6.1 presents the moment coefficient values for simply supported isotropic panels subjected to uniformly-distributed lateral load. The values for $\alpha_x$ were evaluated from the first four terms of the Series (6.3), as demonstrated in Appendix 1(a), Series (A1.15). The values for $\alpha_y$ were evaluated using Series (A1.16) in Appendix 1(a).

**Table 6.1**: Bending moment coefficients for simply supported panels subject to uniformly distributed load.

| Aspect Ratio | Coeff.X, $\alpha_x$ | Coeff.Y, $\alpha_y$ |
|---|---|---|
| 0.1 | 0.11460 | 0.01259 |
| 0.2 | 0.12229 | 0.01705 |
| 0.3 | 0.12215 | 0.02300 |
| 0.4 | 0.11419 | 0.02922 |
| 0.5 | 0.10193 | 0.03481 |
| 0.6 | 0.08833 | 0.03922 |
| 0.7 | 0.07512 | 0.04225 |
| 0.8 | 0.06317 | 0.04393 |
| 0.9 | 0.05280 | 0.04445 |
| 1 | 0.04403 | 0.04403 |
| 1.1 | 0.03673 | 0.04292 |
| 1.2 | 0.03071 | 0.04134 |
| 1.3 | 0.02577 | 0.03946 |
| 1.4 | 0.02172 | 0.03741 |
| 1.5 | 0.01840 | 0.03529 |
| 1.6 | 0.01567 | 0.03318 |
| 1.7 | 0.01342 | 0.03112 |
| 1.8 | 0.01155 | 0.02914 |
| 1.9 | 0.01000 | 0.02726 |
| 2 | 0.00870 | 0.02548 |

For walls spanning in one direction, the panel can be treated as a strip of unit width and the design moment calculated from equation (6.5)

$$m = \frac{q_u L^2}{8} \qquad (6.5)$$

As mentioned above, the designer can choose to consider orthotropy when calculating the design moments on the panels. Bending moment coefficients for anisotropic panels with varying support and loading conditions can be found in several textbooks.

In the next chapter, application of the coefficients of Table 6.1 will be demonstrated by way of predicting failure loads of wall panels and comparing to experimental data. Wall capacities will also be predicted using coefficients that take material orthotropy into consideration.

### 6.3.2 Bending Moment Capacity

The strength of laterally loaded, thin jointed concrete-block masonry is governed by both the flexural tensile bond strength of the mortar/unit joint and the modulus of rupture of the units, depending on their relative magnitudes. The bending stress is assumed to vary linearly across the cross-section. Hence, for the prediction of the moment capacity, moment equilibrium for a cross section about the appropriate bending axis is considered, and simple elastic stress analysis equations are applied. Therefore, the ultimate moment of resistance is given by either one of Equations (6.6) or (6.7)

$$M_c = f_u Z \tag{6.6}$$

$$M_c = f_b Z \tag{6.7}$$

Where $f_u$ = mean modulus of rapture of the blocks (UMOR)

$f_b$ = mean flexural tensile strength of the bed joints

$Z = \dfrac{bt^2}{6}$, is the section modulus of the wall appropriate to the plane of bending, where $b$ is the width of the section (equals $H$ if failure plane is perpendicular to bed joints, $L$ if failure plane is parallel to bed joints), and $t$ is the wall thickness.

### 6.3.3 Material Properties

It was observed in Chapter 4, and demonstrated in Chapter 5, that experimental results for laterally loaded, thin jointed concrete-block masonry panels have low variability. On the basis of this observation, it is concluded that a limited number of samples, six, say, is enough to generate a representative average value of the flexural tensile strength $f_b$ to be used in Equation (6.7). Unfortunately, flexural strength is influenced by the geometry of the test specimen, and so, is not an intrinsic material property. Hence, no absolute values of the flexural strength can be given.

Variability of the UMOR values of the blocks tested in Chapter 4 indicates that a few samples will be needed to generate a mean value to be used in equation (6.6). A three-point bending test as described in Section 4.2.3 is a valid method of test. Again, the results of this test are dependent on the geometry of the test specimen. When a single block is tested, the influence of shear stresses is more critical than in the case of a beam specimen. In this research, the value of the UMOR obtained from beam specimens was found to be approximately 90% of the value obtained from single-block specimens (see Chapter 4).

### 6.3.4 Application to Design

The calculation of load capacity of a given wall is determined by applying the appropriate equations, Equations (6.3) – (6.7), based on the failure mode, that is, whether failure is by de-bonding or unit fracturing. In design, however, the failure mode is not known before-hand, hence the least of the load capacity values obtained from equating the corresponding equations should be used as the strength of the wall. Unlike in structural design using other materials, in masonry the size of the wall is determined before hand since standard sizes of masonry units are used. The task is, therefore, to check the adequacy of the wall under design by comparing the predicted load capacity and the design load. The wall is deemed adequate if, taking into consideration all factors of safety, the predicted load capacity exceeds the design load.

### 6.3.5 Safety Aspects

The high flexural strength of thin layer mortar masonry means that it can withstand large forces without cracking. Since the failure of the masonry is very brittle, an appearance of even a small crack could cause concern and result in devastating consequences at these high loads. It is recommended, therefore, that reinforcement be added to obtain ductile behaviour after cracking.

The equations given in the above sections do not include any factors of safety. It is anticipated, judging by the results of the current research, that partial safety factors for material will be lower than currently recommended by the British code for conventional masonry. More research on a wider range of materials will be needed before safety factors can be recommended. In the current study, the value of partial safety factor was set equal to one to allow direct comparison with test data.

## 6.4 CONCLUSIONS

The work reported in this chapter should serve as a foundation for the development of constitutive models and design criteria for thin-jointed masonry wall panels, for eventual inclusion in design codes. As previously stated, there is no need to develop new analysis concepts as the linear elastic analysis technique is likely to yield good results for this material. Hence, elastic analysis has been applied to express the distribution of bending moments on the panels, while simple elastic stress analysis equations have been applied to predict the moment capacity. A material definition simply based on average values was considered.

## 6.5 RECOMMENDATIONS FOR FURTHER WORK

It should be pointed out that the main emphasis of the current study was not to determine the representative values of the flexural strength of thin jointed masonry walls, but to study its load-deformational characteristics in order to select an appropriate prediction model for the material. As such, relevant experiments should be performed to establish representative values of the flexural strength of the masonry based on the properties of its constituents. Investigation to establish partial safety factors for materials will then follow naturally.

# CHAPTER 7: VALIDATION OF ELASTIC THEORY

## 7.1 INTRODUCTION

The analytical procedure proposed in Chapter 6 will need to be validated by comparison to experimental results. However, available experimental results of concrete-block masonry built with thin-layer mortar are scarce, especially experiments performed under lateral loading. Therefore, comparison will be performed using results from concrete-block and clay-brick masonry wall tests, as well as some results from Autoclaved Aerated Concrete block tests.

## 7.2 PREDICTION OF WALL CAPACITIES

### 7.2.1 Kingston University tests

Three different groups of masonry structures will be analysed, using the elastic analysis equations of Chapter 6. The first group concerns the analysis of sub-panels that resulted from failure of the large Grey Wall tested in the current study, the results of which are presented in Chapter 4. The second group deals with clay-brick masonry walls tested previously at Kingston University. The last example concerns the analysis of Autoclaved Aerated Concrete-block wallettes, also tested at Kingston University. Failure mechanisms of all of these tests indicated plate behaviour.

(a) <u>Grey Wall sub-panels</u>

The Grey Wall panel tested in this research showed different stages of crack-formation, as discussed in Section 4.4.4 (Figures 4.20 – 4.22). Load capacities of each of the resulting sub-panels have been predicted by applying the elastic theory procedure discussed in Chapter 6, and the results are presented in Table 7.1. The predicted values are compared to the experimental values in Table 7.2. Note that pragmatic assumptions have been made to determine panels' aspect ratios and the boundary conditions. The aspect ratio of each panel was determined from dividing the average length of the two vertical sides by the average length of the horizontal sides. The boundary condition along the cracked edge was taken as free, that is, unsupported edge.

**Table 7.1**: Failure loads of Grey-Wall Sub-Panels

| Sub-Panel | Aspect Ratio | Moment Coefficient | | Wallette Strength | | Failure Load, w ($kN/m^2$) |
|---|---|---|---|---|---|---|
| | | x-axis | y-axis | x-axis | y-axis | |
| 1 | 0.3218 | 0.1235 | 0.0102 | 1.78 | 1.31 | 14.11 |
| 2 | 1.5536 | 0.1280 | 0.0364 | 1.78 | 1.31 | 13.61 |
| 3 | 0.8807 | 0.1070 | 0.0370 | 1.78 | 1.31 | 8.80 |
| 3a | 0.5309 | 0.1235 | 0.0220 | 1.78 | 1.31 | 10.19 |
| 3b | 0.4631 | 0.1235 | 0.0180 | 1.78 | 1.31 | 7.75 |

**Table 7.2**: Comparison of Theoretical and Experimental failure loads

| *Crack Pattern | unit | Theory (kN) | Experiment (kN) |
|---|---|---|---|
| 1 | Main panel | 8.2 | 7.2 |
| 2 | Sub-panel 3 | 8.8 | 7.2 |
| 3 | -- | -- | 6.9 |
| 4 | Sub-panel 3b | 7.75 | 7.9 |

**Note**: *Crack patterns are described in Section 4.3.3, and shown in Figure 4.14.

(b) Clay-brick Walls [Hogg, 2003]

Four walls and five brick-beams were constructed using Russet clay-brick units and Ankerfix PVM thin joint mortar. The beams were 12 bricks long by 4 bricks high, and the wall panels measured 2.6 metres by 1.7 metres. All specimens were tested after 96 hours of being built. The brick-beams were subjected to uni-axial flexural test, while the wall panels were tested in the bi-axial mode by applying a uniformly distributed pressure with the help of an air bag. All four edges of the wall panels were simply supported.

Results of the tests are presented in Table 7.3, together with the predicted values obtained using elastic analysis equations.

**Table 7.3**: Load capacities by Elastic Theory and by Experiment

| Wall No. | Beam Strength* | Moment Coefficient | | Failure Load (kN/m$^2$) | |
|---|---|---|---|---|---|
| | | x-axis | y-axis | Experiment** | Elastic Theory |
| 1 | 1.69 | 0.01840 | 0.03529 | 8.0 | 14.8 |
| 2 | 1.52 | 0.01840 | 0.03529 | 7.6 | 13.3 |
| 3 | 1.55 | 0.01840 | 0.03529 | 10.9 | 13.5 |
| 4 | 1.59 | 0.01840 | 0.03529 | 11.9 | 13.9 |

**Note**: *Horizontal direction

**Tests performed by Hogg (2003)

### 7.2.2 Elastic Analysis Predictions Considering Material Orthotropy

The two walls tested in this research, that is, the Grey and Yellow walls, have been analysed by elastic analysis equations that take material orthotropy into consideration. The bending moments in the two directions were calculated using Equations 7.1 and 7.2. These equations were reproduced, with slight alterations from Timoshenko and Woinowsky-Krieger. In Timoshenko and Woinowsky-Krieger (1959), an expression $\frac{E''}{E'_x}$ or $\frac{E''}{E'_y}$, where $E'' = \frac{\nu E}{1-\nu^2}$, is used instead of the Poisson's ratio, $\nu$, in Equations 7.1 and 7.2.

$$M_x = \left(\beta_1 + \beta_2 \nu \sqrt{\frac{D_x}{D_y}}\right)\frac{qa^2}{\varepsilon} \tag{7.1}$$

$$M_y = \left(\beta_2 + \beta_1 \nu \sqrt{\frac{D_y}{D_x}}\right)qb^2 \tag{7.2}$$

Where $\varepsilon = \frac{a}{b}\sqrt[4]{\frac{D_y}{D_x}}$, where $a$ is the length of the panel parallel to the x-axis and $b$ is the length of the side parallel to the y-axis.

$q$ is the applied uniformly distributed loading.

$\upsilon$ is the Poisson's ratio.

$\beta_1$ and $\beta_2$ are numerical coefficients given in Table A1.1, Appendix 1(a). The table has been reproduced from Table 80, Timoshenko and Woinowsky-Krieger (1959).

$D_x = \dfrac{E_x h^3}{12(1-\nu^2)}$, is the flexural rigidity with respect to the x-axis

$D_y = \dfrac{E_y h^3}{12(1-\nu^2)}$, is the flexural rigidity with respect to the y-axis

$E_x' = \dfrac{E_x}{1-\nu^2}, E_y' = \dfrac{E_y}{1-\nu^2}$, where $E_x$ and $E_y$ are the moduli of elasticity with respect to the x- and y-axes, values determined from wallette tests, Chapter 4, and reported in Section 5.3. Then $D_x = \dfrac{E_x' h^3}{12}$ and $D_y = \dfrac{E_y' h^3}{12}$.

The moments of resistance for the panel are given by Equations 7.3 and 7.4.

$$m_{cx} = f_{tx}Z \qquad (7.3)$$

$$m_{cy} = f_{ty}Z \qquad (7.4)$$

where $f_{tx}$ is the flexural tensile strength of the masonry in horizontal bending, and $f_{ty}$ is the strength in the vertical direction. Z is the section modulus per unit width, and is given by

$Z = \dfrac{h^2}{6}$, where $h$ is the wall thickness.

The failure loads were determined by equating Equation 7.1 to 7.3, and Equation 7.2 to 7.4, and solving for $q$. The results of the analysis are presented in Table 7.5.

**Table 7.4**: Failure Loads of Grey and Yellow Walls – Elastic Analysis Considering Material Orthotropy

| **Panel** | $E_x$ | $E_y$ | $\beta_1$ | $\beta_2$ | $q_x$ | $q_y$ | $q$ (kN/m$^2$) |
|---|---|---|---|---|---|---|---|
| Grey | 10900 | 8700 | 0.0303 | 0.0665 | 0.00807 | 0.0181 | 8.1 |
| Yellow | 10700 | 8600 | 0.0303 | 0.0665 | 0.00673 | 0.0105 | 6.7 |

### 7.3 ANALYSIS

The predicted capacities in Table 7.2 are not very different from the experimental values. However, they are unsafe since they are higher than the test values, with the exception of the prediction for sub-panel 3b (crack pattern 4). It is interesting to note that the method of BS5628, using designation (iii) mortar, predicts the capacities for the main Grey wall panel, sub-panel 3 and sub-panel 3b as 1.8, 0.7 and 1.1 kN/m$^2$, respectively. These are extremely conservative values which would result in wastage of materials.

The predicted load capacities for Hogg's walls are invariably higher than the experimental values. It must be noted that these values are only calculated using horizontal beam strengths since Hogg did not test brick-beams in vertical bending. As a result, the predicted wall panel capacities refer only to horizontal strengths, as it was not possible to check the vertical wall capacities. Results of the walls tested in Chapter 4 (also see Table 7.2 above) of this study show that panel strengths for walls of similar dimensions to Hogg's walls are governed by vertical strength. Coincidentally, however, Hogg's wall panels failed by first developing a vertical crack down the mid-span, followed by two horizontal cracks - one at about one third of the panel height and the other at about two thirds of the height. The vertical crack predominately ran through the units, only de-bonding the perpend joints in few courses. This failure mode (vertical crack appearing first) suggests that the horizontal direction governs the panel strengths in Hogg's walls. Thus, even if vertical beam strength had been obtained, the results in Table 7.3 would likely not be different. The only source of the discrepancy, therefore, can be associated with the support conditions of the walls. Hogg comments that walls number 1 and number 2 did not completely rest on the frame at the top support. Indeed, when elastic theory is employed to calculate the capacities of these walls based on three sides being simply supported, the strengths become 6.3 and 5.7 kN/m$^2$ for wall 1 and wall 2, respectively. One notices that the experimental value lies in between the 3-sided and the 4-sided panel solutions. This strengthens the significance of the boundary conditions.

The predictions by elastic analysis when material orthotropy is taken into consideration are presented in Table 7.5. The predicted failure loads for both wall panels exceed those that are predicted by elastic equations which assume isotropic material behaviour (Table 5.6). The isotropic assumption performed better than the more complicated orthotropic one in the case of the two wall panels tested in the current research, hence, Equations 5.4 and 5.5 (isotropic assumption) as compared to Equations 7.1 and 7.2 (orthotropic assumption) perform better.

## 7.4 DISCUSSIONS

The study of masonry structures demands a combined experimental and numerical approach in order to obtain adequate material characterization, which is used to formulate appropriate constitutive models. This approach was followed in the present study. The experimental data gathered in Chapter 4, which indicated strong material linearity, was used in the numerical simulations of Chapter 5, to validate the applicability of elastic theory in thin joint masonry structures. In this chapter, the performance of the constitutive model has been assessed by comparisons against experimental results available in literature. The assessment of analytical techniques presented in Chapter 3 indicated that elastic analysis is not suitable for handling laterally loaded clay-brick masonry wall panels built with conventional mortars. The material discontinuity introduced by the existence of the joints makes the use of linear elasticity concepts an inappropriate option in those structures. The results of the validation process presented in this chapter, on the other hand, indicate that elastic analysis yields satisfactory results for thin jointed masonry walls. This proves that when thin layer mortars are used, the resulting masonry element behaves as a plate. The flexural strength of the joints is higher than that of the units, but because of their relative size when compared to the units, the joints do not introduce significant material discontinuity as a result of the strength differences.

## 7.5 CONCLUSIONS

The following conclusions are drawn from the work presented in Chapter 7:

- For analysis of the thin-jointed concrete block masonry panels tested in this research, Elastic Theory yielded satisfactory results.
- There was no need to assign orthotropic properties to the masonry panels tested here as the extra tediousness of the calculations did not make any improvements to the predictions. In many cases, the assumption of isotropy yielded results that were as close to experimental data as the results given by orthotropic analysis.

# CHAPTER 8: CONCLUSIONS

## 8.1 RESEARCH FINDINGS

The mechanical behaviour of laterally loaded masonry wall panels made of solid dense concrete blocks and thin layer mortars has been investigated by flexural testing of small-scale wallettes and large wall panels. Numerical modelling has been used to ascertain the observed physical behaviour. An insight into the flexural strength and deformational characteristics of the material from initial application of load until failure has been gained. Limited data on investigation of tensile bond strength of thin jointed concrete block masonry is available in the literature, and information on the flexural response from initial loading to collapse is even more scarce. The main purpose of tracing the Load-Deformation response was to eventually develop constitutive relations for the material behaviour in flexure, which should lead to the development of an analytical prediction model. The results of the tests performed in the research indicated a linear elastic behaviour. The mode of failure indicated that the bonding between the units and the mortar is so strong that the joints have little influence on the nature of the crack pattern, that is, the direction and location of the cracks (failure planes) are independent of the mortar joints. Most failure planes comprised of straight-line cracks that ran in the direction normal to that of the maximum flexural tensile stress. Investigation of the results showed that these cracks were initiated when the principal tensile stress at any point reached the uni-axial flexural tensile strength of the material. These phenomena indicate that the wall panels behave as homogeneous elastic plates. With the results indicating linear elasticity and brittle failure, the next logical step was to examine the applicability of elastic theory in describing the material's behaviour in flexure. This has been done and the results presented in the preceding chapters of this thesis.

The main outcomes of this research are, therefore, summarised as follows:

- The material's behaviour under lateral loading is linear-brittle
- The flexural tensile strength is at least three times higher than that of conventional blockwork built using designation (iii) mortar
- The variability of test results is very low when compared with that of conventional masonry.

Specific points of interest concerning each of these findings have been discussed under the relevant sections of this thesis. In the next section, a summary of the anticipated applications of these findings is presented, and recommendations for further investigations on thin jointed concrete-block masonry structures are outlined.

## 8.2 APPLICATIONS OF RESEARCH FINDINGS

Construction of masonry wall panels using thin layer mortars in combination with bricks or Aircrete blocks is rapidly growing. The extension of the system to include dense concrete blockwork, particularly in the UK, has been slow. For concrete blockwork to enjoy similar success, considerable research work is needed to provide convincing evidence of the benefits to be gained. The current research has gone some way to achieving this objective by providing three major findings listed above. These findings will make an invaluable contribution to the understanding of the behaviour of thin-jointed concrete-block masonry walls in flexure, and will be of benefit to designers, contractors and the authorities charged with the revision and improvement of design Codes. These benefits are summarised here:

- The high flexural tensile strength that has been ascertained will provide confidence to both the designer and the contractor when working with the material. The improved confidence with regards to material strength will be a motivation for designers and contractors to seek new areas of application for the material.

- The current UK code of practice for masonry offers some limited information on thin layer masonry for the first time. The elastic-brittle behaviour in flexure, ascertained by the current investigation, provides a starting point from which the development of constitutive material laws could follow and be included in the code.

- The low variability of test results, also ascertained by the current investigation, is essential for the establishment of partial safety factors for the material, which should be reasonably low for this material. Further, the low variability of test data implies that a large number of tests is not necessary for determining an average value of the material's flexural tensile strength from experiments. This will help to cut down the costs of research.

## 8.3 FURTHER INVESTIGATIONS

Considerable research has been (and continues to be) carried out to ascertain the strength properties of thin layer masonry structures. Early investigations have indicated very favourable improvements over and above traditionally built masonry structures. As a result, this form of construction offers the opportunity to capture new markets. There is danger, therefore, of the system being employed blindly without verifying all of its properties, which may lead to bad practice or wastage. Some of the areas where research data concerning thin jointed concrete block masonry is scarce are cited below:

- Reduction in sound transmittance and water penetration rate needs to be demonstrated. Improvements of thermal and acoustic properties also have to be demonstrated by further investigations.

- The brittle nature of thin jointed masonry inevitably requires inclusion of reinforcements in the walls for most applications. Initially, challenges were how to incorporate reinforcements (and wall ties) in the thin joints. Industry has been innovative in this area and a wide range of reinforcements, including bed-joint mesh for crack-control, are now available in the market. However, data on their effectiveness is insufficient. Research is still needed to investigate and quantify the effectiveness of reinforcements, and to formulate formal design rules for design codes.

- Finally, further development of the research may be focused on design of blocks that are less brittle. Reinforcements might need to be included within dense concrete blocks.

**References**


1. Abboud, B.E., Xin, L. and Becica, I.J., "Deflection of Reinforced Masonry Walls Under Out-of-Plane Loads", Proceedings of the Seventh Canadian Masonry Symposium, Hamilton, Ontario, 1995, pp. 895 – 910.
2. ACI, Building Code for Masonry Structures, The American Concrete Institute; ASCE, Detroit, Michigan, 1992.
3. Adell, J.M., "Integral Masonry System and the Contemporary Façade", Proceedings of the 12th International Brick/Block Masonry Conference, Madrid, June 2000, pp. 107-119.
4. Adell, J.M., "Allwall Clay Brick Plate Test", Proceedings of the 12th International Brick/Block Masonry Conference, Madrid, June 2000, pp. 121-130.
5. Ahmed, A., "Behaviour and Design of High Performance Low Density Aircrete Products", Concrete and Masonry Research Group, Kingston University, London, 2005
6. Anderson, C., "Some Observations on Masonry Wallette Testing", International Journal of Masonry Construction, Vol.2, No.4, 1982, pp. 146-154
7. Anderson, C., "Testing Walls Under Lateral Loading", Research Seminar, Cement and Concrete Association, United Kingdom, July 1981.
8. ANSYS 8.0., Ansys Inc., SAS IP Inc., 2003.
9. Arora, S.K., "Design Based on Load Sharing within Masonry Structures: A Review of Experimental Data", Proceedings of the 10th International Brick and Block Masonry Conference, Calgary, Canada, 1994, Volume1, pp. 163-170.
10. AS 3700 (1988): Masonry Structures, Standards Australia, Sydney
11. AS 3700 (1998): Masonry Structures, Standards Australia, Sydney
12. Baker, I.O., A Treatise on Masonry, Wiley and Son, New York, 1912
13. Baker, L.R., "A Failure Criterion for Brickwork in Biaxial Bending", Proceedings of the 5th International Brick Masonry Conference, Washington, USA, 1979, pp. 71-78.
14. Borchelt, J.G. and Tann, J.A., "Bond Strength and Water Penetration of Low IRA Brick and Mortar", Proceedings of the 7th North American Masonry Conference, Notre Dame, USA, June 1996, pp.206-216.
15. Bouzeghoub, M.C. and Riddington, J.R., "2-D and 3-D Finite Element Analysis of Masonry Walls: A Comparative Study", Proceedings of the 10th International Brick and Block Masonry Conference, Calgary, Canada, 1994, Volume1, pp. 31-40.

16. BRE, "Thin Layer Mortar", Building Research Establishment Website, www.bre.co.uk, 2006
17. British Cement Association, "Approved Document: Basements for Buildings", The Building Regulations, Crowthorne, Berks, 1997.
18. British Masonry Society, "Lateral Loading of Masonry", Society News, Masonry International, London, Winter 2000, pp. ix.
19. Brooks, J.J. and Abu Baker, B.H., "The Modulus of Elasticity of Masonry", Masonry International, Vol. 12, No. 2, Autumn 1998, pp. 58-63.
20. BS EN 1052-2:1999 - Methods of test for masonry: Determination of flexural strength, British Standards Institute, London
21. BS 5628:1992 - Part 1, Code of Practice for Use of masonry, British Standards Institute, London
22. Cajdert, A. and Losberg, A., "The Strength of Horizontally Loaded Brickwork, Analysis of Wind Load", Second Nordic Symposium on Masonry Construction, Copenhagen, 1975.
23. Christiansen P., "Theoretical Determination of Flexural Strength of Unreinforced Masonry", Masonry International, The British Masonry Society, Vol.9 No.3, Winter 1995/96, pp. 84-90.
24. Cowan, H.J., "A History of Masonry and Concrete Domes in Building Construction", Building and Environment, 1977, pp. 12
25. CSAS 304.1, Masonry Design for Buildings, Canadian Standards Association, Rexdale, Ontario, 1995
26. Davies, G.A.O., "Analysis as a Substitute for Full Scale Testing in Aeronautical Structures", Proceedings of a Colloquium held at Burwalls, Bristol University, May 1988, pp.1-11.
27. Department of the Environment, Transport and the Regions, "Rethinking Construction", London, 1998
28. Duarte, R.B., "An Analysis of Brickwork Behaviour in Biaxial Bending", Proceedings of the 12th International Brick/Block Masonry Conference, Madrid, Spain, June 2000, pp.525-534.
29. Duarte, R.B., "The Design of Unreinforced Brickwork Panels with Openings under Lateral Pressure", Masonry International, Volume 11, No 3, February 1998, pp.97-101.
30. Edwards, P.R., "Full-Scale Fatigue Testing of Aircraft Structures", Proceedings of a Colloquium held at Burwalls, Bristol University, May 1988, pp. 13-26.

31. EN 1996-1-1, Eurocode 6: Design of Masonry Structures – Part 1-1: General Rules for Reinforced and Unreinforced Masonry, 1996.
32. Fried, A.N., "Bulletin: Kingston University Sustainable Technology Research Centre", The Structural Engineer, The Institution of Structural Engineers, London, UK, Summer 2005, pp. 45-54.
33. Fried, A.N., "Laterally Loaded Masonry Panels – The Significance of Analytical Methods and Material Properties", PhD Thesis, South Bank Polytechnic, London, 1989.
34. Fried, A.N., "The Influence of Limed and Retarded Mortars on Masonry Bond Strength", Proceedings of the 7th North American Masonry Conference, Notre Dame, USA, June 1996, pp.217-229.
35. Fried, A.N., and Li, S., "The Influence of Moisture Content on Masonry Flexural Strength", Proceedings of the 10th International Brick/Block Masonry Conference, Calgary, Canada, July 1994, pp.939-945.
36. Fried, A.N., Marrocchino, E., Bradsell, C., and Roberts, J.J., "Unreinforced Solid Dense Concrete Block Walls Constructed Using Thin Joint Technology", The Structural Engineer, The Institution of Structural Engineers, London, UK, June 2005, pp.33-37.
37. Fried, A.N., Roberts, J.J., Limbachiya, M.C. and Ahmed, A., "Thin Joint Masonry in the UK", Masonry International, Journal of British Masonry Society, Summer 2005, pp. 85-87.
38. Fried, A.N., Roberts, J.J., and Tovey, A.K., "Unreinforced Masonry Basement Design Using a Revised Method of Analysis", Proceedings of the 6th International Masonry Conference, London, Nov. 2002, pp. 167-171.
39. Fudge, C.A., "Developments with Thin-Joint AAC Masonry in the UK", Proceedings of the 12th International Brick/Block Masonry Conference, Madrid, Spain, June 2000, pp. 633-641.
40. Gazzola, E.A. and Drysdale, R.G., "A Component Failure Criterion for Brickwork in Flexure", Proceedings of Structures Conference, New Orleans, USA, 1986, pp.134-153.
41. Gazzola, E.A., Drysdale, R.G., Antonik, V. and McGrath, R., "Benefits of using The New Canadian Masonry Limit States Design Standard", Proceedings of The Seventh Canadian Masonry Symposium, Hamilton, Canada, Volume 1, 1995, pp. 432-443.
42. Ghali, A., Favre, R., and Elbadry, M., Concrete Structures: Stresses and Deformations, 3rd Edition, Spon Press, London, 2002

43. Ghosh A.K., Made A.M. and Colville J., "Finite Element Modeling of Unreinforced Masonry" Proceedings of the 10th International Brick and Block Masonry Conference, Calgary, Canada, July 1994, pp. 61-70
44. Grandet, J., "Physico-Chemical Mechanisms of the Bond between Clay Products and Cement", Proceedings of the Third International Brick Masonry Conference, Essen, April 1973, pp. 217-221.
45. Groot, C.J.W.P., de Keijser, T.H., and van der Pers, N.M., "Mortar-Brick Bond Problems Studied by Means of X-Ray Diffraction", Proceedings of the 10th International Brick and Block Masonry Conference, Calgary, Canada, July 1994, pp. 947-958.
46. Guggisberg, R. and Thurlimann, B., "Failure Criterion for Laterally Loaded Masonry Walls", Proceedings of the 5th North American Masonry Conference, Urbana-Champaign, USA, 1990, pp.949-958.
47. Hagsten, L.G. and Nielson, M.P., "Laterally Loaded Masonry", Proceedings of the 12th International Brick/Block Masonry Conference, Madrid, Spain, 2000, pp. 841 – 858.
48. Hansen, K.F., "Uniaxial Bending Strength of Masonry Walls", Masonry International, The British Masonry Society, Vol.14 No.3, Winter 2001, pp. 96-100
49. Haseltine, B.A., de Vekey, R.C. and Tutt, J.N., "The Influence of Sand Constituents on the Bond of Mortar and Lateral Performance of Masonry: (ii) Comparison of Wall Results with Design to Yield Line Theory and BS 5628", 10th International Brick/Block Masonry Conference, Calgary, Canada, July 1994, pp.1471-1480.
50. Haseltine, B.A., West, H.W.H., and Tutt, J.N., "Design of Walls to Resist Lateral Loads", The Structural Engineer, October 1977, Vol.55, pp 422 - 430.
51. Haseltine, B.A., West, H.W.H., Hodgkinson, H.R., and Tutt, J.N., "The Resistance of Brickwork to Lateral Loading: Discussion", The Structural Engineer, December 1978, Vol.56A, pp 363 - 374.
52. Hendry, A.W., Structural Brickwork, The MacMillan Press Ltd., London, 1981
53. Heyman, J., Structural Analysis – A Historical Approach, Cambridge, 1998
54. Hetenyi, M., Handbook of Experimental Stress Analysis, Wiley and Son, New York, 1950
55. Hill, R., The Mathematical Theory of Plasticity, Clarendon, Oxford, 1949
56. Hogg, J., "Integrated Procurement Routes for Prefabricated Brickwork", PhD Thesis, Kingston University London, December 2003.

57. Hughes, T.G., Baker, M.G., and Harvey, R.J., "Tensile Strengths of Masonry Components", Masonry International, The British Masonry Society, Volume 13, No.2, 2000, pp.39-43.
58. Jabbar, A., Fried, A., Kanyeto, O.J., and Roberts, J.J., "The Strength of Thin Joint Solid Dense Concrete Blockwork", Seventh International Masonry Conference, London, UK, October/November 2006
59. Jukes, P., and Reddington, J.R. "A Review of Masonry Tensile Bond Strength Test Methods", Masonry International, The British Masonry Society, Volume 12, No.2, 1998, pp.51-57.
60. Jung, E., "The Binding between Mortar and Brick", Proceedings of the 8th International Brick/Block Masonry Conference, Dublin, Ireland, 1988, pp. 182-193.
61. Karihaloo, B.L., Fracture Mechanics and Structural Concrete, Longman Scientific & Technical, Essex, England, 1995.
62. Lange-Kornbak, D., "Mohr-Coulomb Approach to the Ductility of Masonry and Optimum Unit/Block Configuration", Masonry International, The British Masonry Society, Volume 14, No.1, 2000, pp.18-27.
63. Lawrence, S. and Marshall, R, "Virtual Work Method for Masonry Panels under Lateral Load", 12th International Brick/Block Masonry Conference, Madrid, Spain, June 2000, pp.1063-1073.
64. Lawrence, S. and Page, A.W., "Bond Studies in Masonry", 10th International Brick/Block Masonry Conference, Calgary, Canada, July 1994, pp.909-918.
65. Lawrence, S. and Page, A.W., "The Australian Masonry Code", 10th International Brick/Block Masonry Conference, Calgary, Canada, July 1994, pp.1509-1518.
66. Lawrence, S.J., and So, L., "The Influence of some Factors on the Tensile Bond Strength of Masonry", 10th International Brick/Block Masonry Conference, Calgary, Canada, July 1994, pp. 929-938
67. Lawrence, S.J., "Behaviour of Brick Masonry Walls under Lateral Loading", Ph.D. Thesis, School of Civil Engineering, University of New South Wales, November 1983.
68. Lawrence, S.J., "The Behaviour of Masonry in Horizontal Flexure", Proceedings of The Seventh Canadian Masonry Symposium, Hamilton, Canada, Volume 1, 1995, pp.525-536.
69. Lee J.S, Pande, G.N., Middleton, J. and Kralj, "Analysis of Tensile Strength of Masonry" Proceedings of the 10th International Brick and Block Masonry Conference, Calgary, Canada, July 1994, pp. 21-30

70. Li, S., Fried, A.N., and Roberts, J.J., "Deformational Analysis for Reinforced Concrete Blockwork Beams", Proceedings of the Seventh Canadian Masonry Symposium, Hamilton, Ontario, 1995, pp. 501 – 512.

71. Lourenco, B.P. "A Review of Out-of-Plane Behaviour of Masonry", Masonry International, The British Masonry Society, Vol.14, No.3, Winter 2001, pp.67-73

72. Lourenco, P.B., "A Macro-Model for the Out-of-Plane Behaviour of Masonry", 12th International Brick/Block Masonry Conference, Madrid, Spain, June 2000, pp.1101-1114.

73. Lourenco, P.B., Almeida, J.C. and Barros, J.A., "Experimental Investigation of Bricks Under Uniaxial Tensile Testing", Masonry International, The British Masonry Society, Vol.18, No.1, April 2005, pp.11-20.

74. Lourenco, P.B., and Rots, J.G., "On the Use of Homogenisation Techniques for the Analysis of Masonry Structures", Masonry International, Vol. 11, No.1, Summer 1997, pp. 26-32.

75. Lourenco, P.B. and Rots, J.G., "Understanding the Behaviour of Shear Walls: A Numerical Review", Proceedings of the 10th International Brick and Block Masonry Conference, Calgary, Canada, July 1994, pp. 11-20

76. Lourenco, P.B., Rots, J.D., and van der Pluijm R., "Understanding the Tensile Behaviour of Masonry Parallel to the Bed Joints: A Numerical Approach", Masonry International, The British Masonry Society, Vol.12 No.3, Winter 1998/99, pp. 96-103.

77. Lovegrove, R, "A Discussion of Yieldlines in Unreinforced Masonry", The Structural Engineer, Volume 66, No.22, November 1988, pp. 371-375.

78. Maksoud, A.A., and Drysdale, R.G., "Simplified Method for Design of Slender Masonry Walls" Proceedings of the 10th International Brick and Block Masonry Conference, Calgary, Canada, July 1994, pp. 191-200

79. Martens, D.R.W. "Structural Behaviour of Veneer Walls with Thin Layer Mortar", Proceedings of the 12th International Brick/Block Masonry Conference, Madrid, June 2000, pp. 303-307.

80. Maugin, G.A., The Thermo-mechanics of Plasticity and Fracture, Cambridge University Press, 1992.

81. Middleton, A.C. and Drysdale, R.G., "Flexural Capacities of Concrete Block Walls with Openings", Proceedings of The Seventh Canadian Masonry Symposium, Hamilton, Canada, Volume 1, 1995, pp. 537-546.

82. Mullins, P.J., and O'Connor, C. "Brick Walls Spanning Vertically – A Theoretical Investigation of the Capacity to Resist Out-of-Plane Loads",

Proceedings of the 9th International Brick/Block Masonry Conference, Berlin, Germany, October, 1991, pp.800-807.

83. Nichols, J.M., "A Study of the Progressive Degradation of Masonry Shear Walls Subjected to Harmonic Loading", PhD Thesis, University of Newcastle, Australia, 2000
84. Page, A.W., "Finite Element Model for Masonry", Journal of Structural Division, American Society of Civil Engineers, Vol.104, No.8, 1978, pp.1267-1285.
85. Page, A.W., "The Design, Detailing and Construction of Masonry – The Lessons from the Newcastle Earthquake", Civil Engineering Transactions, I.E. Australia, Vol.CE34, No.4, December 1992, pp. 348-353.
86. Pande, G.N., Middleton, J., Lee, J.S., and Kralj, "Numerical Simulation of Cracking and Collapse of Masonry Panels Subject to Lateral Loading" Proceedings of the 10th International Brick and Block Masonry Conference, Calgary, Canada, July 1994, pp. 107-116
87. Park, R and Gamble, W.L, Reinforced Concrete Slabs, 2nd Edition, John Wiley & Sons, Inc., New York, 2000
88. Reeh, H., "Design of Masonry by Simple Rules", Proceedings of the 10th International Brick and Block Masonry Conference, Calgary, Canada, July 1994, pp. 183-190.
89. Roberts, J.J., Fried, A.N. and Tovey, A.K., "Design of Plain Masonry Basement Walls", Journal of the Institution of Structural Engineers, Vol. 80, No. 11, June 2002.
90. Roberts, J.J., Fried, A.N. and Tovey, A.K., "Plain Masonry Basement Walls", Kingston University, Surrey, 1999.
91. Robison, J.I, Thavalingam, A, Ponniah D.A. and Bicanic, N, "Comparative Predictions of the Collapse Load for Masonry Arches Including Backfill Effects", Masonry International, Vol.14, No.3, 2001, pp. 91 – 95.
92. Sakr, K.M., and Neis, V.V., "Full Scale Testing of Masonry Cavity Walls Subjected to Lateral Loading", Proceedings of the 10th International Brick and Block Masonry Conference, Calgary, Canada, July 1994, pp. 629-638.
93. Schubert, P., "Tensile and Flexural Strength of Masonry: Influences, Test Methods, Test Results", 10th International Brick/Block Masonry Conference, Calgary, Canada, July 1994, pp.895-908.
94. Schultz, A., Mueffelman, J.M. and Ojarde, N.J., "Critical Axial Loads for Transversely Loaded Masonry Walls", 12th International Brick/Block Masonry Conference, Madrid, Spain, June 2000, pp.1625-1632.

95. Sinha, B.P. and Chee Liang, Ng., "Behaviour of Brickwork Panels Under Lateral Pressure", Proceedings of the 10th International Brick/Block Masonry Conference, Calgary, Canada, July 1994, pp.649-658.

96. Sinha, B.P., "A Simplified Ultimate Load Analysis of Laterally Loaded Model Orthotropic Brickwork Panels of Low Tensile Strength", The Structural Engineer, December 1978, Vol.56B, pp 81 - 84.

97. Sjostrand, O., "Generalized Design Method of Laterally Loaded Masonry Walls", Proceedings of the 10th International Brick/Block Masonry Conference, Calgary, Canada, July 1994, pp. 151-162.

98. Sui, C., Rafiq, M.Y., Easterbrook, D., Bugmann, G., and Zhou, G., "More Accurate Predictions of the Behaviour of Masonry Panel Subjected to Lateral Loads", Seventh International Masonry Conference, London, UK, October/November 2006.

99. Sui, C., Rafiq, M.Y., Easterbrook, D., Bugmann, G., and Zhou, G., "Uniqueness Study to Update FEA Models of Laterally Loaded Masonry Panels by Genetic Algorithm", Seventh International Masonry Conference, London, UK, October/November 2006.

100. Sui, C., Rafiq, M.Y., Easterbrook, D., Bugmann, G., and Zhou, G., "An Investigation into Numerical Model Updating of Masonry Panels Subjected to Laterally Load", Seventh International Masonry Conference, London, UK, October/November 2006

101. Timoshenko, S.P., and Woinowsky-Krieger, S., Theory of Plates and Shells, Second Edition, McGraw-Hill International Editions, Singapore, 1959.

102. Tovey,, A.K., "Basements 1 – Benefits, Viability and Costs", British Cement Association, Crowthorne, Berks, 1999.

103. Tzamtzis, A.D. and Asteris, P.G., "A 3D Model for Non-Linear 'Microscopic' FE Analysis of Masonry Structures", Proceedings of The 6th International Masonry Conference, London, Nov. 2002, pp. 493-497.

104. van der Pluijm, R., Ruytten, H.S. and Schiebroek, C.S., "Flexural Behaviour of Masonry in Different Directions", Proceedings of the 4th International Masonry Conference, London, UK, 1995, pp.117-123.

105. van Geel, E., and van der Pluijm, R., "The Variability of Tensile Bond Strength", Proceedings of the 10th International Brick/Block Masonry Conference, Calgary, Canada, July 1994, pp. 959-968.

106. Valluzzi, M.R., da Porto, F. and Modena, C., "Mechanical Behaviour of Masonry Made of Flat Blocks and Thin Mortar Joints", Proceedings of the 6th International Masonry Conference, London, Nov. 2002, pp. 503-511.

107. Vekemans, H.J. and Ruben, M.P., "Prefabricated Façades with Glue and Bricks", Proceedings of the 12th International Brick/Block Masonry Conference, Madrid, June 2000, pp. 518-522.

108. Wakefield, D.A., "Mortar and its Effect on Masonry", Proceedings of the 7th North American Masonry Conference, Notre Dame, USA, June 1996, pp.153-166.

# APPENDICES

## Appendix 1: Analytical Equations

(a) Derivation of Elastic Analysis Equations

(b) Yield Line Equations

(c) Fracture Line Equations

(d) Strip Method Equations

## Appendix 2: Finite Element Data

(a) Tables

(b) Stress distributions

## Appendix 3: Data for Chapter 3

(a) Table A3.1

(b) Table A3.2

## Appendix 4: Results of the Testing Programme

(a) Load/Displacement data : Wallettes

(b) Load/Displacement data : Walls

(c) Failure Modes (Pictures)

## Appendix 5: Mathematical Analysis

(a) Best-Fit Polynomials for Wallette Load/Displacement Graphs

(b) Derivation of deflection equation

(c) Calculation of Wall Displacements

# Appendix 1: Analytical Equations

(a) Derivation of Elastic Analysis Equations

(b) Yield Line Equations

(c) Fracture Line Equations

(d) Strip Method Equations

## (a): Derivation of Elastic Analysis Equations

Governing differential equation for deflections

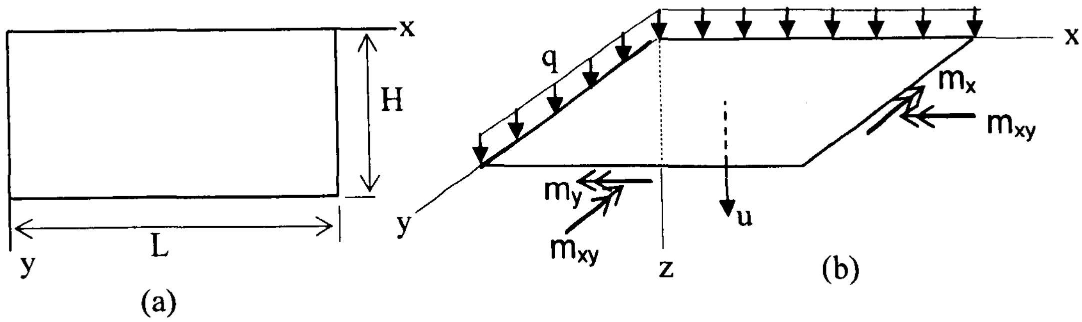


Figure A1.1: Rectangular plate, (a) dimensions, (b) forces and lateral displacement

Elastic deformations of isotropic plates loaded normal to their plane, as in Figure A1.1(b), are governed by a fourth-order partial differential equation:

$$\frac{\partial^4 u}{\partial x^4} + 2\frac{\partial^4 u}{\partial x^2 \partial y^2} + \frac{\partial^4 u}{\partial y^4} = \frac{q}{D} \qquad \text{(A1.1)}$$

where $u$ is the deflection of the plate in the direction of loading at point $(x, y)$, $q$ the load imposed on the plate per unit area, a function of $x$ and $y$, $D$ is the flexural rigidity of the plate. In the case of simply supported rectangular plates loaded with uniformly distributed load, Navier solution [Timoshenko, 1959] of equation (A1.1) is in the form of a series:

$$u = \frac{16q_0}{\pi^6 D}\sum_{m=1}^{\infty}\sum_{n=1}^{\infty}\frac{\sin\frac{m\pi x}{L}\sin\frac{n\pi y}{H}}{mn(\frac{m^2}{L_2}+\frac{n^2}{H^2})^2} \qquad \text{(A1.2)}$$

where $m$ = 1,3,5,..., and $n$ = 1,3,5,...

$q_0$ is the intensity of the uniformly distributed load,

$D = \frac{Et^3}{12(1-v^2)}$, is the flexural rigidity of the plate, of thickness $t$,

$E$ is the modulus of elasticity of the material, and

$v$ is the Poisson's ratio.

The series (A1.2) converges rapidly, and a satisfactory approximation is obtained by taking only the first term of the series. Thus

$$u = \frac{16q_0}{\pi^6 D}\frac{1}{(\frac{1}{L^2}+\frac{1}{H^2})^2}\sin\frac{\pi x}{L}\sin\frac{\pi y}{H} \qquad \text{(A1.3)}$$

The maximum deflection occurs at the centre of the panel, that is, at $x = \frac{L}{2}$ and $y = \frac{H}{2}$. Hence, the maximum deflection is given by

$$u_{\max} = \frac{16q_0}{\pi^6 D} \frac{1}{(1/L^2 + 1/H^2)^2} \tag{A1.4}$$

<u>Bending moments</u>

The bending moment fields are given by the following expressions:

$$m_x = -D(\frac{\partial^2 u}{\partial x^2} + \nu \frac{\partial^2 y}{\partial y^2}) \tag{A1.5}$$

$$m_y = -D(\nu \frac{\partial^2 u}{\partial x^2} + \frac{\partial^2 y}{\partial y^2}) \tag{A1.6}$$

$$m_{xy} = -D(1-\nu) \frac{\partial^2 u}{\partial x \partial y} \tag{A1.7}$$

Where $m_x$ is the bending moment that causes stresses parallel to the x-axis, $m_y$ the moment that causes bending stresses parallel to the y-axis, and $m_{xy}$ is a twisting moment, see Figure A1.1(b). By substituting appropriate partial derivatives of equation (A1.2) into equations (A1.5) – (A1.7), bending moments at any point, $(x, y)$, on the panel can be evaluated. These are given by the following expressions:

$$m_x = \frac{16q_0}{\pi^4} \sum_{m=1,3,\ldots}^{\infty} \sum_{n=1,3,\ldots}^{\infty} \frac{\sin\frac{m\pi x}{L} \sin\frac{n\pi y}{H}}{mn\left(\frac{m^2}{L^2} + \frac{n^2}{H^2}\right)^2} \left(\frac{1}{L^2} + \frac{\nu}{H^2}\right) \tag{A1.8}$$

$$m_y = \frac{16q_0}{\pi^4} \sum_{m=1,3,\ldots}^{\infty} \sum_{n=1,3,\ldots}^{\infty} \frac{\sin\frac{m\pi x}{L} \sin\frac{n\pi y}{H}}{mn\left(\frac{m^2}{L^2} + \frac{n^2}{H^2}\right)^2} \left(\frac{\nu}{L^2} + \frac{1}{H^2}\right) \tag{A1.9}$$

$$m_{xy} = -\frac{16q_0(1-\nu)}{\pi^4 LH} \sum_{m=1,2,\ldots}^{\infty} \sum_{n=1,2,\ldots}^{\infty} \frac{\cos\frac{m\pi x}{L} \cos\frac{n\pi y}{H}}{mn\left(\frac{m^2}{L^2} + \frac{n^2}{H^2}\right)^2} \tag{A1.10}$$

The maximum values of $m_x$ and $m_y$ occur at the centre of the panel, while the maximum twisting moment, $m_{xy}$, occurs at the corners of the panel. The series (A1.8) – (A1.10) are not so rapidly convergent as series (A1.2), and other forms of solution are sometimes preferred. Taking the first 4 terms of the series, we obtain the following expressions for the maximum values of $m_x$ and $m_y$:

$$m_{x\max} = \frac{16q_0}{\pi^4}\left(\frac{1}{L^2}+\frac{\nu}{H^2}\right)\left[\frac{1}{\left(\frac{1}{L^2}+\frac{1}{H^2}\right)^2} - \frac{1}{3\left(\frac{9}{L^2}+\frac{1}{H^2}\right)^2} - \frac{1}{3\left(\frac{1}{L^2}+\frac{9}{H^2}\right)^2} + \frac{1}{9\left(\frac{9}{L^2}+\frac{9}{H^2}\right)^2}\right]$$

.................................................................................................. (A1.11)

$$m_{y\max} = \frac{16q_0}{\pi^4}\left(\frac{\nu}{L^2}+\frac{1}{H^2}\right)\left[\frac{1}{\left(\frac{1}{L^2}+\frac{1}{H^2}\right)^2} - \frac{1}{3\left(\frac{9}{L^2}+\frac{1}{H^2}\right)^2} - \frac{1}{3\left(\frac{1}{L^2}+\frac{9}{H^2}\right)^2} + \frac{1}{9\left(\frac{9}{L^2}+\frac{9}{H^2}\right)^2}\right]$$

.................................................................................................. (A1.12)

Equations (A1.11) and (A1.12) can be expressed, respectively, as:

$$m_x = \alpha_x q_0 L^2 \qquad \text{(A1.13)}$$

and $$m_y = \alpha_y q_0 L^2 \qquad \text{(A1.14)}$$

where $\alpha_x$ and $\alpha_y$ are moment coefficients relative to the x- and y-axis, respectively, and are given by

$$\alpha_x = \frac{16}{\pi^4}\left(1+\frac{L^2\nu}{H^2}\right)\left[\frac{1}{\left(1+\frac{L^2}{H^2}\right)^2} - \frac{1}{3\left(9+\frac{L^2}{H^2}\right)^2} - \frac{1}{3\left(1+\frac{9L^2}{H^2}\right)^2} + \frac{1}{9\left(9+\frac{9L^2}{H^2}\right)^2}\right] \qquad \text{(A1.15)}$$

$$\alpha_y = \frac{16}{\pi^4}\left(\nu+\frac{L^2}{H^2}\right)\left[\frac{1}{\left(1+\frac{L^2}{H^2}\right)^2} - \frac{1}{3\left(9+\frac{L^2}{H^2}\right)^2} - \frac{1}{3\left(1+\frac{9L^2}{H^2}\right)^2} + \frac{1}{9\left(9+\frac{9L^2}{H^2}\right)^2}\right] \qquad \text{(A1.16)}$$

## Bending of Orthotropic Plates

***Table A1.1**: Constants for a Simply Supported Rectangular Orthotropic Plate

| $\varepsilon$ | $\alpha$ | $\beta_1$ | $\beta_2$ |
|---|---|---|---|
| 1.0 | 0.00407 | 0.0368 | 0.0368 |
| 1.1 | 0.00488 | 0.0359 | 0.0447 |
| 1.2 | 0.00565 | 0.0344 | 0.0524 |
| 1.3 | 0.00639 | 0.0324 | 0.0597 |
| 1.4 | 0.00709 | 0.0303 | 0.0665 |
| 1.5 | 0.00772 | 0.0280 | 0.0728 |

*Reproduced from Table 80 (Timoshenko and Woinowsky-Krieger 1959)

## (b): Yield Line Equations

The Yield Line equations used to calculate the panel failure loads of Table 3.1 (Chapter 3) are summarised here.

Notation:

$m$ is the ultimate moment per unit length along bed joint

$\mu$ is the orthogonal strength ratio

$K = \dfrac{E_x}{E_y}$ is the ratio of modulus of elasticity in two directions

$\beta$ is a crack pattern parameter

$L$ is the length of panel

$H$ is the wall height

$\alpha$ is the aspect ratio ($H/L$)

$w$ is the failure pressure

is the simple support

is the continuous support

is the positive fracture line

------ is the negative fracture line

(i) Simply supported along all edges

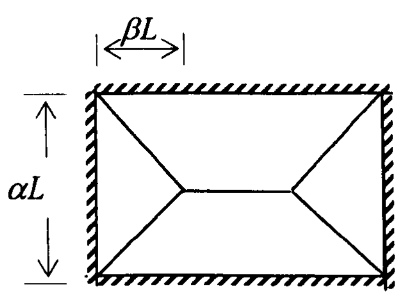


$$w = \frac{m(2\beta\alpha^2 + \mu)}{3\beta L^2(3-2\beta)}, \quad \beta = \frac{\sqrt{\mu^2 + 3\alpha^2\mu} - \mu}{2\alpha^2}$$

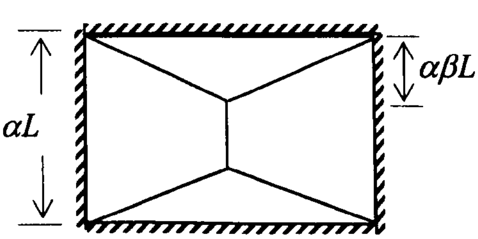


$$w = \frac{m(\alpha^2 + 2\beta\mu)}{3\beta L^2(3-2\beta)}, \quad \beta = \frac{\sqrt{\alpha^2 + 3\alpha^2\mu} - \alpha^2}{2\mu}$$

(ii) All edges built-in

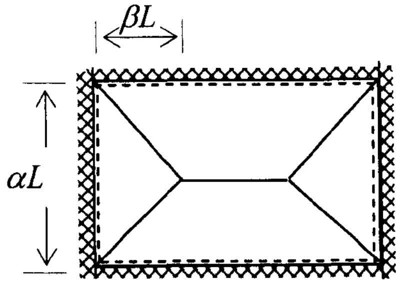


$$w = \frac{2m(2\beta\alpha^2 + \mu)}{3\beta L^2(3-2\beta)}, \quad \beta = \frac{\sqrt{\mu^2 + 3\alpha^2\mu - \mu}}{2\alpha^2}$$

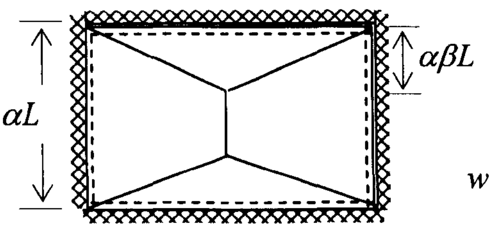


$$w = \frac{2m(\alpha^2 + 2\beta\mu)}{3\beta L^2(3-2\beta)}, \quad \beta = \frac{\sqrt{\alpha^2 + 3\alpha^2\mu - \alpha}}{2\mu}$$

(iii) Simply supported top and bottom, built-in sides

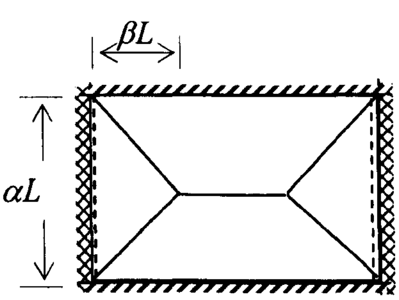


$$w = \frac{2m(\beta\alpha^2 + \mu)}{3\beta L^2(3-2\beta)}, \quad \beta = \frac{\sqrt{4\mu^2 + 6\alpha^2\mu - 2\mu}}{2\alpha^2}$$

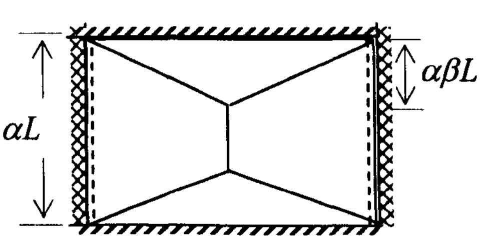


$$w = \frac{m(\alpha^2 + 4\beta\mu)}{3\beta L^2(3-2\beta)}, \quad \beta = \frac{\sqrt{\alpha^2 + 6\alpha^2\mu - \alpha}^{\,2}}{4\mu}$$

(iv) Simply supported bottom, free top, and built-in sides

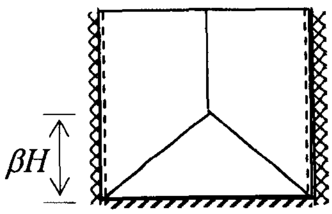


$$w = \frac{6m(\alpha^2 + 8\beta\mu)}{\beta L^2 (3-\beta)}, \quad \beta = \frac{\sqrt{\alpha^2 + 24\alpha^2\mu} - \alpha^2}{8\mu}$$

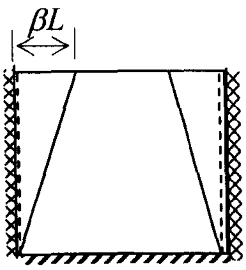


$$w = \frac{6m(\beta^2\alpha^2 + 8\mu)}{\beta L^2 (3-\beta)}, \quad \beta = \frac{\sqrt{64\mu^2 + 72\alpha^2\mu} - 8\mu}{3\alpha^2}$$

(v) Simply supported bottom and sides, free top

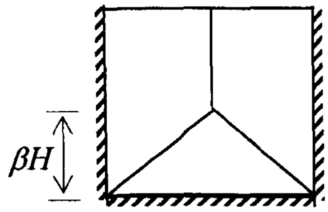


$$w = \frac{6m(\alpha^2 + 4\beta\mu)}{\beta L^2 (3-\beta)}, \quad \beta = \frac{\sqrt{\alpha^2 + 12\alpha^2\mu} - \alpha^2}{4\mu}$$

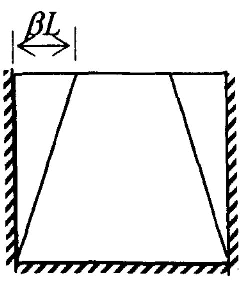


$$w = \frac{6m(\beta^2\alpha^2 + 4\mu)}{\beta L^2 (3-\beta)}, \quad \beta = \frac{\sqrt{16\mu^2 + 36\alpha^2\mu} - 4\mu}{3\alpha^2}$$

(c): Strip Method Equations

The Strip method equations used to calculate the panel failure loads of Table 3.1 (Chapter 3) are summarised here. These equations were derived from equilibrium principles applied to failure mechanisms similar to the yield line crack patterns sketched above. Requirements of the Lower Bound Theorem are satisfied.

Notation:

$m$ is the ultimate moment per unit length along bed joint

$\mu$ is the orthogonal strength ratio

$K = \dfrac{E_x}{E_y}$ is the ratio of modulus of elasticity in two directions

$\beta$ is a crack pattern parameter

$L$ is the length of panel

$H$ is the wall height

$\alpha$ is the aspect ratio ($H/L$)

$w$ is the failure pressure

(i) All sides simply supported, $w = \dfrac{8m}{L^2}(\mu + \alpha^2)$

(ii) All sides built-in, $w = \dfrac{12m}{L^2}(\mu + \alpha^2)$

(iii) Simply supported, $w = \dfrac{4m}{L^2}(3\mu + 2\alpha^2)$

(iv) Simply supported bottom, free top, and built-in sides

$$w = \frac{2m}{L^2}(6\mu + \alpha^2)$$

(v) Simply supported bottom and sides, free top

$$w = \frac{2m}{L^2}(4\mu + \alpha^2)$$

## (d): Fracture Line Theory Equations

The following equations were used to calculate the values in Table 3.1 (Chapter 3). These equations were derived from energy principles by Sinha et al and are reproduced from reference [34].

Notation:

$m$ is the ultimate moment per unit length along bed joint

$\mu m$ is the ultimate moment per unit length normal to bed joint

$K = \frac{E_x}{E_y}$ is the ratio of modulus of elasticity in two directions

| | |
|---|---|
| is the simple support | $L$ is the length of panel |
| is the continuous support | $\alpha$ is the aspect ratio ($h/L$) |
| is the positive fracture line | $w$ is the failure pressure |
| ------ is the negative fracture line | $\beta$ is a factor |

(i) Panels simply supported along four edges

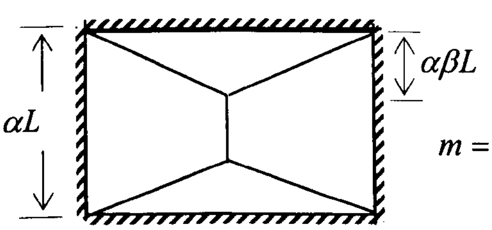


$$m = \frac{w\alpha^2 L^2}{6}\left[\frac{1.5\beta - \beta^2}{1 + \frac{2\mu\alpha^2\beta}{K}}\right], \quad \beta = \frac{K}{2\mu\alpha^2}\left[\sqrt{\frac{3\mu\alpha^2}{K} + 1} - 1\right]$$

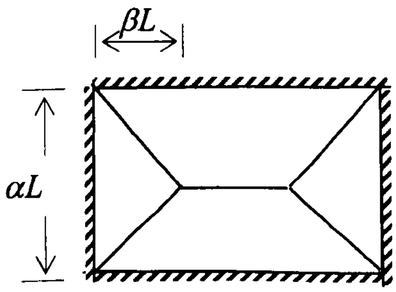


$$m = \frac{w\alpha^2 L^2}{6}\left[\frac{1.5\beta - \beta^2}{2\beta + \frac{\mu\alpha^2}{K}}\right], \quad \beta = \frac{\mu\alpha^2 K}{2K}\left[\sqrt{\frac{3K}{\mu\alpha^2} + 1} - 1\right]$$

(ii) Simply supported along two opposite edges, fully fixed along the third, and free along the fourth edge

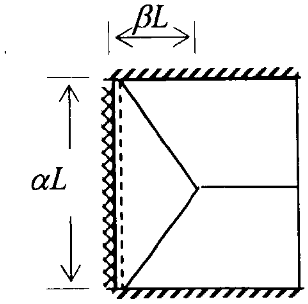


$$m = \frac{w\alpha^2 L^2}{12}\left[\frac{3\beta - \beta^2}{2\beta + \frac{\mu\alpha^2}{K}}\right], \quad \beta = \frac{\mu\alpha^2}{2K}\left[\sqrt{\frac{6K}{\mu\alpha^2}+1}-1\right]$$

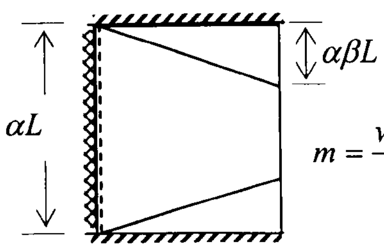


$$m = \frac{w\alpha^2 L^2}{12}\left[\frac{3\beta - \beta^2}{1 + \frac{\mu\alpha^2\beta^2}{K} + \frac{\mu\alpha^{2\beta}}{2K}}\right], \quad \beta = \frac{K}{2\mu\alpha^2}\left[\sqrt{\frac{3\mu\alpha^2}{K}+1}-1\right]$$

(iii) Simply supported along three edges and free along the fourth

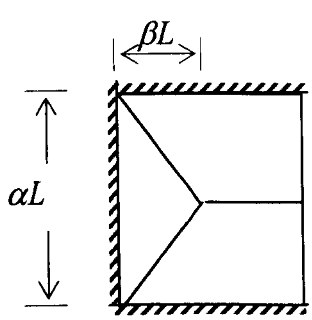


$$m = \frac{w\alpha^2 L^2}{6}\left[\frac{3\beta - \beta^2}{4\beta + \frac{\mu\alpha^2}{K}}\right], \quad \beta = \frac{\mu\alpha^2}{4K}\left[\sqrt{\frac{12K}{\mu\alpha^2}+1}-1\right]$$

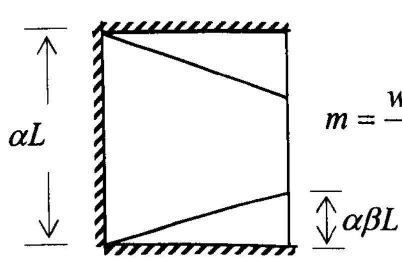


$$m = \frac{w\alpha^2 L^2}{12}\left[\frac{3\beta - \beta^2}{1 + \frac{\mu\beta^2\alpha^2}{K}}\right], \quad \beta = \frac{K}{1.5\mu\alpha^2}\left[\sqrt{\frac{2.25\mu\alpha^2}{K}+1}-1\right]$$

# Appendix 2: Finite Element Data

(a) Tables

(b) Stress distributions

(a) Tables

**Failure Loads for the walls predicted using FEA and Wallette test results**

Maximum Stresses on walls due to unit UDL, obtained by FEA: Sy = 0.14772 Sx = 0.072995 N/mm^2

**Table A2.1: Grey Wall**

| Wallette No. | *Wallette Stress, Sw (N/mm^2) | "Failure Load, Pu (kPa) |
|---|---|---|
| B1 | 1.03 | 6.97 |
| B2 | 1.43 | 9.68 |
| B3 | 1.27 | 8.60 |
| B4 | 1.41 | 9.55 |
| B5 | 1.29 | 8.73 |
| B6 | 1.42 | 9.61 |
| | | |
| P1 | 1.47 | 20.14 |
| P2 | 1.83 | 25.07 |
| P3 | 0.25 | 3.42 |
| P4 | 1.9 | 26.03 |
| P5 | 1.76 | 24.11 |
| P6 | 1.95 | 26.71 |

**Table A2.2: Yellow Wall**

| Wallette No. | *Wallette Stress, Sw (N/mm^2) | "Failure Load, Pu (kPa) |
|---|---|---|
| B1 | 0.78 | 5.28 |
| B2 | 0.74 | 5.01 |
| B3 | 0.75 | 5.08 |
| B4 | 0.63 | 4.26 |
| B5 | 0.76 | 5.14 |
| B6 | 0.87 | 5.89 |
| | | |
| P1 | 1.22 | 16.71 |
| P2 | 1.34 | 18.36 |
| P3 | 1.19 | 16.30 |
| P4 | 1.04 | 14.25 |
| P5 | 1.22 | 16.71 |
| P6 | 1.12 | 15.34 |

* from lab tests
" Failure load of wall, Pu = Sw / Sy,x

| | | | | |
|---|---|---|---|---|
| Swy (avr.) | 1.30833333 | (B-wallettes) | Swy(avr.) | 0.755 |
| Swx(avr.) | 1.782 | (P-wallettes) | Swx(avr.) | 1.1883333 |

(b) Stress Distributions in Walls

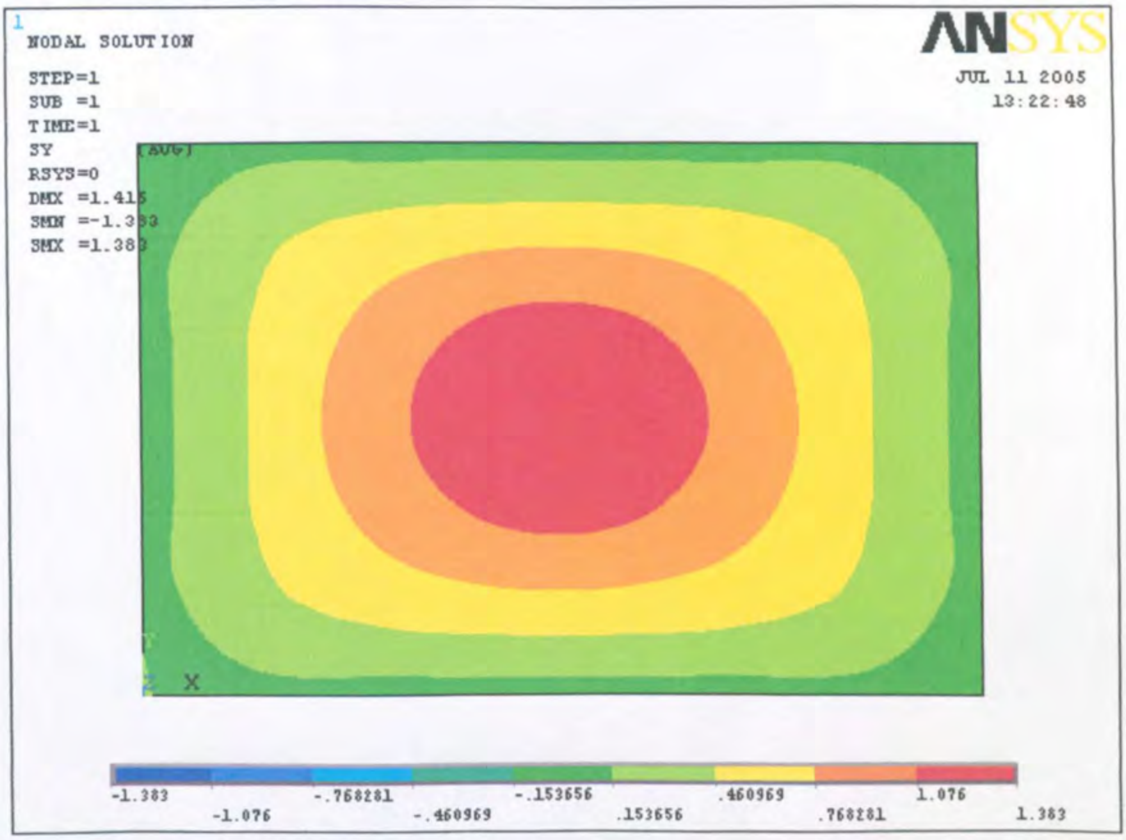


Figure A2.1: Stress distribution in Grey Wall when lateral load = 7.2 kN/m$^2$.

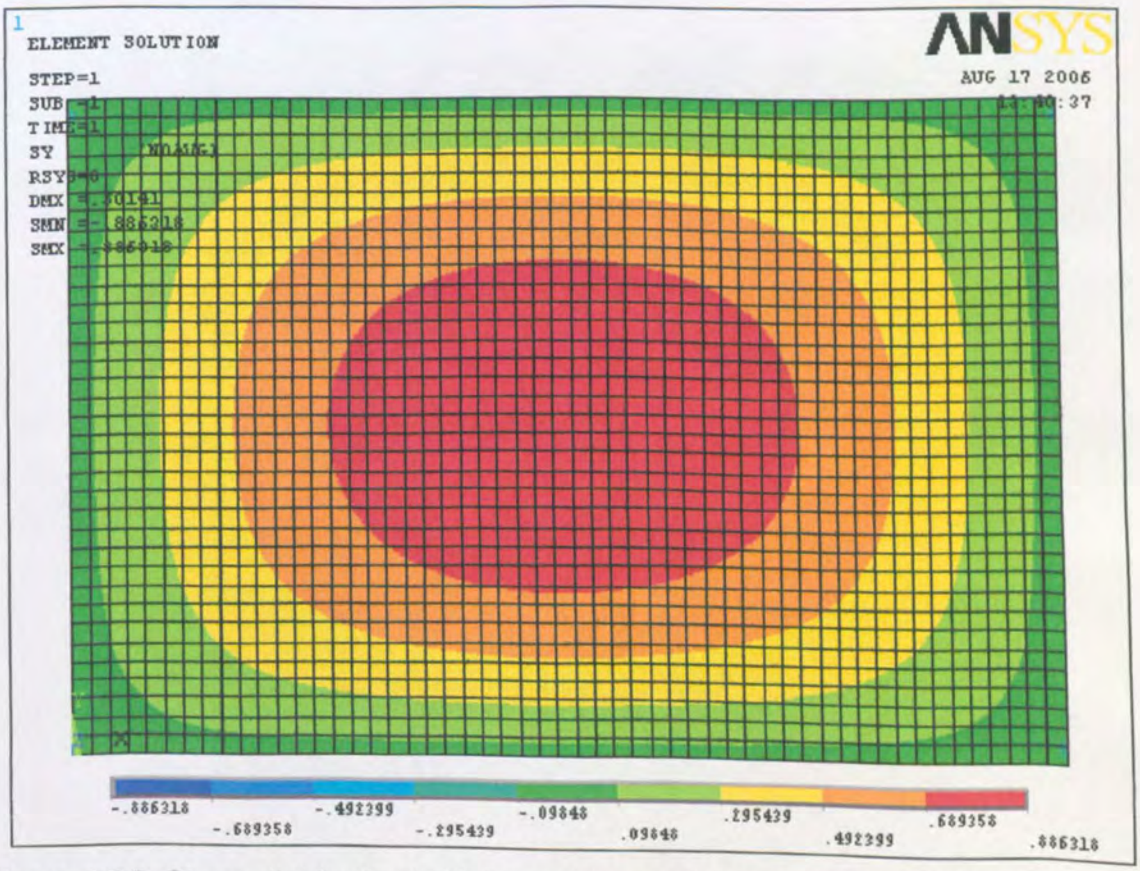


Figure A2.2: Stress distribution in Yellow Wall when lateral load = 6.0 kN/m$^2$.

# Appendix 3: Data for Chapter 3

(a) Table A3.1

(b) Table A3.2

**Table A3.1: Theoretical and Experimental Failure Loads of Panels**

| | | | | | | | | | | | moment coefficient, α | | | | Wk (kPa) | | | | Tests (Lawrence) (kPa) | | |
|---|---|---|---|---|---|---|---|---|---|---|---|---|---|---|---|---|---|---|---|---|---|
| Test # | B.C. | fkx | H | t | L | μ | Asp. ratio | Ex | Ey | β | YL | elastic | Strip | Crk. Line | YL | Elastic | Strip | Crack Line | Full crack | Initial crack | Ulti. Load |
| 6 | 2 | 1.93 | 3 | 0.11 | 6 | 0.810 | 0.500 | 19.05 | 20.81 | | 0.01 | 0.0158 | 0.0173 | | 10.81 | 6.84 | 6.24 | | 4.4 | 1.9 | 8 |
| 7 | 2 | 1.46 | 3 | 0.11 | 6 | 0.699 | 0.500 | 18.46 | 20.67 | | 0.011 | 0.0158 | 0.0177 | | 7.44 | 5.18 | 4.61 | | 4.4 | 2.3 | 8.1 |
| 8 | 1 | 1.96 | 3 | 0.11 | 6 | 0.638 | 0.500 | 16.93 | 21.29 | 0.3003 | 0.024 | 0.0464 | 0.0270 | 0.0394 | 4.57 | 2.37 | 4.07 | 2.79 | 3 | 1.6 | 3.2 |
| 9 | 3 | 2.32 | 3 | 0.112 | 6 | 0.457 | 0.500 | 15.92 | 21.33 | 0.6289 | 0.022 | 0.0142 | 0.0267 | 0.0165 | 6.12 | 9.49 | 5.05 | 8.17 | 2.5 | 1.6 | 5.5 |
| 10 | 5 | 2.1 | 3 | 0.112 | 6 | 0.400 | 0.500 | 16.04 | 20.51 | | 0.031 | 0.022 | 0.0893 | | 3.93 | 5.54 | 1.37 | | 1.7 | 1.7 | 1.7 |
| 12 | 1 | 1.93 | 2.5 | 0.112 | 2.5 | 0.420 | 1.000 | 13.85 | 19.34 | 0.4318 | 0.061 | 0.0479 | 0.0881 | 0.0802 | 10.58 | 13.48 | 7.33 | 8.05 | 8.6 | 7.6 | 8.6 |
| 13 | 2 | 2.08 | 2.5 | 0.112 | 2.5 | 0.413 | 1.000 | 14.07 | 17.35 | | 0.03 | 0.0231 | 0.0590 | | 23.19 | 30.12 | 11.80 | | 9.1 | 9.1 | 12.1 |
| 14 | 3 | 2.06 | 2.5 | 0.112 | 2.5 | 0.519 | 1.000 | 15.77 | 19.93 | 0.4655 | 0.0355 | 0.0244 | 0.0703 | 0.0361 | 19.41 | 28.24 | 9.81 | 19.08 | 11.3 | 11.3 | 20 |
| 15 | 5 | 2.09 | 2.5 | 0.112 | 2.5 | 0.493 | 1.000 | 14.65 | 20.49 | | 0.083 | 0.039 | 0.1683 | | 8.42 | 17.93 | 4.15 | | 7.8 | 7.8 | 7.8 |
| 16 | 4 | 2.17 | 2.5 | 0.109 | 2.5 | 0.336 | 1.000 | 19.16 | 24.49 | | 0.0493 | 0.0972 | 0.1657 | | 13.95 | 7.07 | 4.15 | | 8 | 8 | 14 |
| 17 | 5 | 1.93 | 2.5 | 0.109 | 3.75 | 0.451 | 0.667 | 19 | 25.06 | | 0.067 | 0.03 | 0.1234 | | 4.06 | 9.06 | 2.20 | | 3.4 | 3.4 | 3.4 |
| 18 | 1 | 2.06 | 2.5 | 0.109 | 3.75 | 0.393 | 0.667 | 21.09 | 26.09 | 0.3088 | 0.043 | 0.0498 | 0.0473 | 0.0670 | 6.75 | 5.82 | 6.13 | 4.33 | 4.9 | 2.9 | 4.9 |
| 19 | 3 | 1.76 | 2.5 | 0.109 | 3.75 | 0.432 | 0.667 | 18.74 | 24.63 | 0.5802 | 0.028 | 0.0179 | 0.0431 | 0.0249 | 8.85 | 13.85 | 5.75 | 9.94 | 4.8 | 4.3 | 6.7 |
| 20 | 2 | 1.9 | 2.5 | 0.109 | 3.75 | 0.416 | 0.667 | 16.18 | 22.29 | | 0.021 | 0.0203 | 0.0313 | | 12.74 | 13.18 | 8.56 | | 5.2 | 3.6 | 11.6 |
| 21 | 4 | 1.87 | 2.5 | 0.109 | 3.75 | 0.460 | 0.667 | 18.9 | 24.32 | | 0.0415 | 0.0558 | 0.0998 | | 6.35 | 4.72 | 2.64 | | 3.9 | 3.6 | 4 |
| 22 | 1 | 1.98 | 2.5 | 0.111 | 5 | 0.485 | 0.500 | 18.2 | 24.15 | 0.2761 | 0.029 | 0.0464 | 0.0279 | 0.0449 | 5.61 | 3.51 | 5.84 | 3.62 | 4.7 | 3.1 | 4.7 |
| 23 | 2 | 2.22 | 2.5 | 0.111 | 5 | 0.545 | 0.500 | 18.72 | 23.67 | | 0.015 | 0.0158 | 0.0183 | | 12.16 | 11.54 | 9.95 | | 5.5 | 2.9 | 9.9 |
| 24 | 3 | 2.56 | 2.5 | 0.111 | 5 | 0.512 | 0.500 | 18.2 | 22.87 | 0.6246 | 0.021 | 0.0142 | 0.0262 | 0.0163 | 10.01 | 14.81 | 8.02 | 12.94 | 5 | 2.9 | 6.4 |
| 25 | 4 | 2.09 | 2.5 | 0.111 | 5 | 0.550 | 0.500 | 18.28 | 23.96 | | 0.035 | 0.0293 | 0.0685 | | 4.90 | 5.86 | 2.51 | | 2.6 | 2.6 | 3.9 |
| 26 | 5 | 1.99 | 2.5 | 0.111 | 5 | 0.503 | 0.500 | 19.08 | 24.25 | | 0.056 | 0.022 | 0.0832 | | 2.92 | 7.43 | 1.96 | | 2.7 | 2.7 | 2.7 |
| 27 | 1 | 1.93 | 2.5 | 0.109 | 6 | 0.845 | 0.417 | 17.23 | 22.11 | 0.2932 | 0.018 | 0.04292 | 0.0189 | 0.0284 | 5.90 | 2.47 | 5.61 | 3.73 | 3.1 | 1.9 | 3.1 |
| 28 | 5 | 1.17 | 2.5 | 0.109 | 6 | 0.728 | 0.417 | 18.91 | 23.92 | | 0.043 | 0.022 | 0.0576 | | 1.50 | 2.93 | 1.12 | | 2.3 | 2.3 | 2.3 |
| 29 | 4 | 1.31 | 2.5 | 0.109 | 6 | 0.726 | 0.417 | 17.08 | 21.57 | | 0.03 | 0.01855 | 0.0494 | | 2.40 | 3.88 | 1.46 | | 2.4 | 2.4 | 3.5 |
| 30 | 3 | 1.35 | 2.5 | 0.109 | 6 | 0.704 | 0.417 | 17.91 | 22.4 | 0.6291 | 0.015 | 0.0125 | 0.0183 | 0.0115 | 4.95 | 5.94 | 4.05 | 6.49 | 4.7 | 2.3 | 4.7 |
| 31 | 2 | 1.29 | 2.5 | 0.109 | 6 | 0.768 | 0.417 | 18.6 | 23.93 | | 0.008 | 0.0125 | 0.0128 | | 8.87 | 5.68 | 5.56 | | 4.2 | 1.8 | 6.9 |
| 32 | 1 | 2.33 | 3 | 0.109 | 6 | 0.760 | 0.500 | 20.95 | 30.43 | 0.3374 | 0.0218 | 0.0464 | 0.0263 | 0.0325 | 5.88 | 2.76 | 4.88 | 3.95 | 3.5 | 1.7 | 3.5 |
| 33 | 2 | 1.87 | 3 | 0.109 | 6 | 0.957 | 0.500 | 20.63 | 28.03 | | 0.0095 | 0.0158 | 0.0168 | | 10.83 | 6.51 | 6.12 | | 3.3 | 1.6 | 4.7 |
| 34 | 3 | 1.77 | 3 | 0.109 | 6 | 0.994 | 0.500 | 18.22 | 25.71 | 0.5431 | 0.014 | 0.0142 | 0.0228 | 0.0123 | 6.95 | 6.86 | 4.28 | 7.92 | 3 | 2.2 | 3.9 |
| 35 | 4 | 1.79 | 3 | 0.109 | 6 | 0.760 | 0.500 | 18.41 | 24.82 | | 0.0314 | 0.0293 | 0.0584 | | 3.14 | 3.36 | 1.69 | | 1.7 | 1.7 | 2.5 |
| 36 | 5 | 1.36 | 3 | 0.109 | 6 | 0.904 | 0.500 | 19.52 | 25.86 | | 0.047 | 0.022 | 0.0656 | | 1.59 | 3.40 | 1.14 | | 1.9 | 1.9 | 1.9 |
| 37 | 2 | 1.19 | 2.5 | 0.109 | 2.5 | 1.050 | 1.000 | 20.12 | 27.29 | | 0.0205 | 0.0231 | 0.0406 | | 18.39 | 16.32 | 9.28 | | 10.7 | 9 | 24 |
| 38 | 3 | 1.37 | 2.5 | 0.109 | 2.5 | 0.832 | 1.000 | 18.22 | 27.95 | 0.3805 | 0.0306 | 0.0244 | 0.0556 | 0.0241 | 14.18 | 17.79 | 7.81 | 17.99 | 9 | 9 | 18.8 |

**Boundary categories (B.C.):**

**1 = all sides simply supported**
**2 = all sides built-in**
**3 = simply supported top and bottom, built-in sides**
**4 = simply supported bottom, free top, built-in sides**
**5 = simply supported bottom and sides, free top**

H - Wall height
t - wall thickness
L - length of wall
μ – orthogonal strength ratio = fkx / fky
Asp. Ratio = H / L
Ex - horizontal beam elastic modulus, from wallette tests
Ey - vertical beam elastic modulus, from wallette tests
β – a factor derived for crackline method by Sinah, see reference 3

**Table A3.2: Theoretical Failure Loads of Panels by FEA**

| | | allette Stress | | Wall Dimensions | | | Unit Load Stresses | | Max. Load | | Failure | Tests (Lawrence) (kPa) | | |
|---|---|---|---|---|---|---|---|---|---|---|---|---|---|---|
| Test # | B.C. | fkx | fky | H | t | L | σx | σy | Wx | Wy | Load | Full crack | Initial crack | Ulti. Load |
| 6 | 2 | 1.93 | 1.54 | 3 | 0.11 | 6 | 0.306 | 0.447 | 6.31 | 3.45 | 3.45 | 4.40 | 1.90 | 8.00 |
| 7 | 2 | 1.46 | 1.35 | 3 | 0.11 | 6 | 0.306 | 0.447 | 4.77 | 3.02 | 3.02 | 4.40 | 2.30 | 8.10 |
| 8 | 1 | 1.96 | 1.25 | 3 | 0.11 | 6 | 0.190 | 0.543 | 10.30 | 2.30 | 2.30 | 3.00 | 1.60 | 3.20 |
| 9 | 3 | 2.32 | 1.06 | 3 | 0.112 | 6 | 1.866 | 0.290 | 1.24 | 3.65 | 1.24 | 2.50 | 1.60 | 5.50 |
| 10 | 5 | 2.10 | 0.84 | 3 | 0.112 | 6 | 1.220 | 0.454 | 1.72 | 1.85 | 1.72 | 1.70 | 1.70 | 1.70 |
| 12 | 1 | 1.93 | 0.81 | 2.5 | 0.112 | 2.5 | 0.138 | 0.116 | 14.02 | 6.96 | 6.96 | 8.60 | 7.60 | 8.60 |
| 13 | 2 | 2.08 | 0.86 | 2.5 | 0.112 | 2.5 | 0.191 | 0.169 | 10.90 | 5.09 | 5.09 | 9.10 | 9.10 | 12.10 |
| 14 | 3 | 2.06 | 1.07 | 2.5 | 0.112 | 2.5 | 0.247 | 0.058 | 8.33 | 18.39 | 8.33 | 11.30 | 11.30 | 20.00 |
| 15 | 5 | 2.09 | 1.03 | 2.5 | 0.112 | 2.5 | 0.345 | 0.099 | 6.06 | 10.45 | 6.06 | 7.80 | 7.80 | 7.80 |
| 16 | 4 | 2.17 | 0.73 | 2.5 | 0.109 | 2.5 | 0.319 | 0.051 | 6.79 | 14.28 | 6.79 | 8.00 | 8.00 | 14.00 |
| 17 | 5 | 1.93 | 0.87 | 2.5 | 0.109 | 3.75 | 0.517 | 0.195 | 3.74 | 4.46 | 3.74 | 3.40 | 3.40 | 3.40 |
| 18 | 1 | 2.06 | 0.81 | 2.5 | 0.109 | 3.75 | 0.135 | 0.223 | 15.27 | 3.63 | 3.63 | 4.90 | 2.90 | 4.90 |
| 19 | 3 | 1.76 | 0.76 | 2.5 | 0.109 | 3.75 | 0.385 | 0.154 | 4.57 | 4.94 | 4.57 | 4.80 | 4.30 | 6.70 |
| 20 | 2 | 1.90 | 0.79 | 2.5 | 0.109 | 3.75 | 0.228 | 0.259 | 8.35 | 3.05 | 3.05 | 5.20 | 3.60 | 11.60 |
| 21 | 4 | 1.87 | 0.86 | 2.5 | 0.109 | 3.75 | 0.712 | 0.111 | 2.63 | 7.75 | 2.63 | 3.90 | 3.60 | 4.00 |
| 22 | 1 | 1.98 | 0.96 | 2.5 | 0.111 | 5 | 0.133 | 0.377 | 14.94 | 2.54 | 2.54 | 4.70 | 3.10 | 4.70 |
| 23 | 2 | 2.22 | 1.21 | 2.5 | 0.111 | 5 | 0.211 | 0.310 | 10.51 | 3.90 | 3.90 | 5.50 | 2.90 | 9.90 |
| 24 | 3 | 2.56 | 1.31 | 2.5 | 0.111 | 5 | 0.446 | 0.316 | 5.74 | 4.14 | 4.14 | 5.00 | 2.90 | 6.40 |
| 25 | 4 | 2.09 | 1.15 | 2.5 | 0.111 | 5 | 1.280 | 0.202 | 1.63 | 5.69 | 1.63 | 2.60 | 2.60 | 3.90 |
| 26 | 5 | 1.99 | 1.00 | 2.5 | 0.111 | 5 | 0.849 | 0.316 | 2.35 | 3.17 | 2.35 | 2.70 | 2.70 | 2.70 |
| 27 | 1 | 1.93 | 1.63 | 2.5 | 0.109 | 6 | 0.129 | 0.415 | 15.01 | 3.92 | 3.92 | 3.10 | 1.90 | 3.10 |
| 28 | 5 | 1.17 | 1.50 | 2.5 | 0.109 | 6 | 0.936 | 0.365 | 1.25 | 4.11 | 1.25 | 2.30 | 2.30 | 2.30 |
| 29 | 4 | 1.31 | 1.54 | 2.5 | 0.109 | 6 | 1.761 | 0.263 | 0.74 | 5.86 | 0.74 | 2.40 | 2.40 | 3.50 |
| 30 | 3 | 1.35 | 1.64 | 2.5 | 0.109 | 6 | 0.460 | 0.376 | 2.94 | 4.36 | 2.94 | 4.70 | 2.30 | 4.70 |
| 31 | 2 | 1.29 | 1.69 | 2.5 | 0.109 | 6 | 0.211 | 0.314 | 6.11 | 5.38 | 5.38 | 4.20 | 1.80 | 6.90 |
| 32 | 1 | 2.33 | 1.77 | 3 | 0.109 | 6 | 0.190 | 0.543 | 12.24 | 3.26 | 3.26 | 3.50 | 1.70 | 3.50 |
| 33 | 2 | 1.87 | 1.79 | 3 | 0.109 | 6 | 0.306 | 0.447 | 6.11 | 4.01 | 4.01 | 3.30 | 1.60 | 4.70 |
| 34 | 3 | 1.77 | 1.76 | 3 | 0.109 | 6 | 0.644 | 0.455 | 2.75 | 3.87 | 2.75 | 3.00 | 2.20 | 3.90 |
| 35 | 4 | 1.79 | 1.36 | 3 | 0.109 | 6 | 1.866 | 0.454 | 0.96 | 3.00 | 0.96 | 1.70 | 1.70 | 2.50 |
| 36 | 5 | 1.36 | 1.23 | 3 | 0.109 | 6 | 1.220 | 0.454 | 1.11 | 2.71 | 1.11 | 1.90 | 1.90 | 1.90 |
| 37 | 2 | 1.19 | 1.25 | 2.5 | 0.109 | 2.5 | 0.191 | 0.169 | 6.23 | 7.40 | 6.23 | 10.70 | 9.00 | 24.00 |
| 38 | 3 | 1.37 | 1.14 | 2.5 | 0.109 | 2.5 | 0.247 | 0.058 | 5.54 | 19.60 | 5.54 | 9.00 | 9.00 | 18.80 |

**Boundary Condition (B.C.) categories:**

**1 = all sides simply supported**
**2 = all sides built-in**
**3 = simply supported top and bottom, built-in sides**
**4 = simply supported bottom, free top, built-in sides**
**5 = simply supported bottom and sides, free top**

# Appendix 4: Results of the Testing Programme

(a) Load/Displacement data : wallettes

(b) Load/Displacement data : walls

(c) Failure Modes (Pictures)

(i) GREY WALLETTES

**B-Wallette 1**

| Load (N) | Displcmnt A (mm) | Displcmnt B (mm) | Displcmnt C (mm) | Delta A (mm) | Delta B (mm) | Delta C (mm) | Deflection B Relative to A and C (mm) |
|---|---|---|---|---|---|---|---|
| 1000 | 0.95 | 11.56 | 0.77 | 0.00 | 0.00 | 0.00 | 0.00 |
| 1500 | 1.58 | 12.48 | 1.89 | 0.63 | 0.92 | 1.12 | 0.04 |
| 2000 | 2.32 | 13.28 | 2.80 | 1.37 | 1.72 | 2.03 | 0.02 |
| 2500 | 3.04 | 14.13 | 3.65 | 2.09 | 2.57 | 2.88 | 0.09 |
| 3000 | 3.45 | 14.70 | 4.35 | 2.50 | 3.14 | 3.58 | 0.10 |
| 3500 | 3.88 | 15.23 | 4.94 | 2.93 | 3.67 | 4.17 | 0.12 |
| 4000 | 4.20 | 15.68 | 5.46 | 3.25 | 4.12 | 4.69 | 0.15 |
| 4500 | 4.46 | 16.05 | 5.88 | 3.51 | 4.49 | 5.11 | 0.18 |
| 5000 | 4.75 | 16.44 | 6.29 | 3.80 | 4.88 | 5.52 | 0.22 |
| 5500 | 5.08 | 16.82 | 6.66 | 4.13 | 5.26 | 5.89 | 0.25 |
| 6000 | 5.39 | 17.17 | 6.98 | 4.44 | 5.61 | 6.21 | 0.29 |
| 6500 | 5.65 | 17.46 | 7.24 | 4.70 | 5.90 | 6.47 | 0.32 |
| 7000 | 5.88 | 17.70 | 7.48 | 4.93 | 6.14 | 6.71 | 0.32 |
| 7500 | 6.13 | 17.90 | 7.68 | 5.18 | 6.34 | 6.91 | 0.29 |
| 8000 | 6.33 | 18.10 | 7.86 | 5.38 | 6.54 | 7.09 | 0.31 |
| 8500 | 6.54 | 18.30 | 8.05 | 5.59 | 6.74 | 7.28 | 0.31 |
| 9000 | 6.73 | 18.49 | 8.22 | 5.78 | 6.93 | 7.45 | 0.31 |
| 9500 | | | | | | | |

**B-Wallette 2**

| Load (N) | Displcmnt A (mm) | Displcmnt B (mm) | Displcmnt C (mm) | Delta A (mm) | Delta B (mm) | Delta C (mm) | Deflection B Relative to A and C (mm) |
|---|---|---|---|---|---|---|---|
| 1000 | 3.37 | 1.21 | 0.32 | 0.00 | 0.00 | 0.00 | 0.00 |
| 1500 | 3.93 | 1.85 | 1.12 | 0.56 | 0.64 | 0.80 | -0.04 |
| 2000 | 4.58 | 2.52 | 1.93 | 1.21 | 1.31 | 1.61 | -0.10 |
| 2500 | 5.30 | 3.20 | 2.59 | 1.93 | 1.99 | 2.27 | -0.11 |
| 3000 | 5.96 | 3.85 | 3.20 | 2.59 | 2.64 | 2.88 | -0.10 |
| 3500 | 6.56 | 4.41 | 3.70 | 3.19 | 3.20 | 3.38 | -0.09 |
| 4000 | 7.03 | 4.88 | 4.11 | 3.66 | 3.67 | 3.79 | -0.06 |
| 4500 | 7.41 | 5.28 | 4.50 | 4.04 | 4.07 | 4.18 | -0.04 |
| 5000 | 7.79 | 5.67 | 4.88 | 4.42 | 4.46 | 4.56 | -0.03 |
| 5500 | 8.16 | 6.01 | 5.22 | 4.79 | 4.80 | 4.90 | -0.04 |
| 6000 | 8.46 | 6.30 | 5.52 | 5.09 | 5.09 | 5.20 | -0.05 |
| 6500 | 8.76 | 6.60 | 5.79 | 5.39 | 5.39 | 5.47 | -0.04 |
| 7000 | 9.00 | 6.85 | 6.03 | 5.63 | 5.64 | 5.71 | -0.03 |
| 7500 | 9.19 | 7.10 | 6.28 | 5.82 | 5.89 | 5.96 | 0.00 |
| 8000 | 9.31 | 7.29 | 6.50 | 5.94 | 6.08 | 6.18 | 0.02 |
| 8500 | 9.44 | 7.48 | 6.70 | 6.07 | 6.27 | 6.38 | 0.05 |
| 9000 | 9.53 | 7.65 | 6.88 | 6.16 | 6.44 | 6.56 | 0.08 |
| 9500 | 9.60 | 7.79 | 7.05 | 6.23 | 6.58 | 6.73 | 0.10 |
| 10000 | 9.65 | 7.97 | 7.21 | 6.28 | 6.76 | 6.89 | 0.18 |
| 10500 | 9.71 | 8.07 | 7.39 | 6.34 | 6.86 | 7.07 | 0.16 |
| 11000 | 9.76 | 8.21 | 7.52 | 6.39 | 7.00 | 7.20 | 0.21 |

| | | | | | | | |
|---|---|---|---|---|---|---|---|
| **11500** | 9.81 | 8.31 | 7.64 | 6.44 | 7.10 | 7.32 | 0.22 |
| **12000** | 9.87 | 8.45 | 7.76 | 6.50 | 7.24 | 7.44 | 0.27 |
| **12500** | 9.93 | 8.56 | 7.84 | 6.56 | 7.35 | 7.52 | 0.31 |
| **13000** | 9.97 | 8.67 | 7.95 | 6.60 | 7.46 | 7.63 | 0.35 |
| **13440** | | | | | | | |

**B-Wallette 3**

| **Load (N)** | **Displcmnt A (mm)** | **Displcmnt B (mm)** | **Displcmnt C (mm)** | **Delta A (mm)** | **Delta B (mm)** | **Delta C (mm)** | **Deflection B Relative to A and C (mm)** |
|---|---|---|---|---|---|---|---|
| **1000** | 0.813 | 2.209 | 3.352 | 0.000 | 0.000 | 0.000 | 0.000 |
| **1500** | 1.603 | 3.350 | 4.840 | 0.790 | 1.142 | 1.488 | 0.003 |
| **2000** | 2.478 | 4.284 | 5.888 | 1.665 | 2.075 | 2.536 | -0.025 |
| **2500** | 3.277 | 5.067 | 6.753 | 2.464 | 2.858 | 3.401 | -0.074 |
| **3000** | 3.994 | 5.783 | 7.506 | 3.181 | 3.574 | 4.155 | -0.094 |
| **3500** | 4.574 | 6.375 | 8.122 | 3.761 | 4.166 | 4.770 | -0.100 |
| **4000** | 5.076 | 6.876 | 8.668 | 4.263 | 4.667 | 5.317 | -0.123 |
| **4500** | 5.479 | 7.307 | 9.146 | 4.666 | 5.099 | 5.794 | -0.131 |
| **5000** | 5.893 | 7.748 | 9.630 | 5.081 | 5.539 | 6.278 | -0.140 |
| **5500** | 6.173 | 8.028 | 9.952 | 5.360 | 5.819 | 6.600 | -0.161 |
| **6000** | 6.446 | 8.313 | 10.266 | 5.633 | 6.104 | 6.915 | -0.170 |
| **6500** | 6.670 | 8.582 | 10.600 | 5.858 | 6.374 | 7.249 | -0.179 |
| **7000** | 6.845 | 8.787 | 10.833 | 6.032 | 6.578 | 7.482 | -0.179 |
| **7500** | 7.001 | 8.968 | 11.038 | 6.188 | 6.759 | 7.687 | -0.178 |
| **8000** | 7.158 | 9.145 | 11.233 | 6.346 | 6.937 | 7.881 | -0.177 |
| **8500** | 7.279 | 9.284 | 11.398 | 6.466 | 7.076 | 8.047 | -0.181 |
| **9000** | 7.395 | 9.427 | 11.567 | 6.582 | 7.219 | 8.215 | -0.180 |
| **9500** | 7.501 | 9.549 | 11.704 | 6.688 | 7.340 | 8.352 | -0.180 |
| **10000** | 7.605 | 9.664 | 11.836 | 6.792 | 7.456 | 8.484 | -0.183 |
| **10500** | 7.696 | 9.770 | 11.953 | 6.883 | 7.561 | 8.601 | -0.181 |
| **11000** | 7.780 | 9.866 | 12.056 | 6.967 | 7.657 | 8.705 | -0.179 |
| **11500** | 7.851 | 9.959 | 12.190 | 7.038 | 7.751 | 8.839 | -0.188 |
| **11950** | | | | | | | |

**B-Wallette 4**

| **Load (N)** | **Displcmnt A (mm)** | **Displcmnt B (mm)** | **Displcmnt C (mm)** | **Delta A (mm)** | **Delta B (mm)** | **Delta C (mm)** | **Deflection B Relative to A and C (mm)** |
|---|---|---|---|---|---|---|---|
| **1000** | 0.794 | 0.768 | 0.708 | 0.000 | 0.000 | 0.000 | 0.000 |
| **1500** | 1.843 | 1.793 | 1.709 | 1.049 | 1.025 | 1.002 | 0.000 |
| **2000** | 2.820 | 2.721 | 2.584 | 2.026 | 1.953 | 1.877 | 0.002 |
| **2500** | 3.663 | 3.511 | 3.339 | 2.869 | 2.743 | 2.632 | -0.008 |
| **3000** | 4.449 | 4.280 | 4.117 | 3.655 | 3.512 | 3.410 | -0.021 |
| **3500** | 4.966 | 4.835 | 4.723 | 4.172 | 4.066 | 4.015 | -0.027 |
| **4000** | 5.447 | 5.299 | 5.191 | 4.653 | 4.531 | 4.483 | -0.037 |
| **4500** | 5.790 | 5.674 | 5.610 | 4.996 | 4.905 | 4.902 | -0.044 |
| **5000** | 6.159 | 6.044 | 5.976 | 5.365 | 5.276 | 5.268 | -0.041 |
| **5500** | 6.365 | 6.289 | 6.288 | 5.572 | 5.521 | 5.581 | -0.056 |
| **6000** | 6.562 | 6.524 | 6.540 | 5.768 | 5.756 | 5.833 | -0.044 |

| | | | | | | | |
|---|---|---|---|---|---|---|---|
| 6500 | 6.753 | 6.735 | 6.769 | 5.959 | 5.967 | 6.062 | -0.044 |
| 7000 | 6.877 | 6.891 | 6.960 | 6.083 | 6.123 | 6.253 | -0.045 |
| 7500 | 7.016 | 7.063 | 7.178 | 6.222 | 6.294 | 6.470 | -0.052 |
| 8000 | 7.149 | 7.221 | 7.359 | 6.355 | 6.453 | 6.652 | -0.050 |
| 8500 | 7.233 | 7.339 | 7.509 | 6.439 | 6.571 | 6.801 | -0.049 |
| 9000 | 7.341 | 7.465 | 7.648 | 6.547 | 6.697 | 6.941 | -0.047 |
| 9500 | 7.438 | 7.574 | 7.772 | 6.644 | 6.806 | 7.064 | -0.048 |
| 10000 | 7.534 | 7.681 | 7.881 | 6.740 | 6.912 | 7.174 | -0.044 |
| 10500 | 7.573 | 7.752 | 7.991 | 6.779 | 6.983 | 7.283 | -0.048 |
| 11000 | 7.659 | 7.847 | 8.086 | 6.865 | 7.079 | 7.379 | -0.043 |
| 11500 | 7.751 | 7.941 | 8.173 | 6.957 | 7.173 | 7.466 | -0.038 |
| 12000 | 7.853 | 8.048 | 8.269 | 7.059 | 7.279 | 7.561 | -0.031 |
| 12500 | 7.912 | 8.119 | 8.341 | 7.118 | 7.351 | 7.633 | -0.025 |
| 13000 | 7.974 | 8.195 | 8.408 | 7.180 | 7.427 | 7.701 | -0.014 |
| 13130 | | | | | | | |

**B-Wallette 5**

| Load (N) | Displcmnt A (mm) | Displcmnt B (mm) | Displcmnt C (mm) | Delta A (mm) | Delta B (mm) | Delta C (mm) | Deflection B Relative to A and C (mm) |
|---|---|---|---|---|---|---|---|
| 1000 | 0.124 | 0.150 | 0.166 | 0.000 | 0.000 | 0.000 | 0.000 |
| 1500 | 0.649 | 0.983 | 1.211 | 0.525 | 0.833 | 1.045 | 0.048 |
| 2000 | 1.246 | 1.729 | 2.082 | 1.122 | 1.579 | 1.916 | 0.059 |
| 2500 | 1.588 | 2.279 | 2.805 | 1.464 | 2.128 | 2.639 | 0.077 |
| 3000 | 2.064 | 2.865 | 3.487 | 1.940 | 2.715 | 3.322 | 0.084 |
| 3500 | 2.398 | 3.334 | 4.036 | 2.274 | 3.183 | 3.870 | 0.111 |
| 4000 | 2.737 | 3.753 | 4.527 | 2.614 | 3.602 | 4.361 | 0.115 |
| 4500 | 2.932 | 4.062 | 4.931 | 2.808 | 3.911 | 4.766 | 0.125 |
| 5000 | 3.434 | 4.494 | 5.333 | 3.310 | 4.344 | 5.167 | 0.105 |
| 5500 | 3.778 | 4.814 | 5.671 | 3.654 | 4.664 | 5.505 | 0.084 |
| 6000 | 4.084 | 5.102 | 5.979 | 3.960 | 4.951 | 5.813 | 0.065 |
| 6500 | 4.311 | 5.327 | 6.227 | 4.187 | 5.177 | 6.061 | 0.053 |
| 7000 | 4.547 | 5.567 | 6.504 | 4.423 | 5.417 | 6.338 | 0.037 |
| 7500 | 4.761 | 5.771 | 6.726 | 4.637 | 5.621 | 6.561 | 0.022 |
| 8000 | 4.954 | 5.963 | 6.943 | 4.830 | 5.813 | 6.777 | 0.009 |
| 8500 | 5.116 | 6.129 | 7.131 | 4.993 | 5.979 | 6.965 | 0.000 |
| 9000 | 5.252 | 6.276 | 7.295 | 5.129 | 6.126 | 7.130 | -0.004 |
| 9500 | 5.382 | 6.412 | 7.459 | 5.258 | 6.262 | 7.294 | -0.014 |
| 10000 | 5.502 | 6.542 | 7.612 | 5.378 | 6.392 | 7.446 | -0.021 |
| 10500 | 5.615 | 6.665 | 7.743 | 5.491 | 6.515 | 7.577 | -0.019 |
| 11000 | 5.710 | 6.776 | 7.864 | 5.586 | 6.626 | 7.699 | -0.016 |
| 11500 | 5.807 | 6.893 | 7.981 | 5.683 | 6.743 | 7.815 | -0.006 |
| 12000 | | | | | | | |

**B-Wallette 6**

| Load (N) | Displcmnt A (mm) | Displcmnt B (mm) | Displcmnt C (mm) | Delta A (mm) | Delta B (mm) | Delta C (mm) | Deflection B Relative to A and C (mm) |
|---|---|---|---|---|---|---|---|
| 1000 | 0.289 | 0.415 | 0.529 | 0.000 | 0.000 | 0.000 | 0.000 |

| | | | | | | | |
|---|---|---|---|---|---|---|---|
| 1500 | 0.984 | 1.432 | 1.857 | 0.695 | 1.017 | 1.328 | 0.005 |
| 2000 | 1.680 | 2.336 | 2.972 | 1.391 | 1.920 | 2.444 | 0.003 |
| 2500 | 2.110 | 3.081 | 4.048 | 1.821 | 2.665 | 3.519 | -0.005 |
| 3000 | 2.728 | 3.732 | 4.745 | 2.439 | 3.317 | 4.216 | -0.011 |
| 3500 | 3.111 | 4.204 | 5.317 | 2.822 | 3.789 | 4.788 | -0.016 |
| 4000 | 3.361 | 4.648 | 5.973 | 3.072 | 4.232 | 5.444 | -0.025 |
| 4500 | 3.698 | 5.052 | 6.439 | 3.409 | 4.637 | 5.910 | -0.023 |
| 5000 | 4.027 | 5.413 | 6.828 | 3.738 | 4.998 | 6.300 | -0.021 |
| 5500 | 4.279 | 5.721 | 7.188 | 3.990 | 5.306 | 6.659 | -0.019 |
| 6000 | 4.509 | 5.995 | 7.502 | 4.220 | 5.579 | 6.973 | -0.017 |
| 6500 | 4.725 | 6.245 | 7.790 | 4.436 | 5.830 | 7.261 | -0.019 |
| 7000 | 4.956 | 6.493 | 8.066 | 4.667 | 6.078 | 7.537 | -0.024 |
| 7500 | 5.181 | 6.737 | 8.335 | 4.892 | 6.322 | 7.806 | -0.028 |
| 8000 | 5.376 | 6.943 | 8.565 | 5.087 | 6.528 | 8.037 | -0.034 |
| 8500 | 5.559 | 7.136 | 8.782 | 5.270 | 6.720 | 8.253 | -0.041 |
| 9000 | 5.716 | 7.299 | 8.961 | 5.427 | 6.884 | 8.433 | -0.046 |
| 9500 | 5.869 | 7.459 | 9.148 | 5.580 | 7.043 | 8.619 | -0.056 |
| 10000 | 6.021 | 7.613 | 9.318 | 5.732 | 7.198 | 8.789 | -0.063 |
| 10500 | 6.150 | 7.749 | 9.464 | 5.861 | 7.333 | 8.935 | -0.064 |
| 11000 | 6.267 | 7.868 | 9.592 | 5.978 | 7.453 | 9.063 | -0.068 |
| 11500 | 6.410 | 8.011 | 9.735 | 6.121 | 7.596 | 9.207 | -0.068 |
| 12000 | 6.514 | 8.123 | 9.848 | 6.225 | 7.708 | 9.319 | -0.064 |
| 12500 | 6.655 | 8.258 | 9.967 | 6.366 | 7.842 | 9.439 | -0.060 |
| 13000 | 6.766 | 8.383 | 10.080 | 6.477 | 7.967 | 9.551 | -0.047 |
| 13030 | | | | | | | |

**P-Wallette 1**

| Load (N) | Displcmnt A (mm) | Displcmnt B (mm) | Displcmnt C (mm) | Delta A (mm) | Delta B (mm) | Delta C (mm) | Deflection B Relative to A and C (mm) |
|---|---|---|---|---|---|---|---|
| 1000 | 0.078 | 0.084 | 0.081 | 0.000 | 0.000 | 0.000 | 0.000 |
| 1500 | 0.831 | 0.887 | 0.832 | 0.753 | 0.803 | 0.750 | 0.051 |
| 2000 | 1.768 | 1.845 | 1.769 | 1.690 | 1.761 | 1.688 | 0.072 |
| 2500 | 2.608 | 2.697 | 2.605 | 2.530 | 2.613 | 2.523 | 0.086 |
| 3000 | 3.351 | 3.449 | 3.355 | 3.273 | 3.365 | 3.274 | 0.092 |
| 3500 | 4.160 | 4.213 | 4.005 | 4.082 | 4.129 | 3.923 | 0.126 |
| 4000 | 4.631 | 4.697 | 4.500 | 4.553 | 4.613 | 4.419 | 0.127 |
| 4500 | 4.990 | 5.108 | 4.929 | 4.913 | 5.024 | 4.847 | 0.144 |
| 5000 | 5.364 | 5.483 | 5.291 | 5.286 | 5.399 | 5.209 | 0.151 |
| 5500 | 5.740 | 5.845 | 5.618 | 5.663 | 5.761 | 5.537 | 0.161 |
| 6000 | 5.985 | 6.117 | 5.869 | 5.908 | 6.033 | 5.788 | 0.185 |
| 6500 | 6.238 | 6.399 | 6.117 | 6.160 | 6.315 | 6.036 | 0.217 |
| 7000 | 6.420 | 6.607 | 6.280 | 6.342 | 6.523 | 6.199 | 0.253 |
| 7500 | 6.609 | 6.824 | 6.480 | 6.532 | 6.740 | 6.399 | 0.275 |
| 8000 | 6.726 | 6.967 | 6.616 | 6.648 | 6.883 | 6.535 | 0.292 |
| 8500 | 6.851 | 7.121 | 6.764 | 6.773 | 7.037 | 6.682 | 0.309 |
| 9000 | 6.990 | 7.292 | 6.931 | 6.912 | 7.208 | 6.850 | 0.327 |
| 9500 | 7.075 | 7.405 | 7.053 | 6.997 | 7.321 | 6.972 | 0.337 |
| 10000 | 7.142 | 7.513 | 7.150 | 7.064 | 7.429 | 7.069 | 0.363 |
| 10500 | 7.202 | 7.612 | 7.254 | 7.124 | 7.529 | 7.173 | 0.380 |
| 11000 | 7.264 | 7.716 | 7.370 | 7.186 | 7.632 | 7.289 | 0.394 |
| 11500 | 7.317 | 7.814 | 7.474 | 7.239 | 7.730 | 7.393 | 0.414 |

| | | | | | | | |
|---|---|---|---|---|---|---|---|
| **12000** | 7.356 | 7.891 | 7.566 | 7.279 | 7.807 | 7.485 | 0.426 |
| **12500** | 7.399 | 7.982 | 7.665 | 7.321 | 7.898 | 7.584 | 0.446 |
| **13000** | 7.428 | 8.055 | 7.748 | 7.350 | 7.972 | 7.667 | 0.463 |
| **13500** | 7.458 | 8.124 | 7.827 | 7.380 | 8.040 | 7.746 | 0.477 |
| **14000** | 7.483 | 8.199 | 7.910 | 7.405 | 8.115 | 7.829 | 0.498 |
| **15060** | | | | | | | |

**P-Wallette 2**

| Load (N) | Displcmnt A (mm) | Displcmnt B (mm) | Displcmnt C (mm) | Delta A (mm) | Delta B (mm) | Delta C (mm) | Deflection B Relative to A and C (mm) |
|---|---|---|---|---|---|---|---|
| **1000** | 0.073 | 0.008 | 0.132 | 0.000 | 0.000 | 0.000 | 0.000 |
| **1500** | 0.935 | 0.937 | 1.006 | 0.862 | 0.929 | 0.874 | 0.061 |
| **2000** | 1.864 | 1.953 | 2.054 | 1.791 | 1.945 | 1.922 | 0.089 |
| **2500** | 2.569 | 2.731 | 2.864 | 2.496 | 2.723 | 2.732 | 0.109 |
| **3000** | 3.034 | 3.363 | 3.625 | 2.961 | 3.355 | 3.492 | 0.129 |
| **3500** | 3.460 | 3.925 | 4.273 | 3.387 | 3.917 | 4.141 | 0.153 |
| **4000** | 3.779 | 4.353 | 4.796 | 3.706 | 4.345 | 4.663 | 0.161 |
| **4500** | 4.054 | 4.733 | 5.250 | 3.981 | 4.726 | 5.117 | 0.177 |
| **5000** | 4.232 | 4.999 | 5.579 | 4.159 | 4.991 | 5.447 | 0.188 |
| **5500** | 4.399 | 5.239 | 5.871 | 4.326 | 5.231 | 5.739 | 0.199 |
| **6000** | 4.608 | 5.501 | 6.164 | 4.535 | 5.494 | 6.032 | 0.211 |
| **6500** | 4.741 | 5.697 | 6.395 | 4.668 | 5.689 | 6.263 | 0.224 |
| **7000** | 4.865 | 5.876 | 6.604 | 4.792 | 5.868 | 6.471 | 0.237 |
| **7500** | 4.987 | 6.041 | 6.795 | 4.914 | 6.034 | 6.662 | 0.246 |
| **8000** | 5.085 | 6.180 | 6.960 | 5.011 | 6.173 | 6.828 | 0.253 |
| **8500** | 5.155 | 6.304 | 7.113 | 5.082 | 6.297 | 6.981 | 0.265 |
| **9000** | 5.194 | 6.403 | 7.252 | 5.121 | 6.395 | 7.120 | 0.275 |
| **9500** | 5.212 | 6.495 | 7.382 | 5.139 | 6.487 | 7.250 | 0.293 |
| **10000** | 5.274 | 6.588 | 7.509 | 5.201 | 6.581 | 7.376 | 0.292 |
| **10500** | 5.376 | 6.670 | 7.527 | 5.303 | 6.662 | 7.394 | 0.313 |
| **11000** | 5.422 | 6.739 | 7.587 | 5.349 | 6.731 | 7.455 | 0.329 |
| **11500** | 5.532 | 6.830 | 7.628 | 5.459 | 6.822 | 7.496 | 0.345 |
| **12000** | 5.684 | 6.978 | 7.739 | 5.611 | 6.970 | 7.607 | 0.361 |
| **12500** | 5.652 | 7.000 | 7.790 | 5.579 | 6.992 | 7.658 | 0.373 |
| **13000** | 5.742 | 7.155 | 8.005 | 5.669 | 7.147 | 7.873 | 0.376 |
| **18800** | | | | | | | |

**P-Wallette 3**

| Load (N) | Displcmnt A (mm) | Displcmnt B (mm) | Displcmnt C (mm) | Delta A (mm) | Delta B (mm) | Delta C (mm) | Deflection B Relative to A and C (mm) |
|---|---|---|---|---|---|---|---|
| **1000** | 0.100 | 0.103 | 0.076 | 0.000 | 0.000 | 0.000 | 0.000 |
| **1500** | 1.070 | 1.089 | 0.864 | 0.969 | 0.986 | 0.788 | 0.107 |
| **2000** | 2.049 | 2.330 | 1.749 | 1.948 | 2.226 | 1.673 | 0.416 |
| **2500** | 2.822 | 3.704 | 2.524 | 2.722 | 3.601 | 2.448 | 1.016 |

**P-Wallette 4**

| Load (N) | Displcmnt A (mm) | Displcmnt B (mm) | Displcmnt C (mm) | Delta A (mm) | Delta B (mm) | Delta C (mm) | Deflection B Relative to A and C (mm) |
|---|---|---|---|---|---|---|---|
| 1000 | 0.208 | 0.220 | 0.183 | 0.000 | 0.000 | 0.000 | 0.000 |
| 1500 | 1.407 | 1.430 | 1.276 | 1.198 | 1.210 | 1.092 | 0.065 |
| 2000 | 2.219 | 2.284 | 2.153 | 2.010 | 2.064 | 1.969 | 0.074 |
| 2500 | 3.004 | 3.027 | 2.790 | 2.796 | 2.807 | 2.607 | 0.106 |
| 3000 | 3.690 | 3.688 | 3.388 | 3.482 | 3.468 | 3.205 | 0.125 |
| 3500 | 4.157 | 4.134 | 3.786 | 3.949 | 3.914 | 3.603 | 0.138 |
| 4000 | 4.519 | 4.540 | 4.188 | 4.310 | 4.320 | 4.005 | 0.162 |
| 4500 | 4.741 | 4.789 | 4.472 | 4.533 | 4.569 | 4.289 | 0.158 |
| 5000 | 4.956 | 5.054 | 4.724 | 4.748 | 4.834 | 4.540 | 0.190 |
| 5500 | 5.126 | 5.273 | 4.965 | 4.918 | 5.053 | 4.782 | 0.204 |
| 6000 | 5.265 | 5.466 | 5.120 | 5.056 | 5.246 | 4.937 | 0.250 |
| 6500 | 5.389 | 5.641 | 5.219 | 5.180 | 5.421 | 5.035 | 0.313 |
| 7000 | 5.453 | 5.795 | 5.403 | 5.245 | 5.575 | 5.220 | 0.342 |
| 7500 | 5.562 | 5.948 | 5.554 | 5.354 | 5.728 | 5.370 | 0.366 |
| 8000 | 5.722 | 6.129 | 5.726 | 5.513 | 5.909 | 5.543 | 0.381 |
| 8500 | 5.809 | 6.253 | 5.857 | 5.601 | 6.033 | 5.674 | 0.396 |
| 9000 | 5.886 | 6.360 | 5.983 | 5.678 | 6.140 | 5.800 | 0.401 |
| 9500 | 5.953 | 6.466 | 6.104 | 5.744 | 6.246 | 5.921 | 0.413 |
| 10000 | 6.012 | 6.560 | 6.226 | 5.803 | 6.340 | 6.042 | 0.417 |
| 10500 | 6.077 | 6.654 | 6.331 | 5.869 | 6.434 | 6.147 | 0.426 |
| 11000 | 6.128 | 6.734 | 6.433 | 5.920 | 6.514 | 6.249 | 0.430 |
| 11500 | 6.256 | 6.858 | 6.525 | 6.047 | 6.637 | 6.342 | 0.443 |
| 12000 | 6.330 | 6.946 | 6.618 | 6.122 | 6.726 | 6.434 | 0.448 |
| 12500 | 6.361 | 7.018 | 6.717 | 6.152 | 6.798 | 6.534 | 0.455 |
| 13000 | 6.412 | 7.082 | 6.785 | 6.204 | 6.862 | 6.602 | 0.459 |
| 19550 | | | | | | | |

**P-Wallette 5**

| Load (N) | Displcmnt A (mm) | Displcmnt B (mm) | Displcmnt C (mm) | Delta A (mm) | Delta B (mm) | Delta C (mm) | Deflection B Relative to A and C (mm) |
|---|---|---|---|---|---|---|---|
| 1000 | 0.097 | 0.115 | 0.123 | 0.000 | 0.000 | 0.000 | 0.000 |
| 1500 | 0.948 | 1.069 | 1.090 | 0.851 | 0.953 | 0.968 | 0.044 |
| 2000 | 1.791 | 1.934 | 1.905 | 1.694 | 1.818 | 1.782 | 0.080 |
| 2500 | 2.521 | 2.681 | 2.615 | 2.424 | 2.566 | 2.492 | 0.107 |
| 3000 | 3.212 | 3.363 | 3.199 | 3.116 | 3.248 | 3.076 | 0.152 |
| 3500 | 3.737 | 3.867 | 3.620 | 3.640 | 3.751 | 3.498 | 0.182 |
| 4000 | 4.251 | 4.358 | 4.085 | 4.154 | 4.243 | 3.963 | 0.185 |
| 4500 | 4.680 | 4.760 | 4.399 | 4.583 | 4.644 | 4.276 | 0.215 |
| 5000 | 5.060 | 5.120 | 4.718 | 4.963 | 5.005 | 4.595 | 0.226 |
| 5500 | 5.439 | 5.465 | 4.944 | 5.343 | 5.349 | 4.822 | 0.267 |
| 6000 | 5.718 | 5.710 | 5.134 | 5.621 | 5.595 | 5.012 | 0.278 |
| 6500 | 6.003 | 5.963 | 5.339 | 5.907 | 5.847 | 5.217 | 0.286 |
| 7000 | 6.243 | 6.179 | 5.521 | 6.147 | 6.064 | 5.398 | 0.292 |
| 7500 | 6.444 | 6.369 | 5.702 | 6.348 | 6.254 | 5.579 | 0.290 |
| 8000 | 6.638 | 6.549 | 5.878 | 6.541 | 6.434 | 5.756 | 0.285 |

| | | | | | | | |
|---|---|---|---|---|---|---|---|
| 8500 | 6.789 | 6.699 | 6.058 | 6.692 | 6.584 | 5.936 | 0.270 |
| 9000 | 6.904 | 6.836 | 6.225 | 6.807 | 6.720 | 6.102 | 0.266 |
| 9500 | 6.985 | 6.962 | 6.360 | 6.888 | 6.847 | 6.237 | 0.285 |
| 10000 | 7.100 | 7.083 | 6.466 | 7.003 | 6.968 | 6.344 | 0.294 |
| 10500 | 7.206 | 7.187 | 6.550 | 7.109 | 7.072 | 6.427 | 0.303 |
| 11000 | 7.271 | 7.278 | 6.649 | 7.174 | 7.162 | 6.526 | 0.312 |
| 11500 | 7.317 | 7.366 | 6.747 | 7.220 | 7.251 | 6.624 | 0.328 |
| 12000 | 7.338 | 7.439 | 6.836 | 7.242 | 7.324 | 6.713 | 0.347 |
| 19550 | | | | | | | |

**P-Wallette 6**

| Load (N) | Displcmnt A (mm) | Displcmnt B (mm) | Displcmnt C (mm) | Delta A (mm) | Delta B (mm) | Delta C (mm) | Deflection B Relative to A and C (mm) |
|---|---|---|---|---|---|---|---|
| 1000 | 1.7361 | 1.7554 | 1.6949 | 0.000 | 0.000 | 0.000 | 0.000 |
| 1500 | 2.2447 | 2.3557 | 2.3323 | 0.509 | 0.600 | 0.637 | 0.027 |
| 2000 | 2.7881 | 2.9586 | 2.9734 | 1.052 | 1.203 | 1.279 | 0.038 |
| 2500 | 3.2554 | 3.4375 | 3.4675 | 1.519 | 1.682 | 1.773 | 0.036 |
| 3000 | 3.7406 | 3.9014 | 3.9439 | 2.005 | 2.146 | 2.249 | 0.019 |
| 3500 | 4.1657 | 4.3025 | 4.3557 | 2.430 | 2.547 | 2.661 | 0.002 |
| 4000 | 4.4951 | 4.6267 | 4.6636 | 2.759 | 2.871 | 2.969 | 0.007 |
| 4500 | 4.8151 | 4.9412 | 4.9725 | 3.079 | 3.186 | 3.278 | 0.008 |
| 5000 | 5.0554 | 5.206 | 5.2299 | 3.319 | 3.451 | 3.535 | 0.023 |
| 5500 | 5.228 | 5.4052 | 5.4273 | 3.492 | 3.650 | 3.732 | 0.038 |
| 6000 | 5.3697 | 5.5608 | 5.6052 | 3.634 | 3.805 | 3.910 | 0.033 |
| 6500 | 5.503 | 5.6778 | 5.753 | 3.767 | 3.922 | 4.058 | 0.010 |
| 7000 | 5.6438 | 5.8194 | 5.8841 | 3.908 | 4.064 | 4.189 | 0.016 |
| 7500 | 5.7611 | 5.9365 | 5.9973 | 4.025 | 4.181 | 4.302 | 0.017 |
| 8000 | 5.8662 | 6.0352 | 6.1143 | 4.130 | 4.280 | 4.419 | 0.005 |
| 8500 | 5.8249 | 6.0833 | 6.2575 | 4.089 | 4.328 | 4.563 | 0.002 |
| 9000 | 5.8831 | 6.1576 | 6.3352 | 4.147 | 4.402 | 4.640 | 0.009 |
| 9500 | 5.9675 | 6.2449 | 6.4194 | 4.231 | 4.490 | 4.725 | 0.012 |
| 10000 | 6.0304 | 6.3148 | 6.4905 | 4.294 | 4.559 | 4.796 | 0.014 |
| 10500 | 6.0905 | 6.3847 | 6.5579 | 4.354 | 4.629 | 4.863 | 0.021 |
| 11000 | 6.144 | 6.4415 | 6.6225 | 4.408 | 4.686 | 4.928 | 0.018 |
| 11500 | 6.2228 | 6.5167 | 6.6852 | 4.487 | 4.761 | 4.990 | 0.023 |
| 12000 | 6.3007 | 6.5918 | 6.7488 | 4.565 | 4.836 | 5.054 | 0.027 |
| 19990 | | | | | | | |

(ii) YELLOW WALLETTES

**P-Wallette 1**

| Load (N) | Displcmnt A (mm) | Displcmnt B (mm) | Displcmnt C (mm) | Delta A (mm) | Delta B (mm) | Delta C (mm) | Deflection B Relative to A and C (mm) |
|---|---|---|---|---|---|---|---|
| 1000 | 0.407 | 0.330 | 0.296 | 0.000 | 0.000 | 0.000 | 0.000 |
| 1500 | 1.464 | 1.310 | 1.120 | 1.056 | 0.980 | 0.825 | 0.040 |
| 2000 | 2.436 | 2.194 | 1.892 | 2.029 | 1.864 | 1.596 | 0.052 |
| 2500 | 3.203 | 2.926 | 2.546 | 2.796 | 2.596 | 2.250 | 0.073 |
| 3000 | 3.900 | 3.572 | 3.113 | 3.493 | 3.243 | 2.817 | 0.088 |
| 3500 | 4.608 | 4.199 | 3.644 | 4.201 | 3.869 | 3.349 | 0.095 |
| 4000 | 5.137 | 4.687 | 4.054 | 4.730 | 4.358 | 3.759 | 0.113 |
| 4500 | 5.572 | 5.087 | 4.384 | 5.165 | 4.757 | 4.088 | 0.131 |
| 5000 | 6.014 | 5.491 | 4.716 | 5.607 | 5.161 | 4.420 | 0.148 |
| 5500 | 6.419 | 5.831 | 4.961 | 6.012 | 5.502 | 4.666 | 0.163 |
| 6000 | 6.708 | 6.085 | 5.143 | 6.301 | 5.756 | 4.847 | 0.182 |
| 6500 | 6.967 | 6.311 | 5.306 | 6.560 | 5.982 | 5.010 | 0.197 |
| 7000 | 7.151 | 6.491 | 5.439 | 6.744 | 6.162 | 5.143 | 0.219 |
| 7500 | 7.356 | 6.687 | 5.591 | 6.948 | 6.357 | 5.295 | 0.235 |
| 8000 | 7.505 | 6.834 | 5.708 | 7.097 | 6.505 | 5.412 | 0.250 |
| 8500 | 7.615 | 6.955 | 5.808 | 7.208 | 6.626 | 5.513 | 0.265 |
| 9000 | 7.721 | 7.069 | 5.911 | 7.313 | 6.740 | 5.616 | 0.275 |
| 9500 | 7.808 | 7.169 | 6.001 | 7.401 | 6.840 | 5.705 | 0.287 |
| 10000 | 7.890 | 7.269 | 6.085 | 7.482 | 6.940 | 5.790 | 0.304 |
| 10500 | 7.964 | 7.361 | 6.170 | 7.556 | 7.032 | 5.874 | 0.317 |
| 11000 | 8.017 | 7.446 | 6.246 | 7.610 | 7.117 | 5.951 | 0.337 |
| 11500 | 8.064 | 7.518 | 6.318 | 7.657 | 7.189 | 6.023 | 0.349 |
| 12000 | 8.102 | 7.589 | 6.388 | 7.694 | 7.260 | 6.092 | 0.367 |
| 12500 | 8.1334 | 7.6648 | 6.4522 | | | | |

**P-Wallette 2**

| Load (N) | Displcmnt A (mm) | Displcmnt B (mm) | Displcmnt C (mm) | Delta A (mm) | Delta B (mm) | Delta C (mm) | Deflection B Relative to A and C (mm) |
|---|---|---|---|---|---|---|---|
| 1000 | 0.233 | 0.292 | 0.320 | 0.000 | 0.000 | 0.000 | 0.000 |
| 1500 | 1.181 | 1.380 | 1.460 | 0.948 | 1.088 | 1.140 | 0.044 |
| 2000 | 2.054 | 2.387 | 2.489 | 1.822 | 2.095 | 2.169 | 0.100 |
| 2500 | 2.822 | 3.174 | 3.249 | 2.589 | 2.882 | 2.928 | 0.123 |
| 3000 | 3.543 | 3.874 | 3.922 | 3.310 | 3.582 | 3.601 | 0.126 |
| 3500 | 4.031 | 4.355 | 4.386 | 3.798 | 4.063 | 4.066 | 0.131 |
| 4000 | 4.493 | 4.825 | 4.799 | 4.261 | 4.533 | 4.479 | 0.163 |
| 4500 | 4.897 | 5.246 | 5.158 | 4.664 | 4.954 | 4.838 | 0.203 |
| 5000 | 5.258 | 5.620 | 5.472 | 5.025 | 5.327 | 5.152 | 0.239 |
| 5500 | 5.532 | 5.905 | 5.709 | 5.299 | 5.613 | 5.389 | 0.269 |
| 6000 | 5.761 | 6.169 | 5.936 | 5.528 | 5.877 | 5.615 | 0.305 |
| 6500 | 5.984 | 6.415 | 6.148 | 5.751 | 6.123 | 5.828 | 0.333 |
| 7000 | 6.154 | 6.613 | 6.335 | 5.922 | 6.321 | 6.015 | 0.352 |
| 7500 | 6.353 | 6.838 | 6.537 | 6.121 | 6.546 | 6.217 | 0.377 |
| 8000 | 6.454 | 6.972 | 6.667 | 6.221 | 6.680 | 6.346 | 0.396 |

| | | | | | | | |
|---|---|---|---|---|---|---|---|
| 8500 | 6.497 | 7.094 | 6.836 | 6.264 | 6.801 | 6.516 | 0.411 |
| 9000 | 6.602 | 7.240 | 6.979 | 6.369 | 6.948 | 6.659 | 0.434 |
| 9500 | 6.685 | 7.358 | 7.103 | 6.453 | 7.066 | 6.783 | 0.448 |
| 10000 | 6.741 | 7.454 | 7.207 | 6.508 | 7.162 | 6.886 | 0.464 |
| 10500 | 6.795 | 7.543 | 7.307 | 6.563 | 7.251 | 6.987 | 0.477 |
| 11000 | 6.890 | 7.661 | 7.411 | 6.657 | 7.369 | 7.090 | 0.495 |
| 11500 | 6.960 | 7.761 | 7.502 | 6.728 | 7.469 | 7.182 | 0.514 |
| 12000 | 7.016 | 7.854 | 7.597 | 6.783 | 7.562 | 7.277 | 0.532 |
| 12500 | 7.069 | 7.946 | 7.694 | 6.837 | 7.654 | 7.374 | 0.548 |
| 13000 | 7.107 | 8.023 | 7.768 | 6.874 | 7.731 | 7.448 | 0.570 |
| 13500 | 7.147 | 8.105 | 7.850 | 6.914 | 7.813 | 7.530 | 0.591 |
| 13750 | | | | | | | |

**P-Wallette 3**

| Load (N) | Displcmnt A (mm) | Displcmnt B (mm) | Displcmnt C (mm) | Delta A (mm) | Delta B (mm) | Delta C (mm) | Deflection B Relative to A and C (mm) |
|---|---|---|---|---|---|---|---|
| 1000 | 0.398 | 0.411 | 0.385 | 0.000 | 0.000 | 0.000 | 0.000 |
| 1500 | 1.401 | 1.399 | 1.286 | 1.003 | 0.988 | 0.901 | 0.036 |
| 2000 | 2.225 | 2.211 | 2.045 | 1.828 | 1.800 | 1.660 | 0.056 |
| 2500 | 3.044 | 2.986 | 2.748 | 2.646 | 2.575 | 2.363 | 0.070 |
| 3000 | 3.737 | 3.643 | 3.340 | 3.339 | 3.232 | 2.956 | 0.085 |
| 3500 | 4.290 | 4.178 | 3.808 | 3.892 | 3.767 | 3.424 | 0.109 |
| 4000 | 4.837 | 4.698 | 4.226 | 4.439 | 4.288 | 3.841 | 0.148 |
| 4500 | 5.248 | 5.106 | 4.579 | 4.850 | 4.695 | 4.195 | 0.173 |
| 5000 | 5.581 | 5.436 | 4.864 | 5.183 | 5.025 | 4.479 | 0.194 |
| 5500 | 5.877 | 5.736 | 5.136 | 5.479 | 5.325 | 4.752 | 0.210 |
| 6000 | 6.119 | 5.992 | 5.385 | 5.721 | 5.582 | 5.001 | 0.221 |
| 6500 | 6.336 | 6.225 | 5.612 | 5.938 | 5.814 | 5.227 | 0.231 |
| 7000 | 6.505 | 6.421 | 5.804 | 6.107 | 6.010 | 5.419 | 0.247 |
| 7500 | 6.700 | 6.644 | 6.017 | 6.302 | 6.234 | 5.632 | 0.267 |
| 8000 | 6.819 | 6.793 | 6.168 | 6.421 | 6.382 | 5.783 | 0.280 |
| 8500 | 6.942 | 6.948 | 6.335 | 6.544 | 6.538 | 5.951 | 0.290 |
| 9000 | 7.119 | 7.129 | 6.491 | 6.721 | 6.719 | 6.106 | 0.305 |
| 9500 | 7.214 | 7.247 | 6.613 | 6.816 | 6.837 | 6.228 | 0.314 |
| 10000 | 7.294 | 7.355 | 6.735 | 6.896 | 6.944 | 6.350 | 0.321 |
| 10500 | 7.372 | 7.464 | 6.853 | 6.975 | 7.053 | 6.468 | 0.332 |
| 11000 | 7.434 | 7.557 | 6.952 | 7.036 | 7.146 | 6.567 | 0.344 |
| 11500 | 7.508 | 7.663 | 7.054 | 7.110 | 7.252 | 6.669 | 0.363 |
| 12000 | 7.590 | 7.779 | 7.155 | 7.192 | 7.369 | 6.770 | 0.387 |
| 12250 | | | | | | | |

**P-Wallette 4**

| Load (N) | Displcmnt. A (mm) | Displcmnt. B (mm) | Displcmnt. C (mm) | Delta A (mm) | Delta B (mm) | Delta C (mm) | Deflection B Relative to A and C (mm) |
|---|---|---|---|---|---|---|---|
| 1000 | 0.489 | 0.633 | 0.702 | 0.000 | 0.000 | 0.000 | 0.000 |
| 1500 | 1.444 | 1.802 | 1.943 | 0.955 | 1.169 | 1.241 | 0.071 |
| 2000 | 2.291 | 2.787 | 2.998 | 1.802 | 2.155 | 2.296 | 0.106 |

| | | | | | | | |
|---|---|---|---|---|---|---|---|
| **2500** | 2.929 | 3.526 | 3.787 | 2.440 | 2.893 | 3.085 | 0.131 |
| **3000** | 3.657 | 4.258 | 4.487 | 3.168 | 3.625 | 3.785 | 0.149 |
| **3500** | 4.089 | 4.668 | 4.939 | 3.600 | 4.035 | 4.237 | 0.117 |
| **4000** | 4.522 | 5.083 | 5.304 | 4.033 | 4.450 | 4.602 | 0.133 |
| **4500** | 4.858 | 5.425 | 5.640 | 4.369 | 4.793 | 4.938 | 0.139 |
| **5000** | 5.184 | 5.786 | 6.008 | 4.695 | 5.154 | 5.306 | 0.153 |
| **5500** | 5.456 | 6.106 | 6.337 | 4.967 | 5.473 | 5.635 | 0.172 |
| **6000** | 5.694 | 6.332 | 6.534 | 5.205 | 5.700 | 5.832 | 0.182 |
| **6500** | 5.910 | 6.569 | 6.766 | 5.421 | 5.937 | 6.064 | 0.194 |
| **7000** | 6.076 | 6.767 | 6.953 | 5.587 | 6.134 | 6.251 | 0.215 |
| **7500** | 6.245 | 6.960 | 7.136 | 5.756 | 6.327 | 6.434 | 0.232 |
| **8000** | 6.379 | 7.115 | 7.276 | 5.890 | 6.483 | 6.574 | 0.251 |
| **8500** | 6.534 | 7.288 | 7.420 | 6.045 | 6.656 | 6.718 | 0.274 |
| **9000** | 6.687 | 7.452 | 7.549 | 6.198 | 6.819 | 6.847 | 0.296 |
| **9500** | 6.788 | 7.582 | 7.664 | 6.299 | 6.949 | 6.962 | 0.319 |
| **10000** | 6.934 | 7.731 | 7.775 | 6.445 | 7.099 | 7.073 | 0.340 |
| **10500** | 7.026 | 7.854 | 7.869 | 6.537 | 7.222 | 7.167 | 0.370 |
| **10680** | | | | | | | |

**P-Wallette 5**

| **Load (N)** | **Displcmnt A (mm)** | **Displcmnt B (mm)** | **Displcmnt C (mm)** | **Delta A (mm)** | **Delta B (mm)** | **Delta C (mm)** | **Deflection B Relative to A and C (mm)** |
|---|---|---|---|---|---|---|---|
| **1000** | 0.098 | 0.108 | 0.111 | 0.000 | 0.000 | 0.000 | 0.000 |
| **1500** | 0.847 | 1.017 | 1.069 | 0.750 | 0.909 | 0.958 | 0.055 |
| **2000** | 1.910 | 2.034 | 2.016 | 1.812 | 1.926 | 1.905 | 0.067 |
| **2500** | 2.691 | 2.792 | 2.719 | 2.594 | 2.683 | 2.608 | 0.083 |
| **3000** | 3.315 | 3.384 | 3.261 | 3.217 | 3.276 | 3.150 | 0.093 |
| **3500** | 3.804 | 3.926 | 3.821 | 3.706 | 3.818 | 3.710 | 0.110 |
| **4000** | 4.244 | 4.334 | 4.159 | 4.147 | 4.226 | 4.048 | 0.129 |
| **4500** | 4.582 | 4.684 | 4.472 | 4.485 | 4.576 | 4.360 | 0.154 |
| **5000** | 5.215 | 5.080 | 4.593 | 5.117 | 4.972 | 4.482 | 0.172 |
| **5500** | 5.525 | 5.379 | 4.748 | 5.427 | 5.271 | 4.637 | 0.239 |
| **6000** | 5.793 | 5.617 | 4.881 | 5.695 | 5.508 | 4.769 | 0.276 |
| **6500** | 6.015 | 5.821 | 4.990 | 5.917 | 5.713 | 4.879 | 0.315 |
| **7000** | 6.212 | 5.993 | 5.091 | 6.114 | 5.885 | 4.980 | 0.338 |
| **7500** | 6.273 | 6.040 | 5.151 | 6.175 | 5.931 | 5.040 | 0.324 |
| **8000** | 6.415 | 6.172 | 5.226 | 6.318 | 6.064 | 5.115 | 0.348 |
| **8500** | 6.540 | 6.295 | 5.302 | 6.442 | 6.186 | 5.191 | 0.370 |
| **9000** | 6.649 | 6.408 | 5.372 | 6.551 | 6.299 | 5.261 | 0.393 |
| **9500** | 6.748 | 6.518 | 5.465 | 6.651 | 6.409 | 5.353 | 0.407 |
| **10000** | 6.814 | 6.592 | 5.527 | 6.716 | 6.484 | 5.415 | 0.418 |
| **10500** | 6.876 | 6.670 | 5.590 | 6.778 | 6.561 | 5.479 | 0.433 |
| **11000** | 6.932 | 6.742 | 5.648 | 6.835 | 6.634 | 5.537 | 0.448 |
| **11500** | 6.981 | 6.817 | 5.711 | 6.883 | 6.709 | 5.600 | 0.468 |
| **12000** | 7.015 | 6.880 | 5.763 | 6.917 | 6.772 | 5.652 | 0.487 |
| **12500** | 7.048 | 6.972 | 5.837 | 6.950 | 6.864 | 5.726 | 0.526 |
| **12520** | | | | | | | |

**P-Wallette 6**

| Load (N) | Displcmnt A (mm) | Displcmnt B (mm) | Displcmnt C (mm) | Delta A (mm) | Delta B (mm) | Delta C (mm) | Deflection B Relative to A and C (mm) |
|---|---|---|---|---|---|---|---|
| 1000 | 1.5794 | 1.4653 | 1.679 | 0.000 | 0.000 | 0.000 | 0.000 |
| 1500 | 2.0871 | 2.1556 | 2.4006 | 0.508 | 0.690 | 0.722 | 0.076 |
| 2000 | 2.6361 | 2.8442 | 3.0557 | 1.057 | 1.379 | 1.377 | 0.162 |
| 2500 | 3.1494 | 3.4209 | 3.5677 | 1.570 | 1.956 | 1.889 | 0.226 |
| 3000 | 3.6318 | 3.9093 | 3.9767 | 2.052 | 2.444 | 2.298 | 0.269 |
| 3500 | 4.0503 | 4.3331 | 4.3071 | 2.471 | 2.868 | 2.628 | 0.318 |
| 4000 | 4.4548 | 4.7193 | 4.615 | 2.875 | 3.254 | 2.936 | 0.348 |
| 4500 | 4.7635 | 5.0216 | 4.8124 | 3.184 | 3.556 | 3.133 | 0.398 |
| 5000 | 5.076 | 5.3196 | 5.0118 | 3.497 | 3.854 | 3.333 | 0.440 |
| 5500 | 5.3219 | 5.5739 | 5.1803 | 3.743 | 4.109 | 3.501 | 0.487 |
| 6000 | 5.5171 | 5.7766 | 5.315 | 3.938 | 4.311 | 3.636 | 0.524 |
| 6500 | 5.7104 | 5.9872 | 5.4563 | 4.131 | 4.522 | 3.777 | 0.568 |
| 7000 | 5.9037 | 6.2056 | 5.6024 | 4.324 | 4.740 | 3.923 | 0.616 |
| 7500 | 6.083 | 6.4284 | 5.8036 | 4.504 | 4.963 | 4.125 | 0.649 |
| 8000 | 6.2218 | 6.6023 | 5.9458 | 4.642 | 5.137 | 4.267 | 0.682 |
| 8500 | 6.341 | 6.757 | 6.075 | 4.762 | 5.292 | 4.396 | 0.713 |
| 9000 | 6.4321 | 6.8924 | 6.1405 | 4.853 | 5.427 | 4.462 | 0.770 |
| 9500 | 6.4921 | 6.9946 | 6.2416 | 4.913 | 5.529 | 4.563 | 0.792 |
| 10000 | 6.5597 | 7.1117 | 6.3548 | 4.980 | 5.646 | 4.676 | 0.818 |
| 10500 | 6.6413 | 7.2323 | 6.4578 | 5.062 | 5.767 | 4.779 | 0.847 |
| 11000 | 6.6929 | 7.3389 | 6.527 | 5.114 | 5.874 | 4.848 | 0.893 |
| 11500 | 6.7521 | 7.4883 | 6.6206 | 5.173 | 6.023 | 4.942 | 0.966 |
| 11500 | | | | | | | |

Scan Session: "Grey Wall Test"
Start Time: 18/10/2004 10:48:26

**Table A4.1: Load/Displacement Data for Grey Wall**

| | | | | | | | | | | | | | |
|---|---|---|---|---|---|---|---|---|---|---|---|---|---|
| Assignment | | | | C1R4 3277 on char | 5640 on char | 3265 on char | 3271 on char | 6188 on char | 8199 on char | 3274 on cha | 3263 on cha | 3267 on char | 3266 on chan |
| Reduction Method | | | | mm | mm | mm | mm | mm | mm | mm | mm | mm | mm |
| **ID** | **psed** | **Minutes** | **(mb)** | **C1R4** | **C2R4** | **C3R4** | **C4R4** | **C5R4** | **C1R3** | **C2R3** | **C3R3** | **C4R3** | **C5R3** |
| 91 | 90.1 | 1.50 | 0 | -0.0028 | 0 | 0.0009 | 0 | -0.0009 | 0.003 | 0.0009 | -0.0009 | -0.0019 | 0.0019 |
| 301 | 300.1 | 5.00 | 0.1 | 0.015 | 0.0187 | 0.0234 | 0.0151 | 0.0245 | 0.0139 | 0.0009 | 0.0177 | 0.0196 | 0.0218 |
| 500 | 499.1 | 8.32 | 0.1 | 0.1708 | 0.1792 | 0.1937 | 0.1967 | 0.2132 | 0.1417 | 0.0766 | 0.1593 | 0.1729 | 0.1805 |
| 631 | 630.1 | 10.50 | 0.2 | 0.5734 | 0.603 | 0.6392 | 0.6615 | 0.6929 | 0.4768 | 0.4327 | 0.531 | 0.5627 | 0.5719 |
| 751 | 750.1 | 12.50 | 0.3 | 0.9647 | 1.0138 | 1.0772 | 1.116 | 1.163 | 0.8098 | 0.7841 | 0.899 | 0.961 | 0.9709 |
| 861 | 860.1 | 14.34 | 0.4 | 1.5869 | 1.6961 | 1.7988 | 1.8763 | 1.9678 | 1.356 | 1.3616 | 1.512 | 1.6153 | 1.6644 |
| 871 | 870.1 | 14.50 | 0.5 | 1.722 | 1.8464 | 1.9617 | 2.0485 | 2.146 | 1.469 | 1.4896 | 1.6461 | 1.7593 | 1.8192 |
| 911 | 910.1 | 15.17 | 0.6 | 2.1875 | 2.3533 | 2.5129 | 2.6395 | 2.7673 | 1.8625 | 1.9204 | 2.1147 | 2.2641 | 2.355 |
| 961 | 960.1 | 16.00 | 0.9 | 2.8341 | 3.0879 | 3.344 | 3.5607 | 3.7713 | 2.4117 | 2.54 | 2.8329 | 3.0642 | 3.2281 |
| 981 | 980.1 | 16.34 | 1 | 3.1109 | 3.4137 | 3.7277 | 3.9992 | 4.2475 | 2.6476 | 2.8194 | 3.1562 | 3.4718 | 3.647 |
| 1006 | 1005.1 | 16.75 | 1.2 | 3.4084 | 3.7965 | 4.1947 | 4.5581 | 4.8757 | 2.9003 | 3.1624 | 3.5708 | 3.928 | 4.1999 |
| 1021 | 1020.1 | 17.00 | 1.4 | 3.5163 | 3.9411 | 4.381 | 4.7868 | 5.1317 | 2.9935 | 3.2951 | 3.7375 | 4.1299 | 4.4336 |
| 1091 | 1090.1 | 18.17 | 1.6 | 3.7453 | 4.2669 | 4.8021 | 5.3109 | 5.7373 | 3.1987 | 3.5969 | 4.1279 | 4.5954 | 4.9818 |
| 1126 | 1125.1 | 18.75 | 2 | 3.8851 | 4.5068 | 5.1391 | 5.7475 | 6.2545 | 3.3286 | 3.8249 | 4.4334 | 4.9964 | 5.4416 |
| 1171 | 1170.1 | 19.50 | 2.5 | 4.024 | 4.7925 | 5.5621 | 6.3093 | 6.9457 | 3.4792 | 4.1109 | 4.8405 | 5.5386 | 6.0828 |
| 1211 | 1210.1 | 20.17 | 3 | 4.1207 | 5.0156 | 5.9 | 6.7657 | 7.4979 | 3.5992 | 4.3464 | 5.1824 | 5.9873 | 6.6157 |
| 1251 | 1250.1 | 20.84 | 3.5 | 4.1976 | 5.1873 | 6.1704 | 7.1298 | 7.9436 | 3.7032 | 4.5464 | 5.4628 | 6.3566 | 7.0537 |
| 1291 | 1290.1 | 21.50 | 4 | 4.2755 | 5.3516 | 6.4231 | 7.4639 | 8.3411 | 3.8291 | 4.7529 | 5.7432 | 6.7174 | 7.4669 |
| 1326 | 1325.1 | 22.09 | 4.5 | 4.3431 | 5.4907 | 6.6337 | 7.7424 | 8.6653 | 3.9491 | 4.9417 | 5.9873 | 7.0268 | 7.8118 |
| 1361 | 1360.1 | 22.67 | 5 | 4.3562 | 5.6233 | 6.8424 | 8.0162 | 8.9965 | 4.071 | 5.1314 | 6.2314 | 7.3334 | 8.1595 |
| 1381 | 1380.1 | 23.00 | 5.5 | 4.3994 | 5.6998 | 6.9585 | 8.1687 | 9.1695 | 4.1582 | 5.2538 | 6.386 | 7.5176 | 8.3637 |
| 1411 | 1410.1 | 23.50 | 6 | 4.4604 | 5.8128 | 7.1344 | 8.403 | 9.4439 | 4.2801 | 5.4295 | 6.6096 | 7.7924 | 8.6706 |
| 1436 | 1435.1 | 23.92 | 6.5 | 4.5101 | 5.8968 | 7.2692 | 8.5874 | 9.664 | 4.3723 | 5.5697 | 6.7847 | 8.0074 | 8.9147 |
| 1461 | 1460.1 | 24.34 | 7.2 | 4.5693 | 5.9948 | 7.4161 | 8.7878 | 9.9271 | 4.4754 | 5.7332 | 6.9869 | 8.2635 | 9.1988 |
| 1861 | 1860.1 | 31.00 | 7.2 | 4.9425 | 6.5421 | 7.4929 | 11.0283 | 14.3641 | 4.5745 | 8.4396 | 11.1799 | 14.4958 | 14.5007 |
| 1911 | 1910.1 | 31.84 | 5.5 | 5.7121 | 7.0241 | 7.7194 | 11.6541 | 15.4109 | 4.7658 | 9.0862 | 12.2569 | 15.941 | 15.8231 |
| 1921 | 1920.1 | 32.00 | 6 | 6.0214 | 7.4321 | 7.7512 | 11.7689 | 15.6154 | 4.8065 | 9.2077 | 12.4562 | 16.2177 | 16.0739 |
| 1941 | 1940.1 | 32.34 | 6.5 | 6.6421 | 7.6421 | 7.7924 | 11.9749 | 15.9981 | 4.8818 | 9.4367 | 12.84 | 16.7224 | 16.5631 |
| 1951 | 1950.1 | 32.50 | 7 | 6.9451 | 7.7212 | 7.8008 | 12.0671 | 16.1746 | 4.9145 | 9.5507 | 13.0319 | 16.9898 | 16.812 |
| 1971 | 1970.1 | 32.84 | 5.5 | 7.5556 | 8.1201 | 8.512 | 12.3636 | 16.961 | 5.42 | 10.6198 | 14.719 | 19.4502 | 18.9286 |
| 2160 | 2159.1 | 35.99 | 5.5 | 8.5556 | 8.7073 | 9.8546 | 12.2252 | 17.3236 | 5.5697 | 11.2898 | 16.0298 | 20.8972 | 20.7877 |

**Table A4.1 (Continued)**

| :278 on cha | 3269 on chan | eds calibratin | eds calibratir | €358 on cha | 3264 on chan | 3270 on chan | 3261 on chan | 3268 on chan | 3239 on channel 20 |
|---|---|---|---|---|---|---|---|---|---|
| mm | mm | mm | mm | mm | mm | mm | mm | mm | mm |
| **C1R2** | **C2R2** | **C3R2** | **C4R2** | **C5R2** | **C1R1** | **C2R1** | **C3R1** | **C4R1** | **C5R1** |
| 0 | 0.0009 | -0.0009 | 0 | 0 | 0.0009 | -0.0009 | -0.0009 | 0 | -0.0009 |
| 0 | 0.0161 | 0.0131 | -0.0009 | 0.0186 | 0.0092 | 0.0112 | 0.0129 | 0.0159 | 0 |
| 0.0009 | 0.1306 | 0.1389 | 0.1131 | 0.155 | 0.0955 | 0.1072 | 0.1137 | 0.1225 | 0 |
| 0.2735 | 0.4257 | 0.4524 | 0.4372 | 0.4695 | 0.3123 | 0.3478 | 0.3662 | 0.3843 | 0.1667 |
| 0.5489 | 0.7247 | 0.7631 | 0.765 | 0.7981 | 0.5364 | 0.5922 | 0.6205 | 0.6555 | 0.4434 |
| 1.0009 | 1.2139 | 1.2859 | 1.3153 | 1.3747 | 0.9065 | 0.9913 | 1.0449 | 1.1137 | 0.9249 |
| 1.0968 | 1.3189 | 1.3975 | 1.4374 | 1.5023 | 0.9827 | 1.0771 | 1.1374 | 1.2118 | 1.0311 |
| 1.4211 | 1.6841 | 1.7974 | 1.8648 | 1.954 | 1.2472 | 1.3793 | 1.461 | 1.5653 | 1.4102 |
| 1.8816 | 2.2271 | 2.415 | 2.5516 | 2.6919 | 1.6256 | 1.8269 | 1.9696 | 2.1422 | 2.0501 |
| 2.0789 | 2.4731 | 2.7069 | 2.8758 | 3.0542 | 1.7873 | 2.0348 | 2.2119 | 2.4218 | 2.3687 |
| 2.2961 | 2.7712 | 3.0748 | 3.3013 | 3.5387 | 1.9682 | 2.2848 | 2.5281 | 2.794 | 2.8027 |
| 2.3769 | 2.8913 | 3.2259 | 3.4827 | 3.7504 | 2.0389 | 2.3883 | 2.6585 | 2.9548 | 2.9946 |
| 2.563 | 3.1647 | 3.575 | 3.8966 | 4.2279 | 2.1988 | 2.6251 | 2.9655 | 3.3204 | 3.4203 |
| 2.688 | 3.3767 | 3.8623 | 4.2647 | 4.6406 | 2.3117 | 2.8117 | 3.2189 | 3.6533 | 3.7882 |
| 2.8449 | 3.6577 | 4.2593 | 4.7837 | 5.2359 | 2.4651 | 3.0793 | 3.5878 | 4.1302 | 4.3443 |
| 2.9831 | 3.9065 | 4.6056 | 5.22 | 5.7514 | 2.6065 | 3.3236 | 3.9235 | 4.5519 | 4.8417 |
| 3.1156 | 4.1279 | 4.9069 | 5.5962 | 6.181 | 2.7507 | 3.5521 | 4.2194 | 4.9203 | 5.2683 |
| 3.2829 | 4.3739 | 5.2223 | 5.9697 | 6.5965 | 2.9454 | 3.8198 | 4.543 | 5.3 | 5.6911 |
| 3.453 | 4.6009 | 5.5048 | 6.2947 | 6.9534 | 3.1402 | 4.0706 | 4.8343 | 5.6375 | 6.0516 |
| 3.6259 | 4.8318 | 5.7863 | 6.6296 | 7.3148 | 3.3413 | 4.3289 | 5.1274 | 5.9844 | 6.4205 |
| 3.7575 | 4.9898 | 5.9712 | 6.8379 | 7.5381 | 3.4993 | 4.5136 | 5.3262 | 6.2098 | 6.6542 |
| 3.938 | 5.2159 | 6.2406 | 7.1423 | 7.8685 | 3.7105 | 4.7682 | 5.612 | 6.5315 | 6.998 |
| 4.0771 | 5.3909 | 6.4462 | 7.3838 | 8.1262 | 3.8795 | 4.9659 | 5.8302 | 6.7802 | 7.2625 |
| 4.2415 | 5.5943 | 6.6855 | 7.6639 | 8.4185 | 4.0806 | 5.1971 | 6.0873 | 7.0701 | 7.5615 |
| 6.531 | 9.182 | 11.3033 | 13.0536 | 12.8253 | 5.6374 | 7.9771 | 9.9728 | 11.664 | 11.1885 |
| 6.8064 | 9.8774 | 12.3658 | 14.3959 | 14.022 | 5.8881 | 8.6178 | 10.9474 | 12.8535 | 12.2513 |
| 6.8562 | 10.0051 | 12.5582 | 14.6464 | 14.2461 | 5.9341 | 8.7306 | 11.1194 | 13.0723 | 12.4506 |
| 6.9586 | 10.2464 | 12.9252 | 15.133 | 14.6864 | 6.025 | 8.947 | 11.4486 | 13.4921 | 12.8381 |
| 7.0075 | 10.3665 | 13.1073 | 15.3745 | 14.9131 | 6.0691 | 9.0551 | 11.6141 | 13.7044 | 13.0402 |
| 7.218 | 11.2852 | 14.7235 | 18.0779 | 18.187 | 6.1122 | 9.7592 | 12.9808 | 16.4937 | 16.3683 |
| 7.3618 | 11.7062 | 15.5945 | 19.597 | 20.3988 | 6.0388 | 10.0091 | 13.6642 | 18.0029 | 18.1185 |

**Scan Session: "Yellow Wall Test"**
Start Time: 04/10/2004 10:07:32

**Tabble A4.2: Load/Displacement Data for Yellow Wall**

| Reduction Method | | | | mm | mm | mm | mm | mm | mm | mm | mm | mm | mm |
|---|---|---|---|---|---|---|---|---|---|---|---|---|---|
| **ID** | **Seconds Elapsed** | **Minutes** | **Pressure (kPa)** | **C1R4** | **C2R4** | **C3R4** | **C4R4** | **C5R4** | **C1R3** | **C2R3** | **C3R3** | **C4R3** | **C5R3** |
| 181 | 180.1 | 3.00 | 0 | 0.0009 | -0.0028 | -0.0037 | -0.0035 | -0.0019 | -0.005 | -0.0037 | -0.0065 | -0.0028 | -0.0047 |
| 541 | 540.1 | 9.00 | 0.1 | 0.5659 | 0.5676 | 0.5718 | 0.5662 | 0.5759 | 0.4619 | 0.4682 | 0.4723 | 0.4795 | 0.4693 |
| 721 | 720.1 | 12.00 | 0.5 | 2.8669 | 2.8546 | 2.8798 | 2.811 | 2.8747 | 2.372 | 2.4484 | 2.4277 | 2.4435 | 2.4092 |
| 781 | 780.1 | 13.00 | 0.9 | 4.3769 | 4.3705 | 4.4016 | 4.2466 | 4.3756 | 3.6636 | 3.781 | 3.7329 | 3.742 | 3.667 |
| 841 | 840.1 | 14.00 | 2 | 6.327 | 6.3719 | 6.4784 | 6.3078 | 6.474 | 5.3923 | 5.6314 | 5.5876 | 5.6415 | 5.5385 |
| 901 | 900.1 | 15.00 | 3 | 6.9632 | 7.1271 | 7.2926 | 7.1886 | 7.3594 | 6.0098 | 6.3911 | 6.413 | 6.5332 | 6.4371 |
| 951 | 950.1 | 15.84 | 4 | 7.363 | 7.6965 | 7.9711 | 7.9375 | 8.0783 | 6.4817 | 7.0284 | 7.1592 | 7.3568 | 7.2703 |
| 997 | 996.1 | 16.60 | 5 | 7.5422 | 8.0755 | 8.4775 | 8.605 | 8.7078 | 6.7314 | 7.4929 | 7.7787 | 8.1093 | 8.0702 |
| 1036 | 1035.1 | 17.25 | 6 | 7.8121 | 8.3864 | 8.9145 | 9.1494 | 9.2226 | 6.9535 | 7.8854 | 8.2799 | 8.7085 | 8.7162 |
| 1081 | 1080.1 | 18.00 | 2.9 | 8.2112 | 8.7541 | 9.2314 | 9.9751 | 10.5682 | 4.6538 | 7.5041 | 9.8552 | 12.4448 | 12.0298 |
| 1561 | 1560.1 | 26.00 | 4 | 9.454 | 9.0123 | 9.7625 | 12.2723 | 13.5962 | 4.2454 | 8.5994 | 12.2084 | 16.284 | 15.2474 |
| 1649 | 1648.1 | 27.47 | 4.2 | 9.7812 | 9.4645 | 9.8589 | 12.5414 | 14.0075 | 4.0591 | 8.6947 | 12.5568 | 16.9449 | 15.8031 |

**Table A4.2 (Continued)**

| mm | mm | mm | mm | mm | mm | mm | mm | mm | mm |
|---|---|---|---|---|---|---|---|---|---|
| **C1R2** | **C2R2** | **C3R2** | **C4R2** | **C5R2** | **C1R1** | **C2R1** | **C3R1** | **C4R1** | **C5R1** |
| -0.0056 | -0.0028 | -0.0075 | -0.0054 | -0.0062 | -0.0046 | -0.0028 | -0.0046 | -0.0075 | -0.0065 |
| 0.3806 | 0.3794 | 0.3867 | 0.3861 | 0.3667 | 0.3012 | 0.3077 | 0.3107 | 0.3161 | 0.2962 |
| 1.9878 | 2.0105 | 2.0395 | 2.0192 | 1.978 | 1.6082 | 1.6516 | 1.6506 | 1.6747 | 1.6421 |
| 3.1109 | 3.1449 | 3.1771 | 3.1236 | 3.0338 | 2.5487 | 2.6242 | 2.6058 | 2.6219 | 2.5447 |
| 4.6701 | 4.7883 | 4.8665 | 4.8178 | 4.7168 | 3.9061 | 4.0874 | 4.0927 | 4.1554 | 4.063 |
| 5.2895 | 5.5291 | 5.6972 | 5.6752 | 5.6017 | 4.4857 | 4.8111 | 4.8898 | 5.0166 | 4.9339 |
| 5.843 | 6.2292 | 6.5156 | 6.5614 | 6.5079 | 5.0817 | 5.5748 | 5.7386 | 5.9433 | 5.9054 |
| 6.1588 | 6.7618 | 7.228 | 7.4062 | 7.43 | 5.4151 | 6.1418 | 6.4978 | 6.8653 | 6.9281 |
| 6.4464 | 7.2084 | 7.809 | 8.0832 | 8.1794 | 5.7201 | 6.6184 | 7.1016 | 7.5956 | 7.7357 |
| 6.3759 | 9.3324 | 11.935 | 14.2791 | 14.1974 | 7.9712 | 10.7533 | 13.2398 | 16.4497 | 15.8169 |
| 6.797 | 11.1329 | 15.2097 | 19.2828 | 18.4979 | 8.8033 | 13.2041 | 17.0393 | 21.8395 | 21.0488 |
| 6.8581 | 11.4527 | 15.7728 | 20.1662 | 19.3775 | 8.987 | 13.6648 | 17.7513 | 22.9054 | 22.1712 |

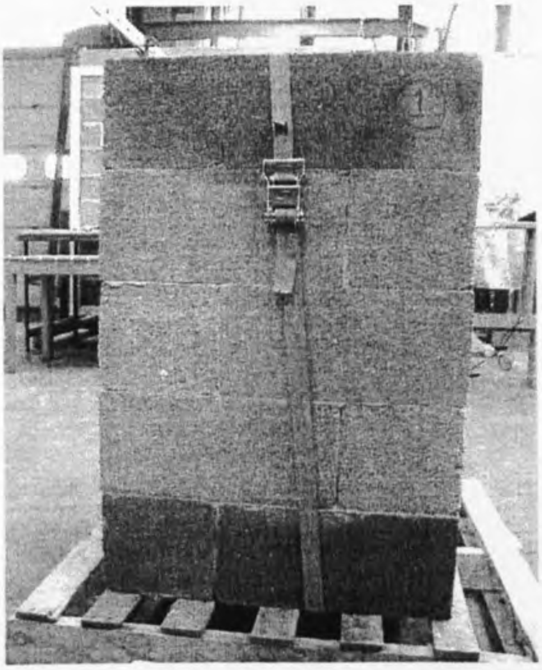

(a) Specimen before test

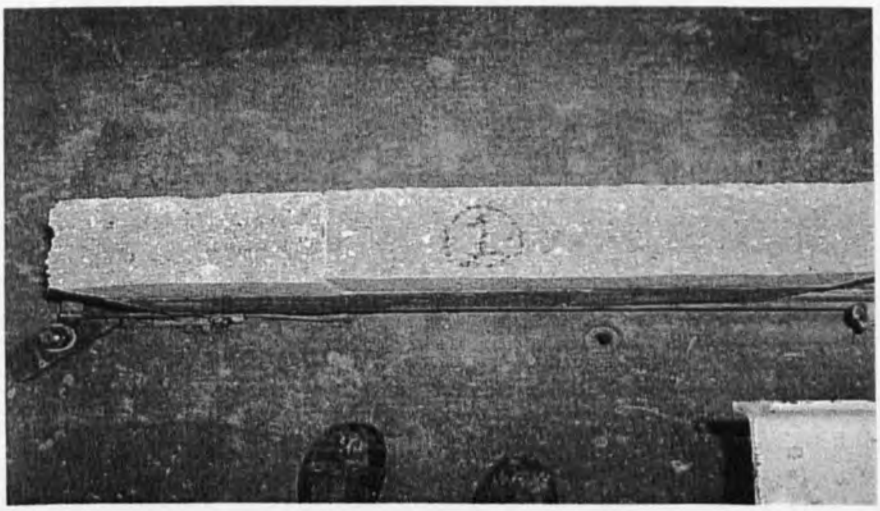

(b) Failure plane

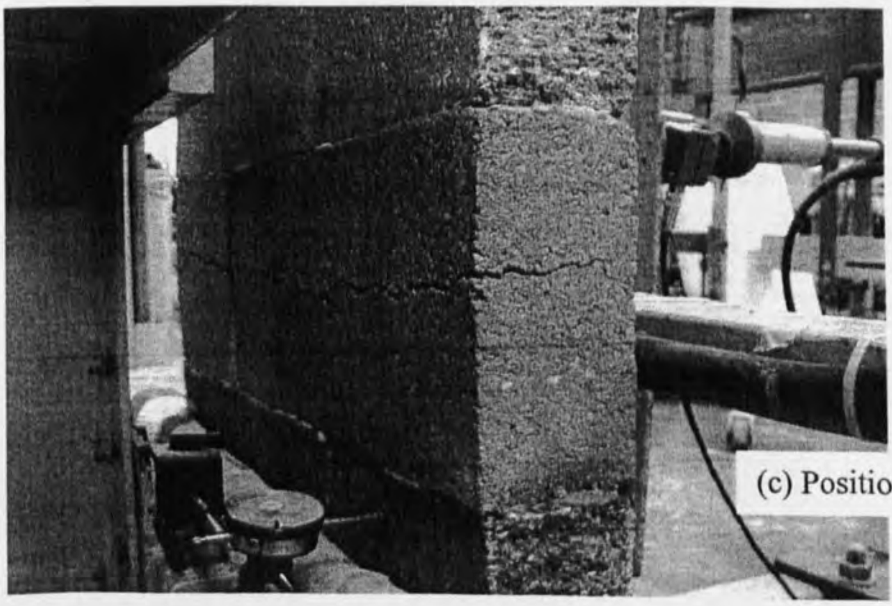

(c) Position of Failure Plane

**Slide 1: Grey B-Wallette No.1**

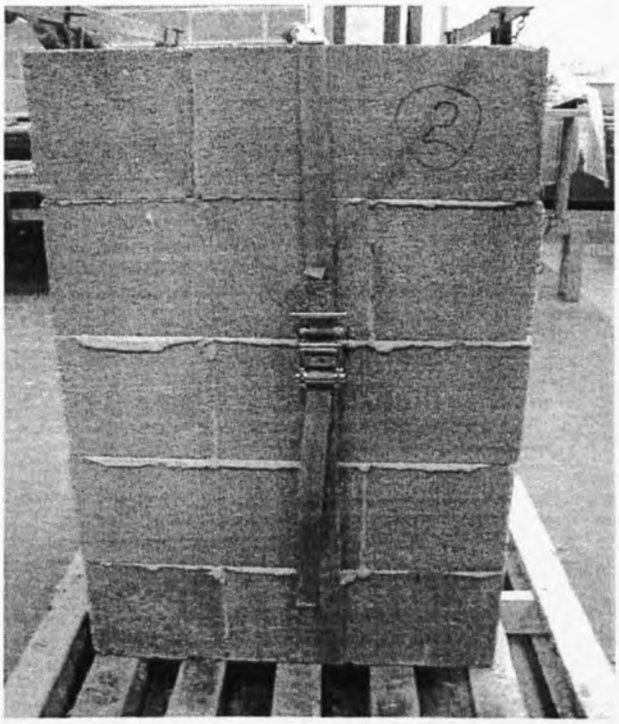

(a) Test Specimen

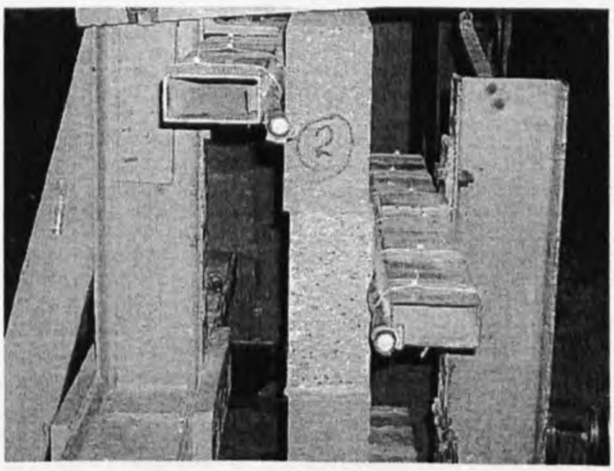

(b) Specimen in position

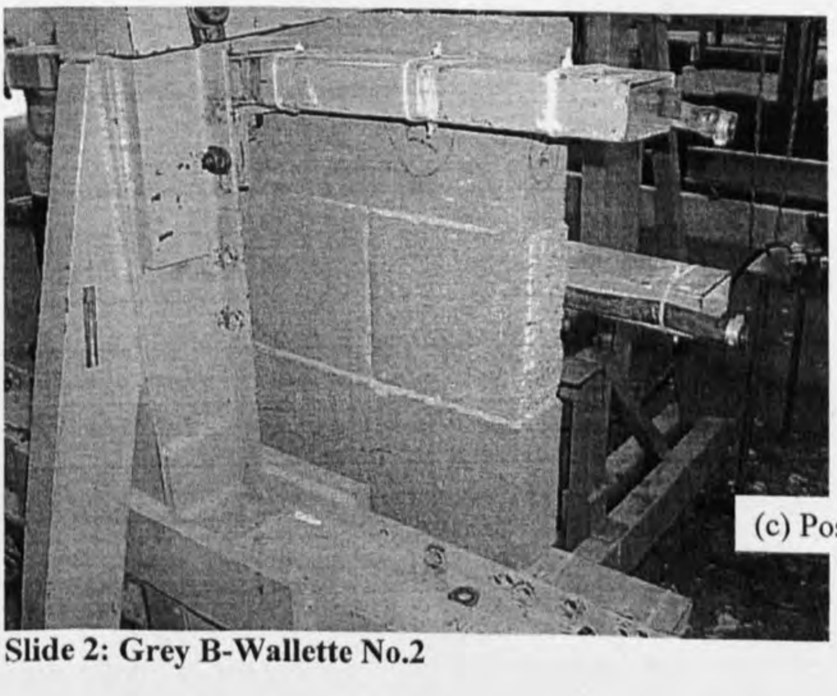

(c) Position of failure plane

**Slide 2: Grey B-Wallette No.2**

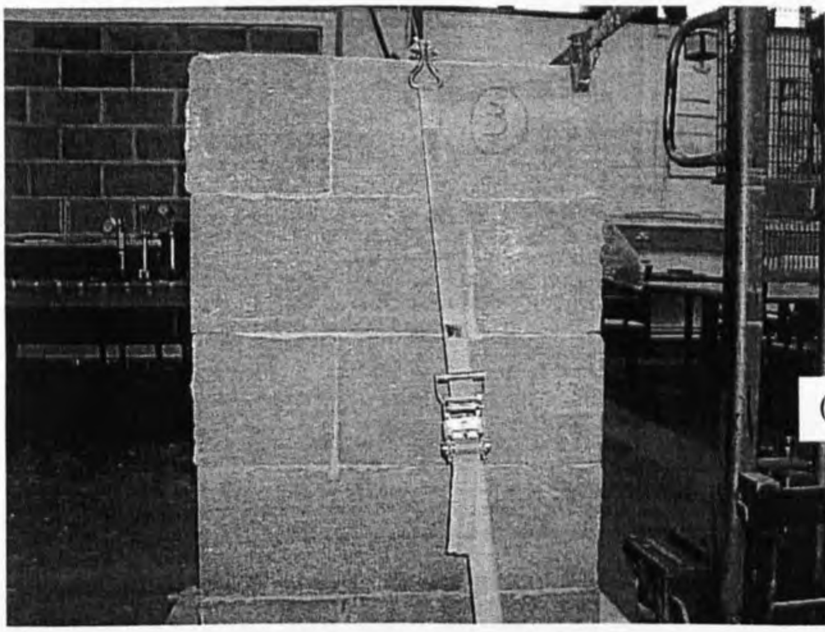


(a) Test Specimen

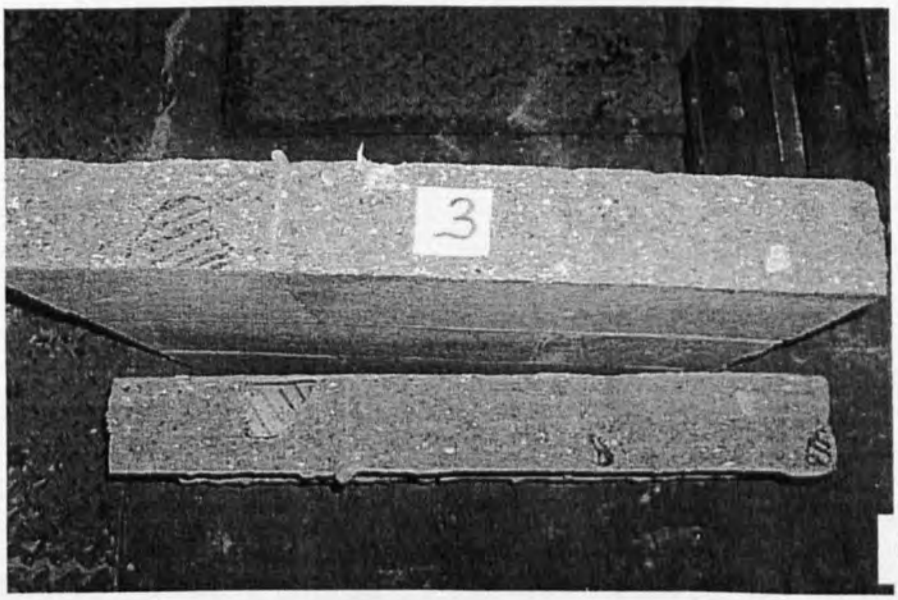


(b) Failure Plane

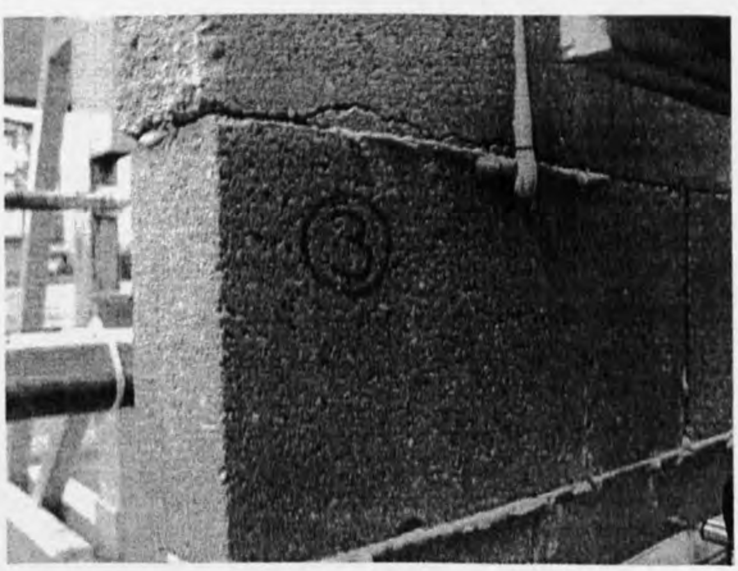


(c) Position of failure plane

**Slide 3: Grey B-Wallette No.3**

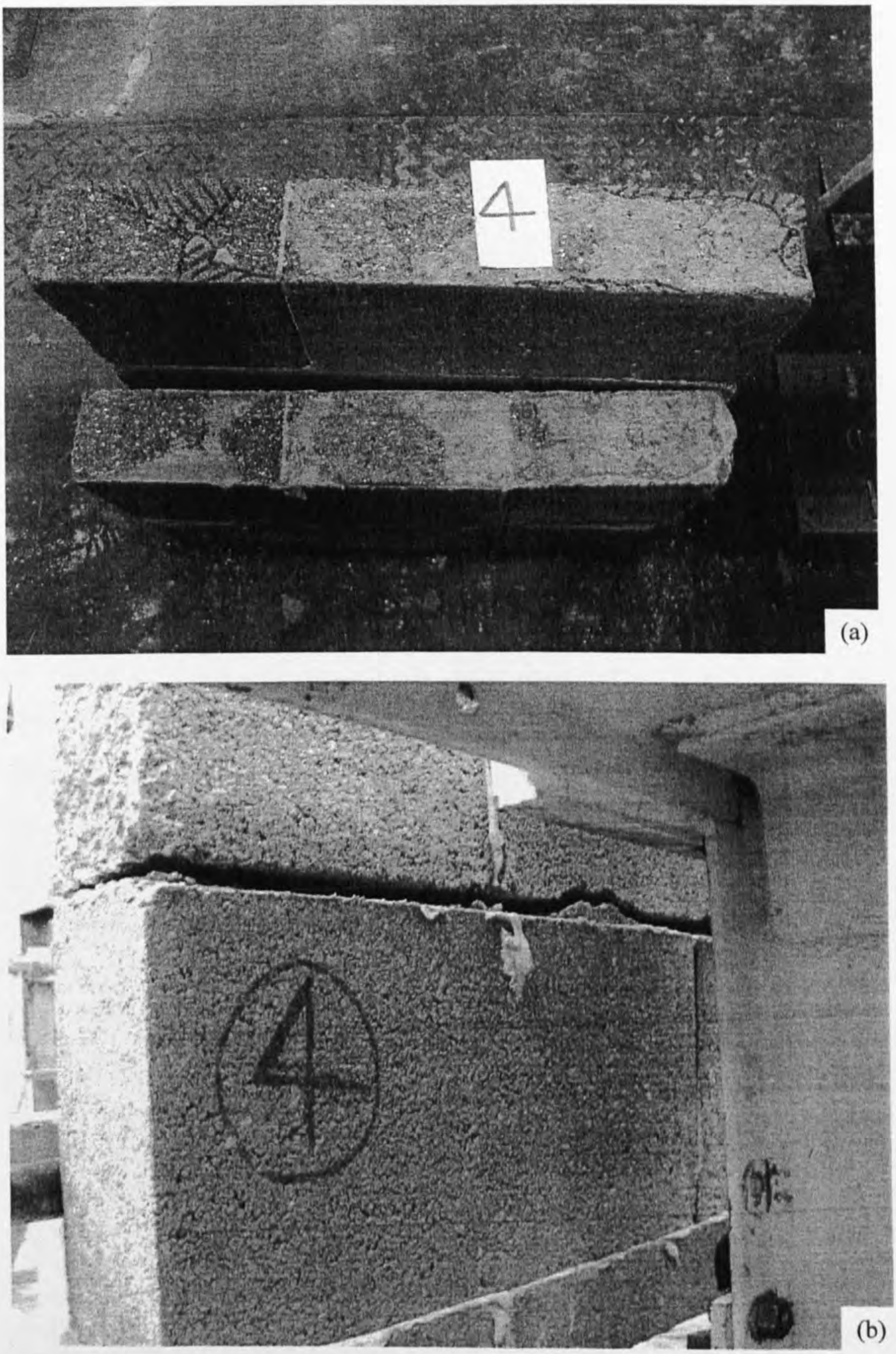


**Slide 4: Grey B-Wallette No.4 - (a) Failure plane, (b) Position of the failure plane**

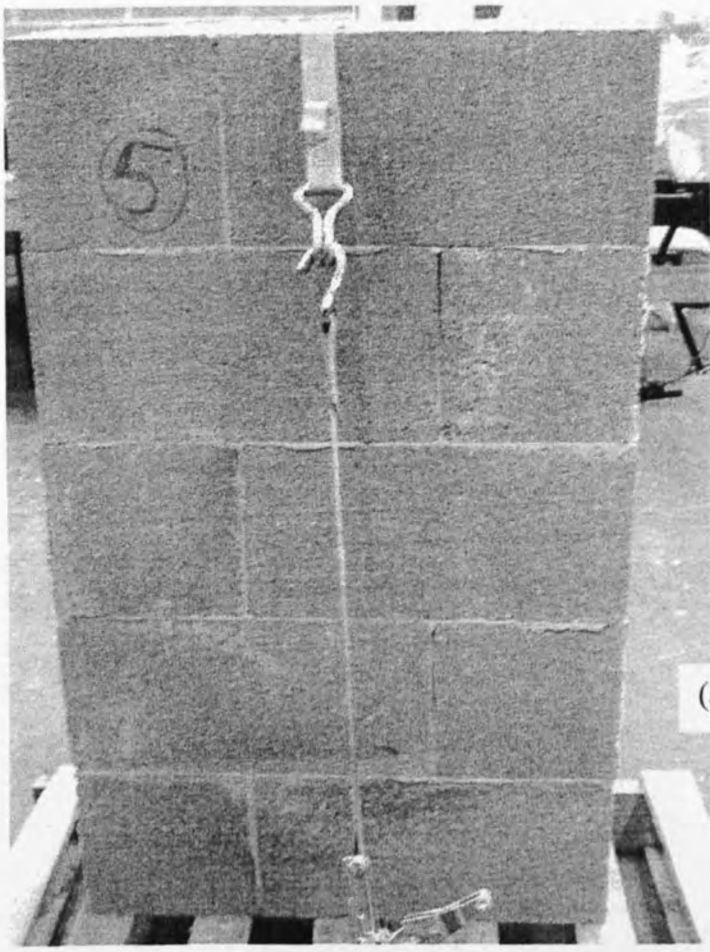


(a) Test Specimen

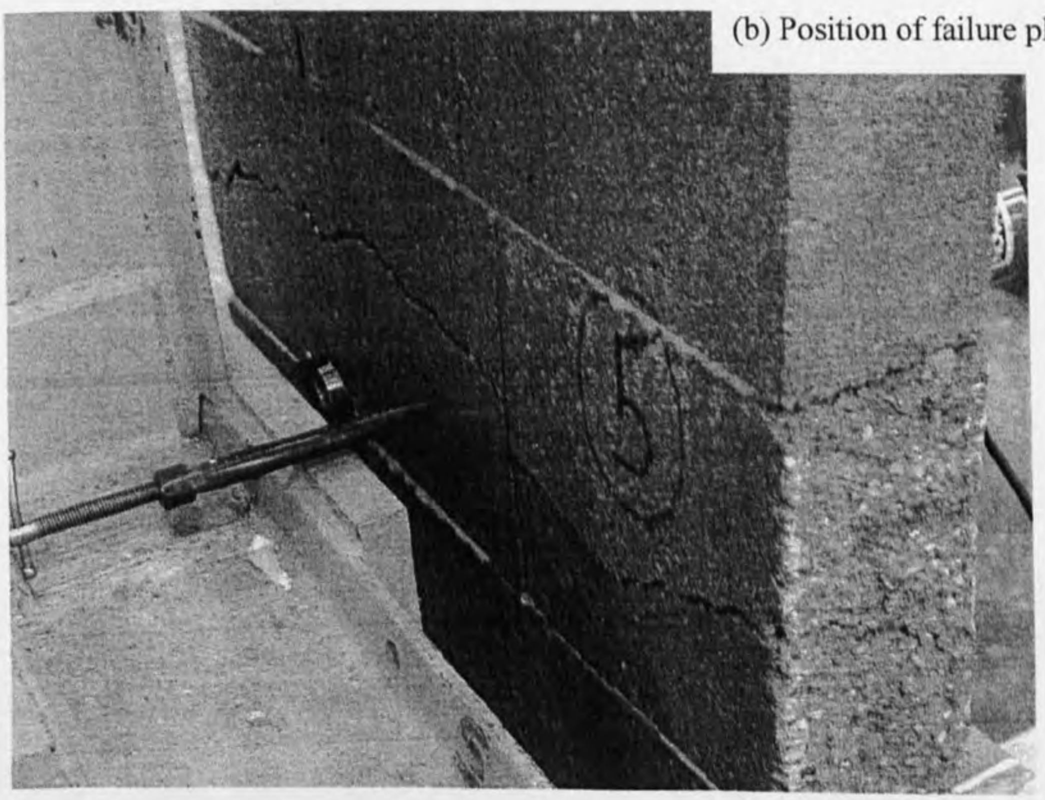


(b) Position of failure plane

**Slide 5: Grey B-Wallette No.5**

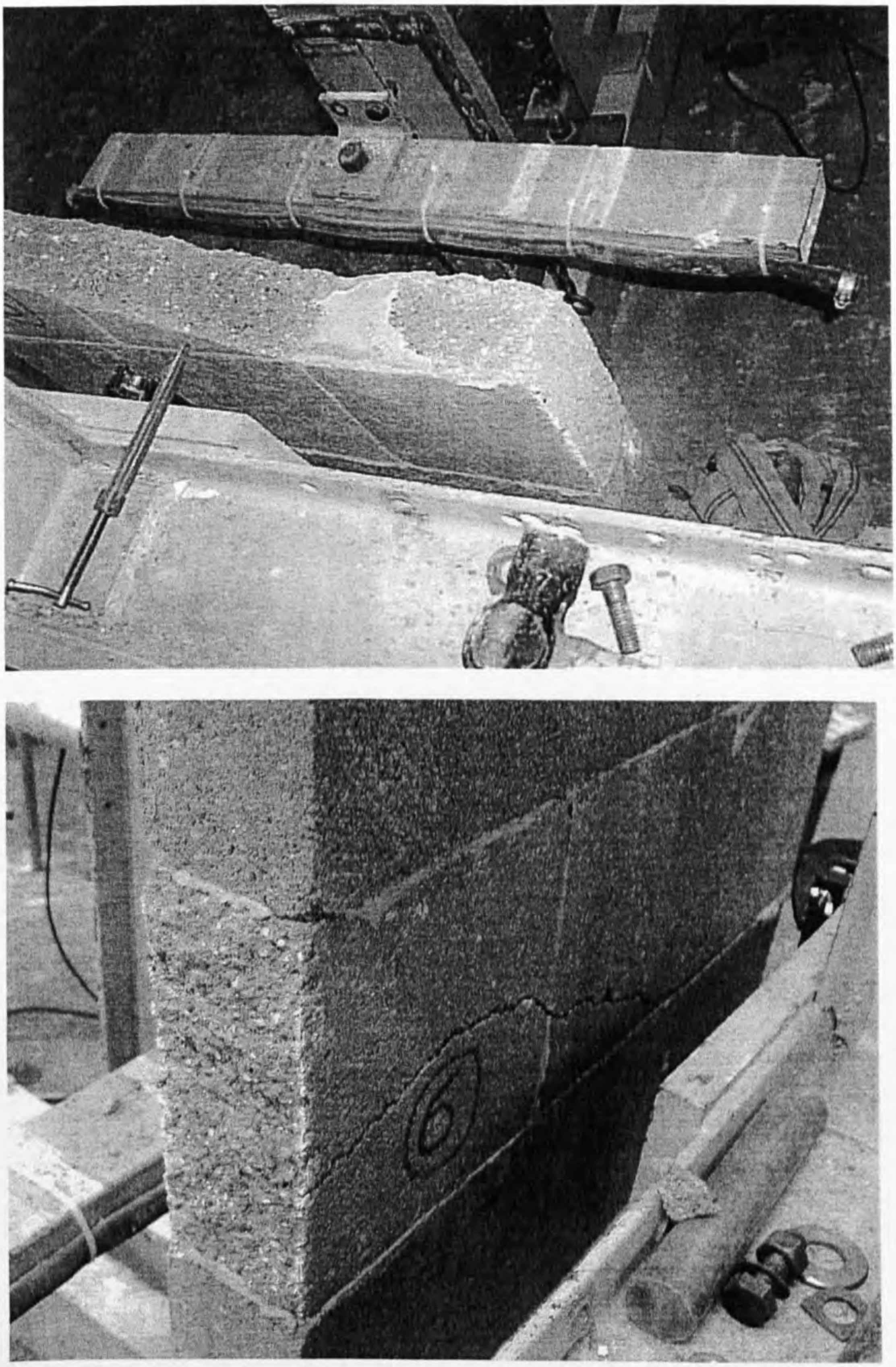

**Slide 6: Grey B-Wallette No.6 – (a) Failure plane, (b) Position of failure plane**

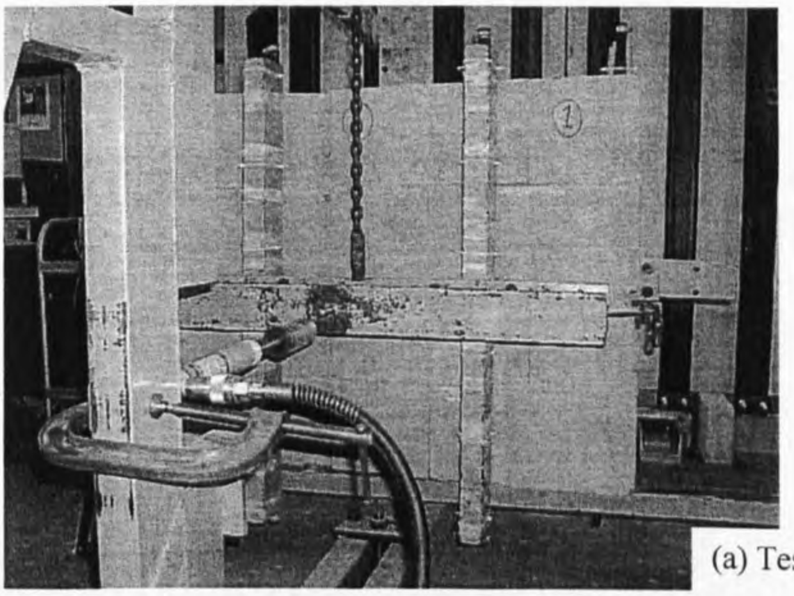

(a) Test specimen in position

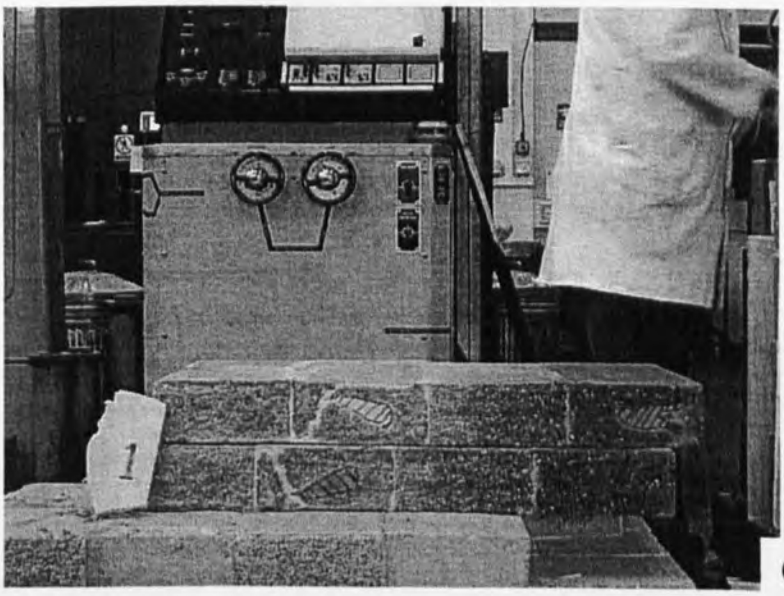

(b) Failure plane

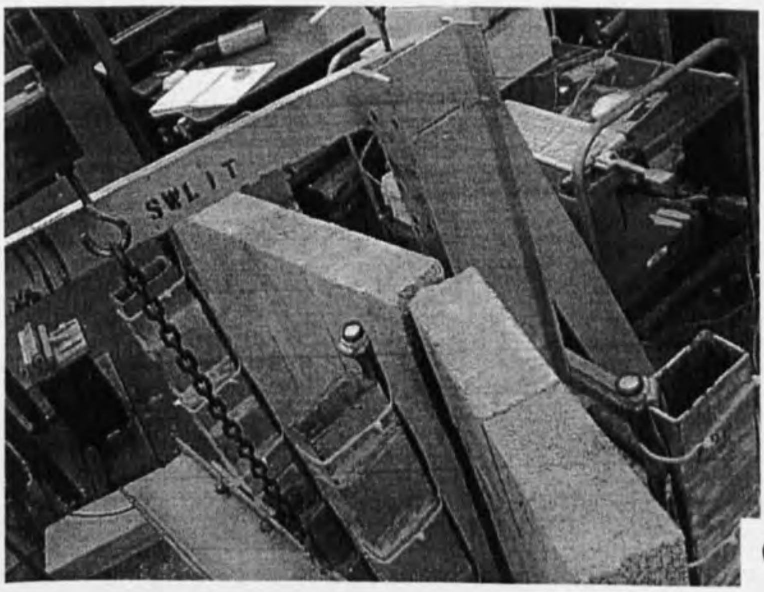


(c) Position of failure plane

**Slide 7: Grey P-Wallette No.1**

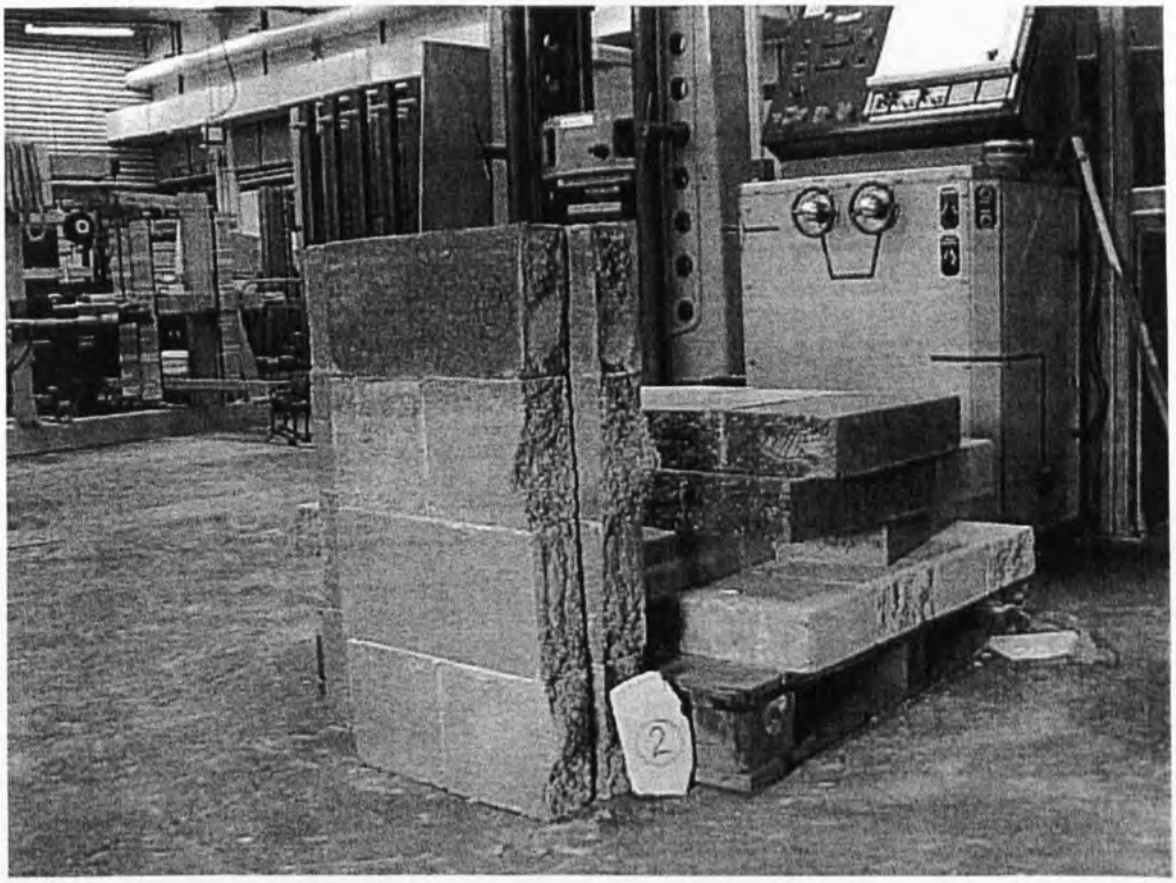

**Slide 8: Grey P-Wallette No.2 – Failure plane**

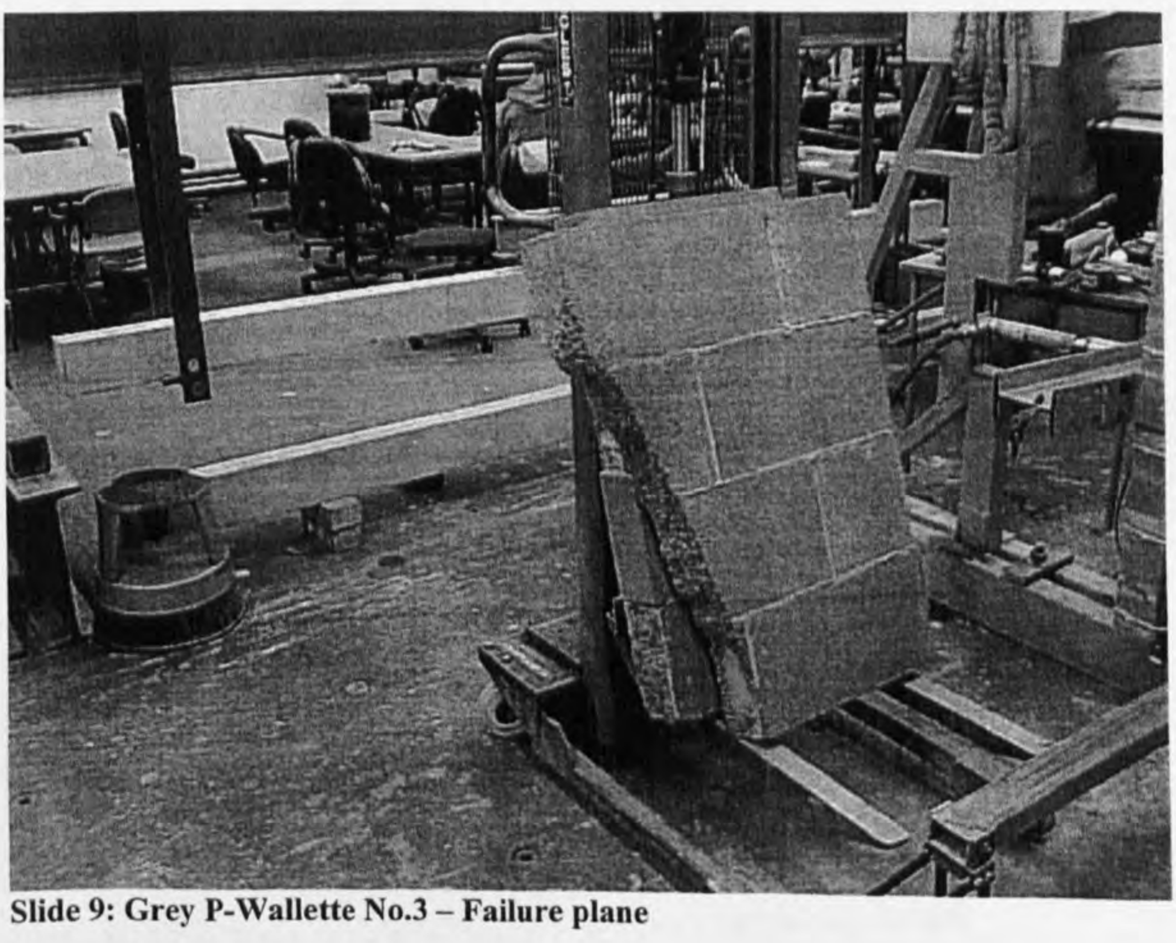

**Slide 9: Grey P-Wallette No.3 – Failure plane**

(a)


(b)

**Slide 10: Grey P-Wallette No.4 – (a) Failure plane, (b) Position of failure plane**

(a) Failure Plane

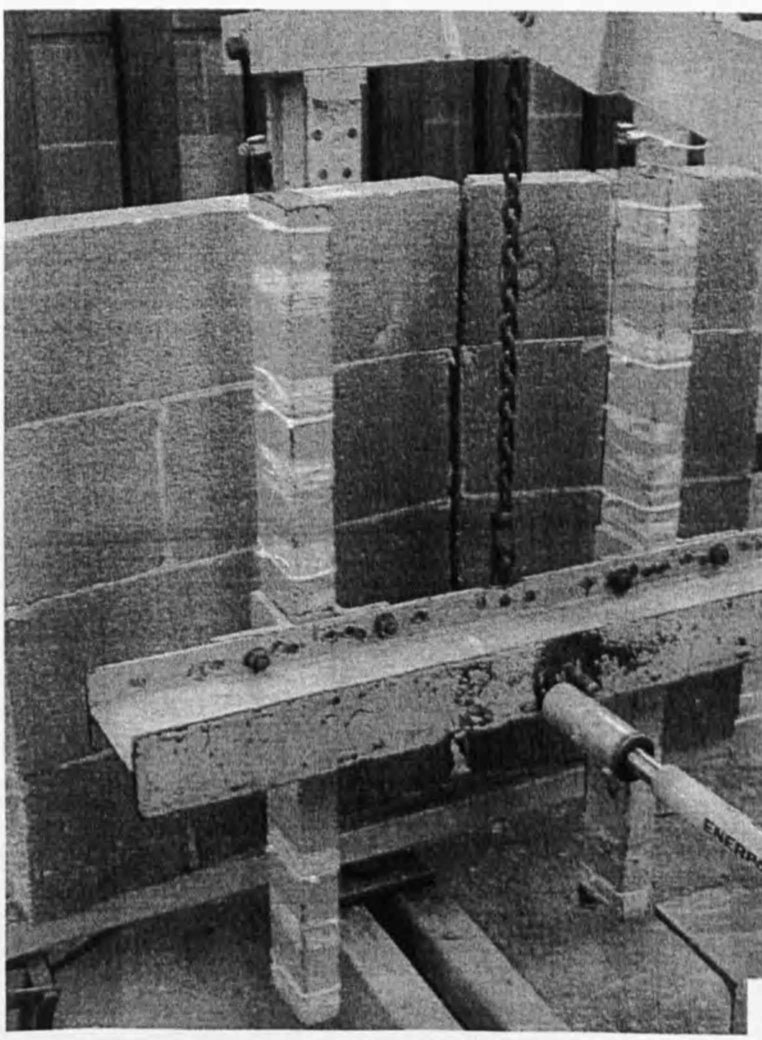

(b) Position of failure plane

**Slide 11: Grey P-Wallette No.5**

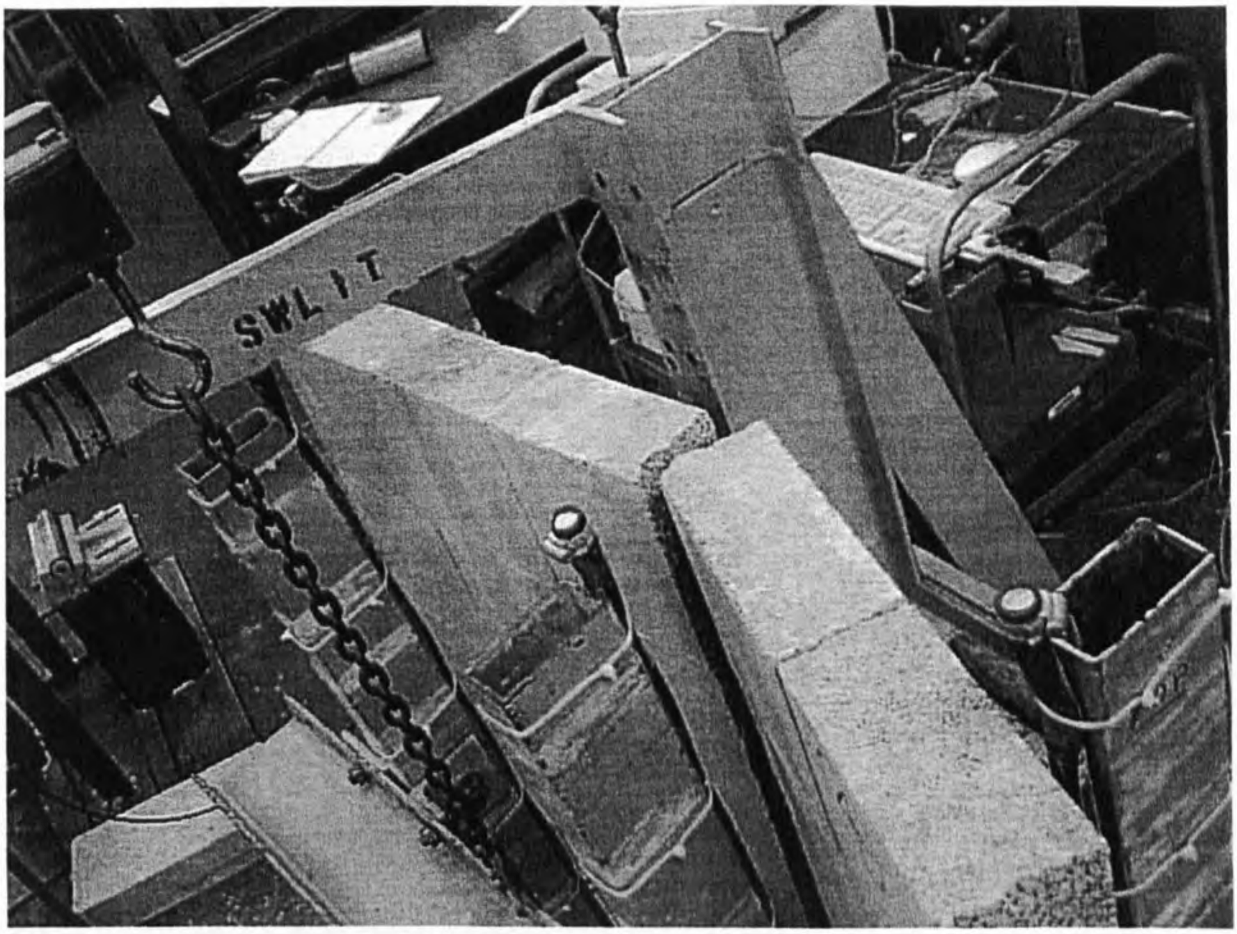


**Slide 12: Grey P-Wallette No.6 – Position of failure plane**

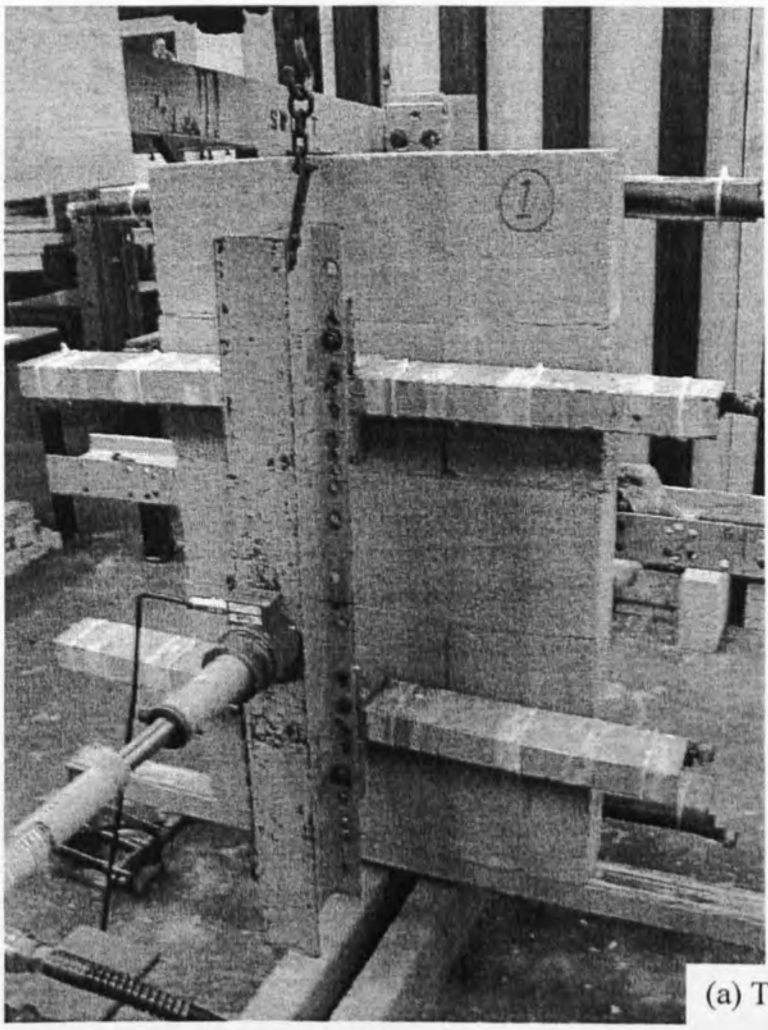

(a) Test specimen in position

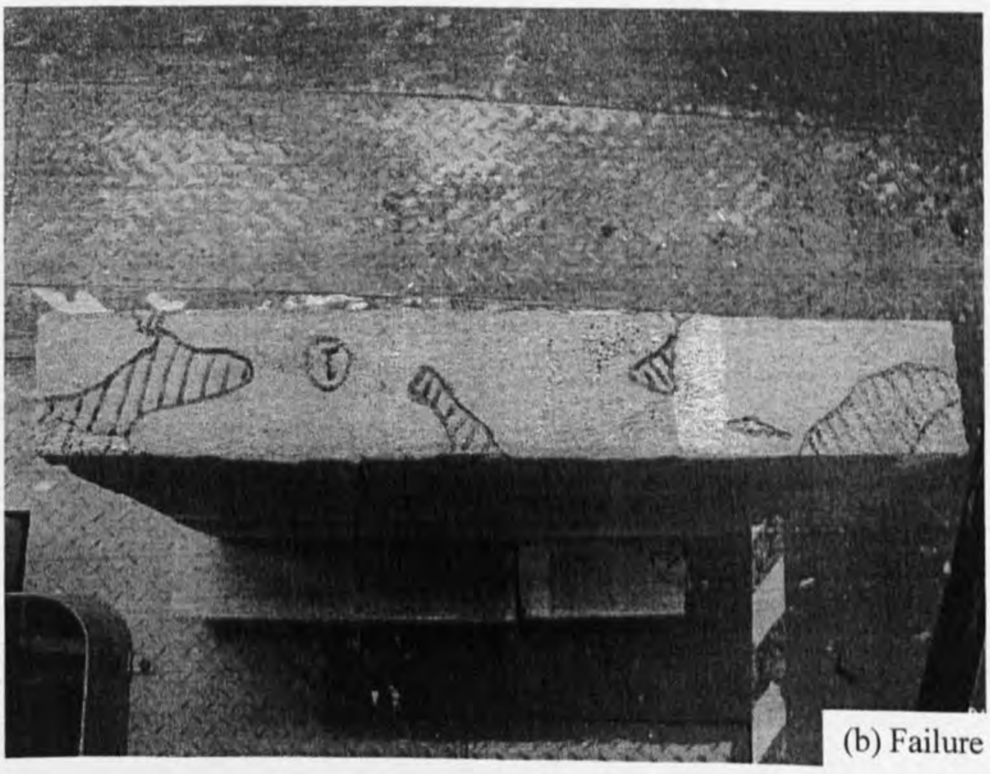

(b) Failure plane

**Slide 13: Yellow B-Wallette No.1**

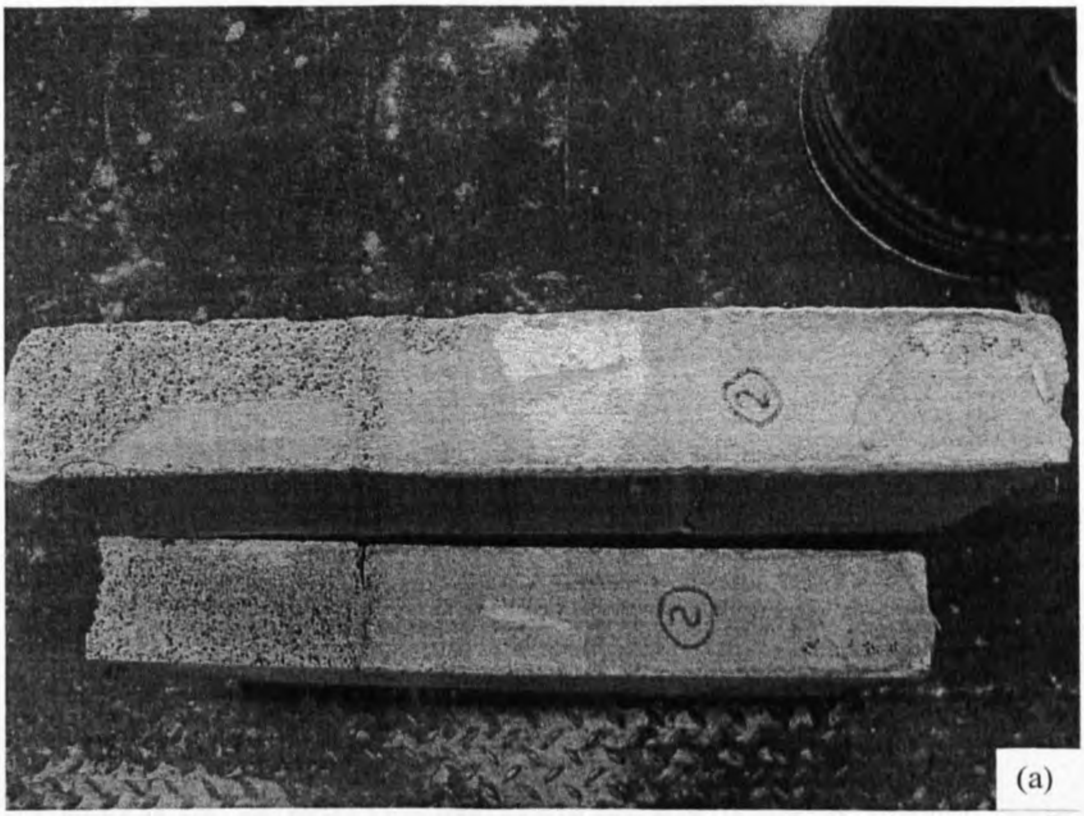


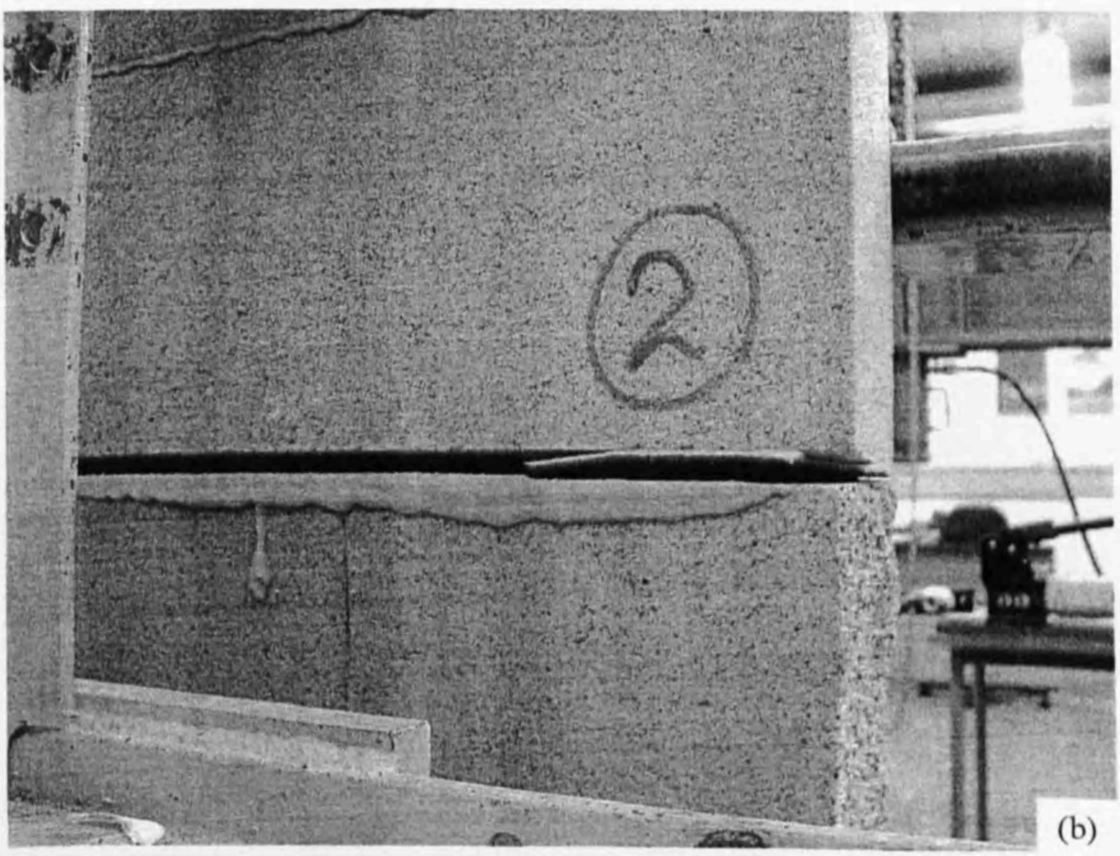


**Slide 14: Yellow B-Wallette No.2 – (a) Failure plane, (b) Position of failure plane**

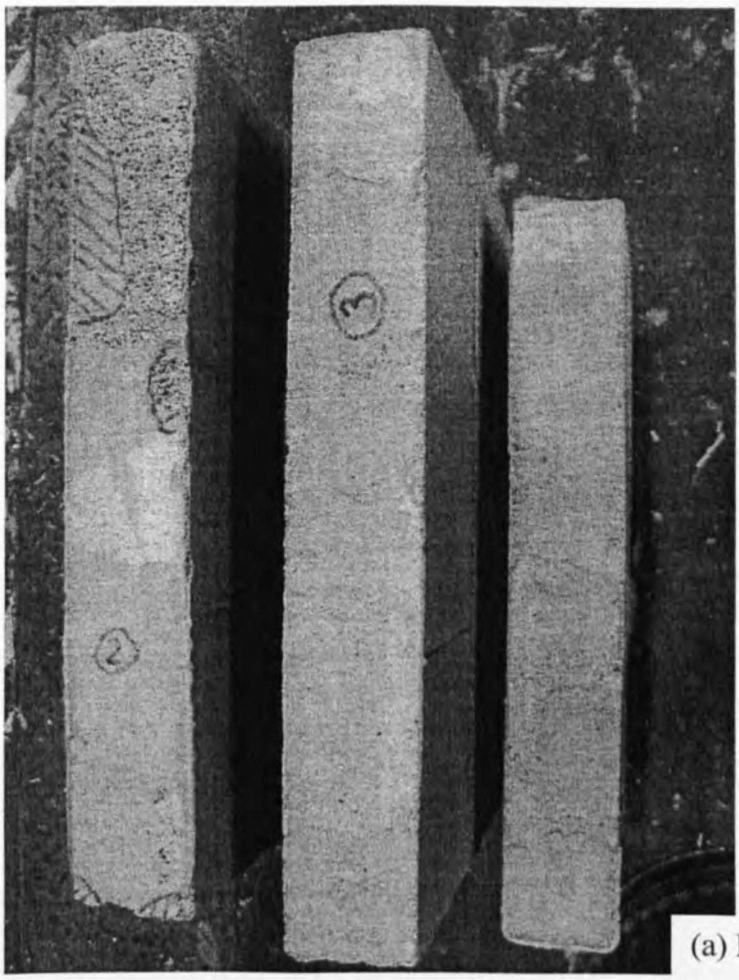

(a) Failure plane

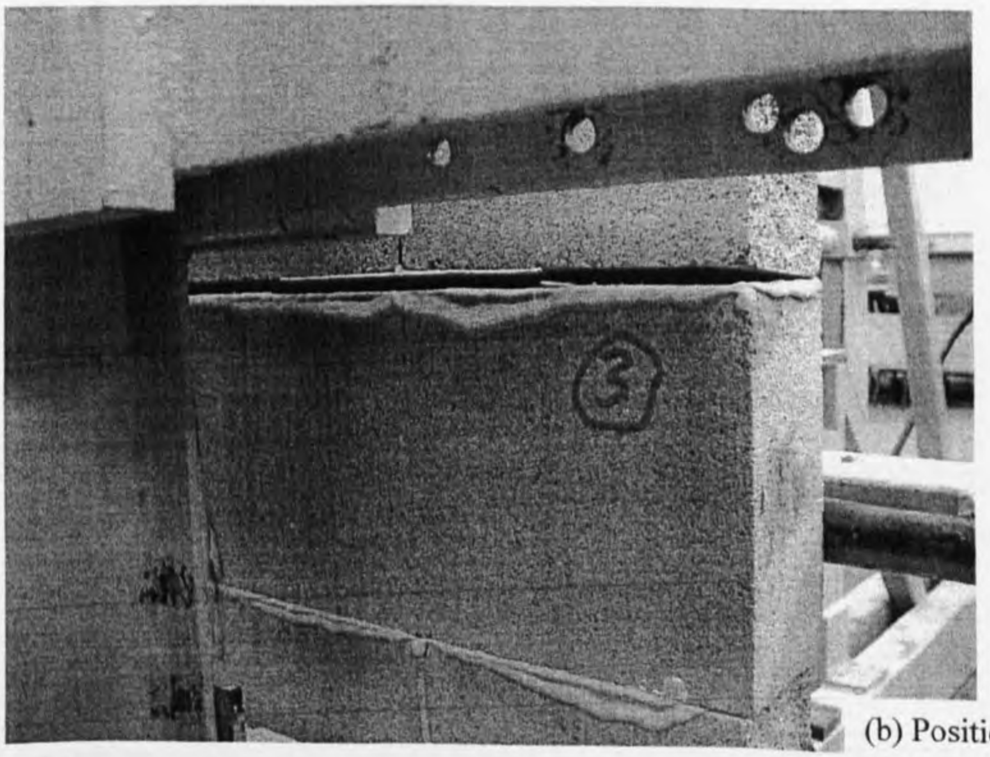

(b) Position of failure plane

**Slide 15: Yellow B-Wallette No.3**

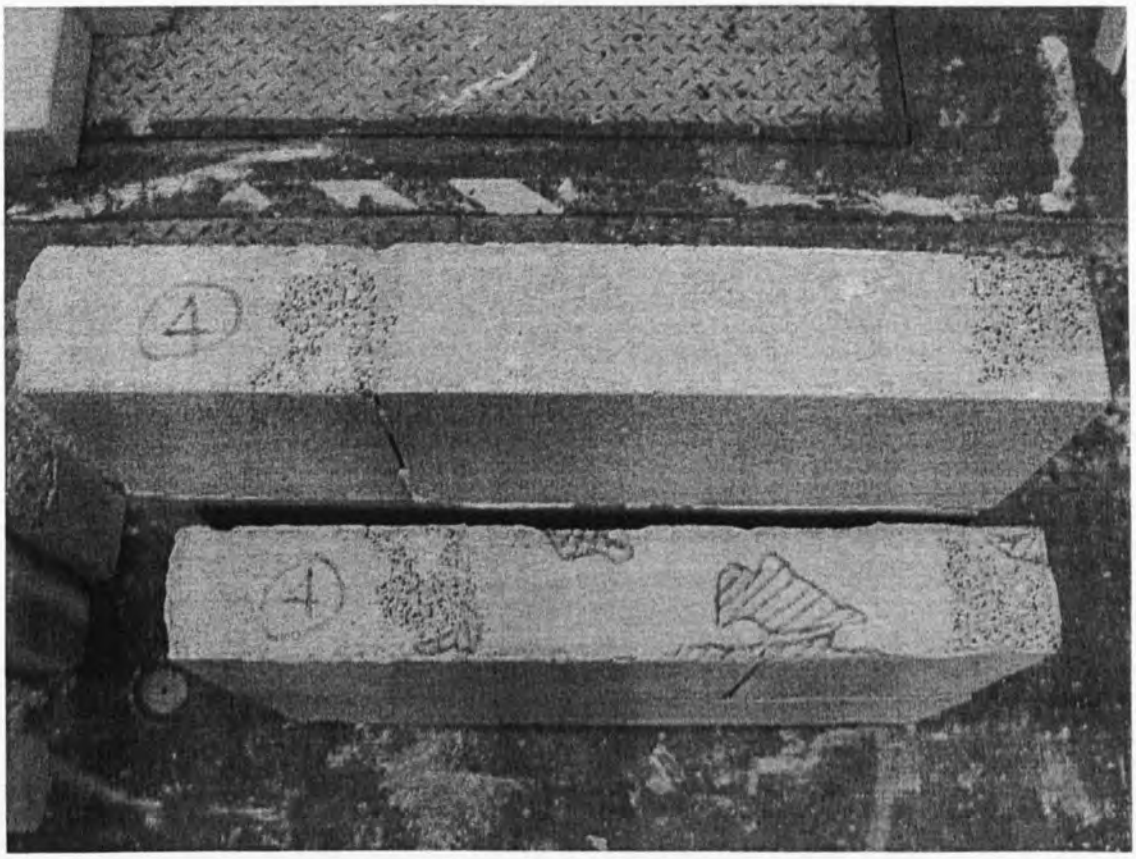

**Slide 16: Yellow B-Wallette No.4 – failure plane**

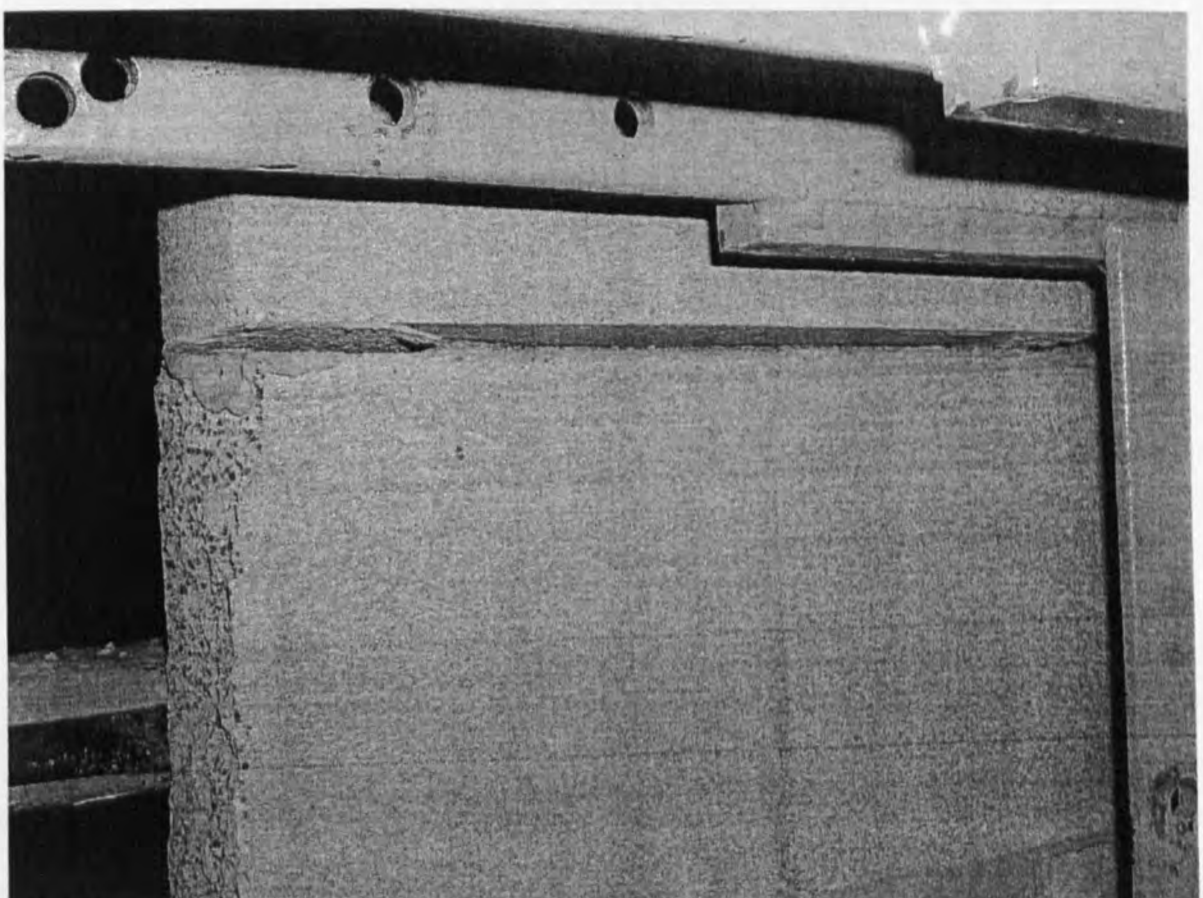

**Slide 17: Yellow B-Wallette No.5 – Position of failure plane**

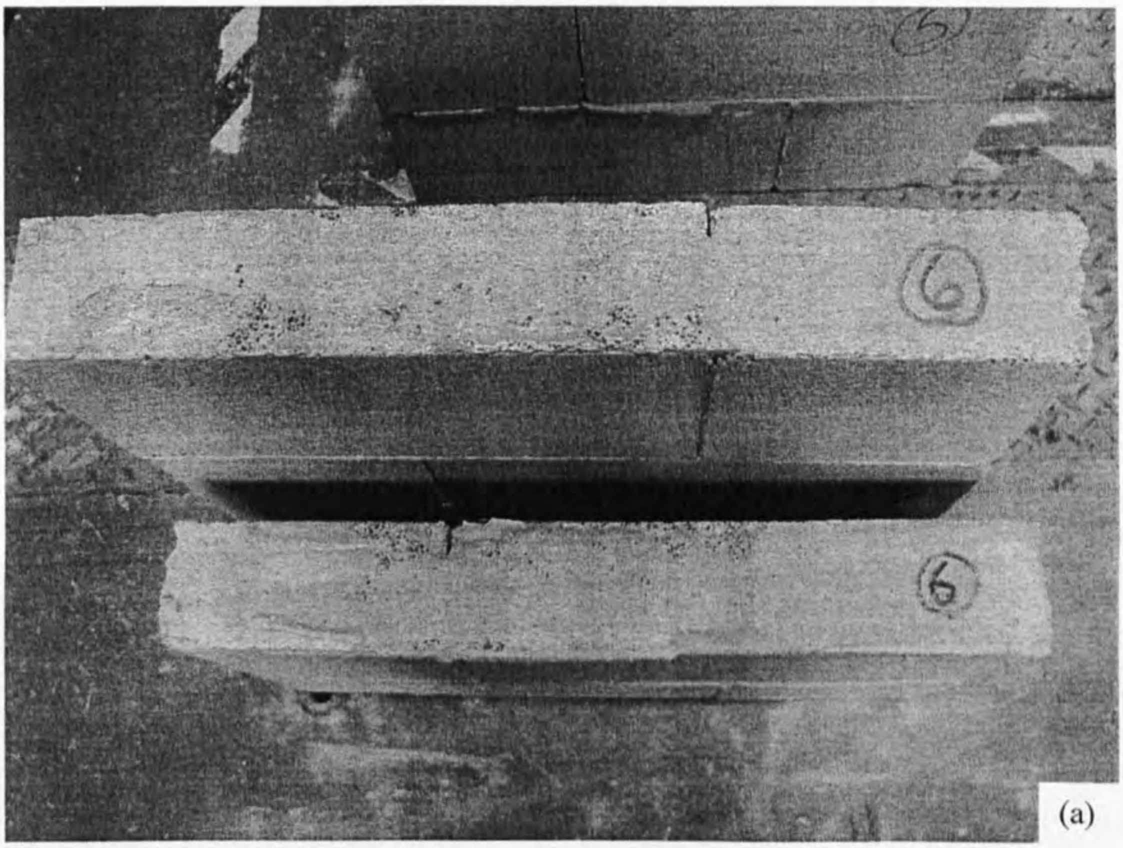

(a)

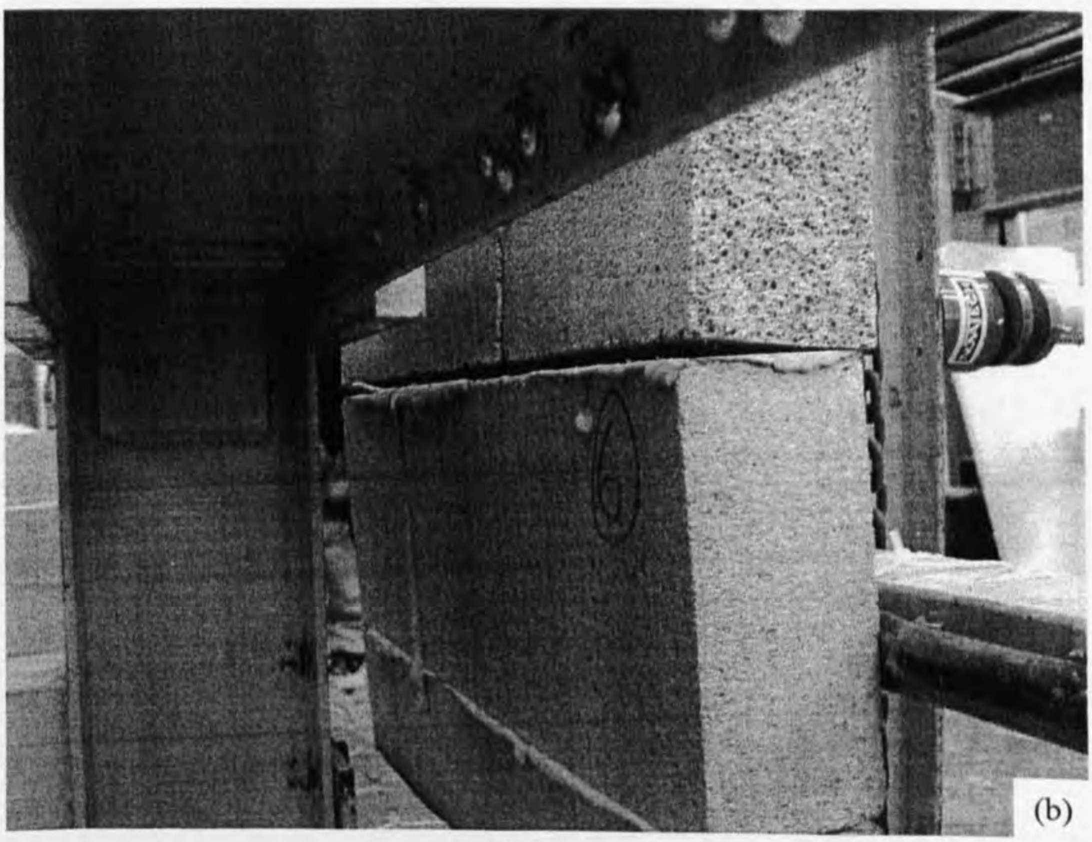

(b)

**Slide 18: Yellow B-Wallette No.6 (a) Failure plane, (b) Position of failure plane**

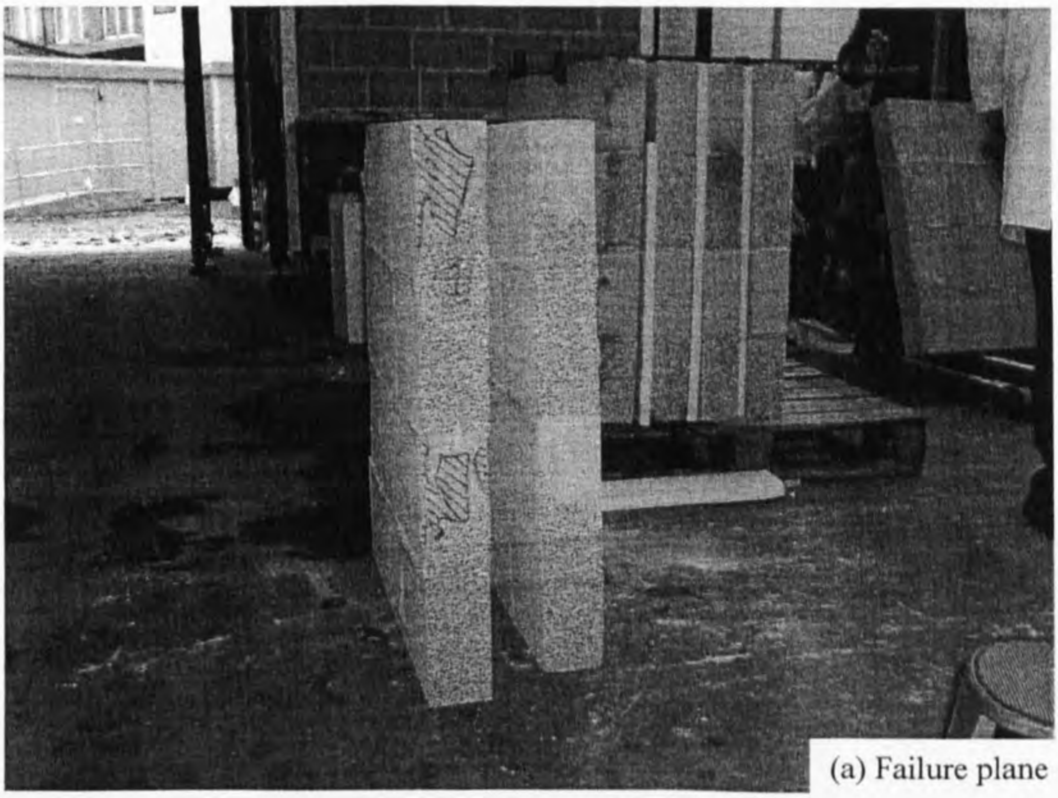

(a) Failure plane

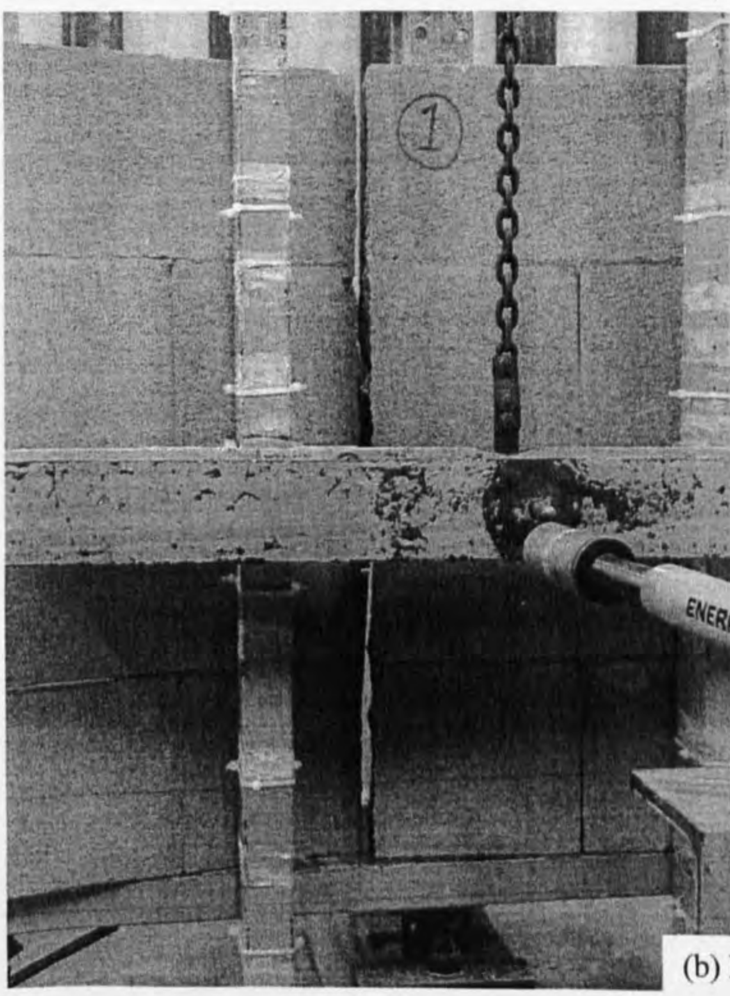

(b) Position of failure plane

**Slide 19: Yellow P-Wallette No.1**

(a) Failure plane

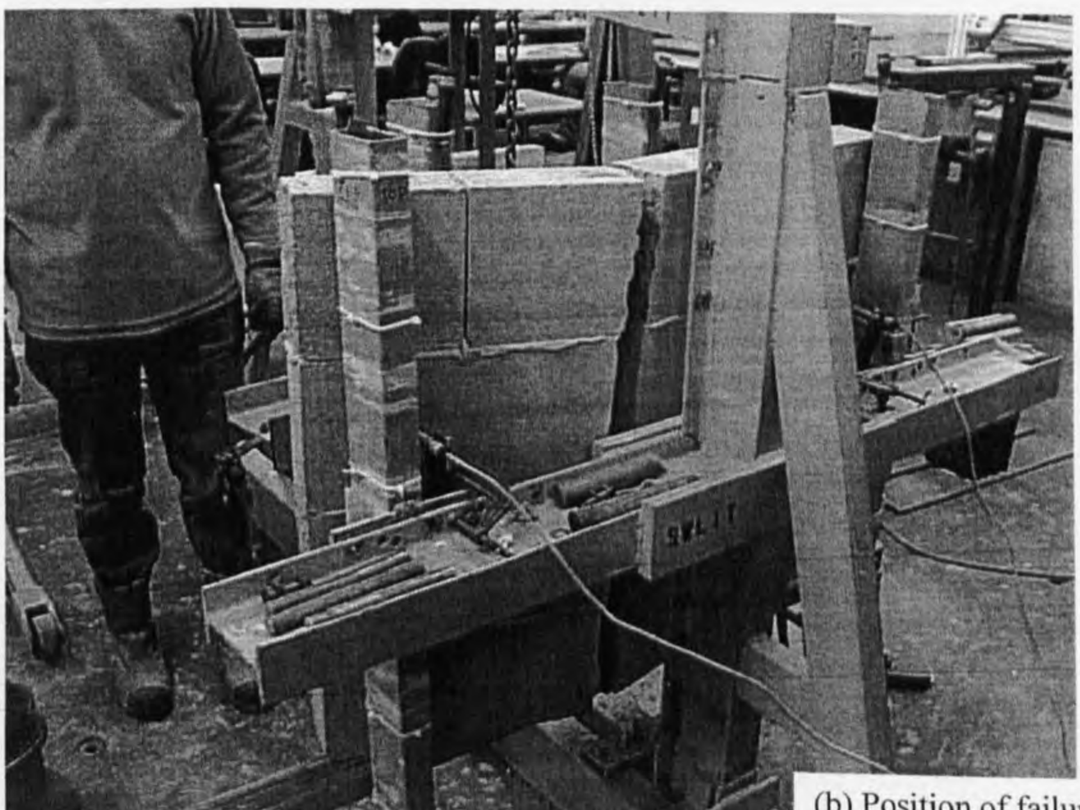

(b) Position of failure plane

**Slide 20: Yellow P-Wallette No.2**

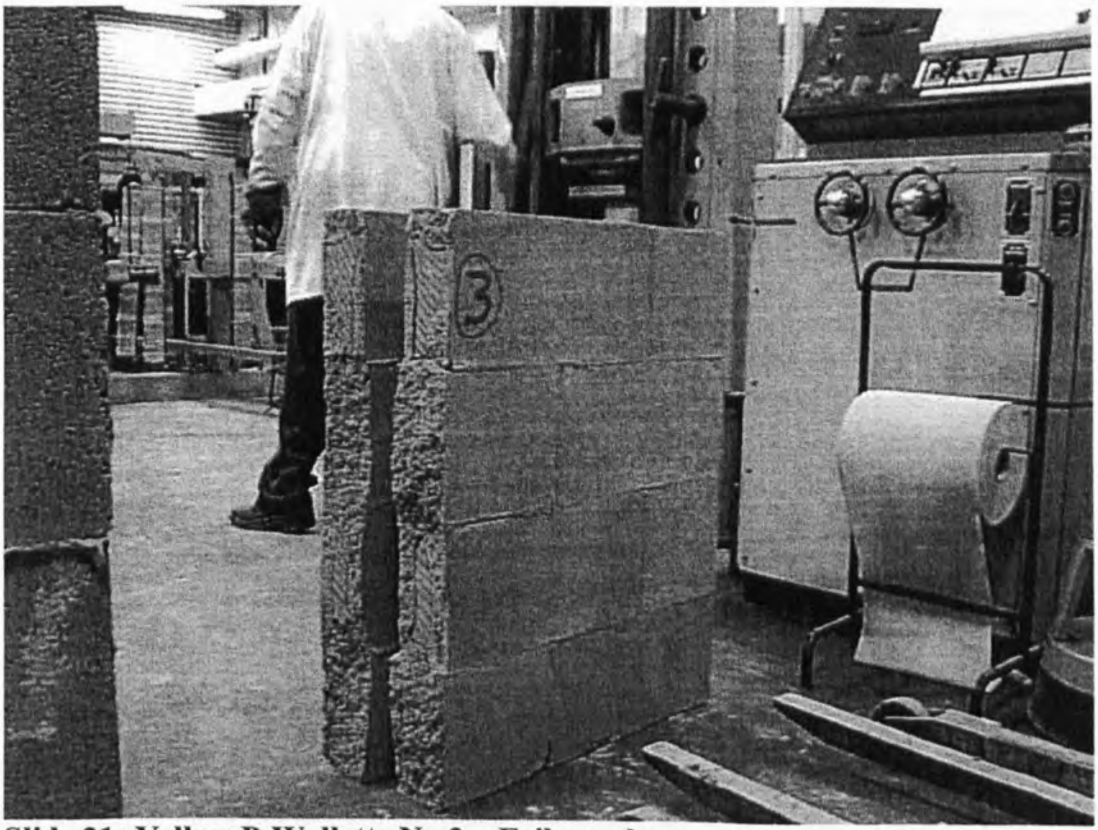

**Slide 21: Yellow P-Wallette No.3 – Failure plane**

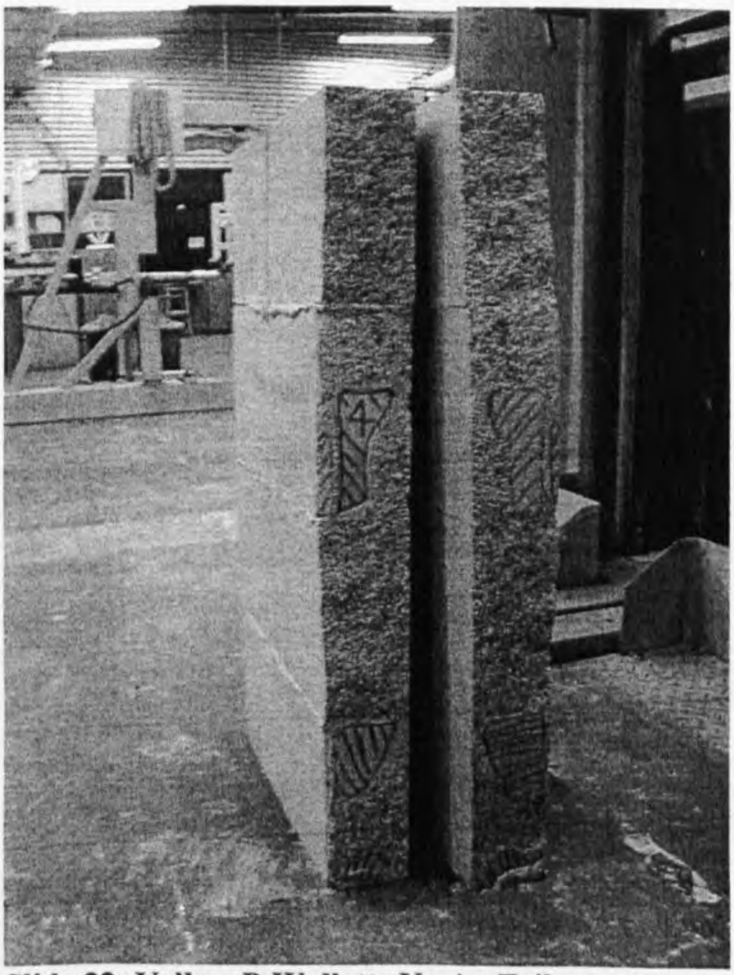

**Slide 22: Yellow P-Wallette No.4 – Failure plane**

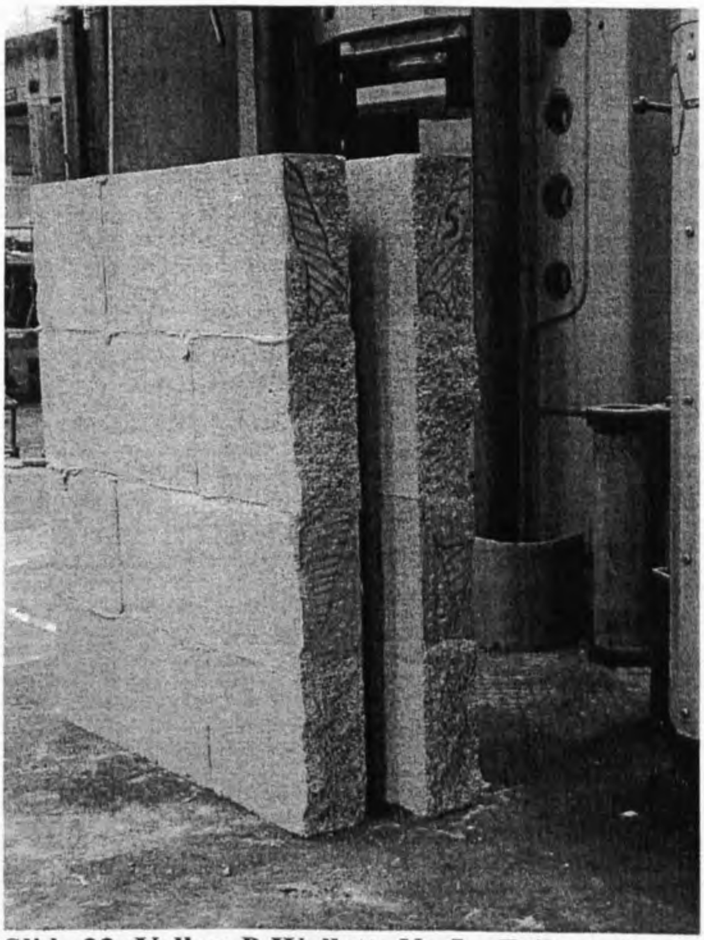

Slide 23: Yellow P-Wallette No.5 – Failure plane

Slide 24: Yellow P-Wallette No.6 – Failure plane

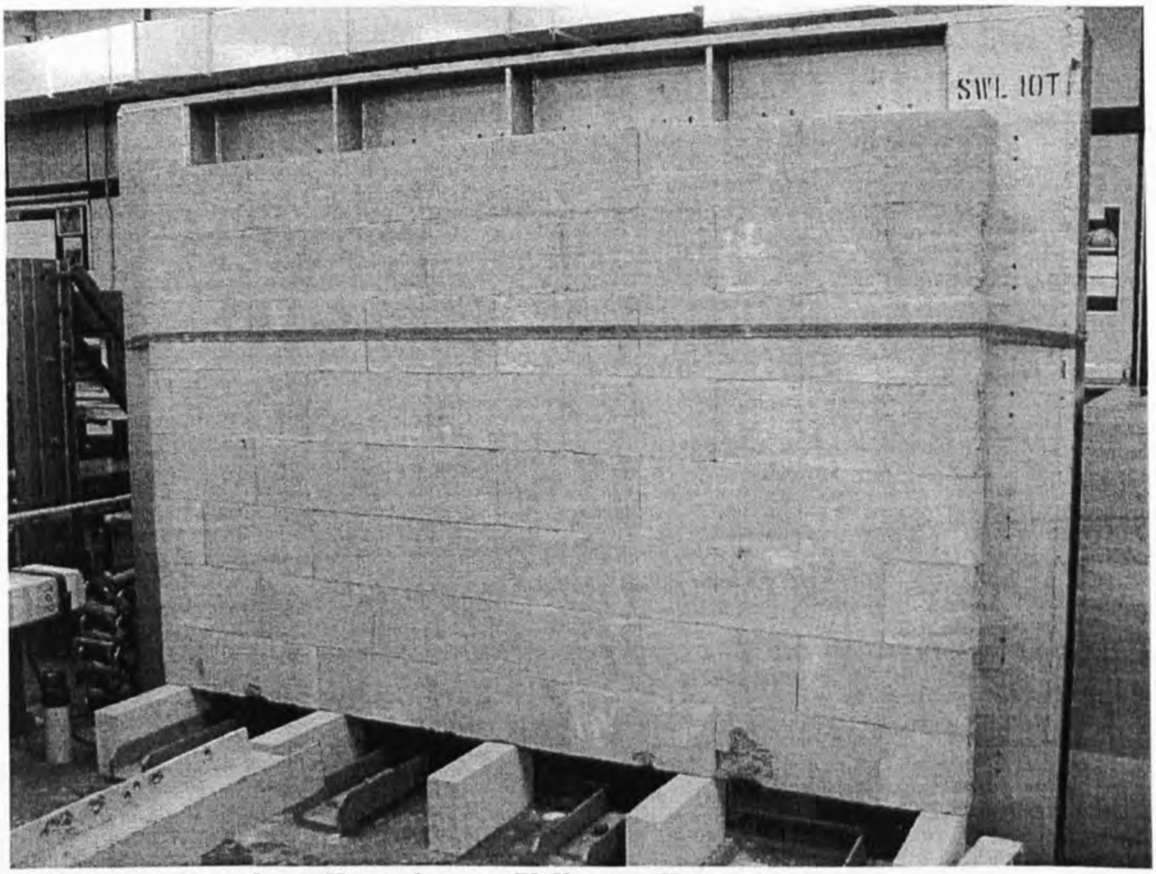

Slide 25: Full-scale wall specimen – Yellow wall panel

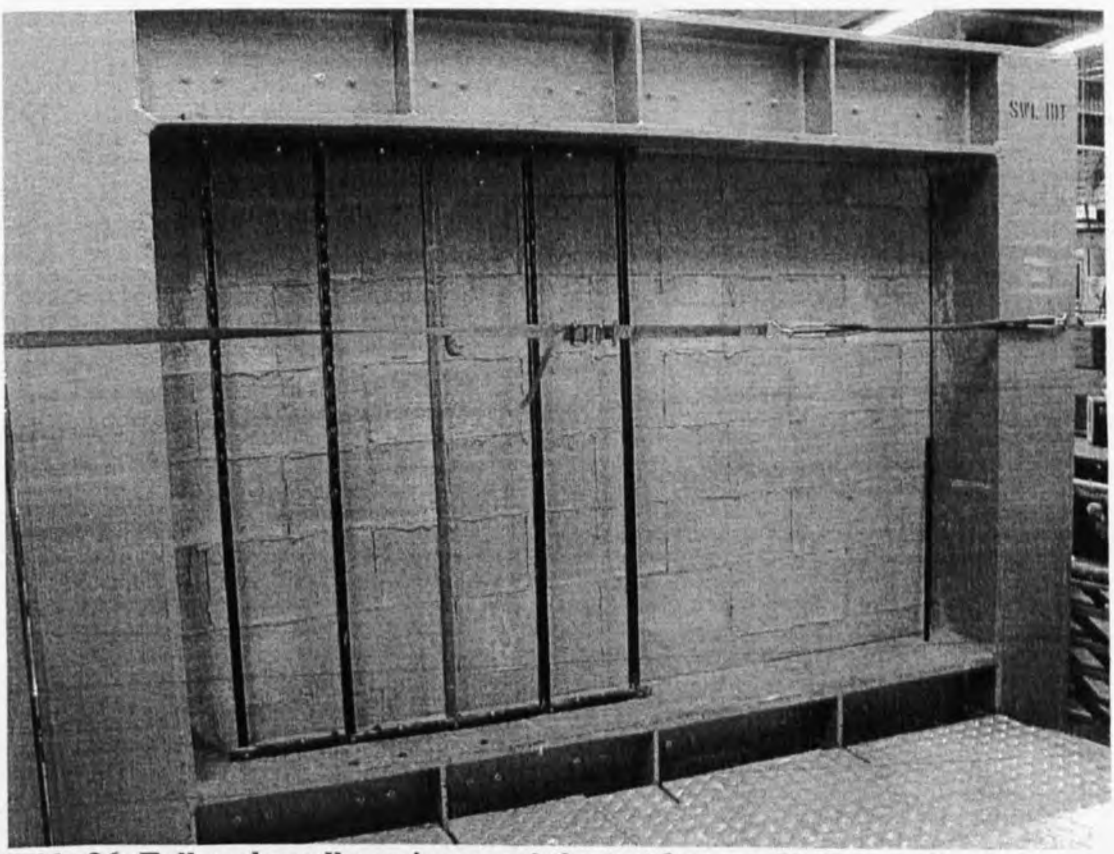
Slide 26: Full-scale wall specimen and the test frame – Yellow wall panel

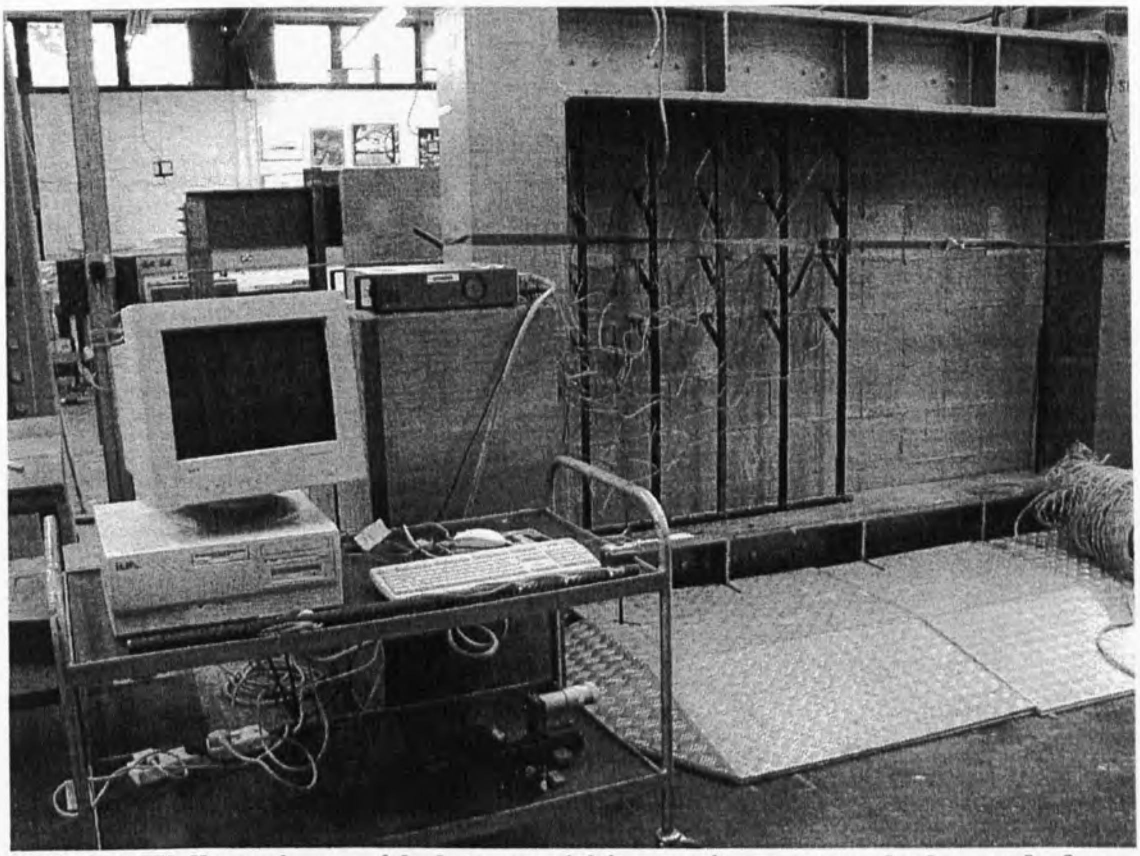

**Slide 27: Wall specimen with data acquisition equipment attached – ready for testing.**

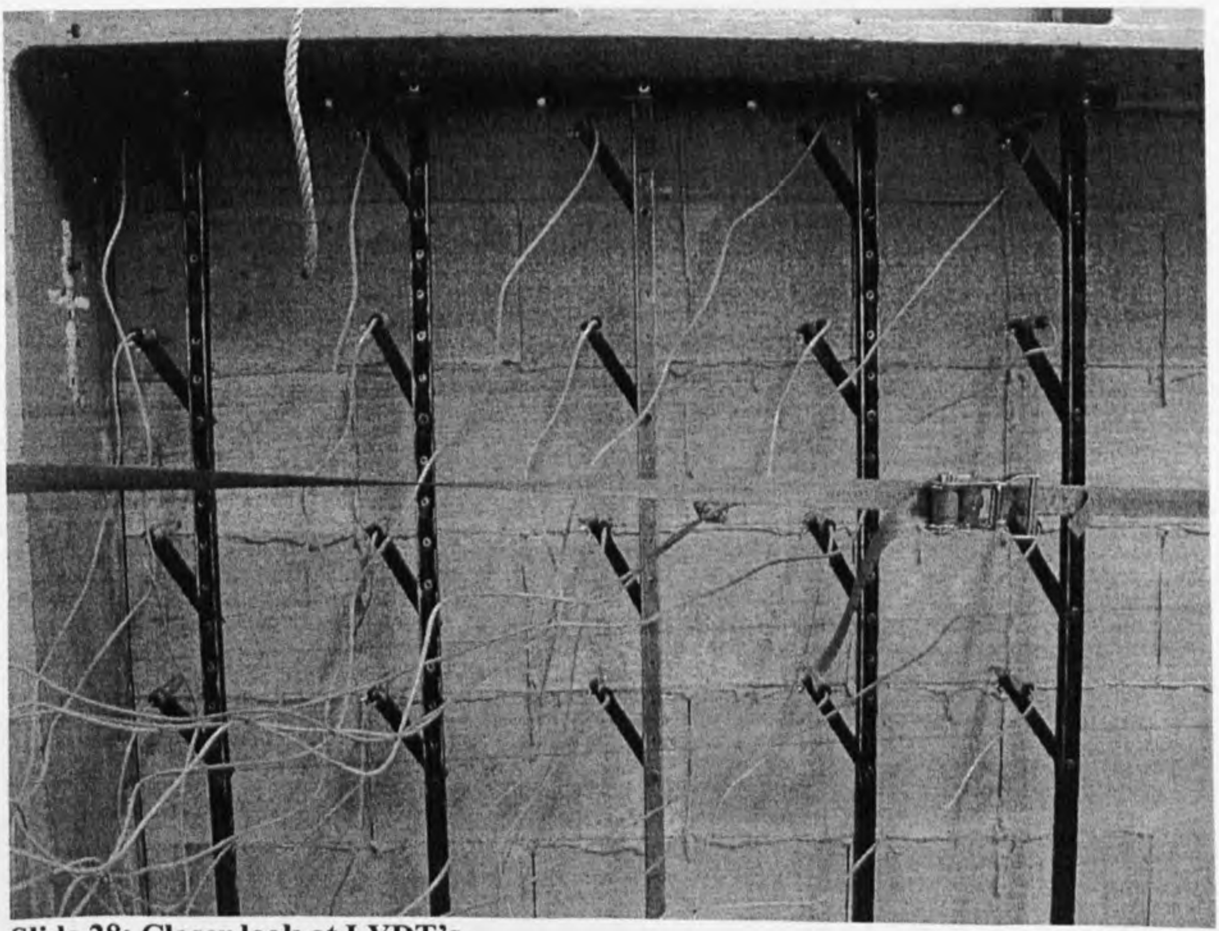

**Slide 28: Closer look at LVDT's**

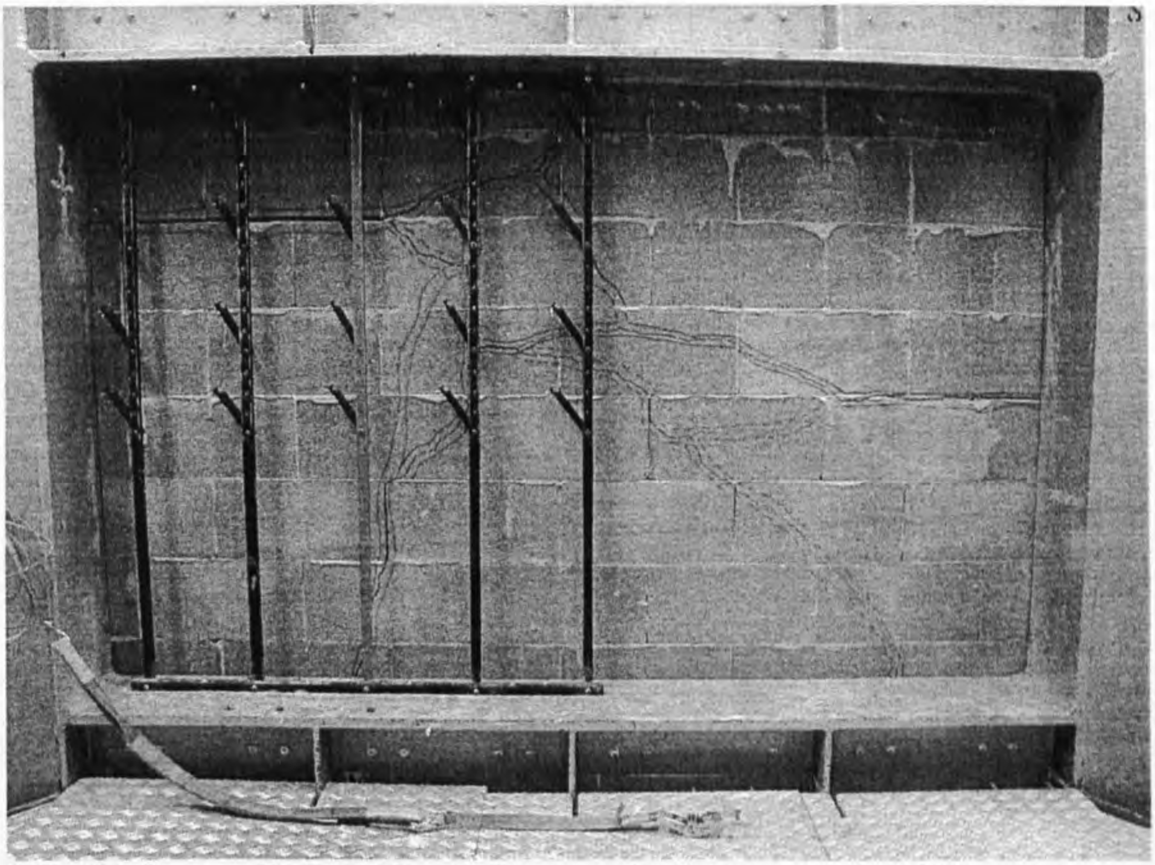

**Slide 29: Grey wall panel after testing – cracks that appeared at different stages have been highlighted with different colours**

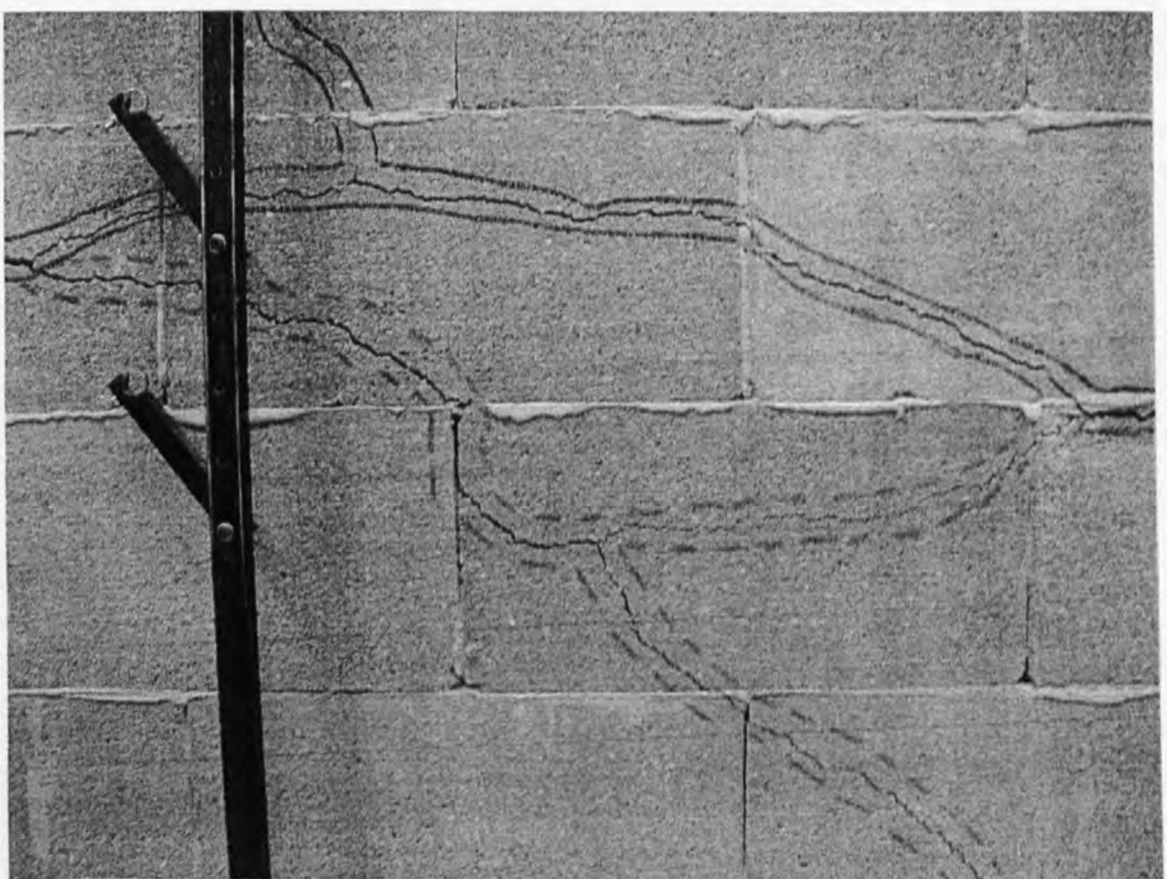

**Slide 30: Detail of some cracks in the Grey panel – cracks neither follow mortar joints nor any particular pattern**

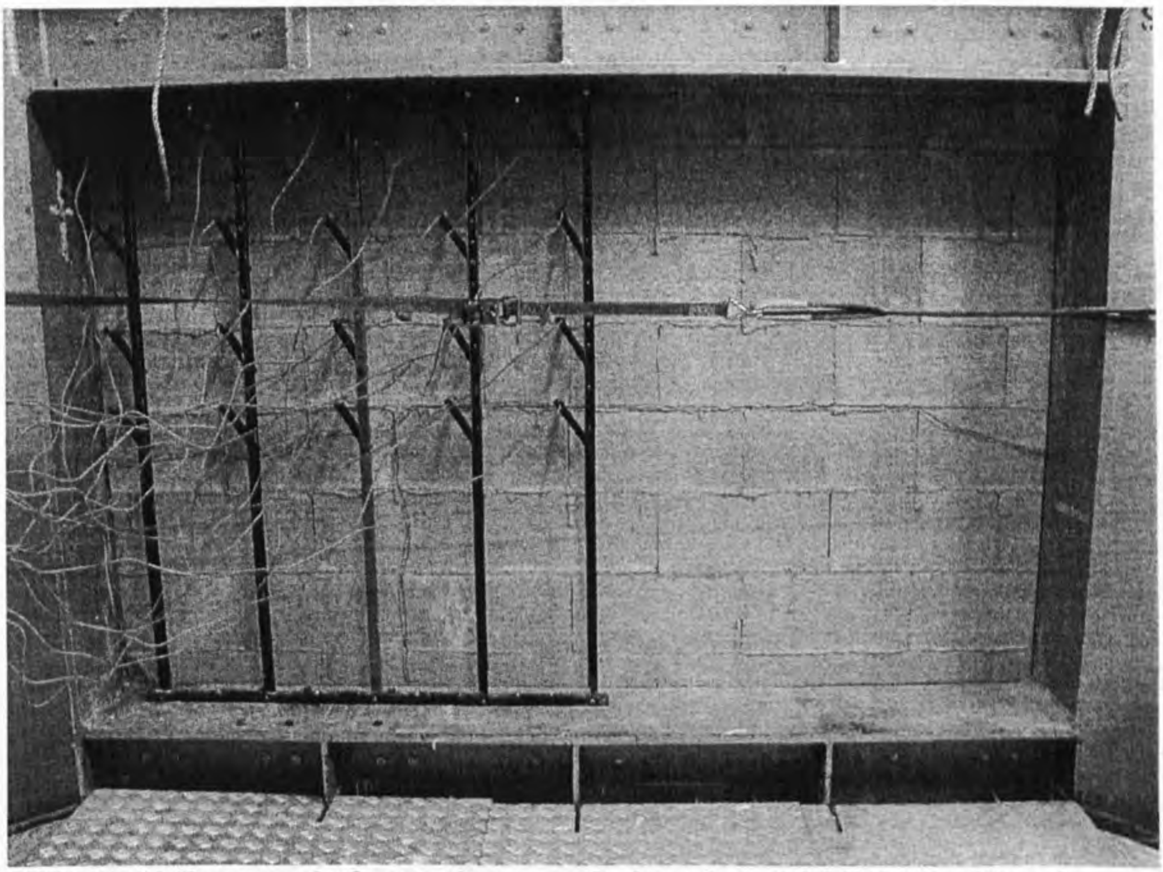

**Slide 31: Yellow panel after testing – cracks have been highlighted with red marker**

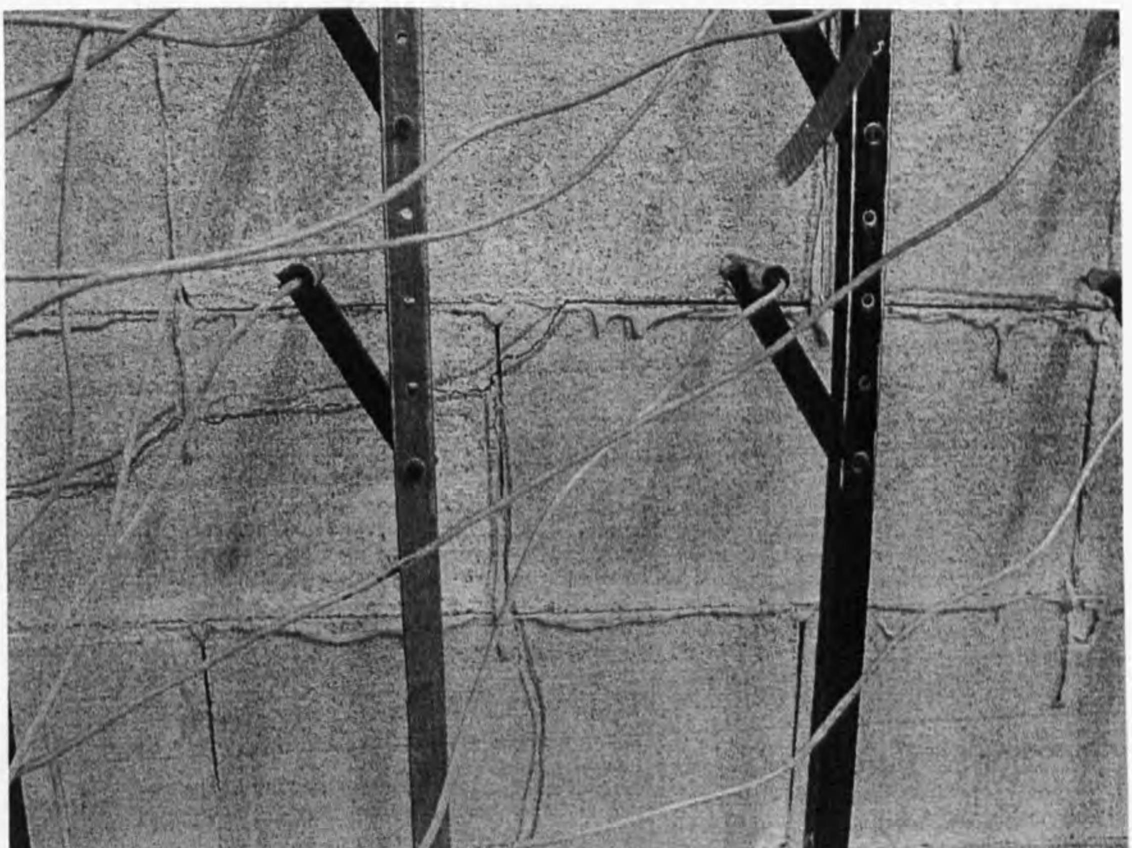

**Slide 32: Detail of the cracks in the Yellow panel – cracks mostly follow mortar joints**

**Slide 33: Further detail of cracks in the Yellow panel. Crack moves from mortar joints into the units.**

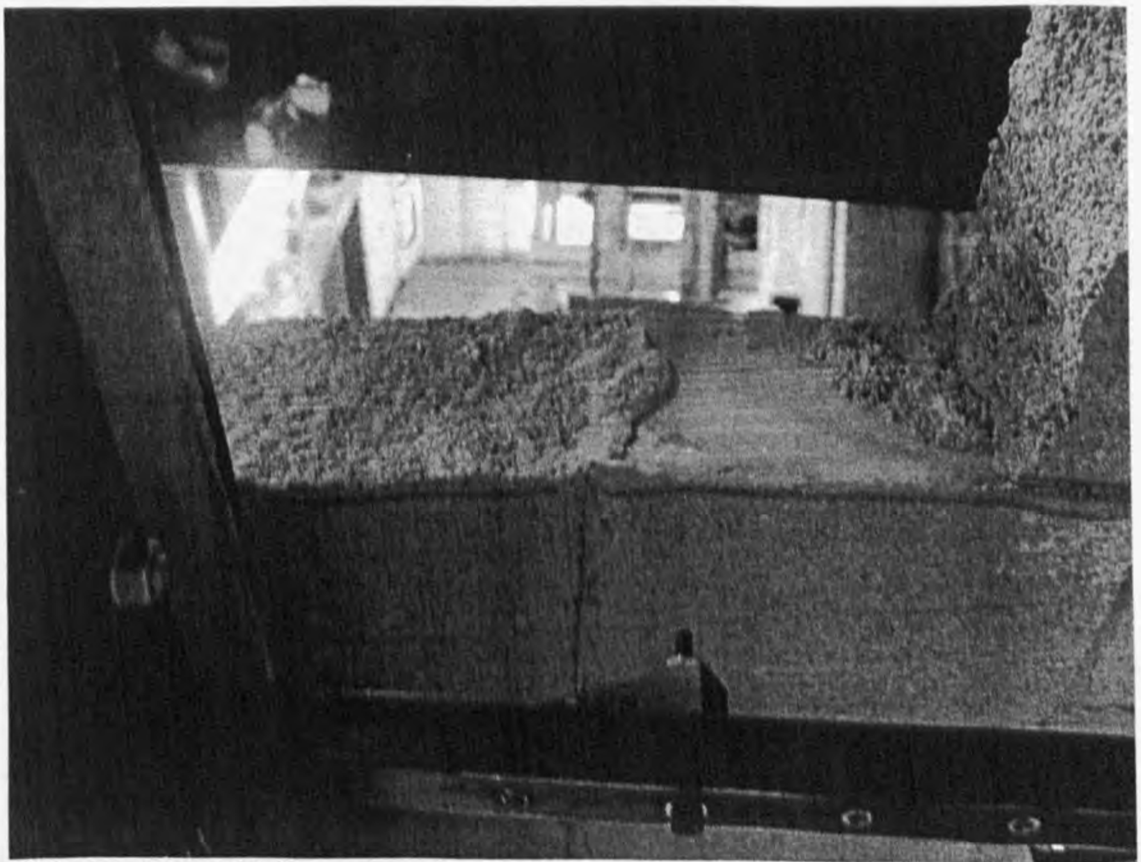

**Slide 34: Part of failure plane in the Yellow panel – notice the plucked-away concrete-block material**

# Appendix 5: Mathematical Analysis

(a) Best-Fit Polynomials for Wallette Load/Displacement Graphs

(b) Derivation of Deflection Equation and Modulus of Elasticity

(c) Calculation of Wall Displacements

(d) Tables (E vs Stress, etc)

5(a): Best-Fit Polynomials for Load/Displacement Graphs of Wallettes

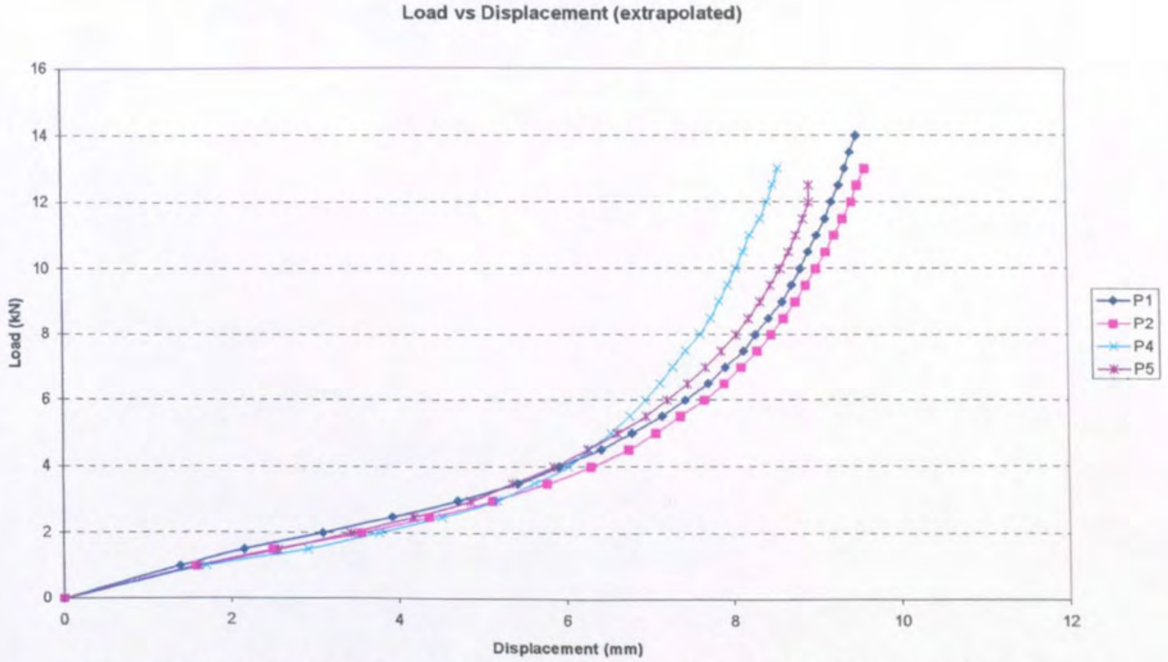


**Figure A5.1**: Normalized Load/Displacement graphs of Grey wallettes

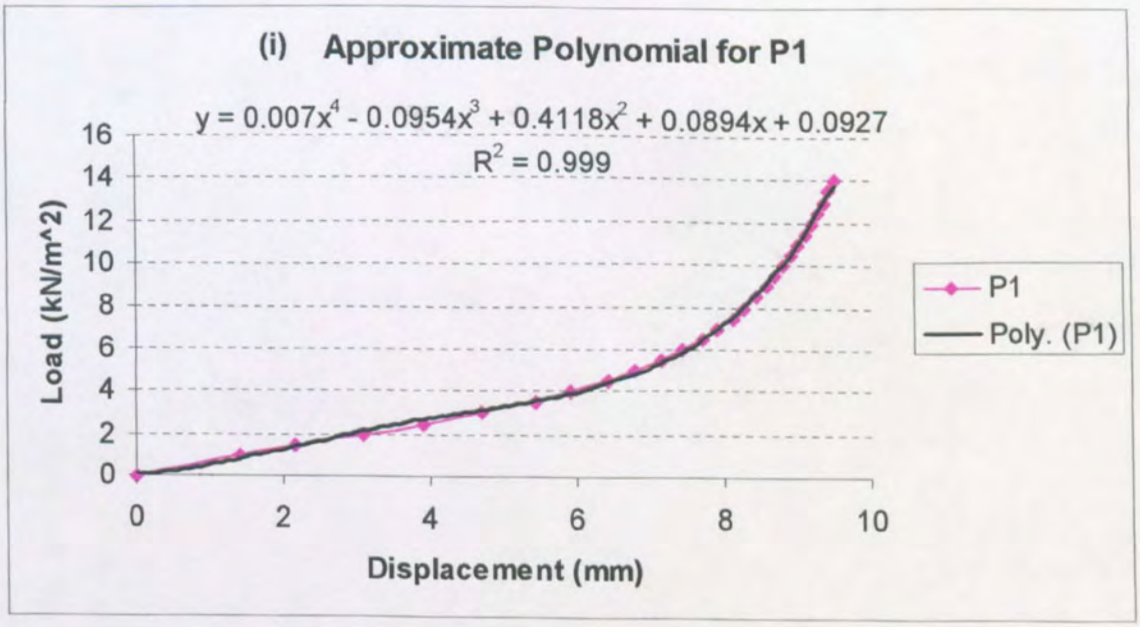

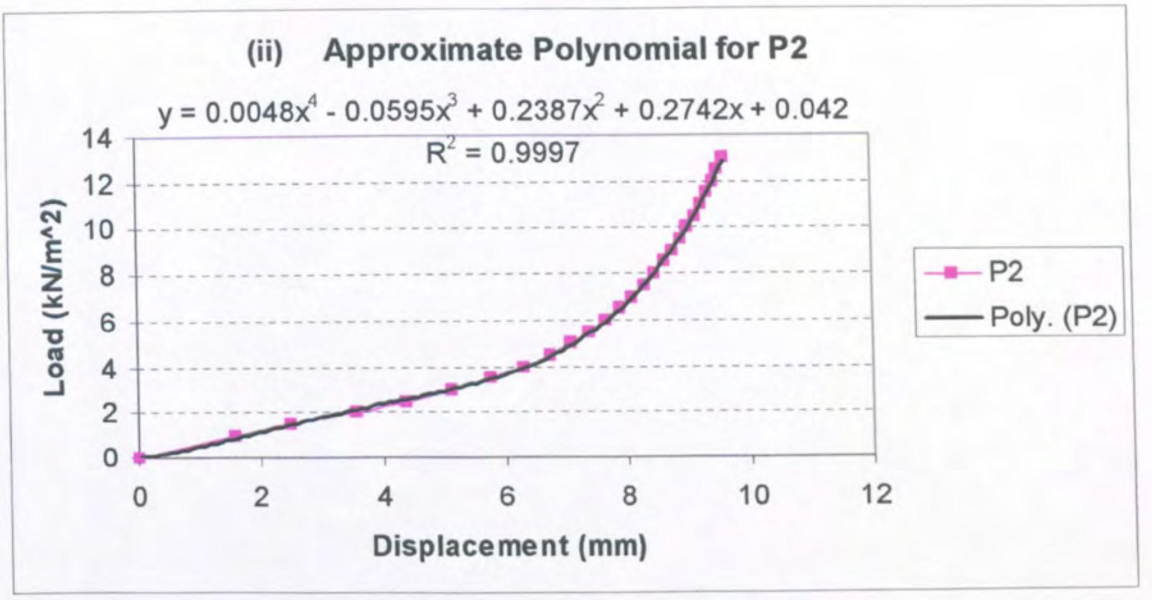


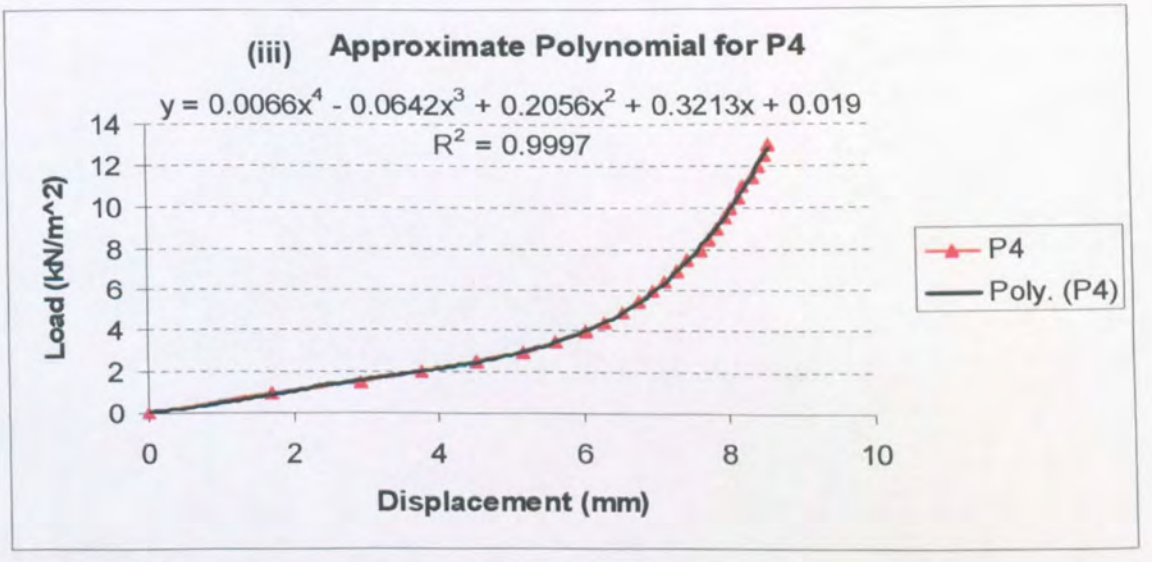


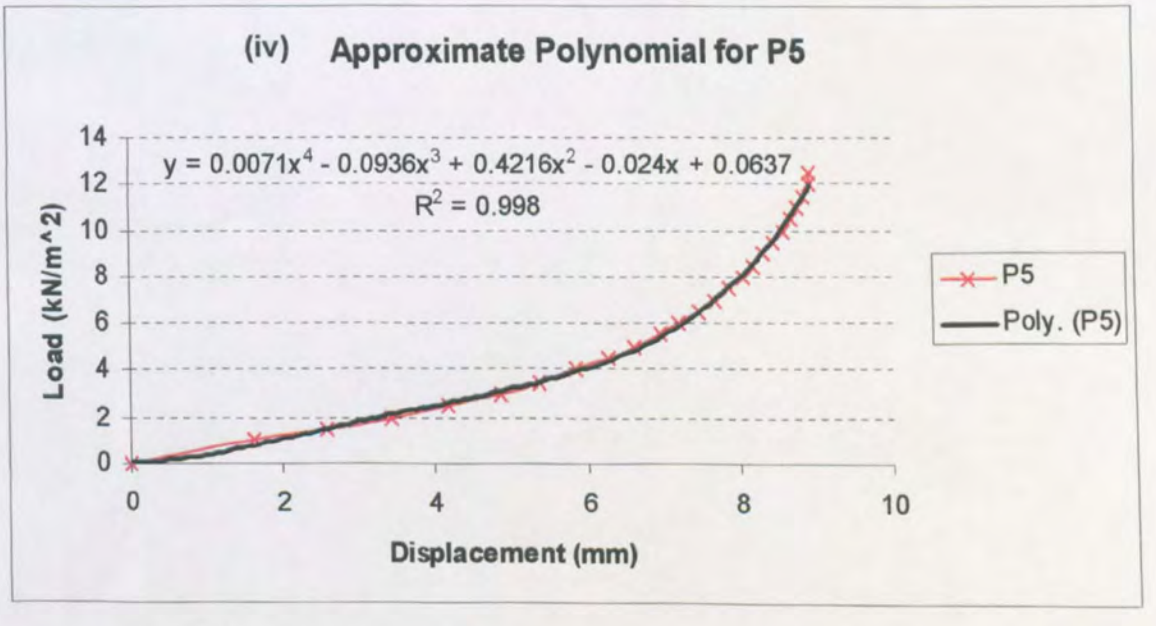


**Figure A5.2**: Equations for best-fit polynomials to the Load-Displacement graphs

**Table A5.1**: Normalized Loads and Displacements for plotting average polynomial, grey-block wallettes

| Normalized Displ. ($U/U_{max}$) | Normalized Loads ($P/P_{max}$) | | | | Avr. nomlzd Load |
|---|---|---|---|---|---|
| | P1 | P2 | P4 | P5 | |
| 0 | 0.0066 | 0.0032 | 0.0015 | 0.0051 | 0.0041 |
| 0.1 | 0.033821 | 0.036663 | 0.031475 | 0.025351 | 0.031827 |
| 0.2 | 0.08484 | 0.084088 | 0.069847 | 0.072488 | 0.077816 |
| 0.3 | 0.139319 | 0.132476 | 0.107763 | 0.12745 | 0.126752 |
| 0.4 | 0.186802 | 0.176376 | 0.142914 | 0.17986 | 0.171488 |
| 0.5 | 0.226719 | 0.217894 | 0.179538 | 0.228031 | 0.213045 |
| 0.6 | 0.268384 | 0.266684 | 0.228413 | 0.278967 | 0.260612 |
| 0.7 | 0.330998 | 0.339953 | 0.306866 | 0.348358 | 0.331544 |
| 0.8 | 0.443645 | 0.462463 | 0.438765 | 0.460583 | 0.451364 |
| 0.9 | 0.645294 | 0.666524 | 0.654524 | 0.648711 | 0.653763 |
| 1 | 0.9848 | 0.992 | 0.9911 | 0.9545 | 0.9806 |

$P1 = 0.007U^4 - 0.0954U^3 + 0.4118U^2 + 0.0894U + 0.0927$
$P2 = 0.007U^4 - 0.0954U^3 + 0.4118U^2 + 0.0894U + 0.0927$
$P4 = 0.0066U^4 - 0.0642U^3 + 0.2056U^2 + 0.3213U + 0.019$
$P5 = 0.0071U^4 - 0.0936U^3 + 0.4216U^2 - 0.024U + 0.0637$

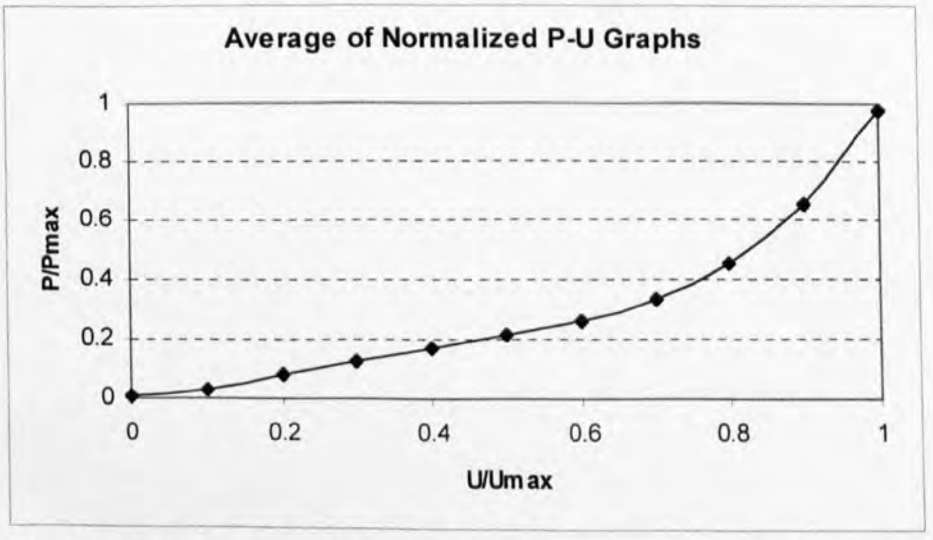


**Figure A5.3**: Average of Normalized Load/Normalized Displacement graphs

The equation of the graph in Figure A5.3 is:

$$\left(\frac{P}{P_{\max}}\right) = 3.403\left(\frac{U}{U_{\max}}\right)^4 - 4.594\left(\frac{U}{U_{\max}}\right)^3 + 2.053\left(\frac{U}{U_{\max}}\right)^2 + 0.114\left(\frac{U}{U_{\max}}\right) + 0.004$$

**Table A5.2**: Normalized Loads and Displacements for plotting average polynomial, yellow-block wallettes

| Normalized Displ., U/Umax | Normalized Loads, P/Pmax | | | | | Average |
|---|---|---|---|---|---|---|
| | P1 | P2 | P3 | P4 | P5 | |
| 0 | 0.0037 | 0.0027 | 0.0015 | 0.0004 | 0.0039 | 0.0020 |
| 0.1 | -0.0128 | 0.0021 | 0.0161 | 0.0221 | -0.0040 | 0.0206 |
| 0.2 | 0.0314 | 0.0414 | 0.0585 | 0.0589 | 0.0420 | 0.0720 |
| 0.3 | 0.0973 | 0.0939 | 0.1106 | 0.1016 | 0.1048 | 0.1347 |
| 0.4 | 0.1606 | 0.1444 | 0.1630 | 0.1470 | 0.1619 | 0.1961 |
| 0.5 | 0.2116 | 0.1891 | 0.2143 | 0.1972 | 0.2059 | 0.2530 |
| 0.6 | 0.2555 | 0.2355 | 0.2716 | 0.2601 | 0.2437 | 0.3111 |
| 0.7 | 0.3123 | 0.3029 | 0.3505 | 0.3495 | 0.2973 | 0.3854 |
| 0.8 | 0.4165 | 0.4216 | 0.4746 | 0.4846 | 0.4033 | 0.5001 |
| 0.9 | 0.6177 | 0.6336 | 0.6763 | 0.6904 | 0.6132 | 0.6885 |
| 1 | 0.9799 | 0.9923 | 0.9960 | 0.9976 | 0.9931 | 0.9932 |

5(b): Derivation of Deflection Equation and Modulus of Elasticity for Wallettes

(i) Derivation of deflection equation

Consider a beam loaded as in Figure A5. The bending moment varies along the length as follows:

For $0 \le x \le a$, $M = Px$
For $a \le x \le b$, $M = Pa$
For $b \le x \le c$, $M = P(L-x)$

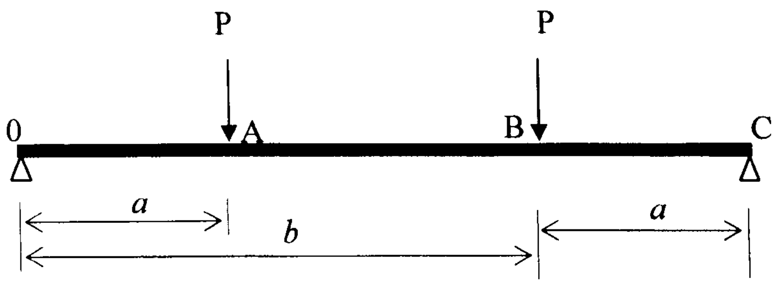


The general differential equation of the deflection curve is

$$\frac{d^2u}{dx^2} = -\frac{M}{EI}, \qquad \text{(i)}$$

where $M$ is the bending moment function that varies with $x$, $E$ is the modulus of elasticity of the material forming the beam, $I$ is the second moment of area of the section resisting bending and, $u$ is the lateral deflection of the beam at a point located at a distance $x$ from the left hand support.

Integrating eq.(i) with respect to $x$ twice, and substituting the expression for bending moment between 0 and $a$, gives the slope and deflection equations for that portion of the beam, and these are given by:

$$\frac{du}{dx} = \frac{-Px^2}{2EI} + C_1 \qquad \text{(ii)}$$

$$u = -\frac{Px^3}{6EI} + C_1x + C_2 \qquad \text{(iii)}$$

Enforcing the boundary conditions at the supports for eq.(iii) yields the value of the constant of integration, $C_2 = 0$.

Proceeding as above for the portion of the beam between $a$ and $b$, yields the following equations:

$$\frac{du}{dx} = -\frac{Pax}{EI} + C_3 \qquad \text{(iii)}$$

$$u = -\frac{Pax^2}{2EI} + C_3 x + C_4 \tag{iv}$$

Boundary conditions; at $x = \frac{L}{2}$, slope of the deflection curve is equal to zero,

at $x = a$, eq.(ii) = eq.(v)

Using these boundary conditions yields the values of $C_1, C_3$ and $C_4$, as follows:

$$C_1 = -\frac{Pa^2}{2EI} + \frac{PaL}{2EI} \tag{v}$$

$$C_3 = \frac{PaL}{2EI} \tag{vi}$$

$$C_4 = -\frac{Pa^3}{6EI} \tag{vii}$$

Therefore, deflection equations are:

$$EIu = -\frac{Px^3}{6} + \frac{Pax}{2}(L-a), \text{ for } 0 \le x \le a \tag{viii}$$

$$EIu = -\frac{Pax^2}{2} + \frac{PaLx}{2} + \frac{Pa^3}{6}, \text{ for } a \le x \le b \tag{ix}$$

The central deflection, that is, at $x = \frac{L}{2}$, is given by

$$EIu = -\frac{PaL^2}{8} - \frac{Pa^3}{6} \tag{x}$$

(ii) Magnitudes of Modulus of elasticity

**Table A5.3**: Modulus of Elasticity at Various Stress Levels – Grey-block wallettes

| Stress (N/mm^2) | E (N/mm^2) P1 | P2 | P3 | P4 | P5 |
|---|---|---|---|---|---|
| 0.149 | 11597 | 9716 | 5549 | 9140 | 13512 |
| 0.199 | 10947 | 8927 | 1903 | 10666 | 9837 |
| 0.248 | 11436 | 9066 | 973 | 9371 | 9205 |
| 0.298 | 12944 | 9211 | | 9495 | 7808 |
| 0.348 | 10967 | 9029 | | 10037 | 7590 |
| 0.397 | 12475 | 9834 | | 9737 | 8571 |
| 0.447 | 12324 | 10082 | | 11242 | 8292 |
| 0.497 | 13056 | 10506 | | 10409 | 8755 |
| 0.547 | 13501 | 10930 | | 10685 | 8141 |
| 0.596 | 12826 | 11272 | | 9504 | 8523 |
| 0.646 | 11845 | 11473 | | 8207 | 8995 |
| 0.696 | 10961 | 11687 | | 8088 | 9493 |
| 0.745 | 10775 | 12081 | | 8114 | 10213 |
| 0.795 | 10849 | 12512 | | 8313 | 11087 |
| 0.845 | 10876 | 12663 | | 8498 | 12438 |
| 0.894 | 10882 | 12947 | | 8868 | 13395 |
| 0.944 | 11145 | 12842 | | 9088 | 13202 |
| 0.994 | 10905 | 13543 | | 9474 | 13433 |
| 1.043 | 10920 | 13262 | | 9755 | 13681 |
| 1.093 | 11031 | 13222 | | 10123 | 13936 |
| 1.143 | 10976 | 13193 | | 10272 | 13846 |
| 1.192 | 11147 | 13140 | | 10603 | 13691 |
| 1.242 | 11086 | 13238 | | 10864 | |
| 1.292 | 11101 | 13664 | | 11204 | |
| 1.342 | 11193 | | | | |
| 1.391 | 11123 | | | | |

**Table A5.4**: Modulus of Elasticity at Various Stress Levels – Yellow-block wallettes

| Stress (N/mm^2) | E (N/mm^2) P1 | P2 | P3 | P4 | P5 |
|---|---|---|---|---|---|
| 0.149 | 14942 | 13605 | 16432 | 8366 | 10766 |
| 0.199 | 15239 | 7933 | 14098 | 7461 | 11717 |
| 0.248 | 13515 | 8051 | 14073 | 7564 | 11954 |
| 0.298 | 12528 | 9412 | 13990 | 7973 | 12805 |
| 0.348 | 12222 | 10586 | 12663 | 11850 | 12623 |
| 0.397 | 12103 | 9701 | 10706 | 11934 | 12305 |
| 0.447 | 12057 | 8766 | 10313 | 12798 | 11582 |
| 0.497 | 12119 | 8290 | 10192 | 12902 | 11479 |
| 0.547 | 11957 | 8090 | 10372 | 12627 | 9102 |
| 0.596 | 12049 | 7772 | 10731 | 13069 | 8597 |
| 0.646 | 12694 | 7711 | 11108 | 13257 | 8163 |
| 0.696 | 12660 | 7859 | 11219 | 12863 | 8187 |
| 0.745 | 12610 | 7874 | 11123 | 12801 | 9155 |
| 0.795 | 12675 | 7984 | 11289 | 12614 | 9092 |
| 0.845 | 12663 | 8172 | 11571 | 12272 | 9086 |
| 0.894 | 12926 | 8204 | 11667 | 12014 | 9050 |
| 0.944 | 13104 | 8388 | 11951 | 11790 | 9225 |
| 0.994 | 13025 | 8516 | 12318 | 11643 | 9466 |

| | | | | | |
|---|---|---|---|---|---|
| **1.043** | 13105 | 8710 | 12509 | 11234 | 9595 |
| **1.093** | 12919 | 8787 | 12645 | | 9708 |
| **1.143** | 13029 | 8851 | 12528 | | 9727 |
| **1.192** | 12943 | 8917 | 12251 | | 9737 |
| **1.242** | | 9015 | | | 9405 |
| **1.292** | | 9019 | | | |
| **1.342** | | 9036 | | | |

5(c): Wall Displacements

**Table A5.5:** Displacements across Mid-Height at different load cases --Grey Wall

| | Displacement at: | | | |
|---|---|---|---|---|
| **Position** | Failure load | 75% load | 50% load | 25% load |
| 0 | 7.4693 | 6.5012 | 6.0214 | 4.4015 |
| 21 | 7.8693 | 6.9121 | 6.4907 | 4.71023 |
| 49.5 | 8.2648 | 7.49892 | 6.9064 | 5.09834 |
| 77 | 8.7461 | 8.02314 | 7.3102 | 5.3851 |
| 104.5 | 9.2878 | 8.50032 | 7.7001 | 5.60024 |
| 131 | 9.9271 | 8.9142 | 7.9436 | 5.7373 |
| 134 | 9.9271 | 8.9142 | 7.9436 | 5.7373 |
| 160.5 | 9.2878 | 8.50032 | 7.7001 | 5.60024 |
| 188 | 8.7461 | 8.02314 | 7.3102 | 5.3851 |
| 215.5 | 8.2648 | 7.49892 | 6.9064 | 5.09834 |
| 244 | 7.8693 | 6.9121 | 6.4907 | 4.71023 |
| 265 | 7.4693 | 6.5012 | 6.0214 | 4.4015 |

**Table A5.6:** Displacements down Mid-Span at different load cases -- Grey Wall

| | Displacement at: | | | |
|---|---|---|---|---|
| **Position** | Failure load | 75% load | 50% load | 25% load |
| 0 | 7.5115 | 6.5012 | 5.6541 | 4.4361 |
| -13 | 7.8615 | 6.8542 | 6.0195 | 4.7042 |
| -38.5 | 8.6185 | 7.6381 | 6.61024 | 5.09821 |
| -63 | 9.3488 | 8.3637 | 7.1537 | 5.5201 |
| -83.5 | 9.9271 | 8.90695 | 7.6436 | 5.7373 |
| -91.5 | 9.9271 | 8.90695 | 7.6436 | 5.7373 |
| -112 | 9.3488 | 8.3637 | 7.1537 | 5.5201 |
| -136.5 | 8.6185 | 7.6381 | 6.61024 | 5.09821 |
| -162 | 7.8615 | 6.8542 | 6.0195 | 4.7042 |
| -175 | 7.5115 | 6.5012 | 5.6541 | 4.4361 |

**Table A5.7**: Displacements across Mid-Height at different load cases -- Yellow Wall

| | Displacement at: | | | |
|---|---|---|---|---|
| **Position** | Failure load | 83% load | 50% load | 33% load |
| 0 | 7.32863 | 7.0241 | 6.5142 | 5.9564 |
| 18 | 7.8121 | 7.5422 | 6.9632 | 6.327 |
| 45.8 | 8.3864 | 8.0755 | 7.1271 | 6.3719 |
| 73.6 | 8.9145 | 8.4775 | 7.2926 | 6.4784 |
| 101.4 | 9.1494 | 8.605 | 7.1886 | 6.3078 |
| 129.2 | 9.2226 | 8.7078 | 7.3594 | 6.474 |
| 135.8 | 9.2226 | 8.7078 | 7.3594 | 6.474 |
| 163.6 | 9.1494 | 8.605 | 7.1886 | 6.3078 |
| 191.4 | 8.9145 | 8.4775 | 7.2926 | 6.4784 |
| 219.2 | 8.3864 | 8.0755 | 7.1271 | 6.3719 |
| 247 | 7.8121 | 7.5422 | 6.9632 | 6.327 |
| 265 | 7.32863 | 7.0241 | 6.5142 | 5.9564 |

**Table 5.8**: Displacements down Mid-Span at different load cases -- Yellow Wall

| | Displacement at: | | | |
|---|---|---|---|---|
| **Position** | Failure load | 83% load | 50%load | 33% load |
| 0 | 7.3859 | 6.7124 | 4.5351 | 3.6841 |
| -14 | 7.7357 | 6.9281 | 4.9339 | 4.063 |
| -38.8 | 8.1794 | 7.43 | 5.6017 | 4.7168 |
| -63.6 | 8.7162 | 8.0702 | 6.4371 | 5.5385 |
| -84.4 | 9.2226 | 8.7078 | 7.3594 | 6.474 |
| -90.6 | 9.2226 | 8.7078 | 7.3594 | 6.474 |
| -111.4 | 8.7162 | 8.0702 | 6.4371 | 5.5385 |
| -136.2 | 8.1794 | 7.43 | 5.6017 | 4.7168 |
| -161 | 7.7357 | 6.9281 | 4.9339 | 4.063 |
| -175 | 7.3859 | 6.7124 | 4.5351 | 3.6841 |